Dipl.-Ing. Elisabeth Wruß

On the Reliability and Predictive Power of Density Functional Theory for the Description of Inorganic/Organic Interfaces

DOCTORAL THESIS

to achieve the university degree of

Doktorin der technischen Wissenschaften

submitted to

Graz University of Technology

Supervisor

Ao.Univ.-Prof. Dipl.-Ing. Dr.techn. Egbert Zojer

Co-Supervisor

Dipl.-Ing. Dr.techn. Oliver T. Hofmann

Institute of Solid State Physics

Graz, July 2018

AFFIDAVIT

I declare that I have authored this thesis independently, that I have not used other than the declared sources/resources, and that I have explicitly indicated all material which has been quoted either literally or by content from the sources used. The text document uploaded to TUGRAZonline is identical to the present doctoral thesis.

Date

Signature

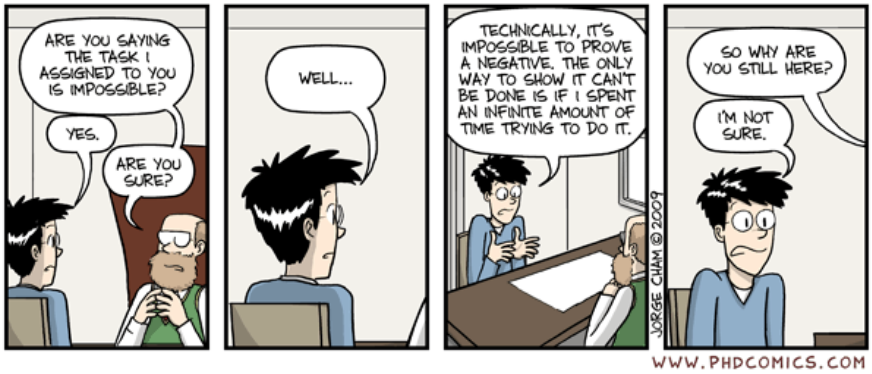

Acknowledgements

At this point I would like to mention several people and organizations who supported me and made the realization of this thesis possible (and also pleasurable).
Most of all I thank my supervisors Egbert Zojer and Oliver T. Hofmann for their guidance, support and patience.
Secondly, my thanks go to all the numerous members of the Advanced Materials Modeling Team who came and went during my time, for countless (not always quite) scientific discussions. Particular mention should be made of David A. Egger, who also supervised one of the projects included in this thesis, Thomas C. Taucher, for IT support, and Gernot J. Kraberger, who came by our office whenever a more theoretical viewpoint was needed (and also on other occasions).
Tomáš Bučko hosted me at Comenius University in Bratislava, which was a very informative and also pleasurable stay, in spite of the bad weather.
I also want to thank Daniel Lüftner for providing me with helpful computational methodology, and Christian Zwick, Frank Schreiber and Alexander Gerlach for experimental input along with scientific challenges and discussions.
For valuable reflection periods and humorous (and sometimes scientific) input, I am thankful to Jorge Cham, Zach Weinersmith, Randall Munroe, Johanna Hermann, Olivia Kettner and Elisabeth Verwüster.
Special thanks go to Elisabeth Stern, for her help, positivity and for always lifting the mood.
I gratefully acknowledge financial support by the Austrian Science Fund (FWF): P24666-N20, P28051-N36 and P27868-N36, and also want to thank the support team of the Vienna Scientific Cluster VSC3, where all the calculations presented in this work have been performed.
Finally, I want to thank my partner Michael, my parents, friends and legionnaire Fidibus, for moral support.

Abstract

The problem of understanding geometric structure and electronic properties of inorganic/organic interfaces can be approach from two different directions, namely by doing experiments, or by doing computer simulations. Among the computational approaches, density functional theory is by far the most popular one, which is owed to its versatility and the fact that it offers a reasonable compromise between computational effort and accuracy. While a huge number of different "flavors" of density functional theory exist, for most applications, some standard approaches have been established.

This thesis is concerned with the applicability, reliability and predictive power of density functional theory for the description of interfaces. Its centerpiece are simulations of several systems consisting of organic molecules adsorbed on metallic and semiconducting substrates, which are no longer trivial to simulate due to certain aggravating geometric or electronic properties. These examples are used as the foundation to discuss the methodological aspects of standard density functional theory, and to evaluate when the application of more advanced approaches is advisable.

First, the benefits and challenges of describing adsorption geometries with density functional theory are examined. This is done on the basis of several exemplary systems, where it is shown how crucially the knowledge coming from simulations can change the understanding of an interface. In addition, the enhancement of the geometry optimization tool *GADGET* for the simulation of molecular adsorption is discussed.

As soon as the geometry of a system is known, its electronic properties can be elucidated. In this work, the focus lies on charge transfer properties between solid substrates and organic adsorbates. It is shown that the choice of the ideal density functional theory methodology to describe such systems is far from straight-forward, as the obtained results strongly depend on the specific combination of physical properties of the interface and the applied density functional.

Another intriguing aspect of metal-adsorbed organic molecules is the occurrence of magnetic effects. Two exemplary systems, which exhibit contrasting behaviors, namely enhancement or quenching of their magnetic moment upon adsorption, are investigated here. The physical basics of this observation and its description within the applied simulation methodology is discussed.

In conclusion, this work demonstrates that the application of standard density functional theory methods to investigate inorganic/organic interfaces does not automatically lead to a correct prediction of geometric and electronic properties of the system. Rather, a comprehensive understanding of the methodological aspects is required to ideally choose the simulation approach and to be able to correctly interpret the obtained results. Under that condition, density functional theory is a valuable tool to analyze interfaces and is indispensable to reach a conclusive and also fully atomistic understanding of the investigated systems.

Kurzfassung

Anorganisch/organische Grenzflächen können einerseits experimentell, andererseits aber auch mithilfe von Computersimulationen untersucht werden. Den besten Kompromiss in Bezug auf Genauigkeit und Rechenaufwand bietet dabei die sogenannte Dichtefunktionaltheorie. Dieses Simulationsverfahren ist äußerst universell einsetzbar, vor allem da eine Vielzahl an verschiedenen Varianten verfügbar ist und die Methodik damit an die jeweilige Problemstellung angepasst werden kann.
Diese Dissertation beschäftigt sich mit der Frage, wie gut sich die etablierten Dichtefunktionaltheoriemethoden für die Beschreibung von Grenzflächen eignen. Insbesondere wird untersucht, inwieweit sie in der Lage sind, Vorhersagen zu treffen und welche Systeme beziehungsweise welche Observablen den Einsatz von anderen Methoden erfordern.
Als Basis für die Diskussion dieser methodischen Aspekte werden Systeme aus spezifisch ausgewählten organischen Molekülen auf metallischen und halbleitenden Oberflächen herangezogen, die aufgrund bestimmter erschwerender geometrischer oder elektronischer Eigenschaften nicht mehr trivial zu simulieren sind.
Ein wesentlicher Aspekt für die korrekte Beschreibung solcher Grenzflächen ist die Adsorptionsgeometrie. Die Anwendung der Dichtefunktionaltheorie für Geometrieoptimierungen wird anhand mehrerer Beispiele untersucht und es zeigt sich, wie grundlegend Simulationen das Verständnis eines Systems verändern und verbessern können. Des Weiteren wird das Geometrieoptimierungstool *GADGET* diskutiert, das im Rahmen dieser Dissertation für die Anwendung auf molekulare Adsorption verbessert wurde.
Sobald die Geometrie eines Systems bekannt ist, können seine elektronischen Eigenschaften untersucht werden. In dieser Arbeit werden in erster Linie Ladungstransfermechanismen zwischen adsorbierten Molekülen und Oberflächen untersucht. Dabei zeigt sich, dass die Wahl der besten Methodik in diesem Zusammenhang keineswegs trivial ist, da das Ergebnis stark vom Zusammenspiel der physikalischen Eigenschaften des Systems mit dem verwendeten Dichtefunktional abhängt.
Ein weiterer interessanter Aspekt metall-organischer Grenzflächen ist das Auftreten von magnetischen Effekten, die hier anhand der Adsorption zweier ähnlicher Moleküle auf (nichtmagnetischen) Metalloberflächen untersucht werden. In einem Fall wird das magnetische Moment des Moleküls durch die Adsorption verstärkt, während es im anderen Fall verschwindet. Die physikalischen Grundlagen dieser Effekte werden diskutiert, und die Beschreibung solcher Systeme mithilfe der angewendeten Simulationsmethoden wird erörtert.
Zusammenfassend zeigt die vorliegende Arbeit, dass die Anwendung der Dichtefunktionaltheorier auf Grenzflächen nicht notwendigerweise zu einer korrekten Beschreibung der geometrischen und elektronischen Eigenschaften des untersuchten Systems führt. Vielmehr ist ein umfassendes Verständnis der methodischen Aspekte notwendig, sowohl um den bestmöglichen Simulationsansatz zu wählen, als auch um die Ergebnisse richtig interpretieren zu können. Erst unter dieser Bedingung kann die Dichtefunktionaltheorie ihr volles Potential entfalten und wird zu einem unverzichtbaren Werkzeug

für die Untersuchung von Grenzflächen, ganz besonders wenn eine Beschreibung auf atomarer Ebene notwendig ist.

Preface: Structure of this Work

This work consists of six main parts: After the introduction (section 1), the theoretical background of the presented topics is discussed in section 2, including inorganic/organic interfaces (section 2.1), the basics of density functional theory (section 2.2), its challenges and how they are relevant for the description of interfaces (section 2.3), and the applied DFT methodology (section 2.4). The results of the projects pursued during this PhD thesis are subdivided into three chapters. Section 3 is concerned with the geometric properties of inorganic/organic interfaces and includes the discussion of the GADGET tool (section 3.1), the adsorption of the chlorogallium phthalocyanine (GaClPc) molecule on Cu(111) (section 3.2), the adsorption of the chlorinated tin phthalocyanine ($SnCl_2Pc$) molecule on Ag(111) (section 3.3) and the adsorption of the pentacenequinone (P2O) molecule on Ag(111) (section 3.4).
In section 4, charge transfer properties at inorganic/organic interfaces are considered by investigating the tetrafluoro-benzoquinone (TFBQ) molecule adsorbed on Cu and Cu_2O surfaces.
The magnetic properties at interfaces are discussed in section 5, which focuses on systems consisting of copper phthalocyanine (CuPc) and cobalt phthalocyanine (CoPc) adsorbed on Ag(111).
Section 6 summarizes all investigated topics.

This thesis is assembled in a partly cumulative manner and contains two peer-reviewed scientific articles:

- included in section 3.2:
  Adsorption Behavior of Nonplanar Phthalocyanines: Competition of Different Adsorption Conformations.
  Elisabeth Wruss, Oliver T. Hofmann, David A. Egger, Elisabeth Verwüster, Alexander Gerlach, Frank Schreiber, and Egbert Zojer.
  The Journal of Physical Chemistry C **2016** 120(12), 6869-6875

- included in section 4:
  Distinguishing between Charge Transfer Mechanisms at Organic/Inorganic Interfaces Employing Hybrid Functionals.
  Elisabeth Wruss, Egbert Zojer and Oliver T. Hofmann.
  The Journal of Physical Chemistry C **2018** 122(26), 14640-14653

These articles are included as I have extensively contributed to them in the course of my PhD studies. In the corresponding section, the introduction describes the context of the publication within my thesis and elucidates my contribution in detail.

Two further articles to which I have contributed during my PhD are not included here, as they were not the main focus of my studies.
The first one is concerned with structure formation processes in self-assembled monolayers:

- **Exploring the driving forces behind the structural assembly of biphenylthiolates on Au(111).**
  Elisabeth Verwüster, Elisabeth Wruss, Egbert Zojer, and Oliver T. Hofmann
  The Journal of Chemical Physics **2017** 147(2)

The second article discusses the numerical accuracy of different DFT codes and is currently in preparation:

- **Numerical Quality Control for DFT-based Materials Databases**
  Christian Carbogno, Kristian S. Thygesen, Björn Bieniek, Claudia Draxl, Luca Ghiringhelli, Andris Gulans, Oliver T. Hofmann, Karsten W. Jacobsen, Sven Lubeck, Jens J. Mortensen, Mikkel Strange, Elisabeth Wruss, and Matthias Scheffler

Contents

Acronyms

DFT	density functional theory
DOS	density of states
SCF	self-consistent field
SIE	self-interaction error
VCA	virtual crystal approximation
vdW	van der Waals
PES	photoelectron spectroscopy
STM	scanning tunneling microscopy
STS	scanning-tunneling spectroscopy
UPS	ultraviolet photoelectron spectroscopy
XMCD	x-ray magnetic circular dichroism
XSW	x-ray standing wave
GGA	generalized-gradient approximation
HSE	Heyd-Scuseria-Ernzerhof hybrid functional
LDA	local density approximation
PBE	Perdew-Burke-Enzerhof exchange-correlation functional
EA	electron affinity
FCT	fractional charge transfer
HOMO	highest occupied molecular orbital
ICT	integer charge transfer
IE	ionization energy
LUMO	lowest unoccupied molecular orbital
CoPc	cobalt phthalocyanine molecule
Cu_2O	copper-I-oxide
CuPc	copper phthalocyanine molecule
GaClPc	chlorogallium phthalocyanine molecule
P2O	pentacenequinone molecule
Pc	phthalocyanine molecule
$SnCl_2Pc$	doubly chlorinated tin phthalocyanine molecule
TCNE	tetracyanoethylene molecule
TFBQ	tetrafluoro-1,4-benzoquinone molecule
TMPc	transition metal phthalocyanine molecule

1 Introduction

This work is concerned with the description of inorganic/organic interfaces applying density functional theory (DFT). The investigated systems consist of organic molecules, which are adsorbed on metallic or semiconducting surfaces. The applied simulation method, DFT, is one of the most wide-spread methods for the quantum-mechanical description of materials. It is deployable to a huge field of applications, especially as the computational power available to scientific research has increased considerably in recent years. The popularity of computer simulations, and particularly DFT, for the description of interfaces is based on several aspects. First of all, it often allows to gain complementary results to experimental data, and, thereby offers an additional perspective on the investigated system. This is especially true when a full, quantum-mechanical understanding is required. In the case of inorganic/organic interfaces, the computational approach can provide a huge amount of additional insight which is experimentally inaccessible, as the sample often contains only little material or the area of interest is embedded deep within the specimen. In specific cases, computer simulations can even be applied as an alternative approach to experiment. This offers the possibility to test a huge amount of material combinations for their properties without the need to actually fabricate them.
A great benefit of DFT in particular is that it offers a good compromise between efficiency and accuracy.[1] Larger systems containing several hundred or even thousands of atoms can be considered, where the computational cost would become forbiddingly large using higher level simulation methods.
However, when applying DFT, one has to keep in mind that while the method is, in principle, exact, in practice the exchange-correlation functionals are approximations, as the exact functionals are not known. A large variety of different exchange-correlation functionals is available. In addition, DFT comes in different "flavors", e.g. plane wave or LCAO (linear combination of atomic orbitals) based approaches, pseudopotential or all-electron approaches, et cetera.[1] Depending on the investigated system and observables, different methods have proven to be most suitable. While some basic properties can be described properly within most of the available frameworks, like covalent bonds, others have to be surveyed with greater care and are described differently by different methods, e.g. charge transfer effects.[2, 3]
Doing dependable simulations becomes particularly demanding in the case of inorganic/organic interfaces, as two very different classes of materials are combined, where each of them could be described best within contrasting simulation methods.[2] It is, therefore, highly important to survey, for which studies DFT is applicable, to chose the applied methodology with caution, and to consider which simulation results are trustworthy. If the reliability of a method for a given system is not a priori clear from experience, it is desirable to compare some of the obtained results to either higher-level computational results or to experimental data. Ideally, one would want a situation, where some observables are obtained from both simulation and experiment and can be

checked for their consistency, while both methods provide additional, unique insights. In this work, different inorganic/organic interface were simulated and different observables were surveyed. Their description within DFT and the influence of the chosen methodology on the results was investigated. In several cases, the simulated data could be compared to available experimental data.
The application of DFT for interfaces allows the investigation of geometric as well as electronic properties.[2] Concerning geometric properties, the add-on geometry optimization tool GADGET [4] was modified to be more suitable to specifically describe interfaces. This was done in collaboration with the developer of the tool, Tomáš Bučko from Comenius University in Bratislava, Slovakia.
The investigation of the adsorption behavior of nonplanar chlorogallium phthalocyanine GaClPc on Cu(111) demonstrated the difficulties that might arise when trying to bring experimental and simulated data in line. The comparison between experimental and computational results on adsorption heights and work function modifications (caused by the molecular adsorption) was not at all straightforward. However, this example also demonstrates how experimental and simulations results can complement one another to finally reach a throughout understanding of the investigated system. Additionally, GaClPc on Cu(111) is exemplary for the importance of a suitable van der Waals (dispersion) correction method for DFT when simulating inorganic/organic interfaces.
The geometric properties of a similar system, namely the doubly chlorinated tin phthalocyanine Sn_2ClPc, were also simulated to achieve complementary insight to experimental results. The main questions here were, whether the molecule gets dechlorinated, whether the Ag substrate exhibits defect atoms due to molecular adsorption and how the adsorption configuration looks on an atomistic level.
The adsorption of pentacenequinone P2O on Ag(111) was studied to investigate different adsorption regimes, namely physisorption and chemisorption. This system is of special interest, as the experimental findings suggest physisorption of the molecule, while simulation results indicate chemisorption.
The knowledge of the geometry of a system is a necessary prerequisite to properly describe the electronic properties in DFT, as deviations in the geometry might falsify the electronic structure as well.[5, 6] For the investigation of electronic properties, not only semi-local but also hybrid DFT functionals were applied. These functionals have been shown to often improve the prediction of several electronic properties [7, 8, 9] and their use was of crucial importance for the investigations on charge transfer and magnetic properties.
To explore charge transfer at semiconducting/organic and metal/organic interfaces, the adsorption of tetrafluoro-1,4-benzoquinone TFBQ on Cu and Cu_2O was simulated using different DFT functionals. A crucial dependence of the computed charge transfer mechanism (namely fractional or integer charge transfer) on the applied functional could be shown. The methodological origin of this interplay was investigated in detail.
As an exciting example for the influence of the applied DFT methodology on the simulated magnetic properties of an adsorbed molecule, the adsorption of copper ph-

thalocyanine CuPc and cobalt phthalocyanine CoPc on Ag(111) was studied. The interesting aspect about these systems is that several different magnetic solutions can be obtained for every system, with the result depending on the DFT functional. The chosen systems were found to exhibit contrasting behavior, as the magnetic moment of the CuPc molecule could be enhanced upon surface adsorption, while for the CoPc molecule it was always decreased. Again, verification of the results via comparison to available experimental data could be done and methodological aspects of describing such systems with (different) DFT functionals were elucidated.

2 Fundamentals, Theoretical Background and Applied Methods

2.1 Inorganic/Organic Interfaces

The systems investigated in this thesis consist of different organic molecules adsorbed on metallic and semiconducting substrates. Upon molecular adsorption, both system parts can exhibit modifications of their geometric and electronic structures.[10, 11] In this section, some important physical aspects of such interfaces are briefly reviewed, and two concepts that are of central importance in this work, namely the adsorption modes physisorption and chemisorption, and different charge transfer mechanism, are discussed in more detail.

At inorganic/organic interfaces, the organic adsorbate molecules, which exhibit discrete energy levels, are brought into contact with a solid substrate material, which exhibits continuous energy bands. The characteristic energy level of the solid substrate is the Fermi level, with the work function Φ giving the difference between the Fermi level and the vacuum level.[10] The adsorbate molecules exhibit a band gap between the highest occupied HOMO level and the lowest unoccupied LUMO level, with the energy differences between these levels and the vacuum level denoted as ionization energy (IE) and electron affinity (EA), respectively.[10] The energy level alignment at the interface is a crucial aspect for its electronic structure. The adsorbate and substrate materials can interact, e.g., via chemical bonding, dipolar effects and charge transfer effects.[10] The adsorption of an organic layer on a substrate usually causes a work function modification ($\Delta\Phi$), which is an important observable used to characterize such interfaces.[10, 12, 13, 14, 15, 16, 17] Another important observable of the electronic structure is the density of states (DOS) of the interface. It gives insights into the energetic arrangement of molecular and substrate states and the hybridization between them. The DOS obtained from DFT can approximately be compared to experimental photoemission spectra.[10]

2.1.1 Physisorption and Chemisorption

Two main types of interaction between an adsorbate molecule and a surface can be distinguished. Weak interactions occurring only from physical effects such as van der Waals bonding are denoted as physisorption. Chemisorption, on the other hand, appears in case of chemical or ionic bonds being formed between adsorbate and substrate.[18] In case of physisorption, the absence of chemical bonding and charge transfer between the system parts typically leaves the electronic structure of the adsorbate largely unperturbed upon adsorption, and the molecular geometries are typically not strongly

distorted.[11, 18]
While in case of physisorption, the adsorbed molecules interact non-specifically with the whole substrate, the dominant bonding forces in chemisorbed systems usually act between specific atoms (or system parts) of the adsorbate and specific substrate atoms.[11, 18, 19, 20] In that case, also the electronic and the geometric structure of the adsorbate are modified, as new chemical bonds are formed, and charge transfer appears.[18, 19] A typical example are self-assembled monolayers of organic molecules on (metal) substrates, which form from molecules chemically bonding to the substrate, e.g. via thiol groups.[21]
In many cases it is not possible to strictly distinguish whether a system exhibits physisorption or chemisorption. This is particularly true for organic molecules adsorbed on metals, as discussed in this work. Even for strongly interacting chemisorbed molecules, the van der Waals interaction of the molecular parts not participating in the chemical bonding often cause a significant binding energy contribution.[22, 23] It is, therefore, problematic to denote physisorption as a "weak" interaction, as the van der Waals dispersion forces can add up significantly over shared areas of the interacting systems. For the inorganic/organic interfaces investigated in this work, this is particularly true for large molecules adsorbing in a flat-lying manner on the surface.[24, 25]

2.1.2 Charge Transfer Mechanisms

When two classes of materials are brought into contact at an inorganic/organic interface, charge transfer between the system parts might appear. Depending on the interaction strength, different charge transfer mechanism can be found.[11] In case of strong chemical bonding between adsorbate and substrate, hybrid states which are shared by all system parts (i.e. the substrate and all adsorbed molecules) are formed, and charge transfer can happen via these states. Due to their delocalized character, so-called fractional charge transfer FCT appears. This charge transfer mechanism is characterized by fractional charging of all molecules, which appears because the charged hybrid states can be assigned in part to the molecules, and in part to the substrate.[11, 20, 26, 27] In case of a well-ordered adsorbate layer, where the whole molecular layer shares the same delocalized state, all molecules on the surface are equivalent, and receive the same amount of charge.[11, 28]
When the interaction strength between the system parts gets weaker, no hybrid states can be formed, and the above discussed case of physisorption appears. Typically, in that case, no charge transfer appears.[11] However, an intermediate situation exists, where the hybridization is hindered, but electron transfer occurs (e.g. via tunneling) as the work function of the substrate is higher than the molecular ionization energies (or lower than their electron affinities).[11] This can, e.g., occur because of a passivating layer on top of the metal substrate, a semiconducting substrate,[28, 29, 30, 31, 32] or because of spacer groups on the molecules.[33] The resulting situation is denoted as integer charge transfer ICT, as charge is then only transferred in integer numbers.[11] The

transferred charge typically cannot be evenly distributed between all molecules, which leads to a coexistence of charged and uncharged molecules on the surface.[11, 28, 34] This means that FCT and ICT differ mainly by their charge localization. Which charge transfer mechanism appears is then mostly determined by the hybridization between the substrate and the adsorbate (and within the adsorbate layer).[11, 33, 34]
In the systems discussed in this work, mainly molecular adsorption on pristine metal surfaces is considered, which typically results in FCT. In the observables obtained from DFT, this can be easily identified. Due to the shared hybrid states, partly filled peaks appear in the DOS projected onto the molecular layer, which is schematically shown in Fig. 1. Therefore, the DOS is typically non-zero at the Fermi edge.
In case of ICT, no hybrid states appear. Rather, some molecular states become completely filled and are shifted below the Fermi level. When only one electron is transferred to a molecule, this results in a singly occupied molecular orbital SOMO,[28, 32] as shown in Fig. 1. This spin-splitting of the molecular states also becomes apparent in the molecular DOS.
A final distinguishing feature is the translational periodicity within the adsorbate layer, which can be broken in case of ICT. After one molecule in the adsorbate layer is charged, this causes a local change in the electrostatic potential surrounding the molecule. As a consequence, the LUMO of adjacent molecules can be lifted above the Fermi energy, thereby preventing their charging.[28]
A more detailed discussion on ICT and FCT in DFT and how the calculated charge transfer is influenced by the choice of the DFT functional is the main topic of section 4.

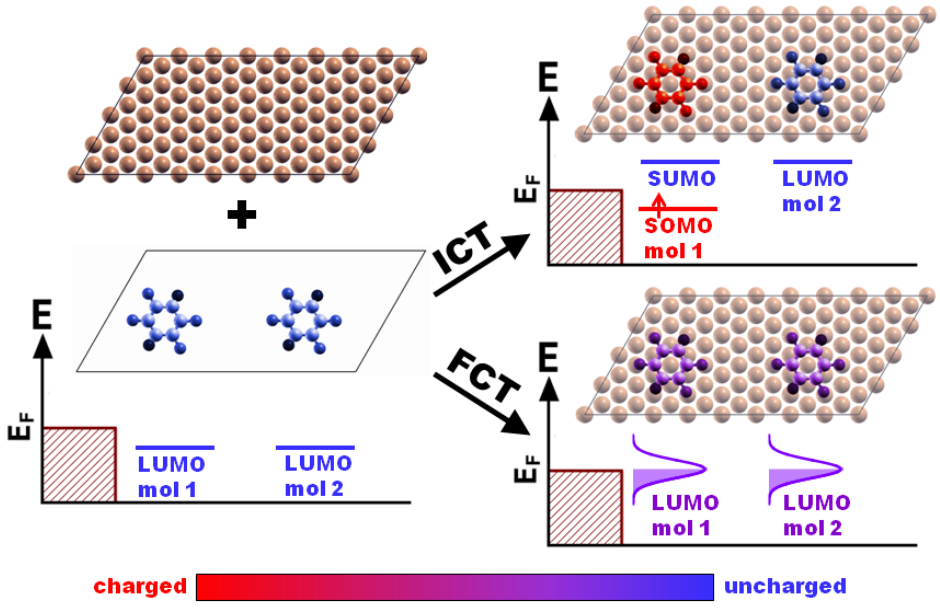

Figure 1: Schematic representation of the molecular levels relative to the substrate Fermi level for fractional and integer charge transfer, as shown in Ref. [6].

2.2 Density Functional Theory and its Application to Interfaces

Density Functional Theory is based on the postulate by Hohenberg and Kohn that the properties of a system of interacting particles can be described as functionals of the ground state density, which only depends on the tree spatial coordinates.[35, 36]
In their two basic theorems on a system of interacting particles in an external potential V_{ext}, Hohenberg and Kohn established that (i) $V_{ext}(\mathbf{r})$ is a unique functional of the ground state density $n_0(\mathbf{r})$, except for a constant shift of the energy and (ii) that a functional E[n] for the total energy exists, which is minimized (and, therefore, gives the ground state energy) by the ground state particle density $n_0(\mathbf{r})$.[35]
With this formulation, the complexity of the system description is significantly decreased compared to the use of wave functions, as the complexity of the latter grows exponentially with system size. However, its applicability is limited at this point, as the correct energy functional is unknown.[1, 36]
The approach that has made DFT applicable in practice was developed by Kohn and Sham, who proposed to replace the complicated interacting many-electron system by an auxiliary system of non-interacting particles. The auxiliary systems has the same ground state particle density as the original, interacting system.[37] This simplifies the problem, as the non-interacting system can be described applying independent-particle equations. The problematic part arising from the particle interactions, including exchange and correlation effects, is joined in the exchange-correlation functional E_{XC}.[36, 37] The ground state energy functional according to Kohn and Sham can then be expressed as follows:[36, 37]

$$E[n] = T_S[n] + \int d\mathbf{r}\, V_{ext}(\mathbf{r})\, n(\mathbf{r}) + E_{II} + J[n] + E_{XC}[n] \tag{1}$$

T_S denotes the kinetic energy of the non-interacting particles, V_{ext} denotes the external potential due to the nuclei, E_{II} denotes the the interaction of the atomic nuclei (which is usually considered a constant according to the Born-Oppenheimer approximation) and J denotes the classical Coulomb electron-electron repulsion (Hartree) energy.
To describe the exchange-correlation energy, approximations are needed, which are the reason for most shortcomings of DFT.[1, 7, 36]
The Kohn-Sham equations are the Schrödinger-like equations of the auxiliary non-interacting system, defining the movement of the non-interacting particles in the Kohn-Sham potential. In this context, it should also be noted that the Kohn-Sham eigenvalues derived in DFT are often used as approximations of orbital energies, although they are not the energies required to add or subtract electrons from/to the interacting system.[36] Therefore, strictly speaking, they do not have a physical meaning (expect for the highest eigenvalue, which corresponds to the negative ionization energy).[36, 38] This implies that for the description of semiconductors and insulators, even with the "exact" Kohn-Sham potential, the band gap should not be reproduced by the band structure derived from the Kohn-Sham equations.[36, 39]
To solve the Kohn-Sham equations, an iterative process is necessary, as several terms

depend on the electron density, which is also the desired solution. Therefore, simulations are started with an initial guess of the electron density, the Kohn-Sham equations are solved, and a new density is derived. This process is repeated until self-consistency is obtained.[36]

2.2.1 Exchange-Correlation Functionals in DFT

A widely used approach is to approximate E_{XC} as a local or semi-local functional of the density, which lowers the required computational effort significantly. This is a viable approach, as in the Kohn-Sham equations, the long-range Hartree terms and the kinetic energies of the independent particles are separated from the exchange-correlation part.[36] More advanced approximations are of non-local character, which can improve the prediction of many properties, but also significantly increases the computational effort.[36, 40]

Local Density Approximation LDA
In the local density approximation LDA, the exchange-correlation energy density is considered to be the same as in a homogeneous electron gas, and the electron density is considered to be a slowly varying function. The exchange-correlation energy solely depends on the value of electron density at the considered point in space. This approximation of the homogeneous electron gas often works well for solids with (almost) free electrons, which exhibit local exchange and correlation effects. For molecular systems, on the other hand, which exhibit inhomogeneous electron densities, it is not well suited and underestimates the exchange energy, while it overestimates electron correlation, leading to an overestimation of bond strengths.[1, 36]

Generalized Gradient Approximation GGA and Meta-GGA Functionals
In generalized gradient approximations, inhomogeneities in the electron density are more effectively considered by including also the gradient of the electron density into the derivation of the exchange-correlation energy. Rapid variations in the electron density can then be modeled more accurately, which improves the description of molecular systems and corrects the LDA over-binding.[1, 36]
In solid state physics, the GGA functional proposed by Perdew, Burke and Enzerhof (PBE),[41, 42] is most commonly used and was also applied in this work.
Meta-GGA methods are still of semi-local character, but the exchange-correlation functional additionally depends on higher-order derivatives of the electron density, or the kinetic energy density.[1]
An example is the TPSS functional (Tao-Perdew-Staroverov-Scuseria),[43] which is a meta-GGA improvement of the PBE functional.

Hybrid (or Hyper-GGA) Functionals
Hybrid functionals are a combination of classical (semi-)local approaches for exchange and correlation, e.g. GGA, with orbital-dependent Hartree-Fock exchange energies.
In this work, the PBEh [44] and the Heyd-Scuserica-Ernzerhof HSE [45] functionals were used, which both built on the PBE functional. In PBEh, the exchange-correlation energy is defined according to

$$E_{XC}^{PBEh} = \alpha E_X^{HF} + (1-\alpha)E_X^{PBE} + E_C^{PBE}, \tag{2}$$

with the Hartree-Fock exchange E_X^{HF}, the PBE exchange and correlation E_X^{PBE} and E_C^{PBE}, and the mixing parameter α, determining the relative portions of exchange from PBE and Hartree-Fock. The optimal portion of Hartee-Fock exchange depends strongly on the investigated system and properties,[1] which will be discussed in detail in section 4.
The HSE functional is a so-called range-separated hybrid functional, where different descriptions of exchange are applied in the short range and in the long range.[45] The ideal choice, again, depends strongly on the application.[36] HSE uses a certain portion of Hartree-Fock exchange in the short range, while in the long range GGA exchange is applied. This significantly reduces the computational effort. Alternatively, functionals exist which predominantly use Hartree-Fock exchange in the long range. The downside of this range separation is that another free parameter, which should also be chosen system-dependently, is added.[46] The system-dependent parameters present in hybrid functionals offer the possibility to specifically tune the functional to a given system, and a variety of approaches to (optimally) tune (range-separated) hybrid functionals has been presented.[47, 48, 49, 50, 51, 52, 53]
The improvement of hybrid functionals over standard (semi-)local functionals arises from the reduction of the notorious self-interaction error (see below), which is present in DFT, but not in Hartree-Fock theory. (Note that this applies only to the single-electron self-interaction error, as discussed below.[54]) While hybrid functionals do not necessarily improve the modeling of all properties for all possible systems (e.g. they often worsen the description of periodic systems like metals [55]), they usually significantly improve the prediction of the electronic structure of molecular systems.[9, 56]
For periodic systems, the problem arises that calculating the Hartree-Fock exchange can be up to two orders of magnitude more demanding than GGA exchange.[44]

2.2.2 Basis Sets

To represent the electronic wave functions in a DFT calculation, basis functions are required. The applied set of basis functions is denoted as the basis set. To achieve a perfectly accurate description of the given system, the basis set would need to be "complete" and to consist of an infinite number of basis functions. To minimize the errors arising from the approximation induced by a finite basis set, it should be chosen

suitably for a given system. Generally, a larger basis set allows a more accurate modeling of the system. In addition, the type of basis functions plays a role, as fewer basis functions are needed to reach the desired level of accuracy when the type of functions is well suited for the system at hand.[1]
The basis set typically applied in DFT are either linear combinations of atomic orbitals LCAO, or plane wave basis sets. LCAOs consist of local basis functions, mostly centered at the atomic nuclei, and are more frequently applied for molecular systems. Plane wave basis sets, on the other hand, are especially suitable to describe periodic crystal systems. These are mostly calculated applying periodic boundary conditions, which suggests the description with a function of infinite range. The size of a plane-wave basis set is usually defined by an energy cutoff.[1]
For the calculation of molecules, this plane-wave approach is disadvantageous, as the use of periodic boundary conditions demands the application large supercells to approximate the situation of isolated molecules.[1]
For plane wave basis sets, so-called pseudopotentials are frequently used, where only the valence electrons are considered explicitly, while inner electron shells are combined into an effective potential to reduce the computational effort.[36] A related, but more advanced approach, which is generally more accurate, is the projector augmented wave PAW formalism.[36, 57]
In this work, FHI-aims[58] and VASP[59] calculations were performed. FHI-aims applies atom-centered orbitals, including all electrons in the system. VASP applies plane wave basis sets and pseudopotentials or the above mentioned PAW method.[59, 60] Here, PAW potentials were used throughout.

2.3 Challenges of DFT

In the previous sections introducing the principles of DFT, several aspects have become apparent which limit the accuracy and applicability of DFT.
These limitations include both errors arising from approximations, but also inherent inabilities of DFT itself. An example of the latter is the above-mentioned band gap problem, as the quantity derived in the simulations - the Kohn-Sham band structure - does not (and should not) model the physical reality, i.e. the band gap of a material. Therefore, the (physical) band gap can not be read out directly from the Kohn-Sham eigenvalues.[7, 36, 39, 61]
The inaccuracies arising from the choice of basis sets can be minimized system-specifically by improving the basis until the desired accuracy is reached. This is usually done in preliminary convergence tests, which are discussed in section 2.4.1.
The most crucial approximations in DFT are usually introduced by the approximate exchange-correlation functionals, which lead to severe shortcomings of many DFT approaches.[7] These include the lack of the derivative discontinuity in the exchange-correlation potential,[62, 63] the missing long-range dispersion effects,[64] the errors arising from self-interaction, [65] and the static correlation error.[3, 7]

For inorganic/organic interfaces as investigated here, the accurate description within DFT is mainly complicated by the lack of long-range dispersion effects (which are particularly important for geometry optimizations) and the errors arising from self-interaction.[2, 66] Therefore, these aspects are discussed in more detail in the following.

2.3.1 Dispersion Correction Methods in DFT

Dispersion forces are a class of attractive van der Waals forces, which arise from long-range correlation effects of the charge density. Due to their non-local nature, they are not included in the mostly applied local and semi-local exchange-correlation functionals, which require on overlap of the electron densities to describe an interaction between two system parts.[64]
While dispersion forces are usually considered to be weak, they can become the dominant interaction for large systems (as they are additive) and determine the structure, e.g. for noble-gas crystals forming at low temperatures, the interaction of graphite sheets or, as discussed in this work, the physisorption of molecules at interfaces.[64]
For several metal/organic interfaces, it has been shown that standard semi-local GGA functionals are not able to model molecular adsorption properly, which makes geometry optimizations with such functionals impossible. [24, 67, 68]
Numerous dispersion (or van der Waals, vdW) correction methods have been developed to overcome this shortcoming of DFT.[64]
In the most basic approaches, the dispersion energy is included non-self consistently by adding a dispersion energy term to the system energy. The dispersion energy of two interacting systems is approximately proportional to the inverse sixth power of their distance R^{-6}. Therefore, dispersion corrections can be done by apply a pairwise additive approach which includes C_6/R^6 terms for every atomic pair in the system, with C_6 being an atom-dependent dispersion parameter.[1, 69] To avoid a divergence of the dispersion energy at small distances, a damping function is employed.[64]
The C_6 correction can be improved by making the C_6 coefficients environment-dependent, e.g. by correcting them according to the atomic "effective volume", with a lower effective volume corresponding to a lower polarizability of the atom.[69, 70, 71] Also higher-order terms (R^{-8}, R^{-10}) can be included to improve the model.
Methods using pairwise additive C_6 methods are computationally cheap, but require the input of C_6 (or other polarizability) parameters and account for pair interactions isolated from the rest of the system, which excludes collective and screening effects.[64]
To improve the description of dispersion effects, various approaches exist to go beyond these pairwise C_6 correction methods.[64] Examples are so-called non-local correlation functionals,[72] functionals building on three-body interactions,[73] many-body dispersion (MBD) interactions,[74, 75, 76] or methods based on the adiabatic connection fluctuation dissipation theorem (ACFDT)[77]. In certain DFT functionals that go beyond the semi-local approach, dispersion is included inherently due to their treatment of cor-

relation, as in functionals based on the random phase approximation.[78, 79, 80, 81, 82] As mentioned before, the use of an adequate dispersion correction method is crucial for DFT simulations of inorganic/organic interfaces. However, in the present case, the large system sizes are a limiting factor due to high computational effort. Therefore, the computationally inexpensive vdW^{surf} dispersion correction method has been applied here.[68] This method is based on the pairwise additive vdW-TS approach, which uses environment-dependent C_6 coefficients calculated from the electron density.[71] The vdW^{surf} method is a modification specifically designed to investigated adsorption at surfaces by including Coulomb screening by the bulk via the Lifshitz-Zaremba-Kohn theory.[68, 83, 84]. It is a computationally cheap energy correction method and has been applied very successfully to describe adsorption geometries of various inorganic/organic interfaces.[24, 25, 68, 85, 86]

2.3.2 Errors Arising from Electron Self-Interaction

In DFT, the self-interaction error (SIE) usually denotes the unphysical interaction of one electron with itself, which occurs in (most) exchange-correlation functionals.[65] Various approaches for self-interaction corrections exist, including hybrid functionals, which apply a specific portion of Hartree-Fock exchange. In the exact treatment of exchange done in Hartree-Fock, the exchange energy for a one-electron system cancels the Coulomb energy. Therefore, Hartree-Fock is free from the (single-electron) SIE, which can thus be mitigated by applying hybrid functionals.[1] However, for many-electron systems, the error arising from self-interaction goes beyond the above discussed effect of one electron interacting with itself.[7] This many-electron self-interaction error [54, 87, 88] is also frequently referred to as delocalization error [46, 89] or deviation-from-straight-line DSLE error [90] and is also present in Hartee-Fock.[54] It influences the energies of fractionally charged systems and leads to charge over-delocalization in semi-local functionals and charge over-localization in Hartree-Fock and hybrid functionals with high amounts of Hartree-Fock exchange.[53, 54, 87, 91, 92] The SIE can, therefore, still be mitigated by using hybrid functionals, but the chosen amount of Hartree-Fock exchange plays a crucial role.

Depending on the applied amount of Hartree-Fock exchange, the delocalization error can lead to unphysical charge distributions being predicted by DFT. For semi-local functionals, which strongly favor fractional charging (and over-delocalizes charge), it can lead to charge transfer between systems even at infinite distances.[87]

One of the main topics of this thesis was how the delocalization error influences charge transfer at inorganic/organic interfaces. Its impact on system and orbital energies, depending on the applied exchange-correlation functional, is discusses in detail in section 4.

An additional problem arising from self-interaction that is relevant for the simulation of inorganic/organic interfaces is the appearance of incorrect orbital ordering in molecules.[9, 25, 93]. Orbital energies are shifted due to self-interaction, with this effect

being more severe for strongly localized orbitals.[9]
In the copper and cobalt phthalocyanine molecules investigated here, this is particularly problematic, as they exhibit strongly localized metal-centered orbitals close in energy to delocalized π-orbitals of the molecular backbone.[9, 93, 94]
In this work, this problem is tackled by the use of hybrid functionals. Another, computationally less expensive approach to improve the descriptions of highly localized orbitals is the LDA+U method, where specific, highly localized orbitals are treated with an additional, orbital-dependent interaction similar to the U term in the Hubbard model.[95, 96] The localized orbitals are, thereby, shifted relative to other, less localized orbitals to correct errors of the exchange-correlation functional.[36]

2.4 Applied Methodology and DFT Settings

Due to the nature of the systems considered here, which combine a crystalline solid with adsorbed molecules, there is no obvious choice for either plane-wave or LCAO approaches. In this work, both were used. The Vienna ab initio simulation package VASP [97] in the version 5.4.1, with the included PAW potentials was applied to do plane-wave calculations. As an atomic-orbital code, FHI-aims [58] was used. The program version was regularly updated with the latest releases.
All interface simulations were performed with periodic boundary conditions in the repeated slab approach. The applied supercells contained a solid substrate of 3-6 layers, with organic molecules adsorbed on top, and a vacuum layer (of at least 20 Å) separating it from the periodic replica in z-direction. To decouple the layers in z-direction electrostatically, a dipole correction was applied.[98] The exchange-correlation functional suggested by Perdew, Burke and Enzerhof PBE [41, 42] was used for semi-local calculations. For hybrid calculations, either the range-separated hybrid HSE,[45, 99] or PBEh,[44] which are both based on PBE, were applied. The choice of functional for every specific system is discussed in the corresponding sections. To account for long-range dispersion forces, the vdW^{surf} [68] energy correction method was used.
For all investigated systems, geometry optimizations were performed. During these optimizations, the upper part of the slab as well as the molecular adsorbate were allowed to fully relax until a maximum remaining force below 0.01 eV/Å was reached. At least one substrate layer was always fixed in its bulk geometry.
The electronic states were occupied according to Methfessel-Paxton[100] (section 3.2) or Gaussian [101] (all other) broadening schemes, and the broadening width was optimized for each system, with a default value of 0.1 eV.
The k-point grids were also optimized for all systems, and set in a Monkhorst-Pack [102] (sections 3.2 and 3.3) or a Γ-centered (all others) mesh.
Every chapter in this work includes a methodology section, where the system-specific computational details and the used unit cells and geometries are explained. All settings that are not given explicitly in the corresponding sections were set as follows:

In VASP, standard PAW-potentials were applied to describe the electronic structure. The plane-wave cutoff was set to the highest value of *ENMAX* suggested in the PAW-potential *POTCAR* files and was checked in convergence tests (see below). For VASP geometry optimizations, the GADGET tool,[4] which is discussed in detail below (see section 3.1), was used.
In FHI-aims, predefined collections of settings for atomic species are given, which contain basis sets, integration grids, and the numerical accuracy of the Hartree potential.[58] For all systems, convergence tests to find the most suitable setting were performed.
All calculations presented in this work were performed at the Vienna Scientific Cluster VSC3.
The graphs presented here were produced using the programs XCrySDen [103] and QtiPlot v0.9.8.9.[104]

2.4.1 Convergence Tests

To choose computational settings suitably for a given system, it is necessary to perform convergence tests. The quantities optimized here were the basis sets (which corresponds to the plane-wave cutoff for VASP, and is included in the atomic settings for FHI-aims), the density of the k-point grid, the number of substrate layers, and numerical accuracy settings to reduce the computational effort. These convergence tests were performed for all applied functionals and for all investigated systems.
The basis sets were converged applying bulk unit cells of the substrate materials, looking at their total energies. Depending on the investigated systems, they were converged to 0.001 or to 0.005 eV per atom.
The k-point grids were converged using surface unit cells, which were fractions of the finally applied unit cells. By doing so, the k-point grids could be scaled according to the unit cell size without changing the k-point sampling itself. As an observable for k-point convergence, the substrate work function was used for metal substrates, and the size of the gap in the DOS for semiconductors, and it was converged to 0.05 - 0.10 eV, depending on the application.
The modification of the work function was used as a convergence parameter for the number of substrate layers, which was increased until the work function was converged to 0.05 eV.
In FHI-aims also several numerical accuracy settings (e.g. *periodic_hf coulomb_threshold*, controlling the threshold of the Coulomb matrix elements) were converged to enhance the calculation speed, especially for hybrid calculations. For the convergence tests, the total system energies of surface unit cells were monitored and a threshold of 0.001 eV for the total energy change was used.
In addition to these convergence tests, geometric properties that were not optimized during the simulations needed to be determined. This included unit cell heights, which need to be sufficiently large to properly decouple periodic replicas in z-direction, and the substrate lattice constants.

To converge the unit cell heights, the electronic potential was written out and it was checked whether it changes by less than 1 meV per Å in the vacuum region.
The lattice constants of all substrate materials were converged by calculating several primitive bulk unit cells of the corresponding materials in a region of usually about $\pm$ 0.2 Å around the experimental lattice parameter in steps of 0.005 Å. The lattice constant was then calculated by performing a Birch- Murnaghan fit.[105, 106] The applied dispersion correction method, vdW^{surf}, was switched off between the substrate atoms in all simulations, as it is not designed to describe dispersion effects in crystalline solids.[68] Therefore, it was also not applied during the lattice constant optimizations. The lattice constants were optimized with all functionals used for the systems in question. For the investigates metals (Cu, Ag), it turned out that the difference in the lattice constants between semi-local PBE and the applied hybrid functionals was below 0.2%. Therefore, the PBE lattice constants were used for all calculations. For the case of Cu_2O, the choice of the lattice constant is discussed in detail in the supporting information of Ref. [6], which is included in section 4.

3 Geometric Properties at Interfaces

An accurate description of the geometric properties of a system is an inevitable prerequisite to receive meaningful results for the electronic properties in DFT simulations. To perform successful geometry optimizations in DFT, several methodological aspects need to be considered. First of all, the applied methodology must be suitable to describe the situation at hand. An example is the simulation of van der Waals bonded systems (e.g. molecules physisorbed on surfaces or the interlayer interaction of graphite sheets). If a semi-local functional without van der Waals correction is applied, the geometry optimization will fail completely and predict no bonding between the individual parts of the system.[64] Secondly, the applied geometry optimization algorithm must be able to predict the minimum structure of the investigated system. This can e.g. be important to properly describe the tilt angles of upright standing molecules, where the degree of freedom describing the tilting is not so easily captured in the geometry optimization.[107]
Another important aspect is that several local minima in the geometry might exist, especially for complex systems like the interfaces discussed here. Depending on the potential energy surface (of the system geometry) and the applied optimization algorithm, it might be necessary to compare different local minima as obtained by different geometry initializations.[107] Otherwise, the global minimum can easily be missed.
The following section analyzes different challenges arising for geometry optimizations in DFT. First of all, the enhancement of the DFT geometry optimization tool GADGET for the application on metal/organic interfaces is presented. Subsequently, three specific systems are discussed, where the geometry optimizations were not straightforward to perform. For these examples it is reviewed in detail how the system geometries could be obtained.

3.1 Enhancement of the GADGET Tool to Optimize Interfaces

GADGET is a geometry optimization tool developed by Tomáš Bučko (Comenius University, Bratislava, Slovakia) and programmed by himself, Jürgen Hafner and János G. Ángyán. GADGET works in conjunction with VASP (or other band-structure codes), which execute the electronic SCF optimizations, while GADGET performs the geometry steps.
The input geometry and output forces of a VASP single-point calculation are used to produce a new geometry. The new geometry is used as input for a subsequent VASP single-point calculation. This procedure is iterated until convergence of the forces (and the energy) is reached.
The main benefits of the GADGET geometry optimization compared to the optimization algorithms implemented in VASP are (i) the use of internal instead of cartesian coordinates and (ii) several possibilities for a more sophisticated initialization of the

Hessian matrix. The use of internal coordinates additionally allows more sophisticated constraining of degrees of freedom in the system during optimizations.
GADGET is especially well suited for complicated geometry optimizations, which go beyond flat-lying molecules on a surface, where mainly the distance needs to be optimized. In contrast to the standard geometry optimization implemented in VASP, GADGET can accurately model the lateral movement of such molecules on the surface, as well as tilting behavior of upright standing molecules and the adsorption of other non-flat molecular structures. Applying both VASP and GADGET for the optimization of various inorganic/organic interfaces, it was shown that GADGET is both faster and also more flexible in the description of such systems than VASP alone.[25, 107, 108, 109, 110, 111, 112]
In the course of my thesis, together with Tomáš Bučko, some additional functionalities to GADGET were implemented. The goal was to further improve its ability to simulate interface adsorption geometries. Additionally, some functionalities were implemented to allow the user a better manual control, e.g. on the definition on the coordinates used by GADGET.
In the following, the relevant functionalities of GADGET are discussed. Then, the implementations conducted in the course of my PhD thesis are presented. These include the option to explicitly define coordinates, an improvement for the description of straight bonds in a system and an improved initial guess for the long range coordinates in the Hessian matrix. Subsequently, some model systems are presented, which were used to test the new implementations.

3.1.1 Geometry Optimizations and GADGET Functionality

In the following, some basic principles of geometry optimizations in DFT and mainly their implementations in GADGET are reviewed, based on Refs. [4] and [113].

Initialization of the Hessian Matrix
The Hessian matrix, or matrix of the force constants, arises from the second derivative of the energy of a system with respect to its geometrical parameters and is used to construct a local quadratic approximation to the potential energy surface of a geometry optimization problem.
Several geometry optimizations methods, such as quasi-Newton methods, require an initial guess of the Hessian matrix. The quality of this initial guess can hugely influence the course of the geometry optimization, potentially leading to significantly faster convergence, but also to divergence in case of a bad guess. The simplest guess that is often applied (e.g. in VASP) is a scaled identity matrix, which assumes all coordinates to be independent of each other. This is, in most cases, a very bad starting guess for the optimization. A good initial guess of the Hessian matrix should already contain information about the chemical structure and connections within the optimized system.

GADGET can apply several different initialization schemes based on the coordinates of the systems, including a simple diagonal matrix or also initialization based on Lindhs model [114], or Fischers model [115], which hugely improve the speed of geometry optimizations in most cases.

Cartesian and Internal Coordinates

The most general and most widely used system to describe atomic positions are cartesian coordinates. However, they do not reflect the chemical structure of the investigated system at all, which makes them not very suitable for geometry optimizations of molecular systems. Additionally, the coordinates are strongly coupled to each other, as the movement of a group of atoms requires corresponding, coupled coordinate changes in all associated atoms. Therefore, a more suitable choice for the geometry optimizations of chemically bonded systems are internal coordinates, which apply bond lengths and valence angles and depict the chemical structure.

For the description of curvilinear motions, like, e.g., the tilt of an upright standing molecule on a surface (as schematically shown in Fig. 2), the choice of coordinates is particularly crucial. Using cartesian coordinates, the tilting requires a coupled change of all molecular coordinates, in accordance with the varying position changes that are induced by the tilting. Obviously, such a simultaneous change of all coordinates is not easily achieved. In fact, it has been seen in cartesian optimizations done with VASP that the geometry optimizations of SAMs always resulted in the same tilt angle that the system was started with, and no further tilting of the molecules could be achieved. In contrast to that, the tilting of the whole molecule can be controlled by angular coordinates directly describing the tilt angle when internal coordinates are applied. This allows a much better description of this degree of freedom.

Internal coordinates also make a good initial guess of the Hessian matrix much easier, due to their chemical nature, which (mostly) connects bonded atoms, while by using cartesian coordinates, relations of atoms are not a priori clear. The coupling of different coordinates is reduced for the initial guess of the Hessian matrix for internal coordinates and also constraints are simpler to handle.

The situation is different for tightly packed crystalline systems like metals. There, internal coordinates are very ambiguous to define, as too many bonds exist. In such systems, the coupling of cartesian coordinates, which is unwelcome for molecular structures, more accurately depicts the nature of the system.

Therefore, the ideal coordinate choice for a given system depends on the nature of this system.

Coordinates in GADGET

GADGET performs optimizations in internal coordinates consisting of bond lengths, bond angles and torsions.

These internal coordinates are detected automatically for a given geometry, connecting every two atoms that are closer than their covalent radii times a bond scaling parameter

called *ASCALE*, and are denoted as short range bonds. For all sets of three connected atoms, a bond angle is created, and for all sets of four atoms, a torsion angle is created. To avoid huge over-definition and a too large number of coordinates, for atoms that have more than a certain number of neighbors (which can be defined explicitly in the input file), e.g. metal atoms in a crystal, the creation of angular coordinates is omitted. When this coordinate creation routine is finished, it is checked whether all atoms in the given system are interconnected. If this is not the case, the existence of several fragments is assumed, as it would, e.g., be the case for a molecule physisorbed on a surface. The large distance between molecule and substrate does not allow interconnecting them by a direct bond, unless *ASCALE* is set to an unrealistically large value. The fragments are connected by so-called long range bonds, which come without associated angles or torsions. These long range bonds are created by looking for atoms that are closer than their covalent radii times *ASCALE* times the long-range scaling parameter *BSCALE*.
The long range bonds can be treated in different ways within the optimization, either simply as bonding distances r, similar to short bonds, but also as inverse coordinates 1/r or inverse-power distance coordinates $1/r^N$.[4] Depending on the system, different methods are more or less beneficial an a good choice of the treatment of long range coordinates can hugely reduce the simulation effort.
This coordinate detection routine works very solid for most systems, but of course it depends on the choice of the parameters *ASCALE* and *BSCALE*. Therefore, it is necessary to check the obtained coordinates, e.g. by checking the number of degrees of freedom that are found for the systems. If this number is too small, it means that the coordinates do not fully represent all degrees of freedom present in the system. As a consequence, the optimization algorithm can not consider all possible translations, which falsifies the optimization.

Substrate Detection
The substrate detection is a feature implemented by Tomáš Bučko specifically to enhance the description of systems of molecules which are (chemically) bonded to a substrate, particularly upright standing molecules as SAMs.
As mentioned previously, the optimization of upright standing molecules is particularly problematic, as the use of cartesian coordinates is unsuitable to describe the tilting of the molecules. Even with more advanced geometry optimization methods, like GADGET, geometry optimizations of SAMs are notoriously difficult.[107, 111, 112] This is caused by the nature of such systems. In principle, an upright standing, chemically bonded molecule on a substrate should ideally be treated as two fragments in the geometry optimization, with the relative positions of substrate and molecule being controlled by several long range coordinates. However, due to the strong bonding between substrate and molecule, the bonding distances between substrate and molecule are small and both parts are interconnected by internal, short range bonds during the coordinate detection. In that case, the whole system is considered as one fragment.

Then, the connection between the two systems consists of one bond (e.g. between S and Au, as depicted in black in Fig. 2) with one corresponding bond angle and torsion. This choice of coordinates does not depict the physical reality of this system very well, as the chemical bonds within the molecule (and within the substrate) are very stiff, while the bond between molecule and substrate is comparably flexible, allowing for different tilt angles.
This can causes problems in the geometry optimization for the following reason: A small change in just one angular coordinate describing the metal-molecule connection causes huge changes in the configuration of the whole system, and, therefore, also can hugely change the energy and forces of the system. This effect becomes even more pronounced in case of large molecules. Looking at the Hessian matrix, this means than one degree of freedom is very flexible, while others, within the molecule, are comparably stiff. The Hessian matrix is then ill-conditioned, with very small as well as very large eigenvalues. The result is a problematic optimization where convergence is hard to achieve.
To solve this problem, it would be beneficial to interconnect molecule and substrate not only by one, but by several bonds. This would usually happen if the molecule and substrate were detected as different fragments, which are then interconnected by a set of long range bonds.
The substrate detection is a tool to force a division of such systems into two fragments, which then triggers the creation of several long range bonds and eases convergence of the geometry optimization. This is shown schematically on the right hand side in Fig. 2, with the additional long range bonds indicated in red.
The division of the systems is done using a parameter called *SUBST*, which gives a minimum number of neighbors that an atom must have to be considered as a substrate atom. All atoms that are thereafter considered to be in the substrate are defined as an independent fragment. In that way, substrate and adsorbed molecule are separated into two different fragments, and are additionally connected via long-range bonds. This allows for a more efficient geometry optimization.
Of course the subdivision into fragments needs to accurately depict the actual system, and an incorrect substrate detection will hinder geometry convergence and can completely falsify the obtained results. However, when used adequately, the substrate detection hugely improves the reliability and speed of geometry optimizations.

3.1.2 Definition of Coordinates in a Given System

In the following, the new implementations for GADGET to improve its applicability for metal/organic interfaces are presented.
These improvements included several add-ons for the coordinate choice. The main goal here was to make the coordinate choice, which is normally done by GADGET automatically, better accessible to the user. This can, e.g. be very relevant for interface systems where the substrate contains adatoms. In such a situation, the substrate detection can

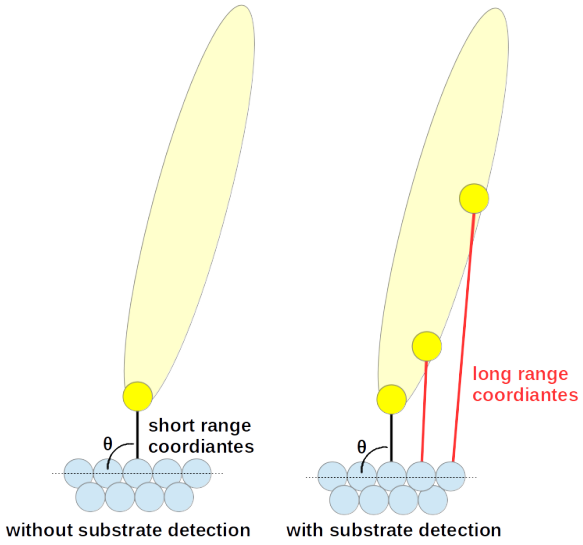

Figure 2: Schematic representation of upright standing molecules on a surface (such as in SAMs) and the influence of the substrate detection method on the coordinate choice.

easily fail, as adatoms have a lower number of neighbors than bulk and surface atoms. This might lead to them being treated as a part of the adsorbed molecule. This obviously results in a coordinate choice which is not ideal to describe the system at hand and will hinder geometry convergence.

Manual Definition of Fragments and Substrate

In some complicated systems, it was found that the automatic substrate and fragment detection does not work properly. To overcome this problem, a manual substrate and fragment specification routine was implemented.

This can be done in a file called *FRAGMENTS*, which lists groups of atoms that are then treated as one fragment in the calculation. Additionally, one of them can be defined as the substrate, which influences how coordinates between it and the other fragments are found, as described above.

This feature is especially beneficial in cases where several similar systems have to be calculated with different starting geometries, e.g. as performed by Elisabeth Verwüster et al.,[112] who investigated different adsorption motifs of one SAM. To ease the comparability of different geometry optimizations of a chemically identical system, the coordinate choice should be consistent. If the starting configurations are very different, this is hard to achieve with the automatic detection scheme, and a manual definition of the system parts is very helpful.

Also in the above mentioned case of systems with adatoms, they can be manually defined to be part of the substrate.

Computationally, this is realized by a two-step procedure. First of all, the parameters *ASCALE* and *BSCALE* are increased until all atoms in the system are interconnected. Then, all short range bonds between atoms defined to be in different fragments are exchanged for long range bonds, and the corresponding bond angels and torsions are removed.

Forcing the System to Consist of a Single Fragment

For consistency reasons, it can sometimes be necessary to have only one fragment in the system, e.g. if the automatic substrate detection should be used. If more than one fragment is found, this routine cannot be applied. Instead of manually increasing the scaling parameters *ASCALE* and *BSCALE*, the tag *IFCON* can be used, which forces the system into detecting only one fragment.

Two different routines exist to achieve this. While *IFCON=1* gradually increases *ASCALE* (in steps of 5%) until only one fragment remains in the system, *IFCON=2* adds all long range bonds to the short range bonds (and, consecutively, also creates bond angles and torsions for them) and checks whether all system atoms are connected. If this is not the case, *BSCALE* is increases and the procedure is repeated until full connectivity is reached.

Due to how these procedures work, the found coordinates are not necessarily ideal to describe the system. Therefore, this method should only be used if the application of the automatic substrate detection is really necessary, as the use of *IFCON* might slow down the geometry optimization.

Tests on various systems have shown that while the first implementation *IFCON=1* performs very well, *IFCON=2* often leads to a divergence of the geometry. This is, most likely, due to an unfortunate choice of coordinates.

Applying Cartesian Coordinates for the Substrate

While the use of internal coordinates is mostly beneficial for the description of molecular systems, for the metal substrates, cartesian coordinates can be a better choice. The reason for that is the crystalline nature of the metal, where all atoms are interconnected by a large number of bonds and the definition of internal coordinates becomes very ambiguous.

Therefore, a method was implemented into GADGET which allows the use of cartesian coordinates for the substrate, while all other bonds are still described in internal coordinates. Ideally, this method should allow a faster optimization of systems with large metallic substrates that do not deform strongly upon molecular adsorption.

The coordinate definition for this method is done by first creating all internal bonds in the standard GADGET routine. Subsequently, all bonds, bond angles and torsions between all groups of atoms where only substrate atoms are included are removed. Finally, cartesian coordinates are added for all substrate atoms.

3.1.3 Improved Internal Coordinate Detection: Straight Bonds

In optimizations applying internal coordinates, a problem can arise from straight bonds between atoms which exhibit bond angles θ of (or close to) 180°.
This situation occurs for systems, which exhibit system parts when three or more atoms lie on one line, as depicted in Fig. 3. In that case, the unambiguous definition of the angular coordinates, relative to the rest of the system, is impossible. Correspondingly, in the definition of the internal coordinates, when $\sin(\theta)$ of the bond angle becomes zero, a singularity arises. Note that this problem only appears when the angles of the considered molecular chain (A, B and C in Fig. 3) have to be defined relative to the rest of a larger system (D and D in Fig. 3).
To avoid this problem, GADGET previously just removed all angles too close to 180°. However, for systems such as straight molecular chains, where atoms are only bonded to their direct neighbors, this often led to situations where the systems are not properly interconnected any more after this coordinate removal. In that case, the simulation considers too few degrees of freedom and the optimization is distorted.
The easiest solution to avoid this problem is to increase $ASCALE$ for the whole system, as this forces more short range bonds, as depicted in red in Fig. 3. However, the large value of $ASCALE$ is then applied to the whole system. A too large value of $ASCALE$ causes an over-definition where too many bonds in the system are considered, which slows down the simulation.
Therefore, a more elegant solution to avoid problems due to straight bonds was implemented.
In a situation as depicted in Fig. 3, with three atoms A, B, C directly in line, the angle θ between them has to be removed. In the new implementation, an alternative bond is searched to replace this problematic straight bond. This is done by checking all neighbors of the outermost atoms B and C, starting with the closest ones. In a situation like in Fig. 3, the bonds between A and D and A and E will be included, despite being further apart than r_c*$ASCALE$. This allows the definitions of bond angles different from 180°, and avoids situations where too few coordinates are defined.

3.1.4 Improved Initial Guess for Long Range Coordinates in the Hessian Matrix

The initial Hessian matrix is constructed from the coordinates of the investigated systems. While good models (like Lindh and Fischer, see above) exist to initialize the matrix elements corresponding to short range bonds, the initialization of elements corresponding to long range bonds is more difficult. In GADGET, the initialization of the Hessian matrix for long range bonds is done using a force constant parameter, with the Hessian matrix element corresponding to the long range bond being set to the inverse of this parameter. A good choice of this parameter can significantly speed up

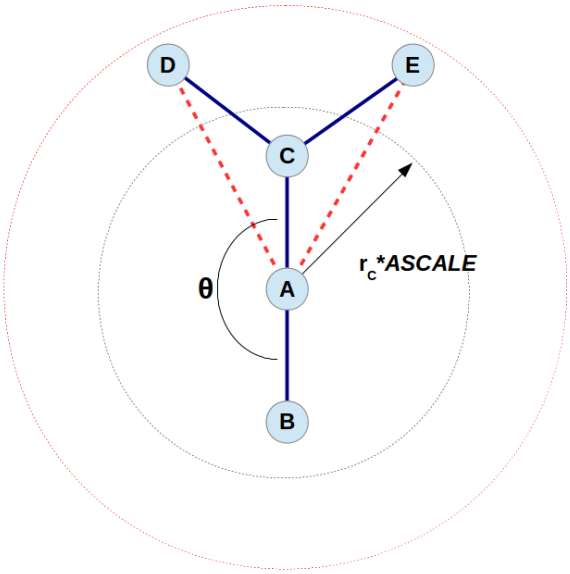

Figure 3: Schematic representation of a system where straight bonds between atoms causes problems in the definition of internal coordinates.

the simulation by providing a better initialization of the Hessian. However, the ideal choice of force constant parameter is strongly system-dependent. In addition, the use of the same force constant parameter for all long range bonds in a system is mostly not ideal.
The better initialization of the Hessian matrix can be done by approximating the forces between the atoms that are connected via these long range bonds. This can be done by applying a van der Waals energy evaluation calculated from C_6 coefficients, as for large distances, the vdW energy is supposedly the largest contribution to the interaction between atoms.
In the newly implemented method called *LRVDW*, the approximate vdW force between two far apart atoms is calculated. This is done by taking the second derivative of the vdW energy term, which contains the C_6 coefficients for the corresponding atomic species and the distance of the atoms. This approach gives a reasonable approximation for the force between two atoms, which is then used to initialize the Hessian matrix, and does not require any tuning.

3.1.5 Performed Tests

To test the performance of the newly implemented functionalities, four small model systems were chosen and are presented in the following sections. They cover several typical scenarios (SAMs as well as chemisorption and physisorption of small organic

molecules) of metal/organic interfaces. The molecules in their gas phase configurations were positioned in a seemingly reasonable position above the substrates and full geometry relaxations were performed. For all compared optimizations it was ensured that they had converged to the same minimum structure.
The optimization were performed with different sets of parameters, including the most relevant tuning parameters *FRAGCOORD*, which defines the treatment of long range coordinates in the geometry optimization, and *POTIM*, which defines the force constants for the Hessian initialization of long range coordinates, as discussed above.
In the following, the test systems are presented and the influence of the newly implemented methods is shortly reviewed. The performance of different settings is compared by comparing the number of geometry steps which were required for full convergence. The latter was defined to be reached as soon as the maximum remaining force was lower than 0.01 eV/Å. Similar settings for the electronic-structure DFT evaluations were applied for all compared calculations.

4-Methylthiolphenol on Au(111)

The 4-Methylthiolpheno molecule (C_7H_7S) adsorbs upright standing on Au, as depicted in Fig. 4. This system served as an example for the calculation of SAMs, as it chemically bonds to the Au surface with its thiol group and forms densely packed monolayers.

In the geometry optimizations, it took between 36 and 60 geometry steps to converge. As the automatic substrate detection caused problems for the tightly packed system, it was used to test manual fragment definition. The automatic coordinate detection scheme finds only one fragment due to the strong bond between the thiol and the Au substrate and the tight packing. Enforcing two different fragments significantly increased the simulation speed by up to 12 steps. The definition of a substrate, both automatically and manually, led to a small increase in the required number of steps and is not necessary for this system, which is most likely due to the small length of the molecular chain and the tight packing, which does no allow for large changes in the tilt angle.

The use of cartesian coordinates for the substrate led to a loss of optimization speed. This is, most likely due to the strong deformation of the topmost Au layer upon molecule adsorption.

The use of the vdW guess of the Hessian matrix did not yield a clear outcome. Depending on the settings of the parameters *POTIM* and *FRAGCOORD*, it resulted either in slower or in faster convergence than the standard procedure.

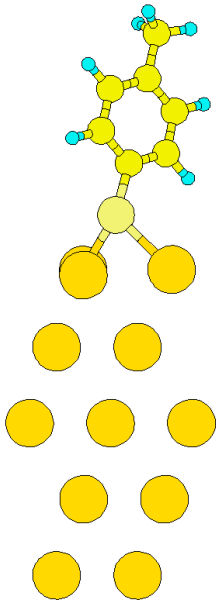

Figure 4: 4-Methylthiolphenol adsorbed on Au(111) in an upright standing configuration. C atoms are depicted in yellow, H atoms in blue and the S atom in light yellow. The Au substrate is depicted in orange.

Tetracyanoethylene TCNE on Cu(111), lying

TCNE (C_6N_4) was adsorbed in a lying geometry on the Cu(111) surface, with all four N atoms bonding to Cu atoms. This system served as an example for flat-lying, strongly bonded interface systems. The geometry is shown in Fig. 5.

The optimization converged in 40 to 65 geometry steps. The definition of fragments and substrate did not cause any relevant changes in the required number of steps. This is not surprising for a flat-lying system, where the main degree of freedom is the adsorption height of the molecule. The definition of different fragments would become relevant here for strong lateral movements of the molecule on the surface, which are better described when no short range bonds between molecule and substrate exist.

The simulation speed for this system seemed to depend mainly on the choice of the long range coordinates made with the parameter *FRAGCOORD*. Also the use of the vdW guess for the Hessian matrix did not yield any improvement. What did cause a significant speedup was the use of cartesian coordinates for the substrate, which is reasonable for this system, where the substrate does not deform strongly upon adsorption of the molecule. This is in contrast to the previous system, where the chemical bonding of the thiol group caused strong deformations of the Au substrate upon adsorption.

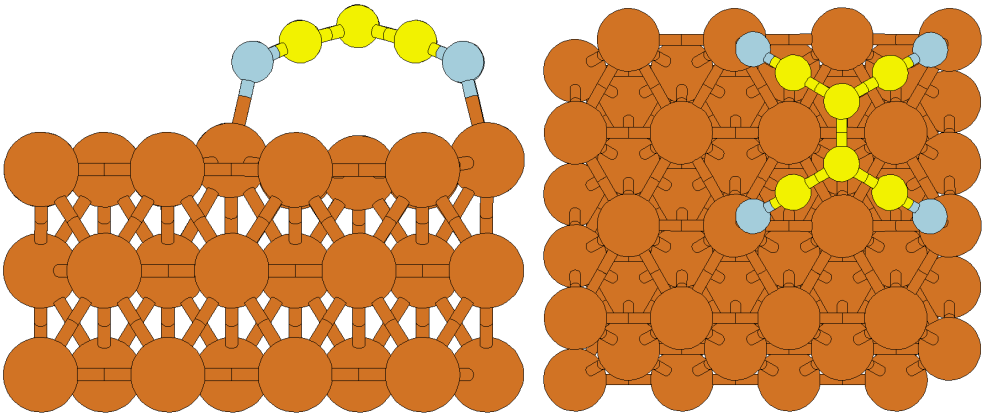

Figure 5: Tetracyanoethylene TCNE on adsorbed on Cu(111) in a lying configuration. C atoms are depicted in yellow, N atoms in grey and the Cu substrate is depicted in brown.

Tetracyanoethylene TCNE on Cu(111), standing

TCNE was also adsorbed in an upright standing geometry on the Cu(111) surface, with two of the four N atoms bonding to Cu atoms. In that case, the molecule-substrate interaction happens via chemisorption, but the bonding is not as strong as for the thiol-bonded SAM. The geometry is shown in Fig. 6.

The optimization took between 31 and 91 geometry steps, and, in some cases where the choice of *POTIM* and *FRAGCOORD* were very unfavorable, did not converge at all.

Manually subdividing the system into two fragments and defining one of them as the substrate led to a massive speedup, decreasing the required number of steps from 91 to 36 steps. In case of Cu substrates, the automatic substrate detection has been shown to be problematic and require an optimized choice of the parameter *ASCALE* to find all substrate atoms correctly. Therefore, for such systems the manual fragment and substrate detection is of great benefit.
Also the use of cartesian coordinates for the substrate increased the calculation speed by up to 16 steps, as the Cu substrate is, again, not strongly modified upon TCNE adsorption.
The use of the vdW guess of the Hessian matrix again performed ambiguously, causing slower or faster convergence depending on the choice of *POTIM* and *FRAGCOORD*.
Additionally, the routine compensating too straight bonds in a system was tested here. When the parameter *ASCALE* was chosen small (e.g. below 1.2), the automatic coordinate detection did not find sufficient degrees of freedom when applying a GADGET version without the above described modification. This indicates that relevant coordinates were discarded due to too straight bonds in the molecular chains. In the new GADGET implementation, however, also at such low values of *ASCALE*, all degrees of freedom were found, which shows that the applied coordinates describe the system accurately.

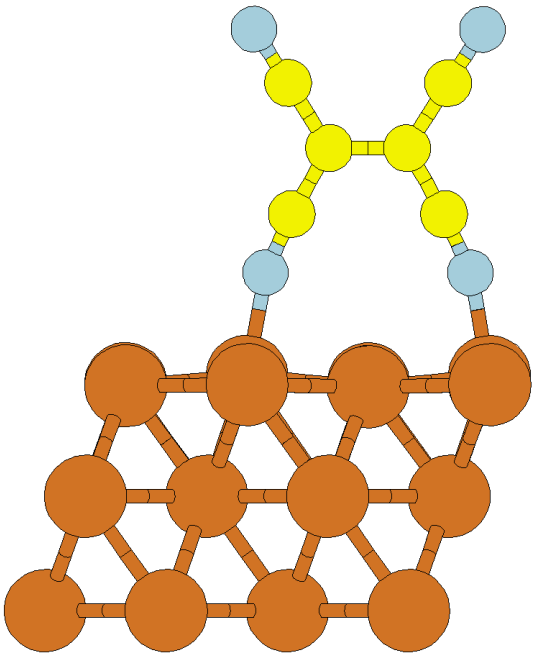

Figure 6: Tetracyanoethylene TCNE on adsorbed on Cu(111) in an upright standing configuration. C atoms are depicted in yellow, N atoms in grey and the Cu substrate is depicted in brown.

Benzene on Ag(111), lying

A benzene molecule was adsorbed on the Ag(111) surface in a lying geometry, where the interaction between molecule and substrate mainly arises from vdW interactions, which is a prototypical physisorption scenario. The geometry is shown in Fig. 7.
The optimization converged after 10 to 51 geometry steps, where the large speed difference arose from the substrate detection. When the system was subdivided into two fragments and the substrate was detected as such, this led to a massive speedup. For this system, the automatic substrate detection worked very well, and the obtained results were similar for automatic and manual substrate detection.
Another factor that caused a strong speedup here was the use of cartesian coordinates for the substrate, which, in the best case, reduced the step number from 36 to 12 steps. Also the use of the vdW guess of the Hessian matrix performed well, always yielding better results than the corresponding calculations without the vdW guess and reducing the required step number by up to 10 steps. For this mainly vdW bonded system, the use of vdW-related coordinates is clearly a good approximation.

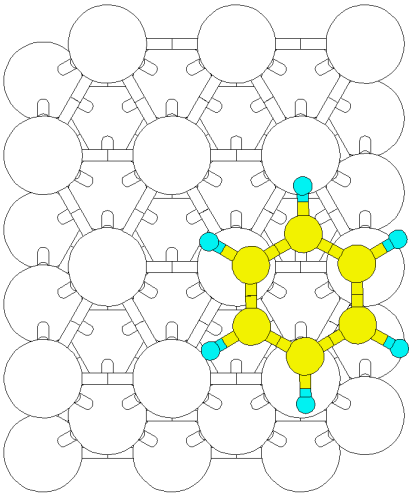

Figure 7: Benzene adsorbed on Ag(111) in a lying configuration. C atoms are depicted in yellow, H atoms in blue and the Ag substrate is depicted in white.

3.1.6 Discussion: GADGET

Several new implementation were included in the GADGET code, trying to improve its applicability to metal/organic interfaces and also allowing the user a more direct control over coordinate choice.
The manual setting of fragments and substrate can be used if different calculations need to be performed in a consistent manner. In addition, this functionality is helpful in cases where the automatic detection routines are not able to properly describe the system, e.g. for strongly bonded closed packed systems as 4-Methylthiolphenol on Au(111) or when the substrate itself causes problems for the substrate detection, as Cu does. In addition to manually detecting the substrate, also a routine to force the detection of only one fragment was included, which helps the automatic substrate detection.
The use of cartesian coordinates for the substrate has been shown to be very useful and to significantly speed up calculations where the substrate is not strongly deformed upon molecular adsorption. This is due to the better suitability of cartesian coordinates for describing crystalline structures. However, for systems where the interaction between molecules and substrate is strong, such as thiol-bonded SAMs, the cartesian coordinates for the substrate are not necessarily beneficial.
The implementation to avoid problems caused by too straight bonds was tested on several systems which contain molecular chains, also including the upright standing TCNE as discussed above. It has improved the choice of coordinates in all cases, avoiding situations where the chosen coordinates do not fully represent all degrees of freedom present of the system.
The use of the vdW guess of the Hessian matrix did, unfortunately, not perform overly well in most cases. Depending on the chosen settings, it improved or worsened the speed of the geometry optimization and only led to a significant improvement for the purely vdW bonded system benzene on Ag(111). However, it has to be kept in mind that the tests performed here included a large number of different settings, which led to wide spreads in the performance. As the use of the vdW initialization method always led to intermediate simulation times, it is indeed helpful as a default setting for the use in calculations where no tuning of the settings is performed.

3.2 Adsorption of Chlorogallium Phthalocyanine GaClPc on Cu(111)

One system where the impact of a proper geometry optimization is very crucial is the nonplanar chlorogallium phthalocyanine GaClPc molecule (see Fig. 8) adsorbed on Cu(111).
This system was already investigated during my master thesis,[23] where it was attempted to reproduce the experimental x-ray standing wave XSW adsorption heights presented by Gerlach et al.[15] via DFT simulations including a vdW correction method. The nonplanar molecular geometry with the Cl atom protruding perpendicular from the molecular plane offers different possibilities for the adsorption configuration, namely Cl-up and Cl-down scenarios.
In the original study of GaClPc adsorption on Cu(111) in Ref. [15], conclusions on the adsorption configuration were drawn from a combination of experimental XSW and ultraviolet photoelectron spectroscopy UPS results and quantum-mechanical DFT calculations. However, at that point, an adequate vdW correction method was not readily available in the applied DFT codes, which made a full geometry optimization impossible. Nonetheless, a conclusion on the adsorption configuration could be reached from the available data, as the Cl-up scenario could be excluded due to the work function modification $\Delta\Phi$ it induces, which does not match the experimentally found value at all. For the Cl-down scenario, on the other hand, experimental and simulated values for $\Delta\Phi$ matched very well.
Surprisingly, the full geometry optimizations of the GaClPc/Cu(111) system performed during my master thesis resulted in adsorption heights differing strongly from the experimental XSW values. This was especially puzzling as the applied van der Waals correction method vdW^{surf} had been shown to yield good agreement with experimental results for various interface systems including phthalocyanine adsorption.[24, 25, 68, 85, 86]
To overcome this disagreement, a third adsorption configuration was considered, with the Cl atom detached from the GaPc molecule (Cl-diss), adsorbing independently on the Cu substrate. In the definitive calculations on that configuration, which were performed during this PhD thesis, good agreement on simulated and experimental adsorption heights could be found.
However, this raised the question on how well the simulated $\Delta\Phi$ value for the Cl-diss scenario matches experiment, as the strong molecular dipole arising for the Ga-Cl bond is no longer present there. Interestingly, $\Delta\Phi$ of the Cl-diss system is very similar to that obtained for the Cl-down system, and, therefore, agrees with the experimentally obtained value. This is the case as the dipole gets compensated due to energetic pinning of states in the molecular backbone to the Fermi level of the Cu substrate. By comparing the values of $\Delta\Phi$ for all investigated configuration to the progression of the work function obtained during deposition, a conclusive explanation on how GaClPc adsorbs could be found. It was shown that the Cl dissociation appears during annealing

of the interface. Finally, also the adsorption energies were investigated. They showed that the Cl-diss scenario is energetically clearly favorable over the Cl-up and Cl-down scenarios.
The different adsorption scenarios and how they compare to experimental results were published in the course of this thesis. The resulting article "Adsorption Behavior of Nonplanar Phthalocyanines: Competition of Different Adsorption Conformations" is included in the following. Before, the author contributions to this article are reviewed in detail, and it is specified what preliminary work has already been performed during my master thesis. The Supporting Information on the article is included subsequently. In section 3.2.3, additional results on the GaClPc/Cu(111) system are presented.

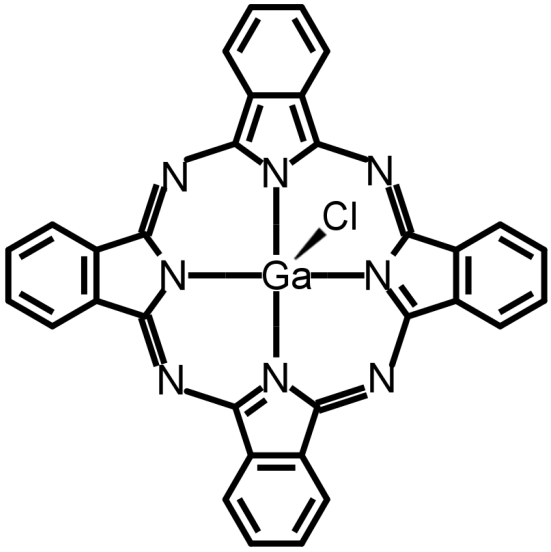

Figure 8: Structure of the chlorogallium phthalocyanine (GaClPc) molecule.

3.2.1 Author Contributions

In the following section, an original publication as published in the Journal of Physical Chemistry C, including the Supporting Information, is inserted.
Reprinted with permission from:
Adsorption Behavior of Nonplanar Phthalocyanines: Competition of Different Adsorption Conformations
Elisabeth Wruss, Oliver T. Hofmann, David A. Egger, Elisabeth Verwüster, Alexander Gerlach, Frank Schreiber, and Egbert Zojer
The Journal of Physical Chemistry C **2016** *120* (12), 6869-6875
DOI: 10.1021/acs.jpcc.6b00312
https://pubs.acs.org/doi/10.1021/acs.jpcc.6b00312

The simulation project on the GaClPc/Cu(111) system was supervised by Egbert Zojer.
The idea that upon the adsorption of GaClPc on Cu(111) the Cl atom could be dissolved was conceived by Elisabeth Verwüster. All presented calculations were performed and analyzed by myself. The interpretation of the obtained data was done by myself, in cooperation with Egbert Zojer, David A. Egger and Oliver T. Hofmann. For the comparison to experimental results (previously published in Ref. [15]), also Alexander Gerlach and Frank Schreiber were included.
The original version of the manuscript was written by myself, and I also created all included figures. Subsequently, the manuscript was modified and improved in close cooperation with Egbert Zojer, Oliver T. Hofmann and David A. Egger.

As mentioned previously, the work on the GaClPc/Cu(111) system is based on preliminary calculations performed during my master thesis.[23] There, the system was investigated with the main focus lying on the simulation of the adsorption geometry by applying an adequate vdW correction methodology. Several different configuration on the surface were considered, and it was found that for these scenarios, no agreement between experimental and simulated adsorption heights could be obtained. As a consequence, a scenario with Cl dissociation was proposed. Although this configuration appeared to be more promising to yield agreement with the experimental findings, no final conclusion could be drawn in the course of my master thesis.
Therefore, the calculations were continued during my PhD thesis, and all calculations which are presented in Ref. [16] were performed in the course of this dissertation. The final results presented there, mainly the adsorption heights of the molecule, are in better agreement with experiment than the previously obtained ones. This is because a better converged unit cell, containing five instead of three substrate Cu layers was applied, and a better knowledge of the applied geometry optimization tool GADGET led to a more suitable choice of parameters and coordinates for the optimizations.
In addition, the theory on why the work function modifications for the different configurations change as they do was verified by further calculations during my PhD thesis. This also allowed to explain the progression of the work function modification with increasing coverage and after annealing as presented in Ref. [15]. Finally, also adsorption energies for the different configurations were calculated and compared.

3.2.2 Original Article: *Adsorption Behavior of Non-Planar Phthalocyanines: Competition of Different Adsorption Conformations*

THE JOURNAL OF PHYSICAL CHEMISTRY C

Article

pubs.acs.org/JPCC

Adsorption Behavior of Nonplanar Phthalocyanines: Competition of Different Adsorption Conformations

Elisabeth Wruss,[†] Oliver T. Hofmann,[†] David A. Egger,[†,‡] Elisabeth Verwüster,[†] Alexander Gerlach,[§] Frank Schreiber,[§] and Egbert Zojer*[,†]

[†]Institute of Solid State Physics, NAWI Graz, Graz University of Technology, 8010 Graz, Austria

[§]Institut für Angewandte Physik, Universität Tübingen, 72076 Tübingen, Germany

Supporting Information

ABSTRACT: Using density functional theory augmented with state-of-the-art van der Waals corrections, we studied the geometric and electronic properties of nonplanar chlorogallium-phthalocyanine GaClPc molecules adsorbed on Cu(111). Comparing these results with published experimental data for adsorption heights, we found indications for breaking of the metal−halogen bond when the molecule is heated during or after the deposition process. Interestingly, the work-function change induced by this dissociated geometry is the same as that computed for an intact adsorbate layer in the "Cl-down" configuration, with both agreeing well with the experimental photoemission data. This is unexpected, as the chemical natures of the adsorbates and the adsorption distances are markedly different in the two cases. The observation is explained as a consequence of Fermi-level pinning due to fractional charge transfer at the interface. Our results show that rationalizing the adsorption configurations on the basis of electronic interface properties alone can be ambiguous and that additional insight from dispersion-corrected DFT simulations is desirable.

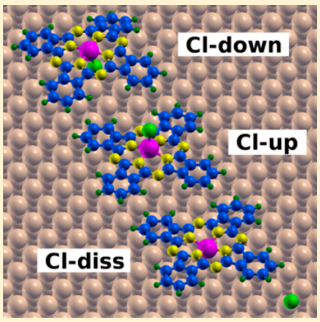

1. INTRODUCTION

Combining experiments and simulations has become a crucial approach in modern surface science for gaining in-depth atomistic insight into processes at interfaces. It also helps to eliminate certain ambiguities that prevail when interpreting experimental data.[1−3] This is particularly true for X-ray standing wave (XSW) experiments, which allow for the determination of adsorption distances with picometer resolution[4] and are, therefore, of crucial importance for rationalizing interface properties.[5−8] At the same time, such experiments allow for the determination of adsorption geometries only modulo the distance between crystallographic planes parallel to the surface.[9−11] Thus, they can provide two or more possible interpretations for the geometry of the adsorbate. This especially applies to large, nonplanar molecules,[7,12] where unambiguously determining the adsorption height by choosing several nonparallel sets of scattering planes[10] can be difficult. Which of the conceivable adsorption geometries is correct can then be determined using density functional theory (DFT). DFT calculations are also highly useful when investigating the coexistence of different phases and adsorption configurations of molecules on surfaces. They have become particularly powerful over the past few years, as recent advances in the treatment of van der Waals interactions within DFT have hugely increased the reliability of the theoretical results.[13−20] This improvement now allows computations to take a more proactive role in this symbiosis. By means of calculations, it becomes relatively straightforward to test scenarios that usually are not automatically considered, including the dissociation of the adsorbed material.[21]

Such an endeavor lies at the heart of the present work, in which we revisit a previously investigated, very well characterized system: chlorogallium-phthalocyanine (GaClPc) on Cu(111).[12] This system serves as an example of an interface between a nonplanar, polar molecule and a metal, where (i) molecule−metal charge-transfer effects crucially impact the electronic properties and (ii) the determination of the adsorption configuration is far from straightforward. Traditionally, for nonplanar, phtalocyanines (Pcs) the considered adsorption configurations comprise situations in which an intact molecule adsorbs with the molecular backbone parallel to the surface and the central metal atom (or metal−halogen bond) protruding perpendicular to it.[7,20,22−24] Deviating from this common view, we find here that, upon annealing or deposition onto sufficiently heated substrates, a situation with Cl dissociated from the molecule becomes a likely scenario. This process might be more common in Cl-bearing Pcs than hitherto discussed.

2. COMPUTATIONAL DETAILS

Using VASP (version 5.3.3),[25] we performed full geometry optimizations, employing the Perdew−Burke−Ernzerhof (PBE) functional[26,27] with projected augmented-wave (PAW)

Received: January 11, 2016
Revised: February 21, 2016
Published: February 29, 2016

DOI: 10.1021/acs.jpcc.6b00312
J. Phys. Chem. C 2016, 120, 6869−6875

potentials[28,29] to treat core−valence interactions (see SI for details). We note that the PBE functional has been shown to cause an incorrect ordering of ligand versus metal-centered states in some metal-Pc[30−32] molecules, which also prevails on noble-metal surfaces.[32,33] For the present interfaces, however, such states do not contribute to the density of states within a few electronvolts of the Fermi energy, as shown in the SI. Thus, we can safely assume that this shortcoming of the PBE functional is not relevant for the present discussion and will not significantly affect the observed charge transfer near the Fermi level. In passing, we note that some of us recently studied the influence of the DFT functional on simulated work functions for the adsorption of various organic molecules on other coinage-metal surfaces.[32,34] The differences in the work functions calculated with either PBE or "conventional" hybrid functionals, such as PBE0 or HSE06, were rather small. We expect that this will be similar for the present system, especially as it is chemically closely related to the systems studied in ref 32. This further justifies the use of the PBE functional.

To account for long-range dispersion forces, the vdW^{surf} algorithm[16] specifically tailored to treat adsorption on metallic surfaces was applied. This computationally efficient post-SCF energy-correction scheme combines the vdW-TS dispersion correction approach[14] with Lifshitz−Zaremba−Kohn theory[35,36] to account for nonlocal Coulomb screening at surfaces.[16] It has been shown to yield adsorption distances in excellent agreement with experiment.[16,18,19,32] The van der Waals coefficients C_6, α, and R for the atoms comprising the GaClPc molecule were taken from ref 14. For Cu, the default settings in VASP 5.3.3 were replaced by the metal-specific parameters from ref 16. A special modification of the VASP code kindly provided by Tomáš Bučko (Comenius University, Bratislava) allowed us to selectively switch off the van der Waals correction between specific atomic species. This was applied here to the interaction between the atoms of the Cu substrate, which is useful because vdW^{surf} is not designed to treat van der Waals interactions in the bulk. It also enabled us to use a PBE-optimized lattice constant for Cu (3.637 Å).

For the plane-wave basis, a cutoff energy of 500 eV was set (early steps of geometry optimizations were done with a cutoff energy of 400 eV). The states were occupied according to the Methfessel−Paxton[37] scheme, and a Monkhorst−Pack[38] (2 × 2 × 1) k-point mesh was applied. To model a surface structure with a metallic substrate, the simulations were performed applying the repeated slab approach with five layers of Cu representing the metal substrate. The periodic replicas of the slab were decoupled by a vacuum region of at least 20 Å containing a self-consistently determined dipole layer compensating for the electrostatic asymmetry of the slab.[39] The geometry optimizations were done using GADGET[40] and VASP. The advanced geometry optimization algorithms implemented in GADGET and the use of a sophisticated model Hessian yield particularly fast convergence properties (see SI for details).[40] During our geometry optimizations, all molecular atoms as well as the top two substrate layers were allowed to relax in all spatial directions until the gradient fell below 0.01 eV/Å. More information on the employed methodology is provided in the SI.

3. RESULTS AND DISCUSSION

3.1. Structure of the Adsorbate Layer. Based on XSW measurements, ref 12 considers two possible adsorption geometries for GaClPc on Cu(111). These are the so-called Cl-down configuration, with the Cl atom between the molecular backbone and the surface, and the flipped Cl-up configuration, with Cl pointing away from the surface. The Cl-up interpretation was considered less likely, as it would lead to a strong, energetically unfavorable shortening of the Ga−Cl bond.[12] DFT calculations of the adsorbed molecules placed at the experimental adsorption distances supported the dominance of the Cl-down phase; full geometry optimization including van der Waals (vdW) corrections could not be performed because, at that time, reliable van der Waals corrections were not yet widely available. The assignment of a Cl-down phase was strongly supported by the observation that the calculated work-function shifts upon GaClPc adsorption in the Cl-down configuration agreed almost perfectly with the ultraviolet photoelectron spectroscopy (UPS) data. Notably, the coexistence of Cl-up and Cl-down conformations (or other situations for that matter) was not analyzed in detail. In passing we note that, in ref 12, the UPS results for the annealed GaClPc monolayer were correlated with XSW measurements where the films were deposited at elevated temperature (rather than annealed).[12] It was then assumed that equivalent molecular configurations on the surface were obtained for the two cases, which is, in fact, corroborated by our findings discussed below.

Building on recent advances in available computational methods (vide supra), it is now possible to go beyond the approach outlined above. As a first step, we investigated the above-mentioned Cl-up and Cl-down configurations with one molecule in a rectangular ∼18 × 18 Å surface cell (corresponding to approximately 80% coverage; for details, see SI). The resulting fully optimized geometries are shown in Figure 1a,b, and the experimental adsorption heights and the corresponding calculated values are reported in Table 1a,b. As the experiments provide adsorption distances relative to the (hypothetical) unrelaxed topmost metal layer (i.e., relative to the bulk lattice),[9,10] equivalent values are also reported for our simulations (although the surface relaxations of the two topmost metal layers were considered explicitly in the geometry optimization).

For the Cl-up scenario, the molecule stays comparably flat, the Ga−Cl bond is perpendicular to the molecular backbone, and the Ga atom is at a greater distance from the substrate than the molecular plane. We find good agreement between calculated and experimental distances for the C and N atoms. For the metal−halogen group in the center of the molecule, however, the heights disagree by more than 1.0 Å. Moreover, whereas experiments predict that the Ga atom is closer to the substrate than the molecular backbone, simulations clearly position it at a larger distance. The incompatibility between theoretical and experimental results for the Cl-up conformation is, actually, not really surprising, considering that adsorption of GaClPc on Cu(111) in the Cl-up configuration was considered to be inconsistent with the experimental and theoretical data already in ref 12.

In the Cl-down configuration, the GaClPc molecule exhibits an umbrella-like shape that is slightly tilted to the side. Remarkably, also for the Cl-down configuration, the full geometry optimizations performed here yielded adsorption distances clearly deviating from the experimental values: In the simulated structure, the molecule is significantly closer to the surface than one would expect from experiment. This effect is particularly large for the C atoms, where the calculated average C position is by more than 1.2 Å lower than the experimental

DOI: 10.1021/acs.jpcc.6b00312
J. Phys. Chem. C 2016, 120, 6869−6875

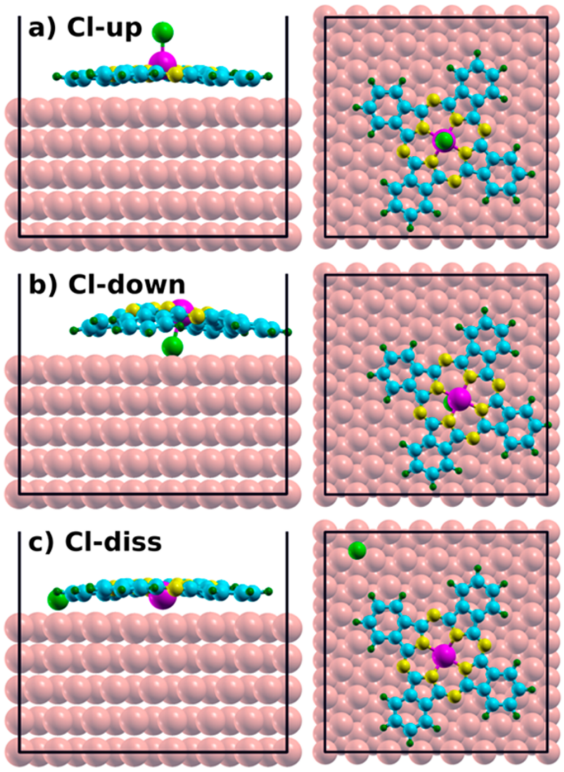

Figure 1. Top and side views of the adsorption geometries of a GaClPc molecule on the Cu(111) surface. Adsorption in the (a) Cl-up, (b) Cl-down, and (c) Cl-diss geometries is shown. The molecular atomic species are depicted as follows: C, light blue; H, dark green; N, yellow; Ga, purple; Cl, light green. The unit cell is indicated by solid black lines.

Table 1. Adsorption Heights (Å) of the Different Atomic Species of the GaClPc Molecule on Cu(111), as Obtained by Experiments (XSW)[12] and Simulations (DFT), for the (a) Cl-up, (b) Cl-down, and (c) Cl-diss Scenarios[a]

	(a) Cl-up		(b) Cl-down		(c) Cl-diss	
atom	XSW	DFT	XSW	DFT	XSW	DFT
C	2.36(7)	2.45	4.44(7)	3.18	2.36(7)	2.51
N	2.63(3)	2.58	4.71(3)	3.72	2.63(3)	2.68
Ga	2.13(5)	3.14	4.21(5)	3.79	2.13(5)	2.14
Cl	3.96(3)	5.36	1.88(3)	1.51	1.88(3)	1.86

[a]To better suit the different molecular configurations, the XSW results were interpreted differently for the three configurations by adding appropriate numbers of bulk lattice plane spacings [2.08 Å for Cu(111)[12]].[9,10]

value. Also the experimental finding that Ga is positioned below the average C adsorption height cannot be reproduced computationally for the Cl-down structure. To clarify the origin of these deviations, we studied a significant number of variations in unit cell size and starting geometry. They all yielded qualitatively similar deviations from the experimental structure (see SI for details).

The lack of agreement between the measured and calculated adsorption distances implies that other, hitherto-uninvestigated adsorbate structures have to be taken into account. In this context, an intriguing aforementioned observation is that, in the Cl-up conformation, the geometry of the backbone is already very close to that observed by experiment, with the discrepancy lying "only" in the positions of the central two atoms. This raises the question which modifications in the adsorption configuration would change that situation. In this context, it is interesting that, in several instances, partial and/or full dechlorination of metal-bonded Cl atoms in organic films on coinage-metal substrates has been reported upon adsorption and/or annealing.[21,41,42] Therefore, considering that the Cu surface can promote molecular dissociation,[43,44] another potentially realistic scenario is that the Cl atom is separated from the rest of the molecule.

In the case of GaClPc on Cu(111), it is clear that the Cl atom remains on the surface, as can be inferred from the XSW results and the associated X-ray photoelectron spectroscopy (XPS) characterization.[12] Therefore, we simulated a situation with the GaPc and Cl fragments adsorbing side by side on the Cu(111) surface separated by more than 4 Å to prevent spurious interactions (structure Cl-diss in Figure 1c). In passing we note that, as a test, we also considered a situation in which the Cl atom was removed from the unit cell, mimicking a situation in which the Cl atom has diffused away from the molecule. This simulation yields adsorption distances for the remaining GaPc system that are virtually identical to those in the Cl-diss case.

The geometry of the molecular backbone of the Cl-diss configuration is very similar to that of the Cl-up configuration, adsorbing essentially flat on the surface. A notable exception is the Ga atom, which—in contrast to the Cl-up case—is located below the organic backbone, that is, between the backbone and the substrate (Table 1c). We attribute this difference to the Ga atom no longer being saturated by the bond to the Cl atom, which triggers a stronger interaction with the Cu surface. Overall, the quantitative agreement between the measured and calculated adsorption distances is excellent for both the molecular constituents and the Cl atom. Remaining deviations are in the range of a few hundredths of an angstrom. Only for the C atoms are they somewhat larger (0.15 Å). In this context, it is interesting to note that the calculated C adsorption heights spread over 0.48 Å. This is related to the 4-fold symmetry of the molecule being reduced to a 2-fold symmetry upon adsorption on the 6-fold symmetric-top layer of the substrate. This leads to two of the four molecular branches bending more strongly and, thus, coming significantly closer to the Cu surface (see SI for details). Regarding the Cl adsorption positions, it is worth mentioning that both the measured and calculated adsorption distances are similar to literature values for isolated Cl atoms on Cu(111).[45] The overall excellent agreement between the measured adsorption distances and the calculations for the Cl-diss conformation implies that the dechlorination of at least some of the GaClPc molecules is a realistic scenario, especially upon deposition at elevated temperature (i.e., for the samples used in the XSW experiments in ref 12) or upon annealing of the films (as in the UPS experiments, vide infra).

3.2. Configuration-Dependent Adsorption Energy.

The possibility of a splitting-off of the Cl atom at the Cu(111) surface is further supported by the relative adsorption energies. These energies were obtained for the different configurations by subtracting the energies of the separately geometry-optimized isolated molecule ($E_{molecule}$, optimized in a converged 45 × 45 × 40 Å^3 unit cell) and the geometry-

DOI: 10.1021/acs.jpcc.6b00312
J. Phys. Chem. C 2016, 120, 6869−6875

optimized metal slab (E_{slab}) from the total energy of the combined system discussed so far (E_{system})

$$E_{ads} = E_{system} - E_{molecule} - E_{slab} \quad (1)$$

The results are reported in Table 2, together with the corresponding contributions arising from van der Waals interactions. The latter strongly contribute to the adsorption energies, which implies that suitable theoretical tools for describing van der Waals interactions are a crucial prerequisite for reliably optimizing the geometries of such systems.[15,16,18,19,32] The significantly lower (i.e., less negative) adsorption energy of Cl-down compared to the two other configurations is a consequence of the much larger adsorption distance of the molecular backbone and, thus, a significantly reduced van der Waals attraction. While Cl-up and Cl-diss lie at very similar adsorption distances, Cl-diss is more strongly bonded to the surface.

Table 2. Adsorption Energies (E_{ads}) and van der Waals Contributions ($E_{ads,vdW}$) per Molecule for GaClPc on the Cu(111) Surface in the (a) Cl-up, (b) Cl-down, and (c) Cl-diss Configurations

configuration	E_{ads} (eV)	$E_{ads,vdW}$ (eV)
(a) Cl-up	−4.72	−6.47[a]
(b) Cl-down	−2.65	−4.24
(c) Cl-diss	−5.10	−6.47[a]

[a]Note that the identical values of $E_{ads,vdW}$ for Cl-up and Cl-diss are a coincidence.

At this point, it should be stressed that adsorption energies only point to the thermodynamically most stable configuration, neglecting any kinetic effects. In the present case, it appears likely that a certain activation barrier is associated with the splitting-off of the Cl atoms. As a consequence, depending on the film growth and the annealing conditions, the coexistence of several configurations (Cl-up, Cl-down, Cl-diss) is certainly a viable scenario with a considerable impact on the expected experimental data. This possibility would be consistent with Cl dissociation appearing especially when films are grown on substrates at elevated temperatures (for XSW experiments) or when a sample is annealed (as for the UPS measurements discussed below).[12] It should also be mentioned here that the exact value of the adsorption energy for the Cl-diss scenario depends on the fate of the Cl atom. Although it is known from XSW experiments that the Cl atom remains on the Cu(111) surface, it might adsorb in different positions, such as at step edges, and/or Cl atoms could form islands. Although our simulations do not focus on elucidating the detailed mechanism of the dechlorination reaction, it is worth mentioning that some mechanistic insight can be gained from previous studies on related systems.[21,46]

3.3. Adsorption-Induced Work-Function Modification.

The fact that our simulations of geometry and binding energies support a Cl-diss scenario raises an important issue: A strong argument for the prevalence of the Cl-down configuration has been that the computed work-function modification, $\Delta\Phi$, for this conformation (−0.55 eV for the Cl-down structure simulated in ref 12) is in excellent agreement with that measured after annealing the sample at 300 °C (−0.60 eV measured by UPS).

This calls for an in-depth investigation of the work-function changes caused by the organic adsorbate layer. Interestingly, the value of $\Delta\Phi$ that we computed for the fully relaxed Cl-down conformation ($\Delta\Phi$ = −0.58 eV, cf. Table 3) is essentially the same as the computational value reported in ref 12 ($\Delta\Phi$ = −0.55 eV, cf. Table 3) despite the very significant differences in adsorbate geometries: Whereas we fully optimized the geometries, in ref 12, fixed adsorption heights determined from experimental values were used. For Cl-down, the latter approach resulted in a molecular backbone that was more than 1.0 Å higher than when the geometry was fully optimized (cf., Table 1). Even more surprisingly, an equivalent value for the work-function change is obtained for the Cl-diss case ($\Delta\Phi$ = −0.62 eV; see Table 3), which is intriguing considering that the highly polar Ga−Cl bond is no longer intact. In passing, we note that, for the situation with Cl removed from the unit cell, we also obtain a value of $\Delta\Phi$ = −0.65 eV, which, as for all other calculated values mentioned so far, would be consistent with the experimental $\Delta\Phi$ value of −0.60 eV obtained after annealing. The only GaClPc configuration considered in this work that induces a markedly different work-function modification is Cl-up: Its $\Delta\Phi$ of −0.37 eV is, however, very close to the −0.34 eV measured for GaClPc films grown at 80 °C prior to annealing at 300 °C.[12]

Table 3. $\Delta\Phi$ Values of the Cu(111) Surface upon Adsorption of GaClPc in Different Configurations, Including Contributions Originating from the Molecular Dipole ($\Delta\Phi_{dip}$) and the Bonding-Induced Dipole ($\Delta\Phi_{bond}$)[a]

	$\Delta\Phi$ (eV)	$\Delta\Phi_{dip}$ (eV)	$\Delta\Phi_{bond}$ (eV)
Cl-up	−0.37	0.23	−0.58
Cl-down	−0.58	−0.26	−0.30
Cl-diss[b]	−0.62	−0.08	−0.53
experimental[12]			
before annealing	−0.34		
after annealing	−0.60		
Cl-down from ref 12	−0.55	−0.30	−0.25

[a]The minimal deviations from eq 2 arise from the asymmetry of the slab due to rearrangements of the top two Cu rows, which were neglected in the derivation of $\Delta\Phi_{bond}$. [b]To avoid effects of spurious charge transfer in the Cl-diss case between the GaPc molecule and the Cl atom, these two fragments were calculated separately (see SI for details).

To understand the origin of the very similar work-function modifications induced by the Cl-down and Cl-diss configurations, it is useful to split the total work-function change into two parts: first, the contribution stemming from the dipoles of the molecules that form the adsorbate layer, $\Delta\Phi_{dip}$, and second, the contribution from the charge rearrangements at the surface. The latter cause the so-called bond dipole, $\Delta\Phi_{bond}$.[47,48] For the overall work-function change, one then obtains

$$\Delta\Phi = \Delta\Phi_{dip} + \Delta\Phi_{bond} \quad (2)$$

To calculate $\Delta\Phi_{dip}$, the molecules are arranged in a (hypothetical) free-standing monolayer in exactly the geometry they would adopt on the surface. $\Delta\Phi_{bond}$ is obtained by solving Poisson's equation using the bonding-induced charge rearrangements as a source term (see SI for details). The values of $\Delta\Phi_{dip}$ and $\Delta\Phi_{bond}$ for all systems are listed in Table 3. $\Delta\Phi_{dip}$ can be understood from the adsorption geometries of the different conformations: When Cl is significantly above the π-backbone, the orientation of the molecular dipole causes a shift in the work function of +0.23 eV. Reversing the dipole

DOI: 10.1021/acs.jpcc.6b00312
J. Phys. Chem. C 2016, 120, 6869−6875

orientation in Cl-down results in a change in sign of the molecule-related work-function modification, and $\Delta\Phi_{dip}$ becomes −0.26 eV. For Cl-diss, the Ga−Cl dipole disappears ($\Delta\Phi_{dip}$ = −0.08 eV). When comparing $\Delta\Phi_{bond}$ for Cl-down and Cl-diss, one observes that the smaller $\Delta\Phi_{dip}$ value for Cl-diss is accompanied by a larger $\Delta\Phi_{bond}$ value, such that, as a net effect, the total work-function modifications become essentially the same. The fundamental reason for this result is rooted in the filling of the molecular states upon adsorption: As shown in Figure 2, where the density of states projected onto the molecular layer (PDOS) is drawn, in all considered cases, a partially filled molecule-derived band at the Fermi energy is observed. That is, the Fermi level cuts through the peak associated with the band derived from the lowest unoccupied molecular orbital (LUMO).

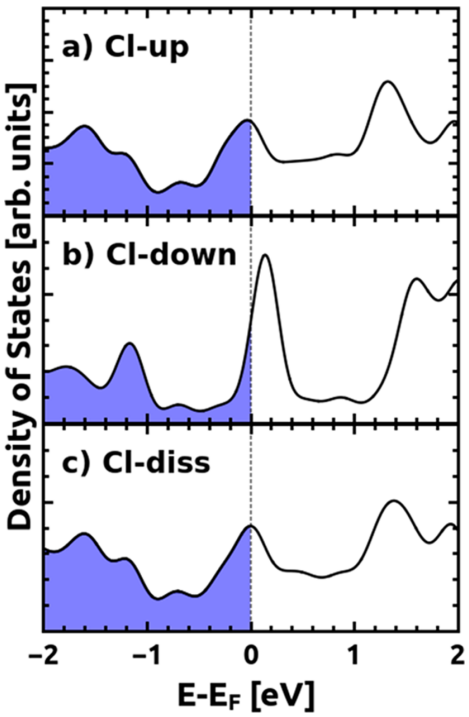

Figure 2. PBE-calculated densities of states projected onto the adsorbed GaClPc layer for the (a) Cl-up, (b) Cl-down, and (c) Cl-diss configurations. The energy is aligned to the Fermi energy, which is indicated by a dotted line. The blue region indicates the filled states. The PDOSs were obtained on the basis of fully optimized geometries.

This scenario results in Fermi-level pinning, namely, a situation in which the system work function becomes independent of the work function of the substrate.[34,49−54] Then, it is essentially the energy of the "molecular pinning level" that determines the work function, at least as long as (i) all molecular dipoles are located spatially between the metal substrate and the molecular states at which the Fermi level is pinned[54] and (ii) the packing density is sufficiently high.[55] In such a case, $\Delta\Phi_{bond}$ has to compensate for differences in $\Delta\Phi_{dip}$. This is exactly what happens here for Cl-down and Cl-diss. The equality of $\Delta\Phi$ for Cl-down and Cl-diss thus implies that the characters and energetics of the LUMO-derived bands after adsorption are essentially the same in the two systems, an assessment that is fully confirmed by calculating the energetic positions of those bands relative to the vacuum energy in the (hypothetical) free-standing molecular monolayers.

The situation is fundamentally different when the molecular dipole is located farther from the substrate than the pinned molecular levels, as is the case for Cl-up. Then, this dipole induces an additional shift in the electrostatic energy beyond the value determined by Fermi-level pinning.[54] Thus, for Cl-up, $\Delta\Phi_{bond}$ is essentially the same as the total work-function shift of Cl-down and Cl-diss (i.e., determined by the energy of the level at which the molecular backbone is pinned). In addition, there is a work-function change of +0.23 eV due to the arrangement of the Ga−Cl dipoles above the molecules.

As mentioned before, the obtained work-function change of −0.37 eV for Cl-up is intriguingly close to the largest work-function reduction of −0.34 eV that is measured for GaClPc films deposited at 80 °C prior to annealing.[12] This potentially indicates that, in this case, a large portion of the molecules adopt the Cl-up configuration, which is energetically favorable over Cl-down (see Table 2). Although it cannot be excluded that part of the GaClPc molecules arriving in a Cl-down configuration lose their Cl atom right upon adsorption [as reported for FeOEP-Cl on Cu(111)[21]], a more substantial loss of Cl atoms apparently occurs only when the films are deposited at elevated temperatures or when the samples are annealed.

4. CONCLUSIONS

The commonly considered geometric configurations for phtalocyanines (Pcs) with central metal-halide substituents comprise situations with the halide groups pointing either toward or away from the substrate. Here, we suggest a different situation to be the thermodynamically most stable case [at least on the Cu(111) surface], namely, dissociation of the molecule with the Cl atom split off from the Pc backbone. The calculated adsorbate geometry for such a situation is in excellent agreement with previously published X-ray standing wave data for that interface. Interestingly, we find essentially identical work-function changes for a number of cases: (i) the experiments, (ii) previous calculations for GaClPc on Cu(111) in the Cl-down configuration (ref 12) at fixed geometries, (iii) a fully optimized Cl-down geometry, and (iv) the geometry with the Cl atom split off the molecular backbone. This is surprising, given that the calculated adsorption geometries in configurations ii−iv are vastly different. This apparent conundrum is resolved by associating the work-function changes with Fermi-level pinning. A situation in which a significant fraction of the GaClPc molecules dissociate and GaPc and Cl adsorb separately is fully consistent with the available experimental data for situations in which enough energy has been provided to overcome the activation energy barrier for dissociation; depending on the annealing time/film growth temperature, the coexistence of different phases (Cl-up, Cl-down, Cl-diss) is also a viable scenario. The described dissociation effects of halogens might play a crucial role for other interfaces as well, especially those including reactive surfaces such as Cu(111).[21,44] This implies that particular care must be taken during any annealing procedures and that scenarios similar to the one presented here have to be taken into account when one is trying to understand experimental observations.

DOI: 10.1021/acs.jpcc.6b00312
J. Phys. Chem. C 2016, 120, 6869−6875

■ ASSOCIATED CONTENT

Supporting Information

The Supporting Information is available free of charge on the ACS Publications website at DOI: 10.1021/acs.jpcc.6b00312.

Details on PAW potentials, GADGET calculations, unit cells, geometry changes during geometry optimizations, additional test calculations, calculations of charge rearrangements and bond dipoles, discussion of symmetry reduction upon adsorption, and densities of states projected onto the adsorbate layer and separately onto the Ga atoms (PDF)

■ AUTHOR INFORMATION

Corresponding Author

*E-mail: egbert.zojer@tugraz.at.

Present Address

‡D.A.E.: Department of Materials and Interfaces, Weizmann Institute of Science, Rehovoth 76100, Israel.

Author Contributions

The manuscript was written through contributions of all authors. All authors have given approval to the final version of the manuscript

Notes

The authors declare no competing financial interest.

■ ACKNOWLEDGMENTS

Financial support by the Austrian Science Fund (FWF) P24666-N20, is gratefully acknowledged. Part of the work of D.A.E. was supported by a DOC fellowship from the Austrian Academy of Sciences. We thank Tomáš Bučko (Comenius University, Bratislava) for support with the computational methods. The computational results presented were achieved using the Vienna Scientific Cluster (VSC) and the clusters of the scientific computing department of Graz University of Technology (ZID).

■ REFERENCES

(1) Hauschild, A.; Karki, K.; Cowie, B. C. C.; Rohlfing, M.; Tautz, F. S.; Sokolowski, M. Molecular Distortions and Chemical Bonding of a Large Pi-Conjugated Molecule on a Metal Surface. *Phys. Rev. Lett.* **2005**, *94*, 036106.

(2) Romaner, L.; Heimel, G.; Brédas, J.-L.; Gerlach, A.; Schreiber, F.; Johnson, R. L.; Zegenhagen, J.; Duhm, S.; Koch, N.; Zojer, E. Impact of Bidirectional Charge Transfer and Molecular Distortions on the Electronic Structure of a Metal-Organic Interface. *Phys. Rev. Lett.* **2007**, *99*, 256801.

(3) Stadtmüller, B.; Lüftner, D.; Willenbockel, M.; Reinisch, E. M.; Sueyoshi, T.; Koller, G.; Soubatch, S.; Ramsey, M. G.; Puschnig, P.; Tautz, F. S.; Kumpf, C. Unexpected Interplay of Bonding Height and Energy Level Alignment at Heteromolecular Hybrid Interfaces. *Nat. Commun.* **2014**, *5*, 3685.

(4) Gerlach, A.; Bürker, C.; Hosokai, T.; Schreiber, F. X-ray Standing Wave and Surfaces X-ray Scattering Studies of Molecule−Metal Interfaces. In *The Molecule−Metal Interface*; Koch, N., Ueno, N., Wee, A. T. S., Eds.; John Wiley & Sons: Weinheim, Germany, 2013; Chapter 6.

(5) Stanzel, J.; Weigand, W.; Kilian, L.; Meyerheim, H. L.; Kumpf, C.; Umbach, E. Chemisorption of NTCDA on Ag(1 1 1): A NIXSW Study Including Non-Dipolar and Electron-Stimulated Effects. *Surf. Sci.* **2004**, *571*, L311−L318.

(6) Gerlach, A.; Schreiber, F.; Sellner, S.; Dosch, H.; Vartanyants, I. A.; Cowie, B. C. C.; Lee, T.-L.; Zegenhagen, J. Adsorption-Induced Distortion of F16CuPc on Cu(111) and Ag(111): An X-Ray Standing Wave Study. *Phys. Rev. B: Condens. Matter Mater. Phys.* **2005**, *71*, 205425.

(7) Stadler, C.; Hansen, S.; Pollinger, F.; Kumpf, C.; Umbach, E.; Lee, T.-L.; Zegenhagen, J. Structural Investigation of the Adsorption of SnPc on Ag(111) Using Normal-Incidence X-Ray Standing Waves. *Phys. Rev. B: Condens. Matter Mater. Phys.* **2006**, *74*, 035404.

(8) Koch, N.; Gerlach, A.; Duhm, S.; Glowatzki, H.; Heimel, G.; Vollmer, A.; Sakamoto, Y.; Suzuki, T.; Zegenhagen, J.; Rabe, J. P.; et al. Adsorption-Induced Intramolecular Dipole: Correlating Molecular Conformation and Interface Electronic Structure. *J. Am. Chem. Soc.* **2008**, *130*, 7300−7304.

(9) Zegenhagen, J. Surface Structure Determination with X-Ray Standing Waves. *Surf. Sci. Rep.* **1993**, *18*, 202−271.

(10) Woodruff, D. P. Surface Structure Determination Using X-Ray Standing Waves. *Rep. Prog. Phys.* **2005**, *68*, 743.

(11) Gerlach, A.; Schreiber, F. The X-ray Standing Wave Technique. In *Handbook of Spectroscopy*, 2nd ed.; Gauglitz, G., Moore, D. S., Eds.; John Wiley & Sons: Weinheim, Germany, 2014; Chapter 44.

(12) Gerlach, A.; Hosokai, T.; Duhm, S.; Kera, S.; Hofmann, O. T.; Zojer, E.; Zegenhagen, J.; Schreiber, F. Orientational Ordering of Nonplanar Phthalocyanines on Cu(111): Strength and Orientation of the Electric Dipole Moment. *Phys. Rev. Lett.* **2011**, *106*, 156102.

(13) Grimme, S. Semiempirical GGA-Type Density Functional Constructed with a Long-Range Dispersion Correction. *J. Comput. Chem.* **2006**, *27*, 1787−1799.

(14) Tkatchenko, A.; Scheffler, M. Accurate Molecular van der Waals Interactions from Ground-State Electron Density and Free-Atom Reference Data. *Phys. Rev. Lett.* **2009**, *102*, 073005.

(15) Mercurio, G.; McNellis, E. R.; Martin, I.; Hagen, S.; Leyssner, F.; Soubatch, S.; Meyer, J.; Wolf, M.; Tegeder, P.; Tautz, F. S.; Reuter, K. Structure and Energetics of Azobenzene on Ag(111): Benchmarking Semiempirical Dispersion Correction Approaches. *Phys. Rev. Lett.* **2010**, *104*, 036102.

(16) Ruiz, V. G.; Liu, W.; Zojer, E.; Scheffler, M.; Tkatchenko, A. Density-Functional Theory with Screened van Der Waals Interactions for the Modeling of Hybrid Inorganic-Organic Systems. *Phys. Rev. Lett.* **2012**, *108*, 146103.

(17) Klimeš, J.; Michaelides, A. Perspective: Advances and Challenges in Treating van Der Waals Dispersion Forces in Density Functional Theory. *J. Chem. Phys.* **2012**, *137*, 120901.

(18) Bürker, C.; Ferri, N.; Tkatchenko, A.; Gerlach, A.; Niederhausen, J.; Hosokai, T.; Duhm, S.; Zegenhagen, J.; Koch, N.; Schreiber, F. Exploring the Bonding of Large Hydrocarbons on Noble Metals: Diindoperylene on Cu(111), Ag(111), and Au(111). *Phys. Rev. B: Condens. Matter Mater. Phys.* **2013**, *87*, 165443.

(19) Egger, D. A.; Ruiz, V. G.; Saidi, W. A.; Bučko, T.; Tkatchenko, A.; Zojer, E. Understanding Structure and Bonding of Multilayered Metal−Organic Nanostructures. *J. Phys. Chem. C* **2013**, *117*, 3055−3061.

(20) Huang, Y. L.; Chen, W.; Bussolotti, F.; Niu, T. C.; Wee, A. T. S.; Ueno, N.; Kera, S. Impact of Molecule−Dipole Orientation on Energy Level Alignment at the Submolecular Scale. *Phys. Rev. B: Condens. Matter Mater. Phys.* **2013**, *87*, 085205.

(21) van Vörden, D.; Lange, M.; Schaffert, J.; Cottin, M. C.; Schmuck, M.; Robles, R.; Wende, H.; Bobisch, C. A.; Möller, R. Surface-Induced Dechlorination of FeOEP-Cl on Cu(111). *ChemPhysChem* **2013**, *14*, 3472−3475.

(22) Duncan, D. A.; Unterberger, W.; Hogan, K. A.; Lerotholi, T. J.; Lamont, C. L. A.; Woodruff, D. P. A Photoelectron Diffraction Investigation of Vanadyl Phthalocyanine on Au(1 1 1). *Surf. Sci.* **2010**, *604*, 47−53.

(23) Baran, J. D.; Larsson, J. A. Structure and Energetics of Shuttlecock-Shaped Tin-Phthalocyanine on Ag(111): A Density Functional Study Employing Dispersion Correction. *J. Phys. Chem. C* **2012**, *116*, 9487−9497.

(24) Niu, T.; Zhou, M.; Zhang, J.; Feng, Y.; Chen, W. Dipole Orientation Dependent Symmetry Reduction of Chloroaluminum Phthalocyanine on Cu(111). *J. Phys. Chem. C* **2013**, *117*, 1013−1019.

(25) Kresse, G.; Furthmüller, J. Efficient Iterative Schemes for Ab Initio Total-Energy Calculations Using a Plane-Wave Basis Set. *Phys. Rev. B: Condens. Matter Mater. Phys.* **1996**, *54*, 11169−11186.
(26) Perdew, J. P.; Burke, K.; Ernzerhof, M. Generalized Gradient Approximation Made Simple. *Phys. Rev. Lett.* **1996**, *77*, 3865−3868.
(27) Perdew, J. P.; Burke, K.; Ernzerhof, M. Generalized Gradient Approximation Made Simple [Phys. Rev. Lett. 77, 3865 (1996)]. *Phys. Rev. Lett.* **1997**, *78*, 1396−1396.
(28) Blöchl, P. E. Projector Augmented-Wave Method. *Phys. Rev. B: Condens. Matter Mater. Phys.* **1994**, *50*, 17953−17979.
(29) Kresse, G.; Joubert, D. From Ultrasoft Pseudopotentials to the Projector Augmented-Wave Method. *Phys. Rev. B: Condens. Matter Mater. Phys.* **1999**, *59*, 1758−1775.
(30) Marom, N.; Hod, O.; Scuseria, G. E.; Kronik, L. Electronic Structure of Copper Phthalocyanine: A Comparative Density Functional Theory Study. *J. Chem. Phys.* **2008**, *128*, 164107.
(31) Marom, N.; Kronik, L. Density Functional Theory of Transition Metal Phthalocyanines, I: Electronic Structure of NiPc and CoPc—self-Interaction Effects. *Appl. Phys. A: Mater. Sci. Process.* **2009**, *95*, 159−163.
(32) Huang, Y. L.; Wruss, E.; Egger, D. A.; Kera, S.; Ueno, N.; Saidi, W. A.; Bucko, T.; Wee, A. T. S.; Zojer, E. Understanding the Adsorption of CuPc and ZnPc on Noble Metal Surfaces by Combining Quantum-Mechanical Modelling and Photoelectron Spectroscopy. *Molecules* **2014**, *19*, 2969−2992.
(33) Lüftner, D.; Milko, M.; Huppmann, S.; Scholz, M.; Ngyuen, N.; Wießner, M.; Schöll, A.; Reinert, F.; Puschnig, P. CuPc/Au(1 1 0): Determination of the Azimuthal Alignment by a Combination of Angle-Resolved Photoemission and Density Functional Theory. *J. Electron Spectrosc. Relat. Phenom.* **2014**, *195*, 293−300.
(34) Hofmann, O. T.; Atalla, V.; Moll, N.; Rinke, P.; Scheffler, M. Interface Dipoles of Organic Molecules on Ag(111) in Hybrid Density-Functional Theory. *New J. Phys.* **2013**, *15*, 123028.
(35) Lifshitz, E. M. The Theory of Molecular Attractive Forces between Solids. *Sov. Phys. JETP* **1956**, *2*, 73−83.
(36) Zaremba, E.; Kohn, W. van der Waals Interaction between an Atom and a Solid Surface. *Phys. Rev. B* **1976**, *13*, 2270−2285.
(37) Methfessel, M.; Paxton, A. T. High-Precision Sampling for Brillouin-Zone Integration in Metals. *Phys. Rev. B: Condens. Matter Mater. Phys.* **1989**, *40*, 3616−3621.
(38) Monkhorst, H. J.; Pack, J. D. Special Points for Brillouin-Zone Integrations. *Phys. Rev. B* **1976**, *13*, 5188−5192.
(39) Neugebauer, J.; Scheffler, M. Adsorbate-Substrate and Adsorbate-Adsorbate Interactions of Na and K Adlayers on Al(111). *Phys. Rev. B: Condens. Matter Mater. Phys.* **1992**, *46*, 16067−16080.
(40) Bučko, T.; Hafner, J.; Ángyán, J. G. Geometry Optimization of Periodic Systems Using Internal Coordinates. *J. Chem. Phys.* **2005**, *122*, 124508.
(41) Müllegger, S.; Schöfberger, W.; Rashidi, M.; Lengauer, T.; Klappenberger, F.; Diller, K.; Kara, K.; Barth, J. V.; Rauls, E.; Schmidt, W. G.; et al. Preserving Charge and Oxidation State of Au(III) Ions in an Agent-Functionalized Nanocrystal Model System. *ACS Nano* **2011**, *5*, 6480−6486.
(42) Heinrich, B. W.; Ahmadi, G.; Müller, V. L.; Braun, L.; Pascual, J. I.; Franke, K. J. Change of the Magnetic Coupling of a Metal−Organic Complex with the Substrate by a Stepwise Ligand Reaction. *Nano Lett.* **2013**, *13*, 4840−4843.
(43) Gutzler, R.; Walch, H.; Eder, G.; Kloft, S.; Heckl, W. M.; Lackinger, M. Surface Mediated Synthesis of 2D Covalent Organic Frameworks: 1,3,5-tris(4-Bromophenyl)benzene on graphite(001), Cu(111), and Ag(110). *Chem. Commun.* **2009**, No. 29, 4456.
(44) Koch, M.; Gille, M.; Viertel, A.; Hecht, S.; Grill, L. Substrate-Controlled Linking of Molecular Building Blocks: Au(111) vs. Cu(111). *Surf. Sci.* **2014**, *627*, 70−74.
(45) Crapper, M. D.; Riley, C. E.; Sweeney, P. J. J.; McConville, C. F.; Woodruff, D. P.; Jones, R. G. Investigation of the Cu(111) ($\sqrt{3} \times \sqrt{3}$)R30°-Cl Structure Using Sexafs and Photoelectron Diffraction. *Surf. Sci.* **1987**, *182*, 213−230.
(46) Guilleme, J.; Martínez-Fernández, L.; González-Rodríguez, D.; Corral, I.; Yáñez, M.; Torres, T. An Insight into the Mechanism of the Axial Ligand Exchange Reaction in Boron Subphthalocyanine Macrocycles. *J. Am. Chem. Soc.* **2014**, *136*, 14289−14298.
(47) De Renzi, V.; Rousseau, R.; Marchetto, D.; Biagi, R.; Scandolo, S.; del Pennino, U. Metal Work-Function Changes Induced by Organic Adsorbates: A Combined Experimental and Theoretical Study. *Phys. Rev. Lett.* **2005**, *95*, 046804.
(48) Rusu, P. C.; Brocks, G. Work Functions of Self-Assembled Monolayers on Metal Surfaces by First-Principles Calculations. *Phys. Rev. B: Condens. Matter Mater. Phys.* **2006**, *74*, 073414.
(49) Hill, I. G.; Rajagopal, A.; Kahn, A.; Hu, Y. Molecular Level Alignment at Organic Semiconductor-Metal Interfaces. *Appl. Phys. Lett.* **1998**, *73*, 662−664.
(50) Crispin, X.; Geskin, V.; Crispin, A.; Cornil, J.; Lazzaroni, R.; Salaneck, W. R.; Brédas, J.-L. Characterization of the Interface Dipole at Organic/ Metal Interfaces. *J. Am. Chem. Soc.* **2002**, *124*, 8131−8141.
(51) Crispin, A.; Crispin, X.; Fahlman, M.; Berggren, M.; Salaneck, W. R. Transition between Energy Level Alignment Regimes at a Low Band Gap Polymer-Electrode Interfaces. *Appl. Phys. Lett.* **2006**, *89*, 213503.
(52) Koch, N. Organic Electronic Devices and Their Functional Interfaces. *ChemPhysChem* **2007**, *8*, 1438−1455.
(53) Braun, S.; Salaneck, W. R.; Fahlman, M. Energy-Level Alignment at Organic/Metal and Organic/Organic Interfaces. *Adv. Mater.* **2009**, *21*, 1450−1472.
(54) Hofmann, O. T.; Egger, D. A.; Zojer, E. Work-Function Modification beyond Pinning: When Do Molecular Dipoles Count? *Nano Lett.* **2010**, *10*, 4369−4374.
(55) Edlbauer, H.; Zojer, E.; Hofmann, O. T. Postadsorption Work Function Tuning via Hydrogen Pressure Control. *J. Phys. Chem. C* **2015**, *119*, 27162−27172.

DOI: 10.1021/acs.jpcc.6b00312
J. Phys. Chem. C 2016, 120, 6869−6875

Supporting Information:

On the Adsorption Behavior of Nonplanar Phthalocyanines: Competition of Different Adsorption Conformations

*Elisabeth Wruss[1], Oliver T. Hofmann[1], David A. Egger[1†], Elisabeth Verwüster[1], Alexander Gerlach[2], Frank Schreiber[2] and Egbert Zojer[1]**

[1] Institute of Solid State Physics, NAWI Graz, Graz University of Technology, 8010 Graz, Austria.

[2] Institut für Angewandte Physik, Universität Tübingen, 72076 Tübingen, Germany.

Corresponding Author

* egbert.zojer@tugraz.at

Present Addresses

† Department of Materials and Interfaces, Weizmann Institute of Science, Rehovoth 76100, Israel.

PAW potentials

The following VASP PAW potentials[1,2] were used:

- PAW_PBE Cu 22Jun2005
- PAW_PBE C 08Apr2002
- PAW_PBE N 08Apr2002
- PAW_PBE H 15Jun2001
- PAW_PBE Ga 08Apr2002
- PAW_PBE Cl 06Sep2000

GADGET calculations

The GADGET calculations were performed with internal coordinates, using the RFO[3] (first step, pre-optimization) and DIIS (second step)[4,5] algorithms for the geometry steps, and the BFGS update algorithm[6–9] for the Hesse matrix.

Unit cells

To our knowledge, no exact unit cell for GaClPc on Cu(111) is known. Numerous test simulations in differently sized unit cells were performed, which led us to finally choose one that covers a surface area of about 321 Å^2. We compared this cell to the one of a quite a similar system, namely ClAlPc on Au(111), which was investigated via STM measurements by Huang et al..[10] The ClAlPc molecule requires a surface unit cell of about 260 Å^2, so we can assume that our calculations represent a coverage of about 80%. Smaller cells with surface areas more similar to the one for ClAlPc on Au were tested, but led to convergence problems (see below). Additionally, a curious tilting of the molecule appeared in several cases, which was presumably

caused by too close packing. The surface unit cell used for GaClPc on Cu(111) with a surface area of about 321 Å^2 and 56 Cu atoms per layer can be described using the following equation, with *A* and *B* denoting the surface unit cell vectors and *a* and *b* denoting the primitive unit cell vectors of the underlying fcc(111) surface:

$$\begin{bmatrix} A \\ B \end{bmatrix} = \begin{bmatrix} 7 & 0 \\ -4 & 8 \end{bmatrix} \begin{bmatrix} a \\ b \end{bmatrix}$$

Geometry change during geometry optimization

Before geometry optimization, the molecular backbone was flat and positioned about 3.5 Å above the Cu surface. All configurations were started with the Ga atom above a hollow position of the Cu(111) substrate, with the Cl atom lying directly above/below the Ga atom (vertical distance 2 Å) for Cl-up and Cl-down. For Cl-diss, the Cl atom was placed in a separate hollow position at least 4 Å from the closest H atom of the GaPc molecule. The molecular lobes were rotated about 27° relative to the borders of the unit cell, inspired by the geometry of ClAlPc on Au(111).[10] During geometry optimization, the molecule moved slightly such that the Ga atom settled at a bridge position of the Cu(111) surface for Cl-up and Cl-diss. For Cl-down, the Cl atom stayed in the hollow position and the rest of the molecule tilted sideways slightly, resulting in a Ga-Cl bond not exactly perpendicular to the Cu surface. The molecules also slightly rotated on the surface. In case of Cl-up and Cl-diss, the angle of the lobes relative to the borders of the unit cell increased to about 30°, while for Cl-down it slightly decreased to 26°.

Additional calculations

Smaller unit cell (48 Cu atoms per surface layer)

Several test calculations were performed in a smaller unit cell with 48 Cu atoms per surface layer and a surface are of about 275 $Å^2$. In some cases this led to a strongly distorted molecular geometry, with the molecular backbone violently bent. Albeit the molecule in principle still adopted a close to flat-lying structure, the backbone carbon atoms spread over a height range of more than 4 Å. This massive distortion was presumably a consequence of a too close packing of the molecules. In addition, this small unit cell led to convergence problems in several cases. The calculation method with one molecule per unit cell and applying periodic boundary conditions demands a commensurable structure. Therefore we employed the next larger unit cell with 56 atoms per Cu layer, which is the one described in detail in the section "Unit cells". The data shown in the main manuscript also have been obtained using that unit cell. In this larger unit cell, the bent geometry was not obtained, not even when we started the geometry optimization with a tilted molecular geometry which should promote this configuration; moreover, no convergence problems were encountered.

Different starting configurations and VASP settings for the Cl-down configuration

As described in the main text, numerous tests on the Cl-down case were performed to make sure that the discrepancies between the simulated geometries and the XSW results are not caused by a bias in the simulation, e.g. an unsuitable starting point.

Starting geometries of the molecule:

In the reference calculations, the molecule was initialized with a flat backbone, meaning that all C, N and H atoms were positioned at the same height, while the Cl atom was positioned 2 Å below the Ga atom. To check the influence of this initialization, we also started simulations from a geometry in which the atoms were placed at the XSW-determined adsorption heights reported in Ref. 11 and choosing an umbrella-shaped geometry for the molecular backbone. We also used the gas-phase structure of the GaClPc molecule, optimized in a large unit cell with dipole corrections in all three spatial directions, as a starting configuration. As mentioned in the main text, the experimental Cl-down configuration places the Ga atom below the molecular backbone, while our simulations find it above. To check the influence of this factor, we initialized the geometry for another simulation by taking the fully relaxed structure of the molecule as obtained from the reference optimization and shifted the Ga atom (and the Cl atom accordingly) to 0.25 Å, respectively, 0.50 Å below the average height of the molecular backbone. Full geometry optimization for all these structures did not cause any significant change in the resulting geometry compared to the reference calculations started from a flat geometry.

Starting position of the molecule:

We also checked the influence of the starting position of the molecule relative to the underlying surface. In the reference calculations, the center of the molecule, namely the Ga and

Cl atom were positioned above a hollow position of the underlying fcc metal. We moved the molecule from this position to positions above the on-top and bridge positions and started geometry optimizations from there. In both cases, the molecule moved back to the hollow position upon geometry optimization.

Starting angle of the molecule:

As mentioned above, the lobes of the molecule were rotated by about 27° relative to the unit cell borders in the reference starting geometry. We also tried to position the molecules parallel to the borders as well as at a 45° angle. In both cases, the molecules did not significantly move out of this configuration during geometry optimization. The final energies were, however, somewhat higher than in the reference calculation. The obtained adsorption heights were again similar to what we found for all other starting configurations.

Calculation of charge rearrangements $\Delta\rho$ and bond dipole $\Delta\Phi_{bond}$

The charge rearrangements $\Delta\rho$ can be calculated by subtracting the charge densities of the isolated slab ρ_{slab} and the (hypothetical) free standing monolayer $\rho_{monolayer}$ from the charge density of the combined system ρ_{system}:

$$\Delta\rho = \rho_{system} - \rho_{monolayer} - \rho_{slab}.$$

In the Cl-diss case, the charge density of the monolayer was subdivided into a contribution from the GaPc molecules and the Cl atoms and they were calculated separately. This was done to avoid spurious charge transfer effects. The bond dipole $\Delta\Phi_{bond}$ can then be obtained from the charge rearrangements by solving Poisson's equation.

Symmetry reduction upon adsorption

For the Cl-up and Cl-diss configurations, the geometries display a symmetry reduction from 4-fold to 2-fold, with two oppositely positioned molecular lobes lying closer to the surface than the other two. This can be assigned to a strong interaction between the lobes of the four-fold symmetric Pc molecule and the underlying six-fold symmetric top Cu(111) layer. Keeping in mind that this interaction is stronger for small adsorption distances of the backbone (Cl-up and Cl-diss), we can understand why we do not observe it for the Cl-down case. The carbon atoms of the branches which are interacting more strongly consistently lie lower than the other ones (height differences for the outermost rings amount to 0.25 Å for Cl-up and 0.31 Å for Cl-diss). Similar effects have been seen for FePc,[12] CuPc[12,13] and CoPc[12,14] on Cu(111) and also for SnPc on Ag(111).[15] Our observations on symmetry reduction are in contrast to the work on ClAlPc on Cu(111) by Niu et al.,[16] who found symmetry reduction for the Cl-down, but nor for the Cl-up configuration. The adsorption distances received by DFT in this work are on average more than one angstrom higher than our adsorption heights, for both Cl-up and Cl-down, which might originate from the use of a different vdW correction method (DFT-D2[17]), which is, to our knowledge, not as well suited for treating interfaces as vdW^{surf}.[18,19] In addition, the different centering metal might also influence the symmetry-reduction effect.

Density of states projected on the adsorbate layer and separately on the Ga atoms

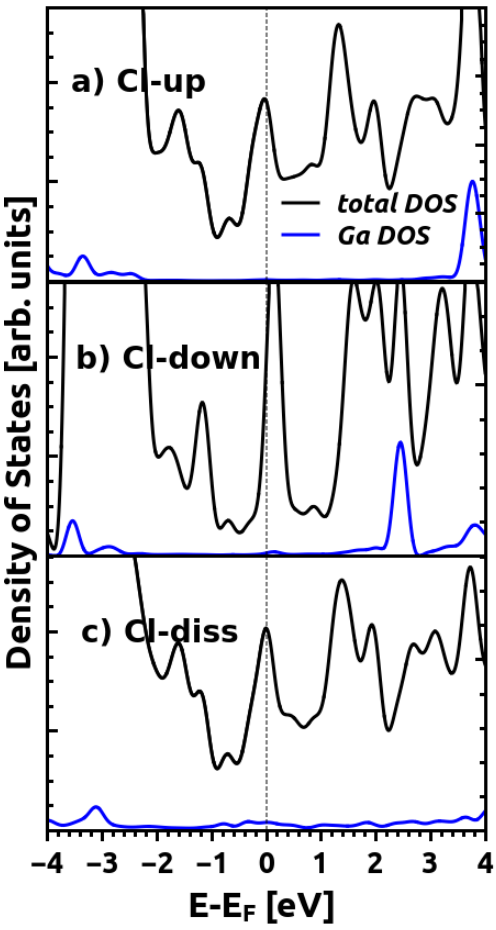

Figure S1. *PBE calculated density of states projected onto the adsorbate layer (black) and separately onto the Ga atoms (blue) for the Cl-up (a), Cl-down (b) and Cl-diss (c) configurations. The energy is aligned to the Fermi energy, which is indicated by the dotted lines. As mentioned in the main manuscript, no Ga-derived states are found close to the Fermi energy.*

References

(1) Blöchl, P. E. Projector Augmented-Wave Method. *Phys. Rev. B* **1994**, *50*, 17953–17979.
(2) Kresse, G.; Joubert, D. From Ultrasoft Pseudopotentials to the Projector Augmented-Wave Method. *Phys. Rev. B* **1999**, *59*, 1758–1775.
(3) Banerjee, A.; Adams, N.; Simons, J.; Shepard, R. Search for Stationary Points on Surfaces. *J. Phys. Chem.* **1985**, *89*, 52–57.
(4) Császár, P.; Pulay, P. Geometry Optimization by Direct Inversion in the Iterative Subspace. *J. Mol. Struct.* **1984**, *114*, 31–34.
(5) Farkas, O.; Schlegel, H. B. Methods for Optimizing Large Molecules. Part III. An Improved Algorithm for Geometry Optimization Using Direct Inversion in the Iterative Subspace (GDIIS). *Phys. Chem. Chem. Phys.* **2002**, *4*, 11–15.
(6) Broyden, C. G. The Convergence of a Class of Double-Rank Minimization Algorithms 1. General Considerations. *IMA J. Appl. Math.* **1970**, *6*, 76–90.
(7) Fletcher, R. A New Approach to Variable Metric Algorithms. *Comput. J.* **1970**, *13*, 317–322.
(8) Goldfarb, D. A Family of Variable-Metric Methods Derived by Variational Means. *Math. Comput.* **1970**, *24*, 23–26.
(9) Shanno, D. F. Conditioning of Quasi-Newton Methods for Function Minimization. *Math. Comput.* **1970**, *24*, 647–656.
(10) Huang, Y. L.; Chen, W.; Bussolotti, F.; Niu, T. C.; Wee, A. T. S.; Ueno, N.; Kera, S. Impact of Molecule-Dipole Orientation on Energy Level Alignment at the Submolecular Scale. *Phys. Rev. B* **2013**, *87*, 085205.
(11) Gerlach, A.; Hosokai, T.; Duhm, S.; Kera, S.; Hofmann, O. T.; Zojer, E.; Zegenhagen, J.; Schreiber, F. Orientational Ordering of Nonplanar Phthalocyanines on Cu(111): Strength and Orientation of the Electric Dipole Moment. *Phys. Rev. Lett.* **2011**, *106*, 156102.
(12) Chang, S.-H.; Kuck, S.; Brede, J.; Lichtenstein, L.; Hoffmann, G.; Wiesendanger, R. Symmetry Reduction of Metal Phthalocyanines on Metals. *Phys. Rev. B* **2008**, *78*, 233409.
(13) Karacuban, H.; Lange, M.; Schaffert, J.; Weingart, O.; Wagner, T.; Möller, R. Substrate-Induced Symmetry Reduction of CuPc on Cu(1 1 1): An LT-STM Study. *Surf. Sci.* **2009**, *603*, L39–L43.
(14) Cuadrado, R.; Cerdá, J. I.; Wang, Y.; Xin, G.; Berndt, R.; Tang, H. CoPc Adsorption on Cu(111): Origin of the C4 to C2 Symmetry Reduction. *J. Chem. Phys.* **2010**, *133*, 154701.
(15) Baran, J. D.; Larsson, J. A. Structure and Energetics of Shuttlecock-Shaped Tin-Phthalocyanine on Ag(111): A Density Functional Study Employing Dispersion Correction. *J. Phys. Chem. C* **2012**, *116*, 9487–9497.
(16) Niu, T.; Zhou, M.; Zhang, J.; Feng, Y.; Chen, W. Dipole Orientation Dependent Symmetry Reduction of Chloroaluminum Phthalocyanine on Cu(111). *J. Phys. Chem. C* **2013**, *117*, 1013–1019.
(17) Grimme, S. Semiempirical GGA-Type Density Functional Constructed with a Long-Range Dispersion Correction. *J. Comput. Chem.* **2006**, *27*, 1787–1799.
(18) Mercurio, G.; McNellis, E. R.; Martin, I.; Hagen, S.; Leyssner, F.; Soubatch, S.; Meyer, J.; Wolf, M.; Tegeder, P.; Tautz, F. S.; et al. Structure and Energetics of Azobenzene on Ag(111): Benchmarking Semiempirical Dispersion Correction Approaches. *Phys. Rev. Lett.* **2010**, *104*, 036102.

(19) Ruiz, V. G.; Liu, W.; Zojer, E.; Scheffler, M.; Tkatchenko, A. Density-Functional Theory with Screened van Der Waals Interactions for the Modeling of Hybrid Inorganic-Organic Systems. *Phys. Rev. Lett.* **2012**, *108*, 146103.

3.2.3 Additional Analysis of GaClPc on Cu(111)

The preliminary calculations on the GaClPc/Cu(111) system have already been discussed in my master thesis, where different unit cells, adsorption sites and methodologies were discussed.[23]
Further insight into the interaction of the molecule with the substrate can be gained from investigating the bonding-induced charge-rearrangements $\Delta\rho$. They can be calculated by subtracting the charge densities of the isolated slab ρ_{slab} and (hypothetical) free standing monolayer ρ_{ml} from the charge density of the combined system.

$$\Delta\rho = \rho_{system} - \rho_{slab} - \rho_{ml} \tag{3}$$

For the Cl-diss system, the two (spin-polarized) monolayer densities of the GaPc molecules and the Cl atom were calculated and subtracted separately to avoid spurious interactions. Fig. 9 shows a 3D representations of $\Delta\rho$, with yellow regions indicating electron accumulation and blue regions indicating electron depletion.
The processes one expects to occur at the interface are (i) Pauli pushback describing the imprint of the molecule on the tailing electron cloud of the metal surface,[116] (ii) charge transfer from the substrate to the π-backbone considering the electron accepting properties typically found for phthalocyanine films on Cu(111),[117, 118] and (iii) additional charge rearrangements due to a bond-formation between the Cl or Ga atoms and the metal surface. Consistent with the partial filling of the LUMO-derived band discussed in the above article, for all three systems, charge accumulation in the π-system of the molecular backbone can be seen. This effect is least pronounced for Cl-down. Also Pauli pushback can be resolved in all cases as an electron-density depletion above the top metal layer. It is laterally confined to the region underneath the molecule and to the (high-electron density) σ-region of the molecules. Again the effect is particularly strong for Cl-up and Cl-diss, which can be understood from the exponential dependence of the wavefunction overlap on the metal-molecule distance. For the two "closer" configurations, the charge rearrangements display a two-fold symmetry as a result of the four-fold symmetric structure of the molecules combined with a six-fold symmetry of the topmost layer of Cu(111). This symmetry reduction effect was already visible from the molecular geometries, where two opposite molecular branches are positioned about 0.25Å lower than the other two for the Cl-up scenario (and 0.31 Å for the Cl-diss scenario). The stronger charge transfer into the lower lying branches of the molecule results in a splitting of the former LUMO, which is, however, rather small and does not become visible in the DOS (see article above). Similar effects have been seen, e. g., also for FePc,[119] CuPc,[119, 120] and CoPc [117, 119] on Cu(111) and SnPc on Ag(111).[121]
The polar Ga-Cl region of the Cl-up configuration which bends away from the surface is not affected by the bonding. This is in sharp contrast to the Cl-down case, where massive charge redistributions occur primarily in the region of this polar Ga-Cl bond. The strong charge rearrangements below the Ga atom in Cl-diss are an indication for

the significant interaction between Ga and the metal substrate, which is absent in the Cl-up case. This finding is consistent with the different positions of the Ga atoms relative to the π-backbone, which seeks stronger interaction with the Cu substrate when it is no longer saturated by the Cl atom, as discussed above.

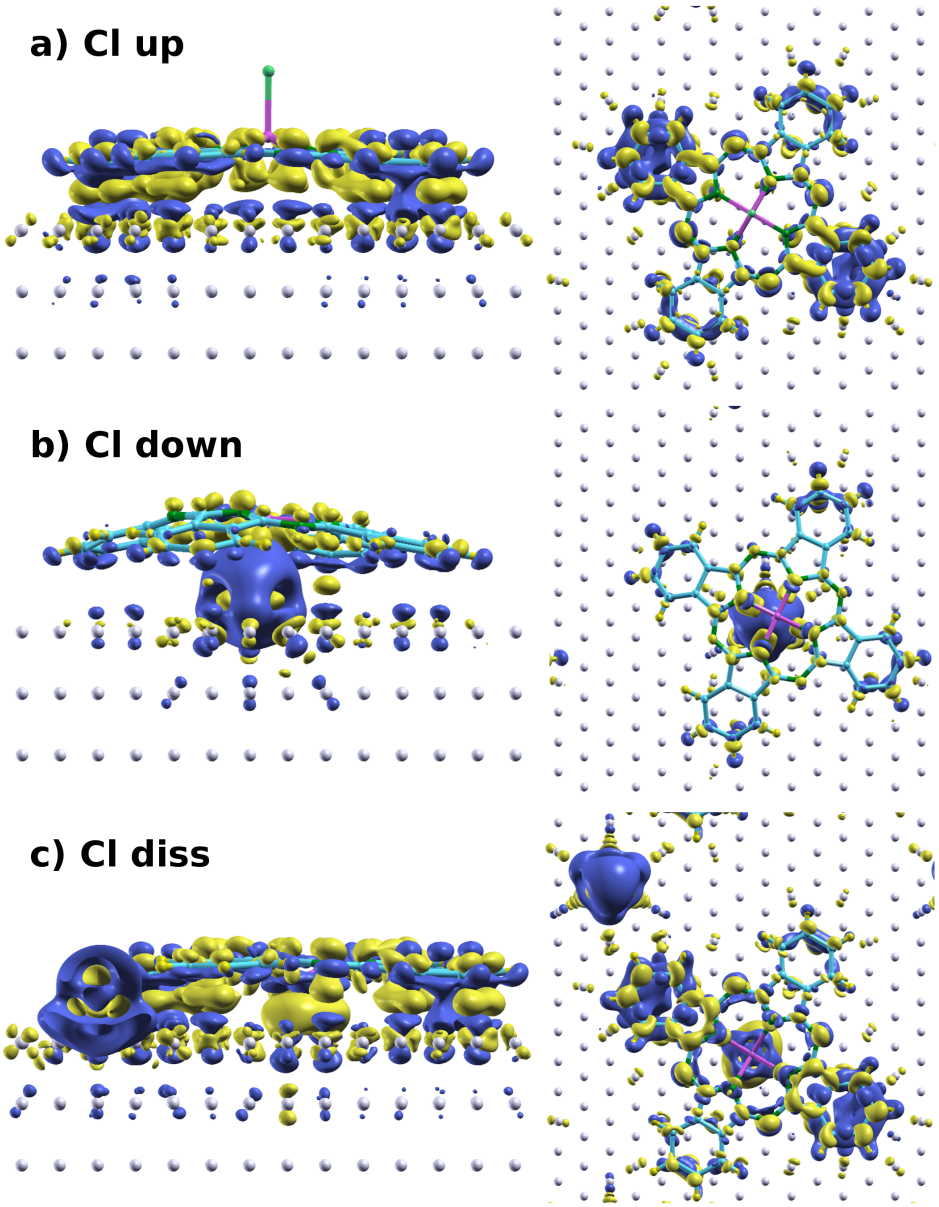

Figure 9: Isodensity plots of the charge rearrangements due to adsorption of the GaClPc molecule on the Cu(111) surface. The Cl-up (a), Cl-down (b) and Cl-diss (c) configurations are shown. The charge rearrangements are derived by subtracting the charge density of the isolated monolayer and slab from the charge density of the combined systems. Yellow regions indicate electron accumulation while blue regions show electron depletion. The isovalue for the plot was set to 0.01 eV/Å^3.

3.3 Adsorption of Chlorinated Tin Phthalocyanine SnClPc on Ag(111)

In this section, a molecule similar to the previously investigated GaClPc is discussed, namely chlorinated tin phthalocyanine SnClPc. The double chlorinated $SnCl_2Pc$ is shown in Fig. 11. The adsorption behavior of (different) chlorinated tin phthalocyanine molecules on Ag(111) surfaces was investigated.
These simulations were done to shed light on the adsorption configuration, which is not clear from experiment alone.
The experimental analysis was done by Christian Zwick, Marco Grünewald and Torsten Fritz from Friedrich Schiller University Jena (Germany), Gerben van Straaten and Christan Kumpf from Forschungszentrum Jülich (Germany) and Takahiro Ueba and Sathoshi Kera from the Institute for Molecular Science Okazaki (Japan).
The experimental results indicate that for $SnCl_2Pc$ adsorption on Ag(111), at least one of the Cl atoms is dissociated from the molecule upon adsorption, resulting effectively in a SnClPc layer. They also suggest that adsorption takes place in a Cl-down configuration. Several indications exist that the Cl atom is penetrating into the Ag substrate without being detached from the molecule.
The main questions to be investigated via simulations are (i) whether the experimentally proposed structure is a viable scenario, (ii) how the structure underneath the adsorbed atoms (concerning possible Ag vacancies) would actually look like and (iii) whether the notion of a Cl atom "digging" into the surface is energetically reasonable.
To answer these questions, several different structures of SnClPc adsorption were simulated, including structures where the Cl atom is dug into the Ag substrate and one (or several) Ag substrate atoms are removed. Additionally, alternative possible adsorption structures were simulated and their consistency with experimental results was checked.
In the following, the experimental results provided by Christian Zwick are summarized briefly. Then, the simulations of plausible adsorption structures are discussed and compared to experiments. The main focus lies on the variety of Cl-down structures. For these configurations, also an estimation for the vacancy formation energy and the adsorption energy is presented.

3.3.1 Experimental Results

As mentioned above, the (unpublished) experimental results were provided by Christan Zwick (and coworkers), and the following discussion is based on my correspondence with him.
In these experiments, $SnCl_2Pc$ was evaporated onto the Ag(111) surface, and different coverages were considered. Here, the full monolayer coverage is discussed.
Low energy electron diffraction LEED and scanning tunneling microscopy STM measurements were used to find the surface adsorption unit cell. The results indicate a unit

cell containing two flat-lying molecules, which form molecular pairs. An STM picture indicating the corresponding structure is shown in Fig. 10.
The STM pictures also suggest that the adsorbed molecule is no longer $SnCl_2Pc$, as an upward pointing Cl atom should be visible as a bright spot in the STM. That means that the molecule either adsorbs in a Cl-down configuration, or both Cl atoms are detached and only SnPc molecules remain.
The adsorption of SnPc can be ruled out experimentally, as data on this system is already published and does not agree with the results discussed here. The LEED patterns as well as the STM structures are very different, and evaporating both SnPc and $SnCl_2Pc$ clearly results in phase separation of two different molecular species on the surface. However, the presence of defect SnPc molecules in the experimentally considered structures is possible.
Therefore, the adsorption in a Cl-down configuration appears to be most likely. Results from differential reflectance spectroscopy DRS show strong broadening of the molecular features, indicating strong hybridization, which usually happens at small adsorption distances.
XSW measurements put the Sn atom at an adsorption height of 2.31 Å above the (unrelaxed) Ag substrate. For the Cl atom, this means that it has to penetrate into the substrate, resulting in a Cl adsorption height of 0.24 Å below the topmost Ag layer. An alternative scenario arises from shifting the whole molecule one Ag layer spacing up, as discussed before for the GaClPc/Cu(111) system. However, this would result in very large adsorption heights, where the above mentioned broadening of molecular features is unlikely to appear. Additionally, in the co-adsorption of SnPc and SnClPc, similar adsorption heights of the different molecules are seen. As the Cl up structure was rendered to be unlikely from STM results, the scenario with Cl penetrating the Ag surface is the only remaining viable solution.
As no strong experimental indication for the Cl penetration could be found, this raises the question, whether such a scenario is likely and energetically reasonable. Surface rearrangements of Ag upon Cl adsorption have been seen experimentally, and the results show a situation with the topmost surface layer being a mixed Cl-Ag structure.[122] In addition, experimental evidence for vacancy formation underneath adsorbed molecules on Ag surfaces exists. For example, for the adsorption of C_{60} on Ag(111), vacancy formation below the adsorbed molecules was found.[123]
As mentioned above, the experimentally proposed scenario is SnClPc adsorption in a Cl-down configuration with Cl lying below the topmost Ag layer, and the formation of Ag vacancies is very likely. However, what is not clear from experiment is the fate of the detached Cl atoms. They might either diffuse into the Ag substrate (which is, however, unlikely according to earlier results about Cl on Ag [124]) or desorb as Cl_2. In STM, the Cl atoms are not seen on the surface, and their adsorption underneath the remaining SnClPc molecules is unlikely due to the low adsorption heights. For similar systems on Cu, different scenarios for detached Cl atoms have been observed. While for GaClPc, the Cl atoms clearly do remain on the surfacer and are seen in experimental XSW results, there are also experimental studies of adsorbed sub-phthalocyanine

molecules where the detached Cl atoms are not seen on the surface and their fate is unclear.[125]

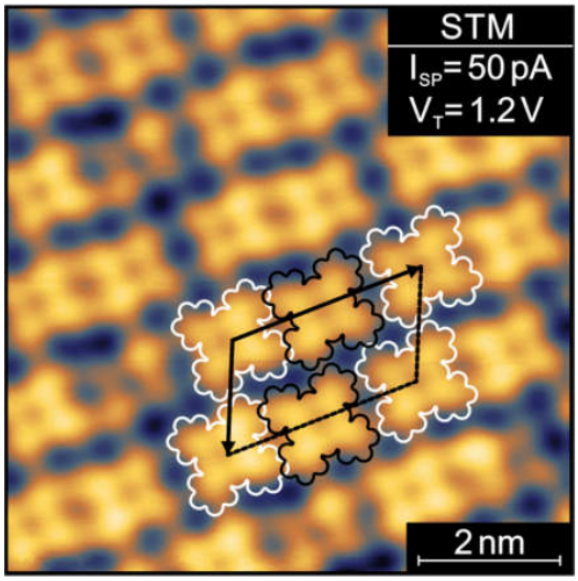

Figure 10: STM picture of SnClPc adsorbed on Ag(111), kindly provided by Christian Zwick. The molecular adsorption positions in the suggested unit cell are indicated.

3.3.2 System and Methodology

The experimentally considered molecule is Sn phthalocyanine with two Cl atoms attached to the central Sn atom, as shown in Fig. 11. Adsorption calculations of this molecule as well as of two (party) dechlorinated derivatives, SnClPc and SnPc, were performed.

Unit Cell
The unit cell was chosen based on the experimental results provided by Christian Zwick. It contains two SnClPc molecules at different adsorption sites and has an epitaxy matrix of $\begin{pmatrix} 6 & 5 \\ 8 & 3 \end{pmatrix}$. The cell is shown in Fig. 12, where also the molecular arrangement as seen from STM, with a pairing of the two SnClPc molecules, is indicated.
For some initial tests, an unit cell with half the surface area and only one molecule was used, to identify general trends of the molecular geometry upon adsorption. Unfortunately, this one-molecule cell showed a very poor convergence behavior. This is most likely caused by the fact that such a cell prohibits the observer molecular pair formation, which results in the surface area assigned per molecule being too small.

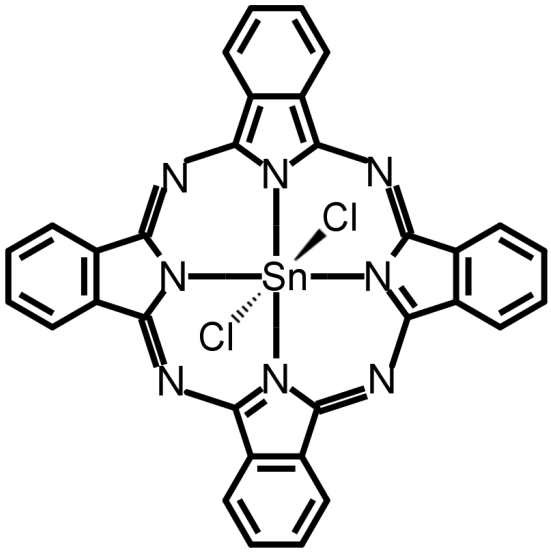

Figure 11: Structure of the doubly chlorinated Sn phthalocyanine ($SnCl_2Pc$) molecule.

Therefore, all further calculations which are presented in the following were performed in the shown two-molecule unit cell, with varying positions of the adsorbed molecules. The starting configurations were generated such that the parallel arrangement of the molecular axes was preserved. The first molecules was always positioned with its central Sn atom close to the unit cell origin (at the next closest desired lattice site, on on-top, bridge or hollow positions of the fcc lattice), while the second one was positioned at a site close to the bisection of the long unit cell axis, as shown in Fig. 12. Depending on the chosen adsorption sites, the distance between the molecules along the long molecular axis amounted to approximately 14.5 Å in both directions. The experimentally observed molecular pairing was, if possible, not initialized to observe whether it would form during geometry optimizations. Note that in the following, the molecular adsorption sites denote the position of the central Sn atom of the Pc molecules at the Ag(111) surface.
Five substrate layers were used to mimic the Ag bulk, and a vacuum gap of at least 20 Å above the molecule was applied.

DFT Methodology
All calculations were performed with the VASP code,[97] applying the PBE exchange-correlation functional.[41, 42] VASP standard PAW potentials with a energy cutoff of 500 eV were used. A Monkhorst-Pack [126] k-point grid of *3x3x1* was applied. The PBE lattice constant for Ag, which was optimized previously, was set to 4.154 Å (compared to a literature value of 4.079 Å [127]). The total SCF energies were converged to 1E-6 eV. To correct for vdW forces, the vdW^{surf} method [68] was used.
GADGET [4] was applied for the geometry optimizations and all molecular atoms and

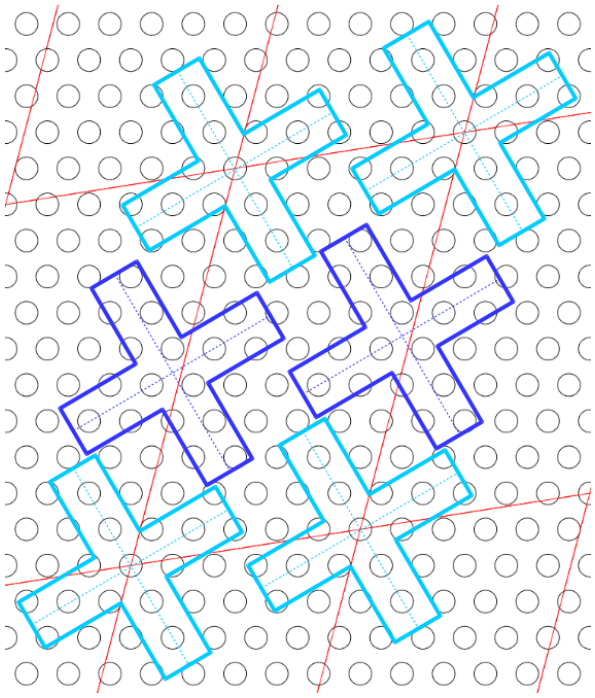

Figure 12: Unit cell of SnClPc on Ag(111) with the adsorption of two molecules, indicated in light and dark blue, in on-top and hollow positions.

the topmost two substrate Ag layers were allowed to relax in all spatial directions. Full geometry convergence was considered to be reached at forces below 0.01 eV/Å. However, not all geometry optimizations were pursued until full convergence was reached, as mainly the general trends were of interest. In the following, for all calculations where the optimization was terminated before full convergence, the maximum remaining forces are given explicitly.

3.3.3 Different Adsorption Scenarios

As discussed previously, the experimentally proposed structure is that SnClPc molecules adsorb in a Cl-down configuration, with the remaining Cl atom penetrating into the Ag surface and low adsorption heights of the molecule. What remained to be determined from simulations was how reasonable this experimentally proposed structure is, and how exactly the molecular configuration underneath the molecule looks, how the Cl atom is buried in the surface, whether vacancies are formed in the Ag substrate and, if so, how many substrate atoms have to be removed upon adsorption. Additionally, it should to be determined whether such a structure is also energetically reasonable.
As a starting point, it was checked whether structures other than Cl-down with Ag substrate vacancies underneath the molecule could also agree with the experimental

results. To do so, all possible scenarios, namely $SnCl_2Pc$ adsorption, SnPc adsorption and SnClPc adsorption in the Cl-up and Cl-down scenario on an unmodified Ag substrate were simulated. What could be compared to experimental results to verify structures were (i) the arrangement of the two molecules relative to each other in the unit cell, and (ii) the adsorption heights of Sn and Cl atoms. In the STM images, a pairing of molecules on the surface is observed. The molecular axes align parallel to each other (see Fig. 12). According to the XSW results, the Cl atoms adsorb at a height lying below the topmost Ag layer (-0.24 Å), while the Sn atoms lie 2.31 Å above the surface.

$SnCl_2Pc$ on Ag(111)

A simulation of $SnCl_2Pc$ on Ag(111) was started with both molecules above on-top sites of the substrate (see Fig. 13a). The initial height of the backbone relative to the topmost surface layer amounted to 4.5 Å.

During optimization, the molecules moved from the on-top position into fcc hollow sites and deformed quite strongly, as shown in Fig. 13c.

The molecules did move closer toward each other, resulting in the experimentally observed pairing. Along the long unit cell axis, a final Sn-Sn distance of 13.8 Å to the closer neighbor and 15.4 Å to the distant neighbor (in the adjoining unit cell) was measured.

The molecules were initially arranged with their axes parallel to each other, but did not preserve this configuration during the optimization, and finally reached a twist angel of about 10° toward each other, as seen in Fig. 13b.

The resulting adsorption heights are given in Tab. 1.

This configuration does not agree well with the experiments regarding both the molecular arrangement and also the adsorption heights. In conclusion, adsorption of the $SnCl_2$ molecule without any dechlorination can be discarded, as it was declared unlikely form experiment alone and additionally the simulated and experimental results do not match for this configuration.

Table 1: Averaged adsorption heights relative to the unrelaxed topmost substrate layer of all atomic species of $SnCl_2Pc$ on Ag(111). The simulated DFT values and the experimental XSW values are given. The experimental heights are corrected by the Cu lattice spacing of 2.36 Å to fit the considered configuration.

	DFT	XSW
C	3.180 Å	
N	3.671 Å	
H	2.827 Å	
Sn	4.280 Å	4.67Å
Cl 1	6.607 Å	6.84 Å
Cl 2	1.566 Å	2.12 Å

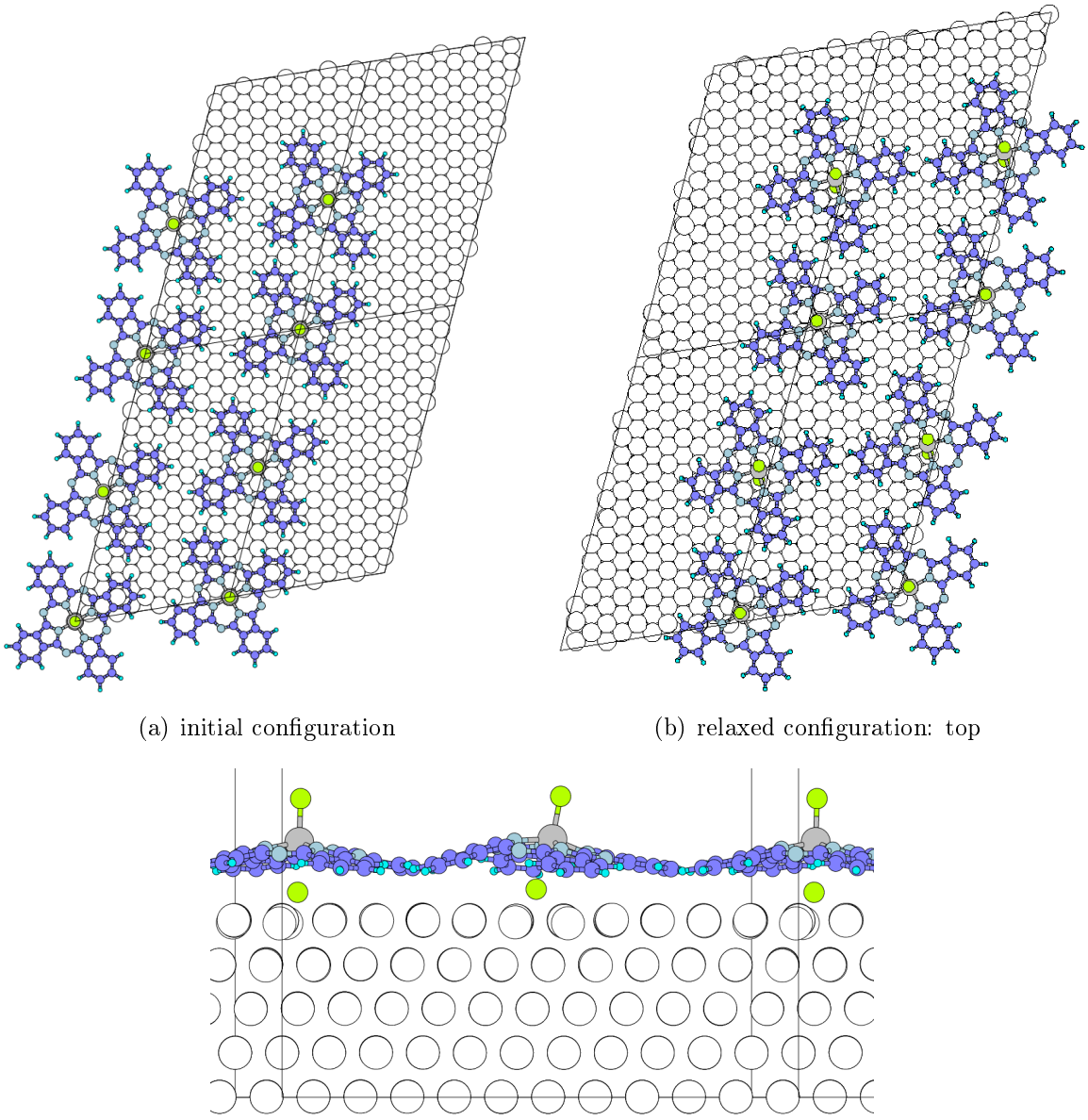

(a) initial configuration

(b) relaxed configuration: top

(c) relaxed configuration: side

Figure 13: Initial and final geometries of $SnCl_2Pc$ on Ag(111)

SnPc on Ag(111)

For the adsorption of SnPc, tests were performed with the molecules initially positioned on different sites, namely on-top, bridge and fcc hollow sites. For both molecules in the cell, equivalent positions were chosen. The on-top and bridge positions resulted in strong lateral movements of the molecules, which where clearly not in a minimum as this position. Therefore, only the fcc hollow site calculation was pursued further and

is discussed in the following.
During geometry relaxation, the molecule at the corner of the unit cell stayed in its initial fcc hollow position, while the second molecule moved toward an hcp hollow site to enlarge the intermolecular distance. The molecular backbone stayed flat, with the Sn atom lying about 0.7 Å closer to the surface than the C and N atoms. All final adsorption height are shown in Tab. 2.
In the final geometry, the Sn-Sn distance amounts to 14.2 Å to the closer neighbor and to 14.8 Å to the distant neighbor along the long unit cell axis.
From the comparison of the present simulation to experimental results, no clear conclusions can be drawn. The lateral structure of the molecules is consistent with the experimental results, as the molecular axes stay parallel and molecular pairs are formed. The adsorption height of Sn differs by 0.12 Å from the experimental XSW results, which is a reasonable agreement. The presence of Cl atoms in the XSW results would then indicate that isolated Cl has to adsorb on the surface. When the experimental Cl adsorption heights are re-interpreted by adding one Ag lattice layer spacing, the isolated Cl atoms would adsorb at 2.12 Å, which is very well in line with experimental results of Cl adsorbing on Ag(111).[128]
The simulation of SnPc adsorption would give reasonably good agreement with experiments, however, this scenario was definitely discarded due to the interpretation of the experimental results (see above).

Table 2: Averaged adsorption heights relative to the unrelaxed topmost substrate layer of all atomic species of SnPc on Ag(111). The simulated DFT values and the experimental XSW values are given.

	DFT	XSW
C	2.94 Å	
N	2.85 Å	
H	2.85 Å	
Sn	2.19 Å	2.31 Å

SnClPc on Ag(111) in Cl-up Configuration
For the simulation of the Cl-up configuration, the molecules were initially positioned with the molecular backbone about 3 Å above the surface and the central Sn atom being positioned above fcc hollow sites of the Ag substrate.
The geometry was converged until the remaining forces were below 0.1 eV/Å.
During the optimization, the molecules moved toward bridge positions of the Ag surface. As showed in Fig. 14c the backbone of the molecule becomes flat on the surface, with the Sn atom protruding away from the surface and the Sn-Cl bond perpendicular to the molecular backbone. The corresponding adsorption heights are contained in Tab. 3.
The Sn-Sn distance amounts to 14.3 Å to the closer neighbor and to 14.7 Å to the

distant neighbor, which means that the molecular pairing seen in experiments is weak, but present for this scenario.
However, although the geometries are not fully converged, the adsorption heights of the Sn atoms above the substrate are clearly much higher than seen in experiment due to the Sn atom lying above the molecular backbone. A situation with the Sn atom below the molecular backbone (but the Cl still pointing away from the surface) was tested by modifying the adsorbed molecular geometry accordingly. The SnPc molecule was rotated to a Sn-down configuration, while the Cl atoms was kept at its position pointing away from the substrate (but reinstalling the Sn-Cl bonding distance of 2.35 Å). A geometry optimization of the such prepared system resulted in the same Cl-up geometry as obtained before.
In conclusion, the SnClPc Cl-up configuration does not match the experimental results. In addition, it was found to be unlikely from STM pictures which do not show any indication of the Cl atom protruding from the center of the molecule.

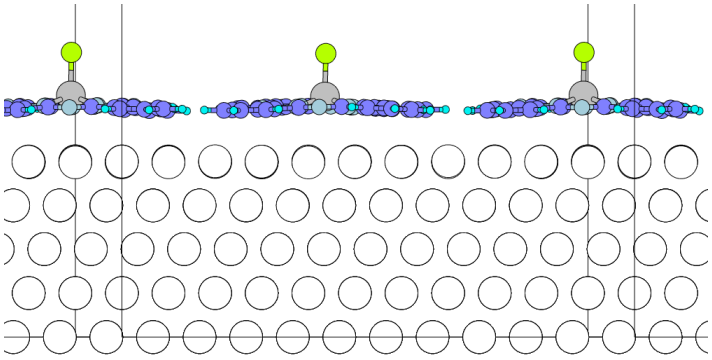

Figure 14: SnClPc in the relaxed Cl-up configuration

Table 3: Adsorption heights relative to the unrelaxed topmost substrate layer of SnClPc on Ag(111) in the Cl-up configuration. The simulated DFT values and the experimental XSW values are given. The experimental Cl heights are corrected by the Cu lattice spacing of 2.36 Å to fit the considered configuration.

	DFT	XSW
C	2.88 Å	
N	2.97 Å	
H	2.82 Å	
Sn	3.55 Å	2.31 Å
Cl	5.895Å	4.48 Å

SnClPc on Ag(111) in Cl-down Configuration
At first, a situation without the formation of vacancies in the Ag substrate was considered for the Cl-down configuration.

The molecules were initially positioned with the Sn and Cl atoms above fcc hollow sites of the Ag substrate, with a distance of about 2 Å between the topmost Ag layer and the Cl atoms.
The geometry optimization was not able to find a stable minimum solution for this configuration. During the optimization, both SnClPc molecules moved and tilted in different directions to avoid each other. This was accompanied by strong deformations of the molecules.
In a second attempt, the SnClPc was positioned closer to the Ag substrate to obtain an anchoring effect of the Cl atom on the Ag substrate, which could stabilize this configuration. Initially, the molecules were positioned above fcc hollow sites, with the Cl atoms positioned at the height of the topmost Ag layer. During the simulations the molecules moved up, pulling the Cl atoms away from the substrate and then remained in a Cl-down position. This resulted in a situation similar to the one described just above, and no geometry convergence could be obtained. Considering the progression of this simulation, where the Cl atom was pushed out of the Ag substrate right away, it appears that a diffusion of the Cl atom without removing any substrate Ag atoms is not a likely scenario.
In conclusion, it appears that no stable solution for the Cl-down configuration in the considered unit cell on an full, unmodified Ag substrate exists.

3.3.4 SnClPc in Cl-down Configuration with Ag Vacancies

The experimentally proposed Cl-down scenario was investigated with different adsorption positions and vacancy scenarios for the Ag(111) substrate. The different configurations are discussed in the following, and all corresponding adsorption heights are contained in Tab. 4.

SnClPc with one Ag per Molecule Removed

Two Ag atoms from the topmost Ag layer were removed per unit cell, and the SnClPc molecules were positioned such that the Cl atom came to lie in these vacancies at the same heights as the topmost Ag layer.
While the Cl-down configuration without vacancies was found to yield no stable solutions, the geometry optimization of the present scenario showed that removing one Ag atom per molecule results in an anchoring effect of the Cl atoms that allows a stable adsorption.
In the course of the optimization, the Cl atoms moved out of the surface, and a slightly bent adsorption geometry of the backbone was obtained, as shown in Fig. 15. As the molecular heights showed no trend to be reduced any further, the optimization was not converged to lower forces than 0.4 eV/Å. The resulting adsorption heights are contained in Tab. 4. They are significantly higher than the ones found from experiment. The Sn-Sn distance amounted to 14.0 Å to the closer neighbor and to 15.0 Å to the

distant neighbor.

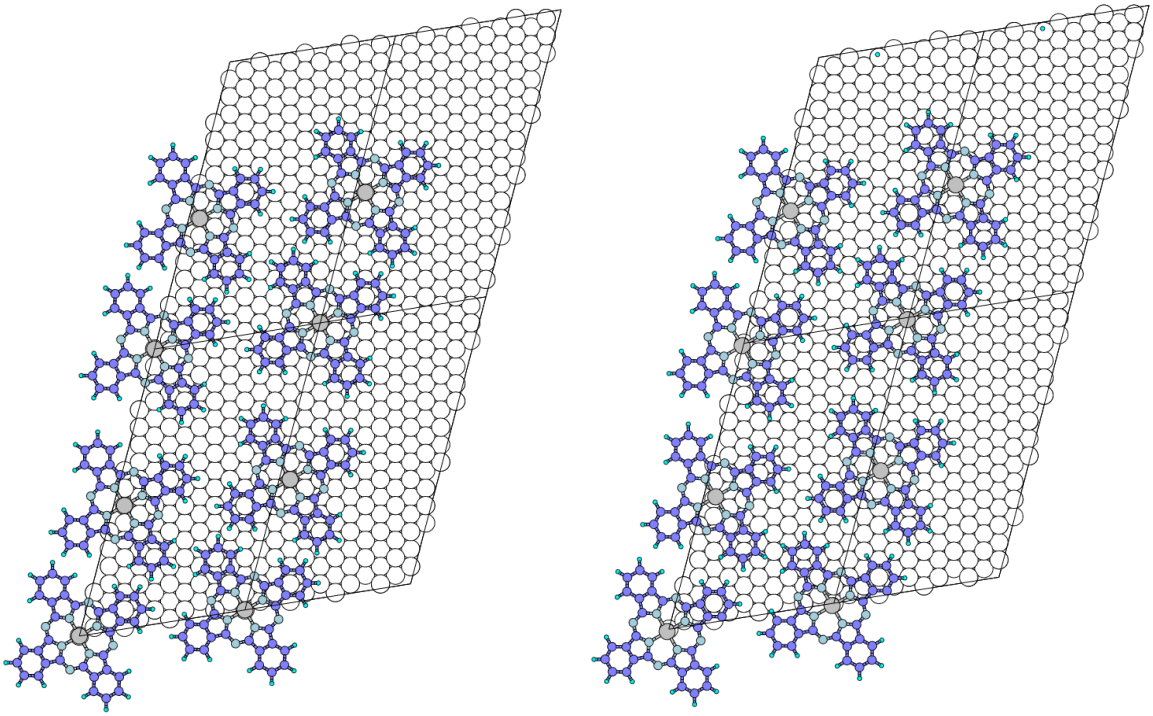

(a) initial configuration

(b) relaxed configuration: top

(c) relaxed configuration: side

Figure 15: SnClPc on Ag(111): Cl-down configuration with one surface atom per molecule removed

Table 4: Adsorption heights are given relative to the unrelaxed topmost substrate layer of SnClPc on Ag(111) in the Cl-down configuration including Ag vacancies for all different considered scenarios. They are labeled by the adsorption sites and the number of Ag atoms removed for each molecule. For comparison, the experimental XSW results are given.

	on-top -1Ag on-top -1Ag	fcc hol. -1Ag fcc hol. -1Ag	fcc hol. -3Ag fcc hol. -3Ag	hcp hol. -4Ag hcp hol. -4Ag	hcp hol. -4Ag on-top -4 Ag	XSW
C	3.10 Å	2.82 Å	2.82 Å	2.72 Å	2.80 Å	
N	3.34 Å	2.85 Å	2.85 Å	2.61 Å	2.81 Å	
H	2.90 Å	2.82 Å	2.82 Å	2.83 Å	2.81 Å	
Sn 1	3.03 Å	2.48 Å	2.48 Å	2.06 Å	2.06 Å	2.31 Å
Sn 2	3.03 Å	1.84 Å	1.84 Å	1.63 Å	2.53 Å	2.31 Å
Cl 1	0.65 Å	0.11 Å	0.11 Å	-0.14 Å	-0.31 Å	-0.24 Å
Cl 2	0.65 Å	-0.26 Å	-0.26 Å	-0.33 Å	0.10 Å	-0.24 Å

SnClPc in Equivalent Hollow Sites of Ag(111) with Three or Four Ag Atoms Removed per Molecule

Positioning both molecules in equivalent hollow sites of the surface (both in fcc or both in hcp hollow sites) was tested, with the Cl atoms of the molecules sitting in the corresponding hollow sites. At the fcc hollow sites, the closest three Ag atoms of the topmost Ag layer were removed for both molecule. In the hcp hollow sites, the closest three Ag atoms of the topmost layer as well as the Ag atom in the second layer below the Cl were removed for both molecules. Due to the symmetry of the substrate, the molecules were distributed quite unevenly in this configuration, with a distance of 13.5 Å to the close neighbor and 15.5 Å to the distant neighbor along the long unit cell axis. The initial geometry of the fcc hollow configuration is shown in Fig. 16a.

The obtained geometries for both cases were very similar. While one of the molecules remained at the original position, the second one moved laterally to obtain a more even distribution of the molecules within the unit cell, resulting in a distances of 14.0 Å to the closer and 15.0 Å to the distant neighbor.

During this lateral movement of the second molecule, its Cl atom stayed in the Ag vacancy. This led to an enlargement of the Sn-Cl distance from 2.35 Å in the gas phase to approximately 3.3 Å, which effectively can be considered to be a dissociation of the Cl atom from the molecule.

In the molecule which stayed intact (molecule 1 at the corner of the unit cell in Fig. 16) the Cl atom (Cl 1) was finally positioned closed to the height of the topmost Ag layer and the Sn atom remained at a height similar to the molecular backbone. In the second molecule, the Sn atom moved down toward the surface and the isolated Cl atom sank deeper into the Ag substrate. The resulting geometry for the fcc hollow configuration is shown in Fig. 16b and c, and the adsorption heights for both configurations, listing Sn and Cl atoms separately, are given in Tab. 4

While the adsorption heights for the intact molecules are reasonably well in line with the experimental XSW results in both cases, the Sn and Cl atoms of the second molecules, where Cl dissociation happens, are significantly lower.

The dissociation of the Cl atoms of one molecule per unit cell is the result of the considered starting geometries, which forced strong lateral movement of one molecule during optimization. Interestingly, the desire of the molecules to obtain the ideal intermolecular distance (and the previously discussed pair formation) is strong enough to cause Cl dissociation in the simulations.

Looking at the final adsorption heights of the intact molecules of both configurations, it appears that removing three to four atoms leads to good comparability to experiment. However, adsorption in equivalent hollow sites for both molecules is clearly not possible, as the intermolecular distance is too small in that case.

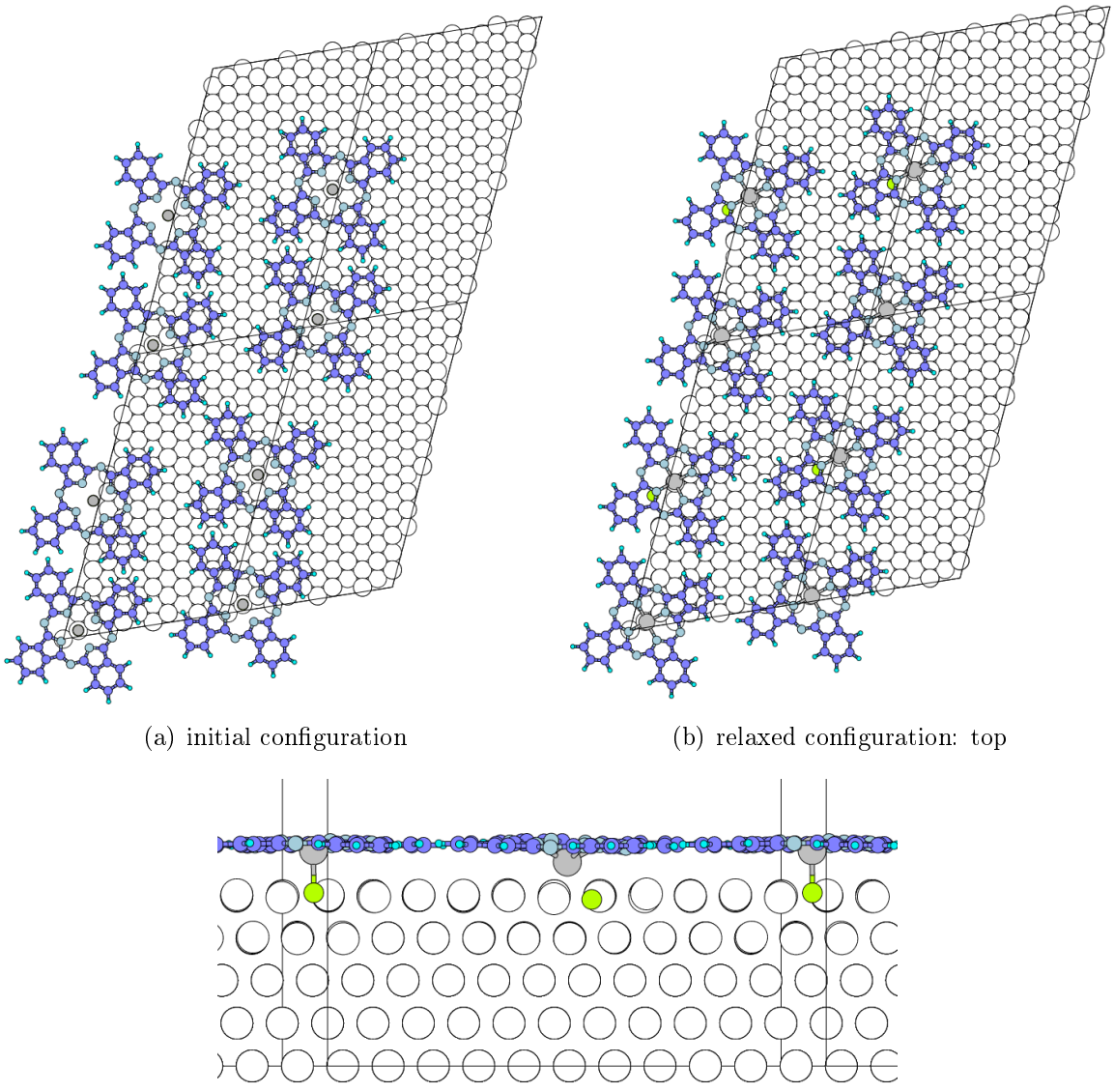

(a) initial configuration

(b) relaxed configuration: top

(c) relaxed configuration: side

Figure 16: SnClPc on Ag(111): Cl-down configuration with three surface atoms removed from the fcc hollow site for each molecule

SnClPc with the Two Molecules at Different Adsorption Sites on Ag(111) with Three or Four Ag Atoms Removed per Molecule

As shown before, the distance between molecule 1 and molecule 2 in the unit cell has to amount to about 14.0 Å, which is not possible when both molecules are put into two equivalent crystal sites, e.g. both in fcc hollow sites, as discussed above. Therefore, adsorption scenarios were considered where the two molecules in the cell are positioned at inequivalent adsorption sites, e.g. the first molecule in a fcc hollow site, while the second one is located in an hcp hollow site. The initial configurations were chosen such that the preferred inter-molecular distance of 14.0 Å was maintained.

For molecules positioned with their Cl atoms in fcc hollow sites, either three or four Ag atoms were removed, with three atoms stemming from the second Ag layer, and the fourth one stemming from the third layer, directly below the adsorption site. For the on-top configuration, one Ag atom from the topmost Ag layer was removed and the molecular Cl atom was put in its position. In the second layer, the three closest Ag atoms were removed. Adsorption in hcp hollow sites was simulated with three Ag atoms of the topmost layer as well as the Ag atom in the second layer directly below being removed.

Several different combinations of these adsorption configurations in one cell were tested. It was found that vacancies of three atoms from fcc hollow sites always resulted in the Cl atoms positioned 0.1-0.3 Å above the topmost Ag layer. Removing also the next Ag atom below, which lies in the third Ag layer, did not change this outcome. The corresponding Sn atoms where then positioned at about 2.5 Å above the unrelaxed Ag surface in all cases. Similar heights were obtained for the molecules being positioned above on-top sites of the substrates. Upon adsorption in hcp hollow sites, the Cl heights were found to lie between 0.2 Å and 0.3 Å below the unrelaxed topmost Ag layer, and the Sn atoms between 2.1 Å and 2.2 Å above it.

The intermolecular distance of approximately 14.0 Å was maintained by the system during geometry optimizations in all cases.

The best agreement with experiments was found for a configuration with one molecule at the on-top site and the second molecule at the hcp hollow site, with four Ag vacancies each. The initial and resulting geometries are shown in Fig. 17 and the corresponding adsorption heights are listed in Tab. 4.

Although the comparison to the experimental adsorption heights is not perfect, this configuration gives the best agreement so far. Additionally, such a "mixed" configuration with the molecules at different adsorption sites results in lateral structures exhibiting the molecular pairing as seen in STM without strong distortion or even Cl dissociation.

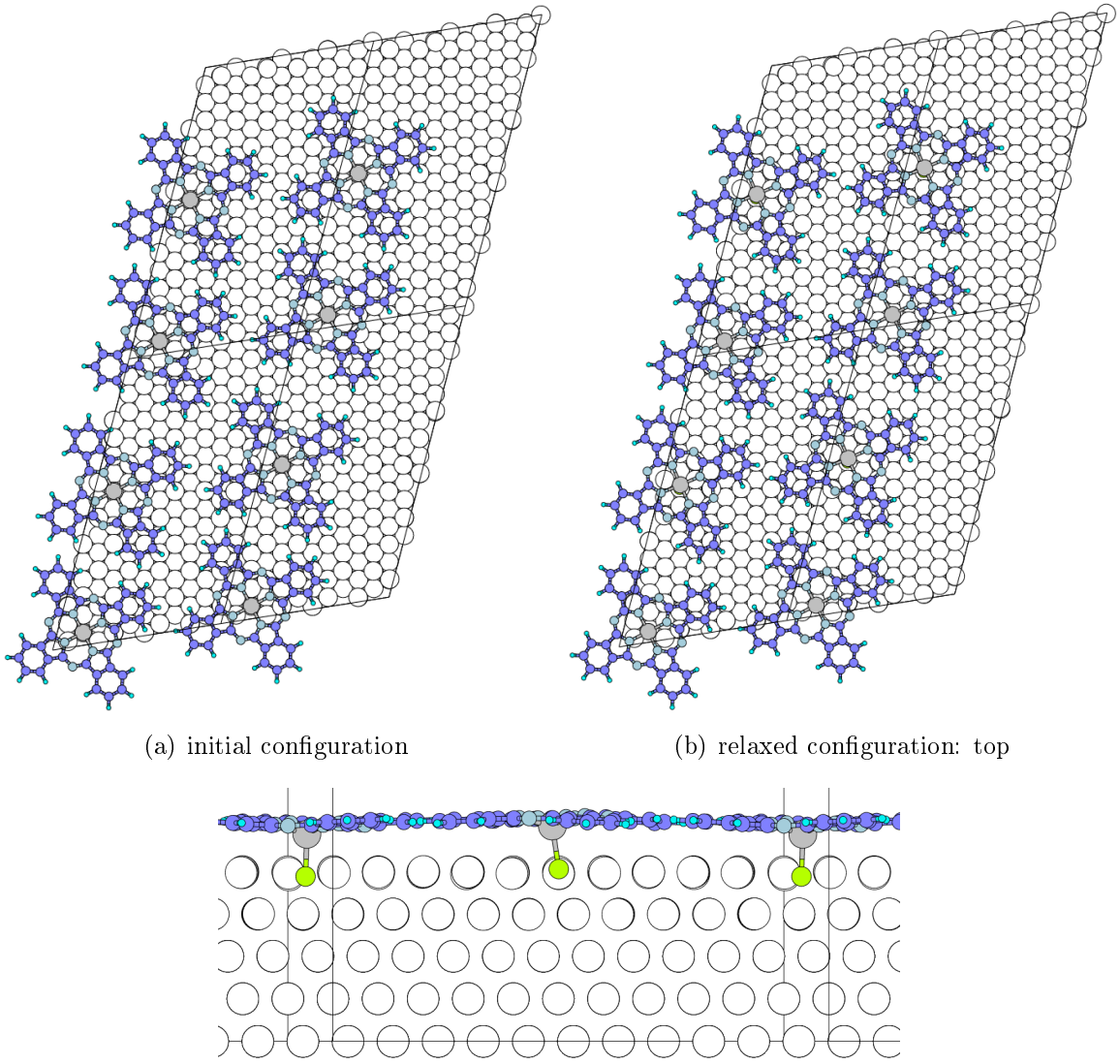

(a) initial configuration

(b) relaxed configuration: top

(c) relaxed configuration: side

Figure 17: SnClPc on Ag(111): Cl-down configuration with four surface atoms from the on-top site (molecule at origin) and four atoms from the hcp hollow site removed

3.3.5 Vacancy Formation and Adsorption Energies

The simulations of SnClPc in different configurations discussed above, along with the experimental results, indicate that the adsorption of SnClPc causes the formation of vacancies in the Ag substrate. The question remains whether such a scenario is energetically reasonable. Therefore, the vacancy formation energy and, subsequently, also the adsorption energy was estimated. This was done for the above presented system with four Ag vacancies at the on-top site and four Ag vacancies at the hcp hollow site, which compares well with experimental adsorption heights.
At first, the vacancy formation energy of the Ag substrate, without considering the adsorbed molecules, was calculated to get an idea about the energy cost of this process. The energy of forming vacancies can be estimated according to Forster-Tonigold and coworkers,[129] where the vacancy Ag atoms are considered by transforming them to bulk atoms.

$$E_{defect} = E_{slab} - E_{slab,full} + n_V * E_{bulk} \tag{4}$$

This term for the defect formation energy contains the energy of the slab including vacancies E_{slab} and the (relaxed) full slab without vacancies $E_{slab,full}$. Additionally, an energy contribution for converting atoms to bulk atom is added, where n_V gives the number of vacancy atoms, and E_{bulk} is the energy of one bulk atom.
For the system considered here, which exhibits eight Ag vacancy atoms in total, a vacancy formation energy of 4.4 eV for the system (2.2 eV per SnClPc molecule) was found.
Also in the calculation of the adsorption energies, the Ag vacancies have to be considered. This can be done in a similar way as described above. Otálvaro et al.[130] have calculated adsorption energies for interface systems containing vacancies as follows:

$$E_{ads} = E_{system} - E_{slab} - E_{molecule} + n_V * E_{bulk} \tag{5}$$

After subtracting the energies of the full slab (without vacancies) and molecule from the total energy, an energy contribution for converting atoms to bulk atoms as above is added.
This was evaluated for the considered system and resulted in an adsorption energy of -1.99 eV per SnClPc molecule, -3.98 eV for the two-molecule unit cell in total, which means that the formation of Ag vacancies upon adsorption is energetically favorable.

3.3.6 Discussion and Outlook: Adsorption of $SnCl_2Pc$ on Ag(111)

The comparison of different dechlorination scenarios of $SnCl_2Pc$ (SnClPc, SnPc) and different adsorption configurations to experimental results showed that the SnClPc molecule adsorbing in a Cl-down configuration, including a formation of Ag vacancies underneath the molecule, is a viable scenario. This is in line with conclusions drawn

from different experimental results by Christian Zwick and coworkers. However, adsorption in a SnPc configuration could not be ruled out from simulation results and would fit the experimental data quite well. In addition, it was seen in the simulations that also the dissociation of the (second) Cl atom can happen quite easily.
For the SnClPc Cl-down adsorption, no distinct answer on the exact adsorption positions and vacancy formation could be given from simulations. Nonetheless, the performed calculations showed that to obtain adsorption heights as seen in experiment, at least three Ag atoms need to be removed underneath every molecule. Additionally, it became clear from simulation that the two molecules in the unit cell must choose different adsorption sites to allow their preferred intermolecular spacing. A pairing of the molecules in the cell is seen in STM as well as in simulation results.
The computational configuration that is closest to the experimental results is the one with four Ag atoms removed at an on-top site, and four Ag atoms removed at an hcp hollow site. The resulting average adsorption heights of Sn and Cl are 2.30 Å and -0.11 Å respectively. From experiment, adsorption heights of 2.31 Å for Sn and -0.24 Å for Cl were found. However, it is not clear whether this specific adsorption configuration will appear, as a huge number of possible configurations exist, while only a few were tested here. Also a scenario without consistent adsorption sites is thinkable, where the molecules adsorb at various different sites. Therefore, the DFT results cannot provide a final adsorption configuration here, but rather suggest reasonable vacancy structures.
It was also discussed whether such vacancy formation is a physically reasonable scenario. As mentioned previously, the formation of vacancies upon adsorption has been observed previously, namely for C_{60} on Ag(111).[123] For the best system as described above, the calculated adsorption energies indicate that adsorption including vacancy formation is still energetically favorable.
To obtain full clarity on this system, it would be necessary to perform a structure search including substrate vacancies. In addition, it would be desirable to compare the adsorption and vacancy formation energies for all considered structures.

3.4 Adsorption of Pentacenequinone P2O on Ag(111)

The occurrence of different adsorption scenarios for a given molecule can not only arise from the molecular geometry, as shown for the two nonplanar Pcs above, but also from the interaction strength with the surface. As discussed in the introductory part (section 2), the adsorbate molecules can exhibit weak physisorption or strong chemisorption, which influences the adsorption heights, but also the molecular geometries. In this section, the interaction strength of an interface system is tuned, attempting to provoke a transition between chemisorption and physisorption.
The system chosen for this investigation was 6,13-Pentacenequinone (see Fig. 18a) on the Ag(111) surface. This work is based on my master thesis,[23] where the adsorption of this molecule and the related 5,7,12,14-pentacenetetrone (P4O) (see Fig. 18b) molecule on coinage metal surfaces were studied. Both molecules exhibit chemisorption on the low work function Cu(111), with adsorption heights below 3 Å, and physisorption on high work function Au(111), with adsorption heights above 3 Å.[23, 131] The adsorption on Ag(111) is an interesting, intermediate case. Experimental XSW results presented by Heimel et al. [131] have shown that the P4O molecule, which has a lower lying LUMO orbital and, therefore, a higher electron affinity, exhibits chemisorption, while P2O exhibits physisorption on that surface.
During my master thesis, I was not able to reproduce this behavior as the performed simulations always yielded strong binding of the P2O molecule to the Ag substrate, which led to chemisorption at low binding distances, differing by about 0.5 Å from the experimental values.
This discrepancy between simulation and experiment is curious, especially as the agreement for the adsorption heights of both molecules is very good for physisorption on Au as well as for chemisorption on Cu and the results vary by less than 0.15 Å for both C and O atoms.
In an attempt to understand this disagreement, the situation was analyzed as follows: In the above mentioned series of systems of P2O and P4O on different coinage metals, a transition between the two different adsorption scenarios appears. Experimentally, the transition takes place on the Ag substrate, when P4O is exchanged by P2O.[131] The DFT simulations performed in my master thesis, on the other hand, find the transition between physisorption and chemisorption at a different point, namely when changing the substrate from Ag to Au.[23] In the simulations, both molecules exhibit physisorption on Au, but chemisorption on Ag.
The appearance of the above described transition between different adsorption scenarios as well as the disagreement between simulation and experiment on the conditions of this transition suggest that a sharp transition between chemisorption and physisorption exists. In that case, a small deviation in the simulation could lead to a quantitatively incorrect result, e.g. concerning the adsorption heights of the molecule. The questions that were raised in the course of my PhD thesis were (i) whether such a sharp transition between adsorption configurations exists and (ii) if the P2O/Ag system can be pushed toward the other, physisorption scenario by applying small changes to the system.

Several different approaches were pursued to answer these questions.
First of all, it was ensured that the difference between simulated and experimental results is not a methodological artifact by applying differing methodological procedures.
Second, the possibility of a two-minimum structure was investigated. In that situation, both the physisorption and the chemisorption case would be stable, local minima and could, therefore, be found in the simulations. This was done by calculating a binding energy curve of the P2O molecule on the Ag substrate.
Then, the existence of the above discussed transition point between different adsorption scenarios was investigated. Several scenarios to trigger this transition were tested, including the modification of the substrate work function and weakening of the bonding between molecular O atoms and substrate Ag atoms. This was accomplished by pursuing different alloying approaches, namely by putting actual heteroatoms in the Ag slab, and also by the virtual crystal approximation.[132] To weaken the substrate-molecule interactions, also the slab lattice constant was modified.
As a final approach, an electric field over the whole unit cell was applied.
To obtain a more complete picture, it was not only tried to weaken the adsorption on Ag, but also several tests to strengthen the adsorption on Au were conducted to approach the transition point from the other direction.

3.4.1 System and Methodology

The structure of the P2O molecule is shown in Fig. 18. For comparison, also the structure of P4O is given.
For the adsorption on the Ag(111) surface, a 6 x 3 unit cell was applied, as depicted in Fig. 19. This cell was adopted from the one presented by Heimel and coworkers.[131] As no STM images of P2O on Ag were available and as Ag and Au have similar lattice constants, it was based on STM images of P2O on Au.
Convergence tests showed that at least four layers of Ag substrate are required for the substrate work function to be converged to within 0.05 eV. In the following calculations, the standard configuration was 5 layers of Ag, as shown in Fig. 20. When a different number of layers was applied, this is stated in the text explicitly.
Note that the adsorption heights given in the following are measured relative to the hypothetically unrelaxed topmost substrate layer to be able to compare them to experimental XSW results.

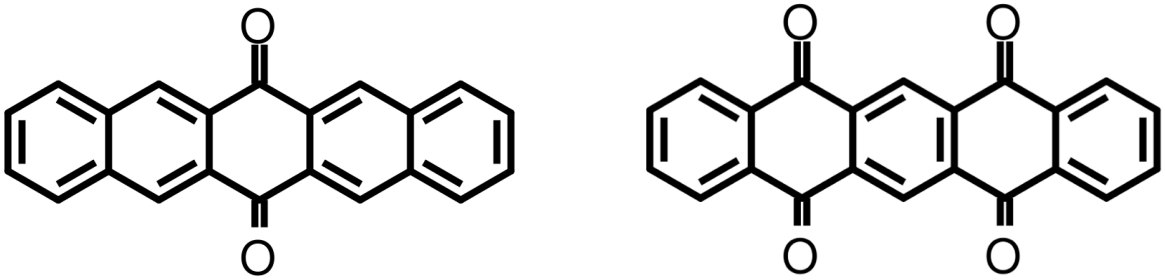

(a) P2O (b) P4O

Figure 18: Structures of the 6,13-Pentacenequinone (P2O) molecule and the 5,7,12,14-pentacenetetrone (P4O) molecule.

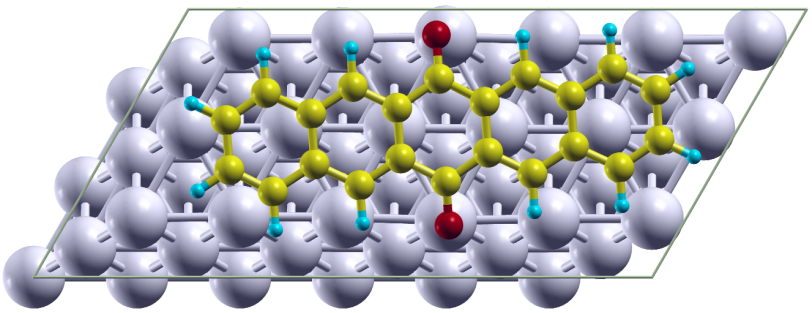

Figure 19: Unit cell of P2O adsorbed on Ag(111). C atoms are depicted in yellow, O atoms in red, H atoms in blue and Ag atoms in grey.

DFT Methodology

The P2O/Ag(111) system was calculated applying both VASP and FHI-aims, using the PBE functional. If not stated differently, the calculations listed in the following were performed using VASP. VASP and FHI-aims agree almost perfectly on the adsorption heights of P2O on Ag(111) (see Tab. 5).

In both codes, unit cells as described above were applied, with at least 20 Å vacuum between the adjoining unit cells and a dipole correction in z direction. For van der Waals corrections, the vdW^{surf} approach was applied.[68]

The k-point grid was set to 3x6x1 k-points for final calculations, and to 2x4x1 for preliminary geometry optimizations. Such preliminary optimizations were applied when lengthy relaxations were to be expected.

In VASP, a plane-wave cutoff of 400 eV and standard PAW potentials were used. The Ag PBE lattice constant was optimized and found to be 4.1540 Å (compared to a literature value of 4.079 Å [127]).

Using FHI-aims, "tight" settings were applied, and the lattice constant was found to be 4.1496 Å.

3.4.2 Discrepancy Between Simulation and Experiment

The adsorption heights of P2O on Ag(111) were determined with VASP and also FHI-aims calculations and the resulting adsorption heights are compared to experiments in Tab. 5. The corresponding adsorption geometry extracted from the VASP calculation, is shown in Fig. 20.

Table 5: Adsorption heights of P2O on Ag(111) are given relative to the the unrelaxed topmost Ag layer. Both C and O adsorption heights are listed in Å and compared to the experimental XSW results from Ref. [131].

	h_C [Å]	h_O [Å]
VASP	2.86	2.49
FHI-aims	2.87	2.54
XSW	3.32	3.35

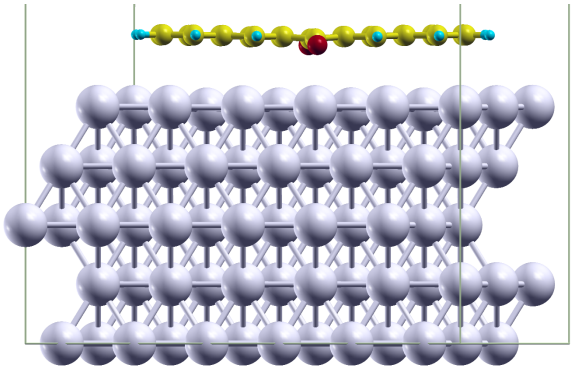

Figure 20: Simulated adsorption geometry of P2O adsorbed on Ag(111). C atoms are depicted in yellow, O atoms in red and H atoms in blue.

Applying both DFT codes, the adsorption heights differ by about 0.4 Å for C and by about 0.8 Å for the O atoms from experimental results. What is clearly visible from the simulation results (see Fig. 20) is that the O atoms are bending down and are by more than 0.3 Å closer to the surface than the C atoms, which is also typical for chemisorption. In case of physisorption, where the main interaction between molecule and surface arises from van der Waals interactions,[18] the molecule stays essentially flat, which is seen in the experimental results.
Note that the simulation results presented in Ref. [131] are closer to the experimental results, but also do not show typical physisorption behavior.

3.4.3 Preliminary Tests on Starting Configuration and Methodology

To make sure that the obtained adsorption heights for the P2O/Ag(111) system are stable and consistent within DFT and do not arise from (i) the geometric initialization or (i) artifacts in one specific calculation method, several different test with varying starting geometries and methods were performed.

Starting Geometries and Unit Cell Sizes

The bonding strength between the O atoms and the substrate might be influenced by several geometric properties. Here, the initial position of the molecule and the initial relaxation state of the substrate were considered to check whether they influence the adsorption heights.

The standard calculations performed of P2O/Ag were initialized with the O atoms directly above Ag substrate atoms in the topmost Ag layer, see Fig. 19. The Ag substrate was not pre-relaxed. The strong bonding that appears between O and Ag could probably be mitigated by initially positioning the O atoms above surface hollow positions. Additionally, a pre-relaxation of the Ag substrate before adding the P2O molecule could minder the reactivity of the surface, e.g. due to bond length changes causing Ag-Ag dimerization in the topmost layer. Several tests were performed with P2O in different starting configurations, with the O atoms above fcc hollow and bridge positions, and on a pre-relaxed Ag substrate. In all cases, the molecule shifted toward a position where the strong bonding toward specific Ag atoms could be restored, and all obtained results were consistent with the ones obtained from the standard initialization.

An influence of the unit cell size on the adsorption heights is imaginable, as the interaction of the molecules with each other could influence their interaction with the substrate. Especially in a closely packed configuration where the molecules form chains and saturate the O atoms of neighboring molecules by forming hydrogen bonds, thereby preventing a strong bonding to the substrate, the adsorption heights could be altered. Several tests applying both smaller and larger unit cells were performed by myself and also by Andreas Jeindl, who additionally did a full structure search applying SAMPLE [133, 134]. By investigating different possible adsorption geometries for P2O on Ag(111), he found that the ideal unit cell for this system is one with an area of 108.4 $Å^2$, which is smaller than the 134.5 $Å^2$ cell applied here. However, none of these tests with differently sized unit cells and differently positioned molecules led to a significant change in the the obtained adsorption heights and the overall binding behavior of the molecule.

vdW Correction Methods

The vdW^{surf} approach [68] has been shown to yield good results for various interfaces comprising flat-lying molecules on metal surfaces. However, to make sure that the obtained results are not an artifact of an unfavorable vdW correction method, also

the Grimme-D3 vdW correction [69] was tested. The obtained adsorption heights were virtually equivalent to the ones obtained with vdW^{surf}.
While the adsorption heights received with vdW^{surf} are mostly in very good agreement with experiment, this method has been shown to exhibit over-binding when adsorption energies are considered.[68, 76, 135] A more advanced approach would be the use of so-called many-body dispersion (MBD) methods.[75, 76, 136] At the time of the execution of this study, an MBD method was being implemented into the VASP code by Tomáš Bučko. Some preliminary tests on the P2O/Ag(111) system could be performed and led to adsorption heights similar to what was found with vdW^{surf}. However, due to the implementation being not fully finalized and tested at that point, it is not clear if the obtained results are trustworthy, and therefore, they are not discussed in detail here.
Completely avoiding the use of a vdW correction method is clearly not a good approach for such a flat-lying organic molecule, where vdW interactions mostly play a significant role for the bonding. Not surprisingly, calculations without such a correction yielded adsorption heights of more than 4 Å for all atomic species.

Geometry Optimization Algorithms
As it has been discussed previously that different geometry optimization algorithms can yield different results in complicated situations, also the use of other algorithms was tested for the P2O/Ag system.
Applying the VASP code, conjugate gradient and damped molecular dynamics methods [137] were applied, where the first one is expected to go directly to the closest local minimum, especially with a small step width, while the second one is also suitable to find geometries that differ more strongly from the initial structure.
Also, the GADGET-implemented quasi-Newton methods "direct inversion of the iterative subspace" (GDIIS)[138] and "rational function optimization" (RFO)[139] were applied.[4] While RFO is supposedly suitable to describe larger structural changes, GDIIS is helpful to achieve fast convergence into the next local minimum.
In FHI-aims, the Broyden-Fletcher-Goldfarb-Shanno (BFGS) optimization algorithm [140] was used.
The obtained adsorption heights stayed virtually the same with all applied methods.

3.4.4 Binding Energy Curve

One possible reason for the discrepancy between simulated and experiment results is a situation where the the geometry optimizations run into the "wrong" minimum structure. This is a problem that does usually not appear for such system consisting of small, flat-lying molecules, where the main degree of freedom is the distance between molecule and surface. For these systems, usually only one minimum structure at a

certain distance exists. However, for some systems it has also been observed that binding energy curves can exhibit barriers, so two local minima occur and two different adsorption scenarios at different distances are found.[141]
During my master thesis, this theory was briefly checked by putting the molecule at different distances to the surfaces in a planar geometry and calculating the binding energies at each distance. This resulted in a smooth binding energy curve with one minimum and without any barriers.[23]
However, in the case that the second minimum is not very pronounced, it might have been missed due to the lack of geometry optimization in this previous test.
To overcome this problem, two different test were performed. At first, a geometry optimization which was constrained to small geometry steps was performed, where the molecule in its gas phase geometry was positioned 4 Å above the substrate. In that way, it should be possible to find also a less pronounced minimum at a larger adsorption distances. However, this simulation led to the same adsorption geometries as observed previously.
Therefore, another binding energy curve was calculated where the molecule (in its gas phase geometry) was positioned at different distances to the surface, and all atoms but the middle C ring (which was constrained in z direction) were allowed to relax fully. The binding energies were calculated by subtracting the energies of the free-standing monolayer (in the gas phase geometry) and the slab (with the topmost two Ag layers fully relaxed) from the energy of the combined system.

$$E_{BE} = E_{System} - E_{Monolayer} - E_{Slab} \tag{6}$$

The binding energies were calculated for distances between 2.8 Å and 3.7 Å, and the resulting binding energy curve is shown in Fig. 21. Clearly, the curve exhibits only one minimum and the hypothesis of a two minimum structure has to be dismissed.

3.4.5 Alloying of the Ag Substrate

If the P2O/Ag system is close to a transition point between physisorption and chemisorption, the obvious tuning parameter to switch between the two scenarios is the work function Φ of the substrate. As mentioned above, on the high work function Au(111) ($\Phi_{experimental}$ = 5.35 eV [142]) P2O exhibits physisorption. The Ag(111) work function ($\Phi_{experimental}$ = 4.46 eV [143]; $\Phi_{simulation}$ = 4.40 eV) needs to be increased to weaken the interaction of molecule and substrate.
Different configurations of the alloying atoms in the Ag substrate were considered, including situations similar to a solid solution, were heteroatoms are distributed in the crystal lattice of the slab, replacing Ag atoms. A possible candidate for such a solid solution in Ag is Au.[144] To test how strongly the work function of Ag can be modified in both directions, also alloying with Pd an Cd atoms was considered, which exhibit

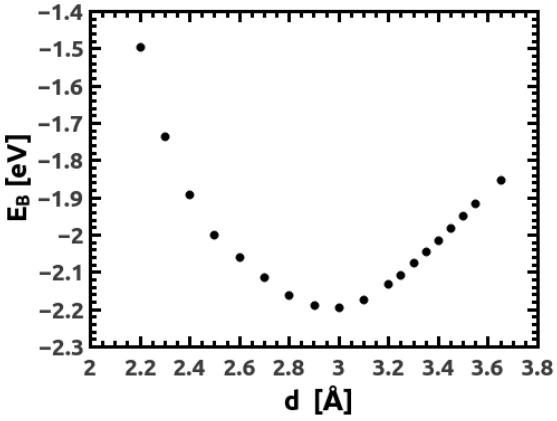

Figure 21: Binding energies in eV of P2O adsorbed on Ag at different distances. The distances are given for the middle C ring relative to the unrelaxed Ag substrate. In the region between 3.2 and 3.6 Å adsorption distance, where the second minimum stemming from chemisorption is expected to occur, calculations were performed at every 0.05 Å, while in the other regions calculations were performed every 0.1 Å.

similar atomic radii as Ag and are soluble in it, but have different numbers of valence electrons than Ag.[144, 145]

Ag Alloyed with Pd and Cd

The unit cell of the P2O/Ag(111) system was considered with different amounts of Pd and Cd alloying atoms in the slab. A four layer slab with 72 Ag atoms was considered, and the impact of Pd and Cd heteroatoms distributed within Ag on the work function was investigated.

Different distributions of the heteroatoms were tested. They were either distributed over the whole slab, or only distributed in the lower layers of the slab to avoid interactions with the P2O molecules in adsorption calculations performed afterwards.

The impact of different numbers of hetero Pd and Cd atoms on the work function of the Ag slab is shown in Fig. 22. Two cases with the heteroatoms distributed evenly over the whole slab were considered, marked as "full". In all other calculations, the heteroatoms were distributed equally in the two bottom layers. The Ag substrate is given for reference. Note that its work function does not agree with the previously reported value due to the avoidance of substrate relaxation, which is usually performed for the the topmost two layers.

The obtained work functions range between 4.67 and 4.42 eV, which means a maximum work function increase of 0.18 eV.

The impact of the maximal work function increase on the adsorption of P2O was tested by performing a full geometry optimization in the corresponding unit cell, containing 24 Pd atoms. In this cell, the presence of the Pd atoms in the topmost Ag layer led to deformations of the molecule due to interactions with these heteroatoms. Therefore,

also the unit cell with 6 Pd atoms was used to test P2O adsorption.
Although the adsorption heights were minimally increased by about 0.1 Å in both cases, the molecule still clearly exhibited chemisorption behavior on the substrate. Apparently, such a small work function change is not enough to break the strong binding between P2O and Ag.

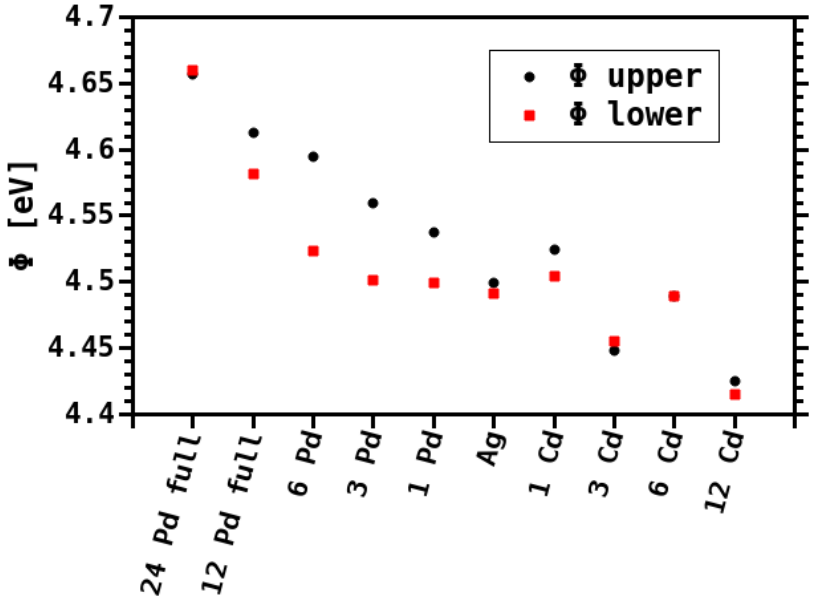

Figure 22: Work functions of the Ag slab alloyed with Pd and Cd at the upper (black) and lower (red) side of the slab. The alloying atoms were distributed evenly in the whole slab (in calculations marked as "full") or in the lower two layers of the 4 layer Ag slab (all other).

Ag Alloyed with Au

For the alloying with Au, a different approach was used and entire substrate layers in the Ag slab were substituted by Au layers. In a 5 layer slab, between one and three complete layers were occupied by Au atoms. Two examples are shown in Fig. 23. The resulting top and bottom work functions as well as the adsorption heights of the P2O molecule on these slabs are listed in Tab. 6.
One layer of Au increases the work function by less than 0.1 eV, three middle layers lead to an increase of 0.15 eV, but in that case, already two thirds of the substrate are Au. With only one Au layer on top, the upper work function is increased to about 5.0 eV, which is closer to Au ($\Phi_{Au,exp} = 5.35$ eV) than to Ag ($\Phi_{Ag,DFT} = 4.40$ eV). This indicates that the work function depends mainly on the surface dipole. Consequently, the adsorption on a substrate with a top Au layer leads to physisorption, while the

adsorption on a mainly-Au substrate with Ag on top still yields chemisorption. This is depicted in Fig. 23.

Table 6: Upper and lower work functions Φ_{top} and Φ_{bottom} in eV and adsorption heights of P2O C and O atoms h_C and h_O in Å of the 5-layer Ag slab with substituted Au layers.

	Φ_{top} [eV]	Φ_{bottom} [eV]	h_C [Å]	h_O [Å]
top and bottom layer Au	5.00	4.99		
top layer Au	5.04	4.53	3.20	3.18
second layer Au	4.57	4.46		
one middle layer Au	4.51	4.53	2.93	2.80
three middle layers Au	4.65	4.61	2.91	2.76

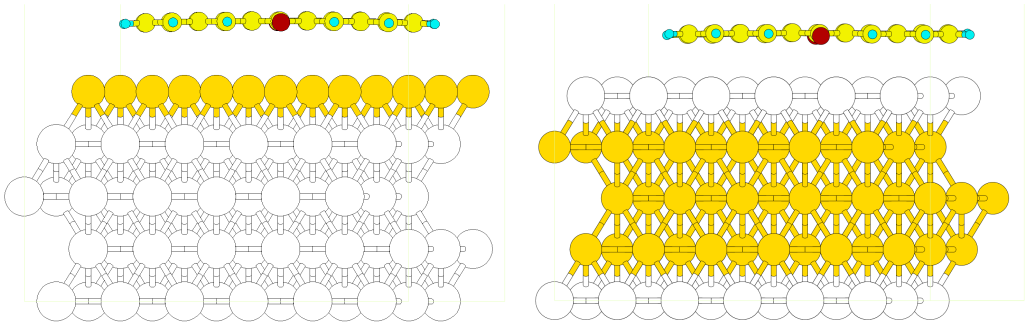

(a) top layer Au (b) three middle layers Au

Figure 23: P2O adsorbed on two different Ag/Au slabs.

3.4.6 Lattice Constant and Layer Distance Variations

An alternative approach to weaken the binding between molecule and substrate is the variation of the substrate lattice constant (and, alternatively, the layer distances), as this allows shifting the Ag d-bands. Mavrikakis et al. have shown that strain-induced shifting of the d-bands of Ru can influence the adsorption strength of O atoms.[146] In the present case, modifying the d-bands of Ag should also influence the coupling of substrate atoms to molecular O atoms, thereby changing the molecular adsorption strength.
How the d-bands of strained Ag and Au are influenced was tested by varying their lattice constants by up +15% and -15%, respectively. The compression is expected to weak the reactivity of the Ag substrate, while the stretching should increase the reactivity of the Au substrate.[146] The resulting DOSs are shown in Fig. 24. While the width of the d-bands is changed significantly upon stretching/compressing in both

cases, their onset stays virtually the same. This is, unfortunately, not very promising for the present study. Anyhow, adsorption tests with P2O on the strained substrates were performed. In the case of Ag, the unit cell size had to be increased from a 6 x 3 cell to a 7 x 4 Ag(111) cell to allow the adsorption of P2O in the 15 % compressed cell. In addition, the substrate could obviously not be relaxed. The adsorption heights of P2O on strained Ag and Au are shown in Tab. 7. Note that the adsorption height of the molecule on the unstrained substrates are not perfectly consistent with the previously reported values due to the avoidance of substrate relaxation in the present case.

While the work functions of the strained substrates do not follow a clear trend, the

Table 7: Adsorption heights h_C and h_O in Å and (lower) work functions Φ_{bottom} in eV of P2O C and O atoms h_C and h_O in Å on strained Ag and Au substrates. While the Ag lattice constant was decreased, the Au lattice constant was increased.

	h_C [Å]	h_O [Å]	Φ_{bottom} [eV]
Ag	2.97	2.85	4.37
Ag -5%	3.02	2.86	4.50
Ag -10%	3.08	2.96	4.60
Ag -15%	3.16	3.01	4.54
Au	3.22	3.19	5.17
Au +5%	3.16	3.15	5.20
Au +10%	3.07	3.10	5.29
Au +15%	2.96	3.05	5.23

adsorption heights do. On Ag, the heights are increased by about 0.2 Å upon 15% compression, while on Au, they are reduced by almost the same amount upon 15% stretching.

On both metals, the P2O molecule moved significantly toward the opposite adsorption scenario, namely toward chemisorption on Au, and toward physisorption on Ag, upon changing the lattice constants. However, what does not appear is the originally expected sudden transition between the adsorption behaviors. Rather, a gradual change of the adsorption heights is seen. On Ag, the binding of the O atoms toward the substrate is still strong, which is indicated by their significantly lowered height compared to the C backbone, while on Au, it is the other way round.

For consistency reasons, tests were performed where not the lattice constant, but the layer distance between adjoining Ag layers in z-direction was modified by up to ± 15%, which corresponds to a situation where strain is applied only in one direction. The results were consistent with the lattice constant changes, leading to slightly smaller changes in the adsorption heights at the maximum deformation of 15%.

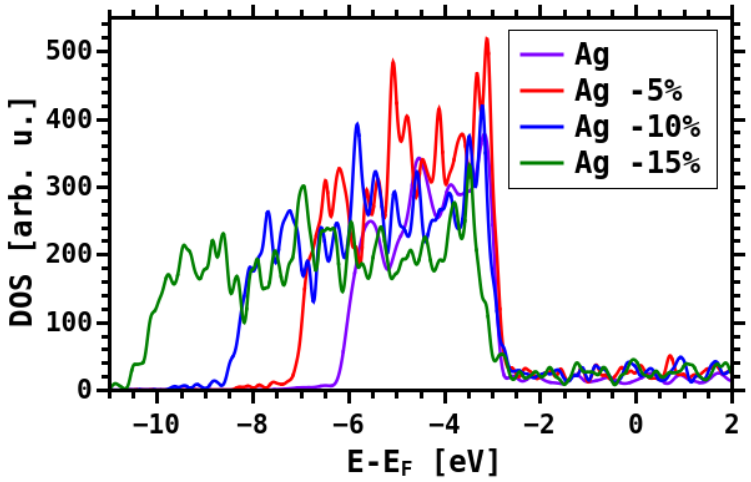

(a) compressed Ag

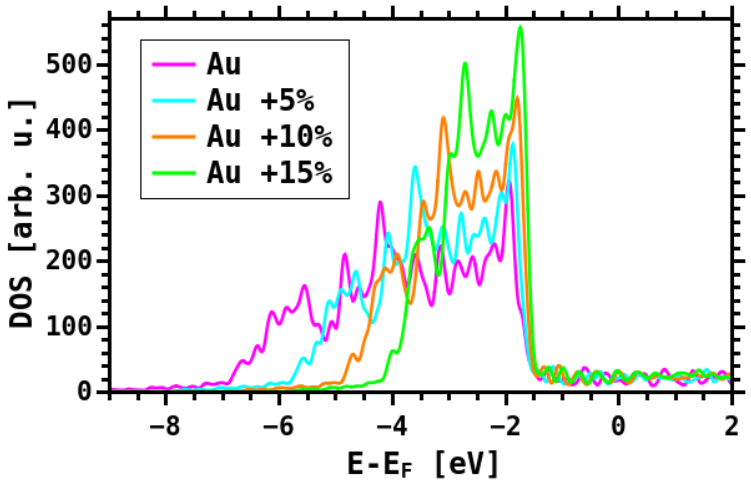

(b) stretched Au

Figure 24: Effect of strain on the DOS of Ag and Au. While Ag was compressed for decreased reactivity, Au was stretched for enhanced reactivity.

3.4.7 Alloying via the Virtual Crystal Approximation

Another viable approach to alter the d-bands of the substrate material is the use of the so-called virtual crystal approximation VCA.[132] This method can be applied in DFT to create a situation similar to alloying or doping of a material by adding or removing (delocalized) negative charge to the valence region, and the corresponding positive charge to the nuclei. Such VCA calculations were performed applying FHI-aims, where the charges of nuclei and valence electrons can easily be modified.
In the present case, the VCA could be useful to tune the substrate work function by

creating a situation similar to alloying and to add extra electrons to the Ag slab or remove electrons from the Au slab. However, in a project performed by Anna Eibel (and co-supervised by me), where the DOS and work function of several metals was investigated upon different "alloying" states induced by the VCA, it was shown that the work function of these materials could not be altered strongly. This is in line with the above discussed findings on the calculation of actual alloys. The d-states of the metals, on the other hand, were shifted quite strongly upon VCA alloying. Therefore, it was tested whether this shifting can be applied to weaken the binding of P2O on the Ag surface, similar to the lattice constant variations as performed previously.
To do so, electrons were added (and, for testing reasons, also removed) to/from the valence region of the Ag atoms. Also some calculations on Au were performed, where electrons were removed from the valence region. The resulting adsorption heights and work functions are shown in Tab. 8.
The obtained results are similar to the previous section. While the adsorption heights

Table 8: Adsorption heights of C and O atoms h_C and h_O in Å and (lower) work functions Φ_{bottom} in eV are shown for P2O adsorption on Ag and Au, applying the VCA. Where and what amount of charge is added/removed for the valence region is given explicitly. The nuclei were charged correspondingly to obtain charge neutrality.

	h_C [Å]	h_O [Å]	Φ_{bottom} [eV]
Ag	2.87	2.54	4.40
Ag +0.25 e^- s-shell	3.16	2.81	4.31
Ag -0.25 e^- s-shell	2.61	2.58	4.61
Ag +0.50 e^- s-shell	3.19	2.91	4.27
Ag +0.25 e^- p-shell	3.17	2.84	4.34
Ag +0.25 e^- d-shell	3.17	2.84	4.35
Au	3.26	3.26	5.13
Au -0.35 e^- s-shell	2.99	3.12	5.46
Au -0.35 e^- d-shell	2.96	3.15	5.49

can, indeed, be changed, the strong bonding of the O atom to the Ag substrate is maintained, and no switching between binding mechanisms is found. On the Au substrate, VCA calculations also yielded similar results as the changing of the lattice constant, with decreased binding distances, but without a switching in the overall binding profile.

3.4.8 Applying an Electric Field

The above discussed approaches all tried to alter the interaction between the P2O molecule and the Ag substrate. However, the desired change of the bonding scenario from chemisorption to physisorption could not be obtained that way. Therefore, a completely different approach was tested. Instead of trying to influence the interaction of

the system parts itself, an electric field was applied over the whole unit cell. The force acting on the system electrons in such a field effectively change the work function of the substrate and should, therefore, strengthen or weaken the binding of the molecule. In VASP, such an external field can be applied in combination with a dipole correction in the corresponding direction, which cancels the field toward the adjoining periodic replica of the unit cell.
The electron potential energy of such a system is depicted in Fig. 25, where the slope of the electron potential energy over the z-direction of the unit cell is clearly visible in the vacuum region.
Geometry optimizations while applying an electric field of up to -0.75 eV/Å (which was the highest field that still allowed convergence of the SCF cycles and the geometry) showed no effect on the binding distance of the molecular C backbone, but reduced the binding of the O atoms to the surface and increased their binding distances by about 0.15 Å.
Subsequently, it was tested whether the weakening of the O-bonds can be combined with the weakening of the total binding strength as obtained by changing the lattice constant. Electric fields of 0.6 eV/Å were applied on a system with a 15% decreased unit cell size. The corresponding adsorption heights are shown in Tab. 9. Note that due to the compression of the unit cell, again a larger unit cell size was necessary to fit the P2O molecule (see section 3.4.6). Note also that no work function can be sensibly given for the present systems due to the gradient in the electron potential energy along the slab.
As previously discussed, the adsorption height of the C atoms is not influenced by the

Table 9: Adsorption heights h_C and h_O in Å of P2O C and O atoms on a compressed Ag substrate. In addition, an electric field of ± 0.6 eV was applied.

	electric field [eV/Å]	h_C [Å]	h_O [Å]
Ag	-	2.97	2.85
Ag -15%	-	3.16	3.01
Ag -15%	0.6	3.17	3.14
Ag -15%	-0.6	3.16	2.91

magnitude of the electric field, but only by the lattice compression. The height of the O atoms, on the other hand, is strongly influenced by the electric field. By applying this combination of straining, which weakens the bonding of the π-system toward the substrate, and electric field, which weakens the binding of the O atoms, the P2O atom could be forced into a situation similar to the physisorption on Au. In that case, an average adsorption height of about 3.15 Å relative to the Ag substrate and a height difference of only 0.02 Å between C and O atoms was obtained.
The initially suggested abrupt change between the different adsorption scenarios could, however, not be obtained. Only by individually weakening the different binding contributions, an overall weakening of the binding could be simulated.

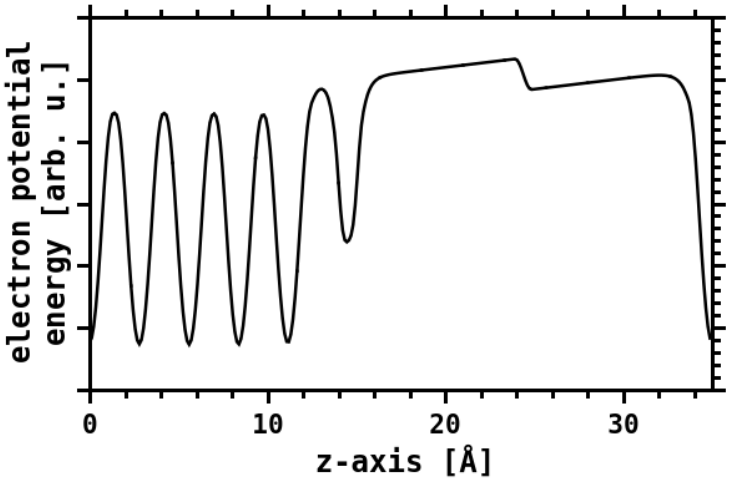

Figure 25: Electron potential energy of a P2O/Ag unit cell with an electric field of 0.2 eV/Å applied in z direction, drawn along the z-axis of the unit cell in Å. The Ag layers are visible at the left, and the P2O molecule lies on top, at about 14 Å. The potential energy in the vacuum gap exhibits a gradient, with the step in the middle being caused by the dipole correction.

3.4.9 Discussion: Adsorption of P2O on Ag(111)

The strong interaction between P2O and the Ag surface arises from (i) the bonding of the O atoms to Ag substrate atoms, (ii) the interaction of the molecular π-system with the substrate and (iii) van der Waals interaction of the whole molecule with the substrate.
When the topmost Ag layer is exchanged by Au, the adsorption behavior of P2O is similar to the adsorption on a complete Au slab, which indicates that mainly the binding directly to the surface atoms is relevant, while the work function of the substrate is not so crucial. Also, changes of up to 0.2 eV in the work function do not change the adsorption behavior at all.
In the performed tests it was found that the binding between molecule and substrate can be lessened by weakening both the interaction of the O atoms (by applying an electric field) and the π-system of the molecule (by compressing the Ag lattice constant). However, no abrupt transition between physisorption and chemisorption could be found. Instead, a gradual increase of the adsorption heights was obtained. Additionally, the necessary system changes to significantly weaken the binding were huge, with lattice constant reduction of 15% and an electric field of 0.6 eV/Å. Note that the obtained binding distances after applying these changes are still by more than 0.15 Å smaller than the ones obtained in experiments, meaning that the molecule still adsorbs too strongly.

Conclusion
No indication for the P20/Ag(111) system being close to a transition between physisorption and chemisorption could be found. The initially presented hypothesis postulating the existence of an abrupt transition between those two states for P2O/Ag has, therefore, to be discarded.

Still, the question remains why the experimental adsorption heights can not be reproduced within the given methodology, especially as good agreement is mostly obtained for similar systems.[25, 68, 85, 86, 131, 135]
From the simulation point of view, considering standard semi-local DFT methodology, the available options appear to be exhausted. The use of hybrid functionals is also not expected to yield different results, as they tend to strengthen surface binding compared to semi-local functional (as discussed in section 4) and would, therefore, most likely lead to even smaller binding distances.
Another possibility is that the the physisorptive scenario is a thermally activated case, which is found in the XSW measurements performed at room temperature, but not in DFT calculations. However, this scenario is not very likely, as some indication of the existence of a physisorbed adsorption scenario should have been visible in the binding energy curve.
As it is highly unlikely that this system can, for some unknown reason, not be described properly within DFT, it appears that some unknown factor disturbs the comparability of simulated and experimental results. An idea that was recently proposed (by Oliver T. Hofmann) suggests the existence of adatoms at the Ag surface. Preliminary tests performed by Andreas Jeindl on such a system indicate that this approach could, at least, prevent the significantly lower adsorption of O atoms compared to the C backbone.
To gain full understanding of the P2O/Ag(111) interface, it would, therefore, be necessary to (i) carry out further calculations to find out whether a configuration of the Ag substrate can be found that allows to reproduce the experimental adsorption heights and (ii) perform further experimental investigations to check if the originally obtained experimental adsorption heights are reproducible, and if some evidence of Ag surface reconstruction can be found.

4 Charge Transfer Properties at Interfaces: Tetrafluoro-Benzoquinone TFBQ on Copper Oxide Cu_2O and Cu

The correct evaluation of the electronic properties of an inorganic/organic interface is, in most cases, only possible when the geometry is described adequately, and vice versa. Several of the above discussed systems demonstrate this interplay of geometric and electronic properties, e.g. GaClPc on Cu, where the impact of the molecular dipole on the work function depends on its relative position. To properly capture the electronic structure at interfaces, the correct description of charge-transfer processes is crucial, as they directly influences molecular geometries, but also other interface properties, such as the work function.[28, 147]

The charge transfer occurring between adsorbed molecules and a substrate depends on the electron affinity (ionization energy) of the adsorbed molecules and the work function of the substrate. While DFT has been shown to give good and consistent results for many electronic properties independent of the details of the methodology, this is, unfortunately, not true for charge transfer at interfaces. Depending on the interface, the amount of transferred charge as well as the charge transfer mechanism can depend on the applied methodology.[2, 90, 148]

For inorganic/organic interfaces, two different charge transfer scenarios have been discussed, namely fractional charge transfer FCT and integer charge transfer ICT, which differ mainly in their charge localization.[11, 28]

During this thesis, the interplay of the charge transfer mechanism and the applied DFT functional, namely the amount of Hartree-Fock exchange α, was investigated in detail. Due to its impact on the charge localization in a system, the parameter α strongly influences the charge transfer properties.[3, 87, 90, 149]

The test system consisted of tetrafluoro-1,4-benzoquinone (TFBQ) molecules (see Fig. 26) adsorbed on a semiconducting copper-I-oxide Cu_2O and on a metallic Cu substrate (for details and structures, see section 4.3). The use of these two different substrates allowed to compare a scenario with strong hybridization as seen on Cu, where FCT is expected to occur, to a scenario where ICT is expected due to the weaker reactivity of the Cu_2O substrate.

The work on these systems was published recently in Ref. [6] and the article as well as the Supporting Information are included in the following. Beforehand, the author contributions to the article are specified.

In addition, preliminary work on charge transfer properties, including the choice of substrate material and molecule, as well as preliminary results on modifying the charge transfer properties by tuning the substrate, are discussed.

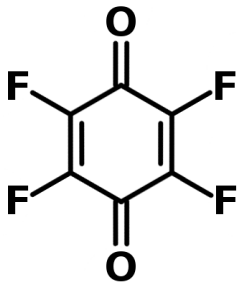

Figure 26: Structure of tetrafluoro-1,4-benzoquinone TFBQ.

4.1 Author Contributions

In the following section, an original publication as published in the Journal of Physical Chemistry C, including the Supporting Information, is inserted.
Reprinted with permission from:
Distinguishing between Charge-Transfer Mechanisms at Organic/Inorganic Interfaces Employing Hybrid Functionals
Elisabeth Wruss, Egbert Zojer and Oliver T. Hofmann
The Journal of Physical Chemistry C **2018** *122* (26), 14640-14653
DOI: 10.1021/acs.jpcc.8b03699
https://pubs.acs.org/doi/10.1021/acs.jpcc.8b03699

The simulation project on charge transfer mechanisms was supervised by Oliver T. Hofmann, and the project plan to investigate charge transfer for small organic molecules at metal and semiconducting substrate as a function of the Hartree-Fock exchange was proposed by him.
All presented calculations were performed and analyzed by me. The interpretation of the obtained data was done by Oliver T. Hofmann and myself. I have written the original version of the manuscript and created all included figures. Subsequently, the manuscript was modified and improved in close cooperation with Oliver T. Hofmann and Egbert Zojer.

4.2 Original Article: *Distinguishing between Charge Transfer Mechanisms at Organic/Inorganic Interfaces Employing Hybrid Functionals*

THE JOURNAL OF PHYSICAL CHEMISTRY C

Article

Cite This: J. Phys. Chem. C 2018, 122, 14640−14653

pubs.acs.org/JPCC

Distinguishing between Charge-Transfer Mechanisms at Organic/Inorganic Interfaces Employing Hybrid Functionals

Elisabeth Wruss, Egbert Zojer, and Oliver T. Hofmann*

Institute of Solid State Physics, NAWI Graz, Graz University of Technology, 8010 Graz, Austria

Supporting Information

ABSTRACT: When modeling inorganic/organic interfaces with density functional theory (DFT), the outcome often depends on the chosen functional. Hybrid functionals, which employ a fraction of Hartree−Fock exchange α, tend to give better results than the more commonly applied semilocal functionals, because they remove or at least mitigate the unphysical electron self-interaction. However, the choice of α is not straightforward, as its effect on observables depends on the physical properties of the investigated system, such as the size of the molecule and the polarizability of the substrate. In this contribution, we demonstrate this impact exemplarily for tetrafluoro-1,4-benzoquinone on semiconducting (copper-I-oxide Cu_2O) and metallic (Cu) substrates and explore how the simulated charge transfer depends on α. We determine the value α^* that marks the transition point between spurious over-localization and over-delocalization of charges. This allows us to shed light on the interplay between the value of α^* and the physical properties of the interface. We find that on the inert semiconducting substrate, α^* strongly depends on surface screening. Furthermore, α has a significant impact on the amount of charge transfer and, in particular, the charge localization. Conversely, for the adsorption on Cu, α affects only the amount of transferred charge, but not its localization, which is a consequence of strong hybridization. Finally, we discuss limitations to the predictive power of DFT for modeling charge transfer at inorganic/organic interfaces and explain why the choice of a "correct" amount of Hartree−Fock exchange is difficult, if not impossible. However, we argue why simulations still provide valuable insights into the charge-transfer mechanism at organic/inorganic interfaces and describe how α can be chosen sensibly to simulate any given system.

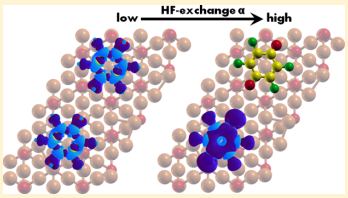

1. INTRODUCTION

With increasing computational power available to scientific applications, computer simulations have become more and more significant in various scientific disciplines. A showcase field concerning this trend is the investigation of inorganic/organic interfaces. As they are often embedded within the specimen, experimental investigations can be troublesome. Moreover, experiments frequently yield only incomplete information and do not provide a full atomistic understanding of the processes relevant at interfaces. Here, first-principles simulations can provide complementary insights and potentially offer an entirely different perspective by making observables accessible that are difficult to track experimentally.

The most widely used simulation method in material science based on the quantum-mechanical description of matter is density functional theory (DFT). The reason for this is mainly that DFT offers a good compromise between computational efficiency and accuracy.[1] Although DFT is in principle exact, in practice approximations need to be made because the exact functional is not known. A large variety of different exchange−correlation functionals is available, and many basic properties, such as covalent bonds, are well described within most of the existing frameworks.[2−4]

Unfortunately, this is not necessarily true for all observables, and inconsistencies between different functionals occur. In particular, when charge transfer at interfaces comes into play, the results of different DFT functionals can differ, varying both the amount of transferred charge and the charge distribution within a given material combination.[5−11] The problem of spurious charge transfer is particularly pronounced at inorganic/organic interfaces, where two very different classes of materials are combined.[10] Conceptually, for such interfaces, two fundamentally different charge-transfer mechanisms have been found both in simulations and in experiments: fractional charge transfer (FCT) and integer charge transfer (ICT).[12] FCT implies that all molecules get equally fractionally charged. It occurs on surfaces where hybrid bands between the substrate and molecules can be formed, which is, for example, the case for interfaces with pristine metals.[13−16] The case of ICT is typically found for less reactive surfaces, such as passivated metals or semiconductors.[17−21] There, charge transfer can occur only in integer electron numbers because of the absence of hybrid bands. This leads to the coexistence of charged and neutral molecules on the surface.[12,20,22] The difference between ICT and FCT, therefore, lies primarily in the localization of charges within the molecular adsorbate.[12] Consequently, the charge-transfer mechanism strongly influences the electrostatic landscape and, therefore, several physical properties of the interface[20] (such as charge injection barriers[23]). In this work, we address the question how well the typically applied

Received: April 19, 2018
Revised: May 17, 2018
Published: May 31, 2018

DOI: 10.1021/acs.jpcc.8b03699
J. Phys. Chem. C 2018, 122, 14640−14653

semilocal and hybrid DFT methods are suited to do reliably describe the properties of such inorganic/organic interfaces.

A complication that arises when trying to distinguish between ICT and FCT in simulations is that semilocal DFT functionals [such as Perdew–Burke–Ernzerhof (PBE),[24,25] which is also applied in this work] spuriously over-delocalize charges.[8,26−29] Consequently, by default, FCT is favored. The problem of over-delocalization can be overcome by admixing a fraction of Hartree–Fock exchange (quantified by the parameter α). This is done in the so-called hybrid functionals.[30] It has been argued that the Hartree–Fock exchange plays a role similar to that of the on-site repulsion term in the Hubbard model (i.e., the $+U$ term),[31−33] and it thus relates to the difference between the first and the second ionization energies, which is naturally system-dependent.

Whereas a too low fraction of Hartree–Fock exchange favors FCT, conversely, when a (too) high amount of Hartree–Fock exchange is chosen, this leads to the opposite case of charge over-localization[11,34] and causes an unphysical favoring of ICT over FCT.[20] Therefore, the charge-transfer mechanism obtained in a simulation can depend strongly on the applied functional, and the simulation does not necessarily reflect the correct physics.

In this contribution, we address several questions concerning the interplay between the chosen functional and the charge-transfer properties obtained when simulating inorganic/organic interfaces. In particular, we investigate whether semilocal and hybrid functionals can predict the charge-transfer mechanism. In addition, we discuss how insights can still be gained in systems where this is not the case. In this context, we also consider the question how well typically applied "default" hybrid functionals, such as PBE0 (which employs $\alpha = 0.25$),[3,30,35] are able to describe charge transfer at interfaces.

We start by reviewing the physics behind the two charge-transfer mechanisms and how they are represented within DFT. Readers who are more interested in the practical application are encouraged to continue with section 4, where we simulate different interfaces and investigate the influence of α. Throughout, we apply the PBEh[30] functional family. We investigate two prototypical interfaces that are expected to exhibit different charge-transfer mechanisms. These comprise the adsorption of tetrafluoro-1,4-benzoquinone (TFBQ, see Figure 1) on a weakly reactive, metallic surface and on an essentially inert semiconducting substrate, where (almost) no hybridization between adsorbate and substrate takes place.

TFBQ is an electron acceptor and, therefore, triggers electron-transfer processes on substrates with a sufficiently small work function. Initially, we analyze the molecule in the gas phase to obtain a starting point for our discussion. We then consider adsorption on the semiconducting copper-I-oxide Cu_2O surface. In the case of intrinsic Cu_2O, the lowest unoccupied molecular orbital (LUMO) of TFBQ lies in the gap of the substrate, and no charge transfer toward the molecule takes place. To obtain a prototypical ICT scenario, charge transfer is enabled by inducing an n-doped situation of the substrate, which results in filling of the molecular LUMO. Then, we simulate adsorption on Cu, where we expect that the hybridization between molecule and substrate will lead to an FCT situation.

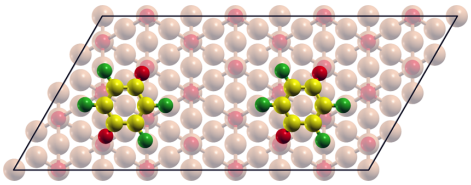

Figure 1. TFBQ on the $Cu_2O(111)$ surface in the 8 × 4 surface supercell. Cu atoms are depicted in brown, O atoms in red, C atoms in yellow, and F atoms in green.

For the discussed systems, we derive the transition value α^*, which is defined such that the applied functional does neither over-localize nor over-delocalize charges. Comparing this value for physically different systems allows us to investigate the interplay of physical properties and the applied functional. We discuss why it is problematic to choose an "ideal" value of α for a given system and how to most reasonably apply DFT for the investigation of different charge-transfer mechanisms.

2. METHODOLOGY

2.1. Computational Settings. All calculations are performed within the FHI-aims simulation package.[36] We apply the PBEh[30] hybrid functional family, which connects PBE and Hartree–Fock exchange according to the equation

$$E_{xc}^{PBEh} = \alpha E_x^{HF} + (1 - \alpha)E_x^{PBE} + E_c^{PBE} \quad (1)$$

with the exchange–correlation energy E_{xc}^{PBEh} consisting of a portion of Hartree–Fock exchange energy E_x^{HF}, the complementary portion of PBE exchange E_x^{PBE}, and the correlation energy E_c^{PBE}. The relative weight of exchange from PBE and Hartree–Fock is determined by the mixing parameter α. The PBEh family contains two commonly used functionals, PBE[24,25] ($\alpha = 0$) and PBE0[3,30,35] ($\alpha = 0.25$). To demonstrate the impact of the fraction of Hartree–Fock exchange, in this work, we vary α between 0 and 1.

Geometry optimizations are performed for all discussed systems with the corresponding functional. In these optimizations, the vdW-TS van der Waals correction[37] is applied, and for adsorption on Cu(111), the surface parameterization by Ruiz et al.[38] is used. We allow the molecule(s) as well as the topmost part of the substrate (i.e., the first O–Cu–O triple layer for Cu_2O and the two topmost layers for Cu) to relax until remaining forces below 0.01 eV/Å are reached. Full geometry optimizations for every applied functional are crucial, as incorrect results are obtained for several observables when hybrid-functional calculations on the basis of PBE geometries are performed: for the systems discussed here, hybrid calculations on the basis of PBE geometries result in work-function differences of up to 0.4 eV, adsorption height modifications of up to 0.25 Å, and the appearance of spurious peaks in the density of states (DOS) compared to consistently applying the hybrid functional (for details, see the Supporting Information). Note that the performed hybrid geometry optimizations for surface systems containing several hundred atoms are computationally extremely costly. This is aggravated by the need for performing all calculations in a spin-polarized manner, as this is a prerequisite for capturing the ICT scenario (see below).

For the smallest possible $Cu_2O(111)$ surface unit cell containing four Cu atoms (and two O atoms) per layer, a k-point grid of 12 × 12 × 1 k-points is applied. For metallic Cu, a denser k-grid is required and we used 16 × 16 × 1 k-points for the equivalent Cu(111) surface unit cell with four atoms per

DOI: 10.1021/acs.jpcc.8b03699
J. Phys. Chem. C 2018, 122, 14640−14653

layer. For the larger unit cells containing adsorbed molecules, the *k*-point grids are scaled accordingly. A Gaussian occupation scheme with a broadening of 0.1 eV is applied.

FHI-aims contains predefined collections of settings for atomic species regarding basis sets, integration grids, and the numerical accuracy of the Hartree potential.[36] During our convergence tests, "light" settings showed sufficient accuracy for the investigated systems when describing observables such as the DOS, orbital energies, and work functions. Details on the convergence tests are provided in the Supporting Information.

2.2. Investigated Systems and Unit Cells. For the surface calculations presented in this work, we consider unit cells containing two molecules of TFBQ on the stable copper-I-oxide $Cu_2O(111)$[39,40] and copper Cu(111) surfaces (as chemically related examples for semiconductor and metal substrates).

Note that the simulation of several molecules in one unit cell is necessary to describe the coexistence of charged and uncharged molecules as it can appear in the ICT case.

By this material choice, similar binding properties for the molecule are preserved, as on both substrates, molecular adsorption is guided by the bonding of the molecular O atoms to substrate Cu atoms. We have chosen the mixed-terminated (111) surface because there the TFBQ molecule exhibits only very weak hybridization with this substrate. We note that stronger hybridization between the adsorbate and a semiconductor can occur, for example, for the Cu-terminated surface (in which case an FCT solution on a semiconducting substrate could theoretically appear).

In hybrid DFT, the band gap of a material (and the level alignment with an adsorbate) depends on the employed functional.[41,42] In our calculations, the gap of Cu_2O varies between nonexistent (metallic, $\alpha = 0.00$) and 6.8 eV ($\alpha = 0.75$), compared to an experimental band gap of 2.1 eV.[43] However, this is less of a concern for the present study because the exact value of the band gap is not relevant as long as a consistent ordering of substrate and adsorbate states (molecular LUMO in the substrate band gap) is maintained. Indeed, for all applied hybrid functionals ($\alpha > 0$), intrinsic Cu_2O is correctly described as a semiconductor with the TFBQ LUMO lying in its band gap. As a consequence, there is no electron transfer to the molecules. The situation is different when $\alpha = 0$ (or very close to 0), where the semiconducting nature of the substrate is not captured and Cu_2O exhibits no band gap. In that case, the molecular LUMO is below the substrate Fermi energy, and charge is spuriously transferred toward the TFBQ molecules. Therefore, the energies for the unoccupied LUMO could not be derived with $\alpha = 0$, and corresponding results could not be used in the following, whenever LUMO energies were required for determining α^*.

The applied coverage is motivated by the structure of the $Cu_2O(111)$ surface, as the 4×4 cell (containing 16 Cu atoms per layer) is the smallest possible unit cell allowing the commensurate adsorption of TFBQ in a flat-lying geometry. We, therefore, apply an 8×4 unit cell for both Cu and Cu_2O substrates, which allows the adsorption of two molecules per unit cell in symmetry equivalent positions (see Figure 1).

To model the Cu substrate, four layers of metal atoms are used. At this slab thickness, the metal work function is converged to within 0.1 eV. To simulate the $Cu_2O(111)$ surface, three O−Cu−O layers of $Cu_2O(111)$ are employed, corresponding to a thin film of Cu_2O. This results in a slightly smaller band gap than in a bulk Cu_2O substrate but does not affect the situation qualitatively, as in all cases, the molecular LUMO is located inside the Cu_2O gap. The lattice constants are set to 3.63 Å for Cu and to 4.27 Å for Cu_2O. Note that, in principle, the lattice constant depends on the applied functional. However, we carefully checked that using a fixed value does not affect the results in this work, which is discussed in detail in the Supporting Information.

As periodic boundary conditions in all three spatial directions are applied, a vacuum gap of at least 20 Å is inserted between the periodic replicas of the slabs in the direction perpendicular to the surface. In addition, a dipole correction[44] is used to electrostatically decouple the periodic replicas.

3. THEORETICAL BACKGROUND: MODELING CHARGE TRANSFER WITH DFT

3.1. Charge-Transfer Mechanisms. A key aspect of the present paper is to understand how the applied DFT methodology influences the charge-transfer mechanism found in simulations. Prior to discussing that, we review the physical aspects that lead to the two possible scenarios, FCT and ICT, and highlight the distinguishing features.

Whether FCT or ICT appears in a specific case depends mainly on the hybridization between electronic states of the adsorbed molecules and states of the underlying substrate. Also, the coupling between adjacent molecules can play a role.[12,22,45−47] To illustrate the two different situations, we consider a model system where all molecules in the layer are notionally equivalent (i.e., they adsorb on equivalent adsorption sites) and where the interaction between the molecules is negligible. This is a good approximation for flat-lying molecules, where the coupling in the first monolayer is typically very small.

At first, we discuss a situation where no strong hybridization between the adsorbed molecules and substrate takes place. This is usually the case when there are spacer groups on the molecule separating it from the substrate[47] or when the molecules are adsorbed on a nonreactive, passivated, or semiconducting substrate.[19−21,48−50] When the adsorbate is electronically decoupled from the surface, charge transfer is limited to integer electron numbers (e.g., via tunneling). The (spin)orbitals of the adsorbed molecules are then either completely filled or completely empty.[12] As soon as one electron is added to the LUMO of an adsorbed molecule, the orbital splits into a singly occupied (SOMO) and a singly unoccupied (SUMO) spin orbital (see Figure 2).[20,21,51] In the corresponding DOS, the resulting spin-split peaks are located above and below the Fermi level, respectively, while no molecular DOS prevails directly at the Fermi edge. In addition, ICT systems exhibit a coexistence of charged and neutral molecules on the surface (where the ratio between the species can adopt a wide range of values).

This breaking of the translational periodicity due to charging can be understood in the following way: Electron transfer is originally triggered by the electron affinities of the molecules in the adsorbate layer being larger than the work function of the substrate (or their ionization energies being smaller). Because of the ensuing transfer of charge to one molecule, the electrostatic energy in its surrounding changes such that further transfer to neighboring molecules is suppressed and neighboring molecules remain neutral.[20] For identical adsorption sites and at low temperatures, this results in the formation of a superlattice of charged molecules. Notably, the charged and neutral molecules exhibit differences not only in their charge

DOI: 10.1021/acs.jpcc.8b03699
J. Phys. Chem. C 2018, 122, 14640−14653

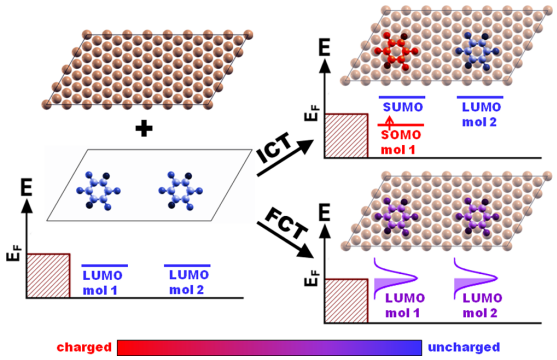

Figure 2. Schematic representation of level alignment upon adsorption of two TFBQ molecules on a substrate. Depending on the interaction, either spin-polarized charging of one molecule (ICT) or spin-unpolarized, equivalent charging of both molecules (FCT) appears.

densities and densities of states but also in their geometries (i.e., bond lengths).

Conversely, for adsorption on moderately reactive surfaces (such as clean coinage metals), strong hybridization between the electronic states of substrate and adsorbed molecules can take place and a hybrid band is formed. The states in this hybrid band are delocalized between substrate and molecules. When a state in such a band becomes occupied, part of the charge density can be associated with the substrate, and part of it with the adsorbate. This leads to a situation where all molecules on the surface become equally, and often fractionally, charged.[12] In case of fractional charging, the Fermi energy cuts through the hybrid band; that is, the molecular DOS is nonzero at the Fermi edge and the net charge on each molecule adopts a noninteger number (see Figure 2). In contrast to the ICT situation, the translational symmetry is not broken and all molecules in the layer exhibit equivalent geometries and electronic structures. The main features distinguishing FCT and ICT systems are summarized in Table 1 and Figure 2.

Table 1. Characteristics of FCT and ICT

	FCT	ICT
spin splitting in molecular DOS	no	yes
molecular DOS at the Fermi edge	yes	no
breaking of translation symmetry in molecular layer	no	yes
equal charging of all molecules	yes	no
fractional charging of molecules	yes	no

3.2. Impact of the Methodology on the Charge Distribution. While there is a vast amount of DFT studies describing FCT systems, theoretical work on ICT systems is comparably scarce. This discrepancy appears because modeling ICT is fundamentally more complicated[20,22] and also computationally significantly more costly than simulating FCT for the following reasons:

The first complication when modeling ICT arises from the periodic boundary conditions, which are required to simulate extended surfaces. To be able to capture symmetry breaking between different molecules in this framework, large supercells containing at least two molecules are required. This already significantly increases the computational effort. Additionally, spin-unrestricted simulations need to be performed, as single (unpaired) electrons are transferred. Although this is, in principle, straightforward to do within most DFT codes, it further increases the computational cost.

The most challenging and computationally most expensive factor is related to the functional required to correctly describe ICT. Whereas FCT can be modeled using semilocal functionals, capturing ICT requires higher-rung methods (such as hybrid functionals).[20] These are computationally up to two orders of magnitude more demanding than their semilocal counterparts.[30]

We note that the simulation of cells with two molecules per supercell does not pose a restriction for the FCT situation where all molecules in the monolayer are equivalent. However, for ICT, it only allows to model the situation where every other molecule is charged (and not, say, one out of four). Allowing for different ratios between charged and neutral molecules would require the use of even larger supercells, which is presently intractable using hybrid functionals. The precise fraction of charged molecules is, however, inconsequential for the present study, which deals with the conceptual differences between FCT and ICT. Thus, also the limitation to two molecules per supercell does not affect the conclusions (see also the low-coverage simulations presented in the Supporting Information).

To understand why the use of hybrid functionals is imperative for the description of ICT, one needs to consider how the energy of a molecule evolves with (fractional) charging. For the ideal, exact functional, the total energy of a system is piecewise linear between integer electron numbers (see the black lines in Figure 3a).[5,8,27,52−55] Because all available exchange−correlation functionals are approximations, errors arise, which cause deviations from this straight-line behavior. The so-called deviation from straight-line error (DSLE)[11] (often referred to as many-electron self-interaction error[26,27]) leads to a systematic over- or underestimation of the total energy for fractional electron numbers (depending on the functional), even if it does not necessarily affect the energy at integer electron numbers.[8,26,27,56−58]

In semilocal functionals such as PBE, the DSLE consistently leads to an underestimation of the energy for fractionally charged moieties[8,11,27,56] and, therefore, to a concave shape in the dependence of the total energy on the particle number (see the blue line in Figure 3a).

To understand how this error affects the charge-transfer mechanism, one needs to consider the energetics of molecular orbitals. In Kohn−Sham DFT, the energy of an orbital is given by the derivative of the total energy with respect to the filling of the orbital.[59]

$$\varepsilon = \frac{\mathrm{d}E}{\mathrm{d}N} \tag{2}$$

This means that for a DSLE-afflicted functional, the orbital energy will generally depend on its occupation. For the case of a semilocal functional with a concave curvature of the total energy with respect to the occupation (the blue line in Figure 3a), the orbital energy will, therefore, increase (i.e., typically become less negative) as it gets filled (see Figure 3b).

Hartree−Fock exhibits a contrary behavior. The total energy of a system with fractional electron numbers is systematically overestimated,[35] which is again due to the DSLE. In this context, it is worth pointing out that, although Hartree−Fock is free from single-electron self-interaction, the many-electron self-interaction error is still present.[27] The total energy is

DOI: 10.1021/acs.jpcc.8b03699
J. Phys. Chem. C 2018, 122, 14640−14653

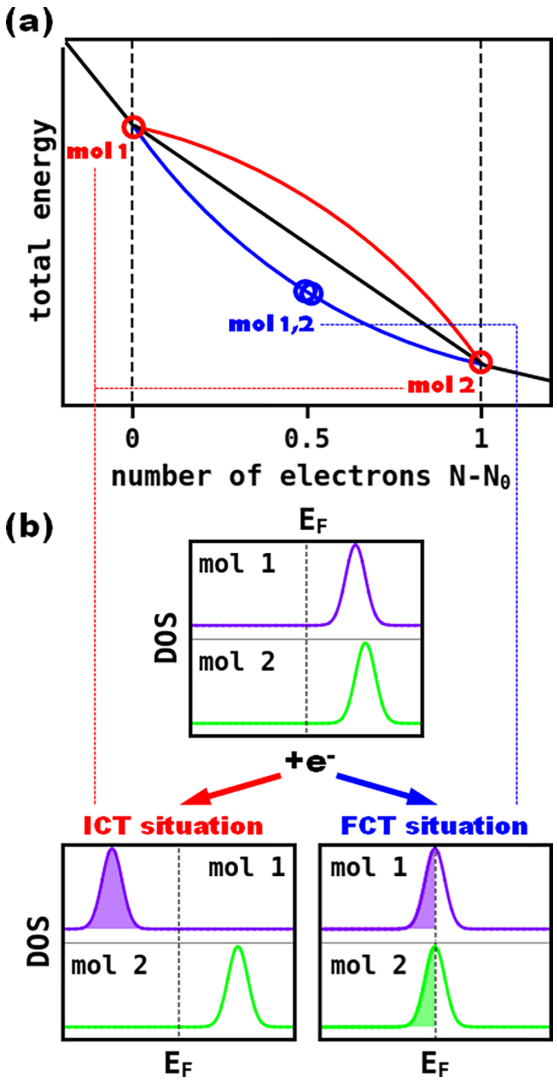

Figure 3. Schematic presentation of over-delocalization and over-localization due to the DSLE. (a) Evolution of the total energy of a system depending on the (fractional) number of electrons it contains. N_0 corresponds to the charge-neutral situation. The black line shows the ideal DSLE-free situation, where the dependence of the energy on the number of electrons is piecewise linear between integer electron numbers. The blue curve depicts the situation of $\alpha = 0$, where over-delocalization of charges appears and the energy at fractional electron numbers is underestimated. The red curve depicts the opposite situation of $\alpha = 1$, where the energy for fractional electron numbers is overestimated and strong over-localization of charges occurs. The lowest energy configuration for the two-molecule system shown in (b) is marked with red ($\alpha = 1$, ICT) and blue ($\alpha = 0$, FCT) circles. (b) One electron is added to the frontier orbitals of a system containing two molecules. Over-localization shifts the orbitals apart and leads to one full and one empty orbital upon charging, which results in the ICT case (red). Over-delocalization, on the other hand, results in two half-filled orbitals and therefore an FCT situation (blue).

curved in a convex form (see the red line in Figure 3a), and therefore, the orbital energy decreases (i.e., typically becomes more negative) with increasing occupation (see Figure 3b).

Knowing this dependence, we can argue what will happen in a charge-transfer system with two molecules. Even when the molecules are notionally identical, their LUMOs will not be perfectly aligned, for example, as a result of dynamic disorder. As soon as a minute amount of charge is transferred to one of the molecules, its lowest-lying unoccupied orbital will become partly occupied. In the case of a semilocal functional ($\alpha = 0$), this results in an upward shift of the orbital energy until it comes into resonance with the lowest-lying empty orbital of the other molecule. This charge-transfer-induced destabilization of the respective orbital inevitably results in an even distribution of charge between both molecules. This resembles the FCT situation (see Figure 3b). Note, however, that the FCT charge distribution does not originate from the physical situation, as it appears even when no hybridization (either between the molecules or to a substrate) occurs. Rather, it is purely a numerical artifact, which arises from the dependence of the orbital energy on its occupation.

For this case, the energetically ideal configuration for the transfer of one electron is marked by the blue circles in Figure 3a. As a consequence, strongly hybridizing systems, which are expected to exhibit FCT, are qualitatively correctly described in the framework of semilocal functionals. The tendency to over-delocalize charges,[26,27,29] however, prevents a successful simulation of ICT systems.[20]

Conversely, for Hartree−Fock (or hybrid functionals comprising a large amount of Hartree−Fock exchange), adding charge to an unoccupied orbital of an adsorbed molecule will result in a downshift of the orbital in energy. The orbital is, therefore, stabilized compared to the corresponding orbitals of neighboring molecules (see Figure 3b). Thus, the orbital of one molecule must become fully charged before charge can be added to the orbitals of another molecule. Consequently, for the model case of one electron being transferred per two molecules, the total energy is minimized by fully charging one molecule while leaving the other one neutral. This is depicted by the red circles in Figure 3a. Therefore, in Hartree−Fock and for large α, the DSLE tends to over-localize charges, favoring the ICT scenario.

Because of the contrasting behavior of the aforementioned methods, it is possible to construct hybrid functionals that aim at compensating the DSLE. This can be done by complementing semilocal functionals with Hartree−Fock exchange (see eq 1),[35] where the residual DSLE depends on the applied mixing ratio expressed by the parameter α. We note that also other methods exist to compensate for the DSLE, including (empirical) self-interaction correction schemes or range-separated hybrid functionals with either a general parameterization, such as the popular CAM-B3LYP[60,61] or the HSE[62,63] functional, or optimally tuned functionals with a system-specific parameterization.[58,64−69] However, even if some of these approaches might be computationally cheaper, they contain more parameters than a simple, global hybrid functional, which makes them harder to interpret physically. Therefore, they are not in the scope of the present work.

The above discussed cases emphasize the relevance of the parameter α, which determines how the energies of the frontier orbitals depend on their (partial) occupation.[70] Irrespective of the actual physical properties of an interface, low values of α (or no Hartree−Fock exchange mixed in at all) will promote an

DOI: 10.1021/acs.jpcc.8b03699
J. Phys. Chem. C 2018, 122, 14640−14653

FCT situation, whereas sufficiently high amounts of α will favor an ICT situation in the simulations. Under certain circumstances, the value of α can, therefore, be the deciding factor whether an FCT or an ICT situation is found in a DFT calculation.

As the DSLE-free situation marks the transition point between over-localization and over-delocalization, it is worthwhile identifying the corresponding value of α (denoted here as α^*).[11,71] Thus, in the following, we will identify this transition point for different interfaces and will also discuss how its value is influenced by the physical situation. Moreover, we will describe which information can be gained by varying α and under which circumstances the choice of α has little or no qualitative impact on the obtained results.

4. RESULTS AND DISCUSSION

4.1. Impact of α on the Electronic Structure of TFBQ in the Gas Phase. The first system for which we determine α^* is the TFBQ molecule in the gas phase. Here, we discuss two possible approaches, namely, enforcing the straight-line condition and comparing the LUMO energies to the electron affinity (EA) of the molecule.

4.1.1. Straight-Line Condition. To assess the straight-line condition, we calculate the LUMO energies of the molecule in the gas phase as a function of α. We consider the neutral molecule as well as the molecule charged by half an electron and by one electron. In the latter case, the considered orbital corresponds to the SOMO of the TFBQ anion. The corresponding values are shown in Figure 4a, where we interpolate linearly between the data points, which is consistent with the results for gas-phase molecules in previous works.[11,70] It follows from eq 2 that the straight-line condition is met when the energy of an orbital becomes independent of its occupation. For low values of α (0.00, 0.25, and 0.50), we find an increase of the orbital energy with filling, whereas for higher values of α (0.75 and 1.00), the orbital energy decreases. The slope $d\varepsilon/dN$ is determined from a linear fit and is plotted as a function of α in Figure 4b. By interpolation, we deduce the value of $\alpha^* = 0.62$ to fulfill the straight-line condition. This value might appear high compared to the amount of Hartree−Fock exchange employed in many commonly used functionals. In this context, it is useful to remember that there is a relationship between the fraction of Hartree−Fock exchange and the Hubbard U term for the on-site charging energy (see Introduction).[31−33] Physically, this parameter describes that it is more difficult to ionize a molecule a second time (even if the second charge is put into the same orbital) because of the Coulomb repulsion between the two charges. This repulsion is larger for more confined orbitals; that is, small molecules typically require large values of U (and, thus, α). The value of $\alpha^* = 0.62$ is also very well in line with the values of α^* around 0.7 obtained for other small molecules such as tetracyanoethylene,[20] tetracyanoquinodimethane,[11] and benzene.[71]

4.1.2. Comparison of EA and LUMO Energy. An alternative approach for obtaining a DSLE-free functional is to tune α such that the (negative) energy of the highest occupied molecular orbital corresponds to the ionization potential of the system.[11,72,73] As the vertical ionization potential of the negatively charged molecular anion is equal to the vertical EA of the neutral molecule, either of the quantities can be considered. Likewise, in the DSLE-free case, the energy of the SOMO of the anion equals the energy of the LUMO$^\alpha$ of the neutral molecule.[11] Consequently, a viable tuning procedure

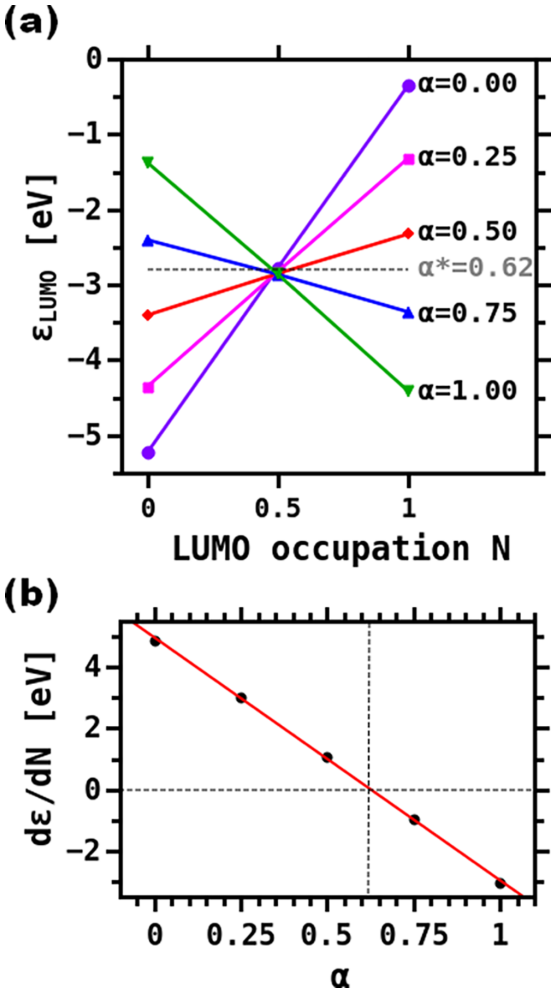

Figure 4. (a) Dependence of the LUMO energy ε on its occupation in the gas-phase TFBQ molecule as a function of the amount of Hartree−Fock exchange α. Three charging levels ($N = 0$, $N = 0.5$, and $N = 1$) have been considered, and the value α^* is marked by the gray dashed line. (b) Dependence of $d\varepsilon/dN$ (the change of the LUMO energy with charging) as a function of α. By applying a linear fit, a value $\alpha^* = 0.62$ for $d\varepsilon/dN = 0$ (i.e., the straight-line condition) is obtained ($R^2 = 0.9994$).

would also be to match the EA of the neutral molecule with its LUMO energy. As this line of arguments is independent of the underlying molecular geometries, it can also be applied to adiabatic quantities (i.e., relaxing geometries of the charged states, as will be done in the following). Such tuning procedures have been applied frequently and have yielded an improved prediction of several electronic properties.[68,71,73,77]

To obtain the EA, we calculate the energy differences between the neutral molecule and the singly negatively charged system.

$$\mathrm{EA} = E_{\mathrm{neutral}} - E_{\mathrm{anion}} = -\varepsilon_{\mathrm{LUMO}} \quad (3)$$

This procedure is known as the ΔSCF approach.[70,78−80] For all hybrid functionals considered here, EA is found to vary by

DOI: 10.1021/acs.jpcc.8b03699
J. Phys. Chem. C 2018, 122, 14640−14653

less than 0.1 eV, which is in line with previous findings that the ΔSCF EA does not strongly depend on the functional.[70] The average EA amounts to 2.84 eV. The TFBQ LUMO energies as a function of α are shown in Figure 5. From this plot, it can be

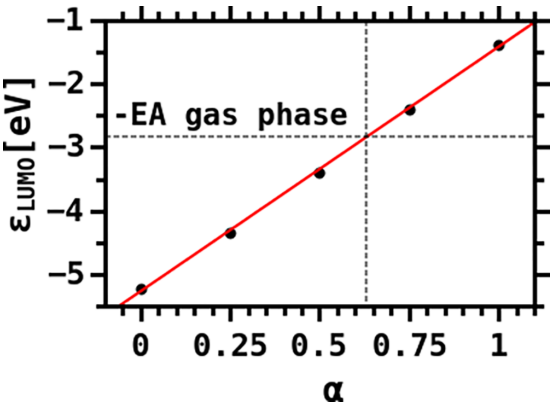

Figure 5. LUMO energies of the TFBQ molecule calculated with different values of α. The dashed lines mark the negative EAs and the corresponding values of α^* calculated for the gas phase (linear fit of LUMO energies: R^2 = 0.9990).

concluded that for matching the LUMO energy with the average EA (dashed line), a value of α^* = 0.63 is required. This is consistent with the value α^* = 0.62 found above, enforcing the straight-line condition.

4.2. Impact of α on the Electronic Structure of the TFBQ/Cu_2O Interface. Knowing α^* for the TFBQ molecule in the gas phase, the question arises how this value compares to α^* for an interface with a monolayer of TFBQ molecules adsorbed on a surface. We first consider adsorption on Cu_2O, where we expect only little hybridization and, therefore, anticipate an ICT situation. Here, the modified α^* is estimated based on the straight-line condition for the lowest unoccupied molecular state at the interface (which, for the sake of consistency, we continue to call LUMO in the following). This is analogous to the first strategy employed for the gas-phase molecule. As a complementary approach, we compare the energies for the ICT and FCT scenarios for different values of α and, from that, determine α^*.

Prior to that, it is useful to discuss how α^* is expected to change due to presence of a substrate. For the following semiquantitative argument, we neglect the impact of hybridization and different geometric relaxations at the interface compared to the gas phase but rather focus on the role played by the dielectric screening of the additional negative charge through the substrate. The screening causes an overall increase of the EA. Conceptually, this should also be reflected in the positions of the unoccupied states derived from the LUMO of the neutral adsorbate. It has, however, been shown that neither semilocal nor hybrid functionals capture this effect.[81−84] Therefore, in a situation with no hybridization and no geometric distortions upon adsorption, the LUMO energies of uncharged molecules are not affected by the presence of a surface. Consequently, a first approximate value for α^* at the interface can be obtained by comparing the EA of the interface with the LUMO energy of the gas-phase molecule.

Ideally, we would like to calculate the EA on the surface via the ΔSCF approach, that is, as an energy difference of the charged and the uncharged moieties. This is, however, not directly possible with periodic boundary conditions because charging of the unit cell would lead to a diverging energy. In practice, this can be avoided by assuming a homogenous charged background in the unit cell. However, especially for interfaces, such an approach does not solve the problem since then the charging energy would diverge with increasing the width of the vacuum gap. In principle, the GW method (which provides charged excitations) would be a viable alternative approach. However, the results of the typically conducted non-self-consistent GW corrections depend on the starting point, that is, the underlying DFT calculations and, therefore, the functional.[85,86] Moreover, for the interfaces investigated in this work, GW is presently far too costly. It has, however, been discussed in the literature that screening in comparable interface systems increases the EA by approximately 1 eV.[81] By comparing this value to the LUMO energies derived in the gas phase (see Figure 5), we conclude that surface screening will significantly lower the required value of α^*. These considerations show that the presence of a screening substrate can be expected to significantly reduce the amount of Hartree−Fock exchange necessary to realize a DSLE-free situation. Considering that the screening energy scales with the dielectric substrate, even more significant reductions of α^* can be expected for molecules adsorbed on more polarizable substrates.

4.2.1. Straight-Line Condition. To obtain a quantitative estimate for α^*, it is necessary to calculate the actual interface, where not only screening effects but also geometric rearrangements and a possible hybridization between TFBQ and Cu_2O states influence the LUMO energies. Then, a value of α^* including all adsorption-induced contributions can be derived from enforcing the straight-line condition. In analogy to section 4.1, this corresponds to finding the value of α for which the LUMO (respectively, SOMO) energy becomes independent of the filling of the state.

To be able to directly compare LUMO and SOMO energies, the ideal strategy is to calculate both a charged and a neutral molecule in one unit cell. To achieve that, we choose a supercell containing two TFBQ molecules on a 8 × 4 Cu_2O(111) substrate, as shown in Figure 1. Note that no calculations applying α = 0.00 could be included here, for the reasons discussed in the Methodology section.

When adding an electron to the unit cell to fill one of the LUMOs, the charge has to be compensated by a positive charge without breaking the translational symmetry within the unit cell. Thus, a positively charged plate is positioned below the Cu_2O substrate (for details, see the Supporting Information).[87,88] This results in a situation that is physically equivalent to n-doped Cu_2O, where free charges are available in the conduction band and can be transferred to the molecules. The additional electron can be donated to either one or both of the electron-accepting TFBQ molecules. For all hybrid functionals applied here, it is possible to achieve a situation where the electron is localized on one molecule while the second molecule remains charge-neutral. The energies of (the essentially nondispersing band derived from) the LUMO of the neutral molecule and of (the band derived from) the SOMO of the charged molecule are shown in Figure 6a. A value of α = 1.00, as applied for the gas phase, could not be considered for the surface because in this case, we were unable

DOI: 10.1021/acs.jpcc.8b03699
J. Phys. Chem. C 2018, 122, 14640−14653

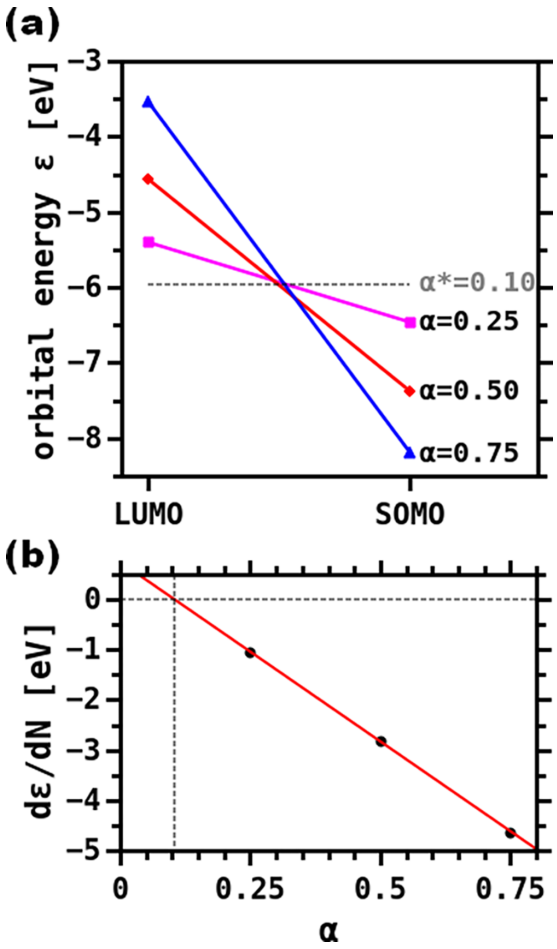

Figure 6. Orbital energies of two TFBQ molecules adsorbed on the $Cu_2O(111)$ surface in an 8 × 4 surface unit cell. (a) The presence of one charged and one neutral molecule in the cell allows the direct comparison of LUMO and SOMO energies for three different values of α. The energies are given relative to the upper vacuum level. (b) Change of LUMO energy for all considered values of α. By applying a linear fit, the value of $\alpha^* = 0.10$ for $d\varepsilon/dN = 0$ is derived (R^2 = 0.9998).

to converge the Cu_2O substrate. In contrast to the gas-phase situation, where only high values of α lead to a decrease in the LUMO energy with charging, on the surface, we find a decrease for all tested functionals. By extrapolating $d\varepsilon/dN$ as a function of α (Figure 6b), the value fulfilling the straight-line condition can be determined to be $\alpha^* = 0.10$. Consistent with the above considerations regarding screening effects, this value is significantly lower than that in the gas phase. Consequently, on the surface, a calculation with $a = 0.10$ or higher will favor an ICT situation, whereas for lower values, the FCT scenario is favored. Therefore, the application of the gas-phase value of α^* (0.63) to the surface situation will create a significant risk of over-localizing charges and strongly favor ICT.

Notably, $\alpha^* = 0.10$ is also significantly below the frequently applied value $\alpha = 0.25$ (as used, e.g., in PBE0[3,30,35]), suggesting that "standard" hybrid calculations would also be biased toward charge over-localization and, thus, toward ICT in the present case.

As we intend to investigate the influence of the surface adsorption, we want to exclude that the derived α^* is influenced and strongly affected by the presence of neighboring (screening) molecules. Therefore, we further reduce the molecular coverage to one-fourth of the previous value. As described in the Supporting Information, this yields $\alpha^* = 0.08$, showing that the considered coverage with one molecule per 126 Å^2 is low enough to render the value of α^* determined above, insensitive to the presence of neighboring molecules.

4.2.2. Charge-Transfer Mechanism for Different Values of α. The unit cell containing two molecules conceptually allows the simulation of the ICT-induced coexistence of two differently charged molecules on the surface. This enables a direct investigation of the charge-transfer mechanism.

As a first step, we consider the DOS projected onto the molecules, which is calculated with different values of α and is shown in Figure 7. For $\alpha = 0.00$, the charge is evenly distributed

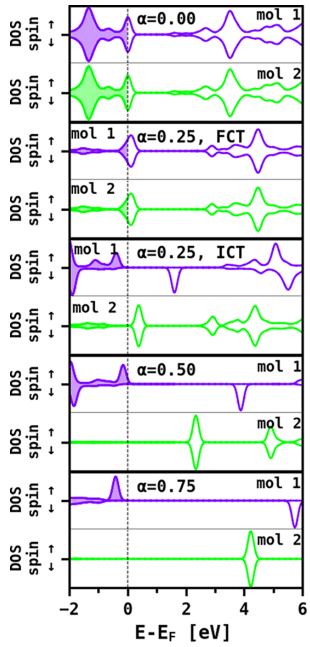

Figure 7. DOSs projected on molecules 1 (purple) and 2 (green) for all applied functionals. For $\alpha = 0.25$, both FCT and ICT solutions are shown. Spin-up and spin-down DOSs are drawn in the positive and negative directions in arbitrary units. The energy axis is aligned to the Fermi energy (and in case of no DOS at the Fermi level, to the valence band maximum of the underlying Cu_2O substrate).

between both molecules and neither symmetry breaking nor spin splitting appears. Thus, this situation can be described by the FCT model. Conversely, for $\alpha = 0.50$ and $\alpha = 0.75$, the projected DOS exhibits symmetry breaking between molecule 1 and molecule 2, and for the charged molecule, the DOS becomes clearly spin-polarized. These calculations can be assigned to the ICT scenario. We note that early discussions of the ICT scenario invoked polaron levels in the gap (sometimes also denoted as ICT levels) as relevant for the charge transfer. Our calculations clearly show that there is no in-gap state.

DOI: 10.1021/acs.jpcc.8b03699
J. Phys. Chem. C 2018, 122, 14640−14653

Rather, as found also by other authors,[51,89,90] the LUMO of the charged molecule splits into a SOMO and a SUMO state, where the SUMO is found at higher energies than the LUMO of the neutral molecule.

For α = 0.25, the situation is less clear. We obtain two solutions, where the projected DOSs shown in Figure 7 imply that one corresponds to an FCT and the other one to an ICT solution. Notably, these differing results are obtained by different initializations of the calculations: whereas the default initialization (which, in FHI-aims, is a superposition of the spherical atomic charge densities)[36] leads to the FCT scenario, any asymmetric magnetic initialization of molecules 1 and 2 converges to the ICT solution.

To further analyze these observations, we establish charge localization on the molecules as an observable to distinguish between the charge-transfer mechanisms. This is done by calculating the charges of individual molecules and defining a charge localization parameter, L, as

$$L = \frac{Q_{mol1} - Q_{mol2}}{Q_{mol1} + Q_{mol2}} \quad (4)$$

When the charge is evenly distributed between both molecules, the localization parameter becomes zero, which corresponds to an ideal FCT case. Charging of one molecule with the other one remaining neutral results in a localization of L = 1 (or L = −1). This corresponds to an ideal ICT situation.

However, determining the charges faces two challenges: First of all, it is important to keep in mind that atomic or molecular charges are not unambiguously defined observables, and different partitioning schemes usually lead to varying results. Additionally, although TFBQ interacts only weakly with the Cu_2O substrate, there is a small, but nonzero, hybridization between the substrate and deeper-lying σ orbitals. As a result of these two complications, an "uncharged" molecule (with no charge transfer into the LUMO) may become nominally positively charged. In the present case, the high-α ICT solutions exhibit such positive charging if the LUMO of the molecule remains empty. This leads to the nonintuitive situation of a nominal charge localization L > 1. For the determination of the localization parameter, here we use Mulliken charges[91] on the molecules. In order to exclude positive charging due to hybridization and/or Mulliken artifacts, we set the positively charged molecule to Q = 0. In the Supporting Information, we report the results for three alternative strategies: considering only the LUMO occupation of the two molecules, considering the full Mulliken charges, or partitioning via Hirshfeld[92] charges. We emphasize that for all of these choices, the conclusions drawn hereafter prevail.

Figure 8 shows the absolute value of L for TFBQ on Cu_2O for different values of α. For α = 0.00, L = 0, consistent with the FCT situation discussed above. For α = 0.50 and α = 0.75, a value of L = 1 is obtained with one molecule being charged and the other one remaining neutral. For α = 0.25, the FCT solution exhibits L = 0, whereas for the second solution, L = 0.8 is obtained. The meaning of L being neither 1 nor 0 as well as the reason for the coexistence of FCT and ICT solutions for α = 0.25 will become clear from the following discussion of the relative energetics of the FCT and ICT scenarios.

4.2.3. Relative Energies of FCT and ICT Solutions. When we reconsider the energy progression in Figure 3a, we see that the relative energies of the FCT and ICT solutions have to change upon varying α. For our system (two TFBQ molecules on Cu_2O + one extra electron per unit cell), this leads to the relative energies schematically shown in Figure 9.

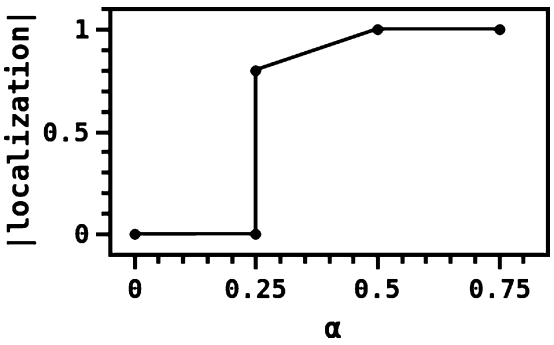

Figure 8. Absolute value of localization of charges for two TFBQ molecules on Cu_2O for different amounts of α. For α = 0.25, both obtained solutions are shown.

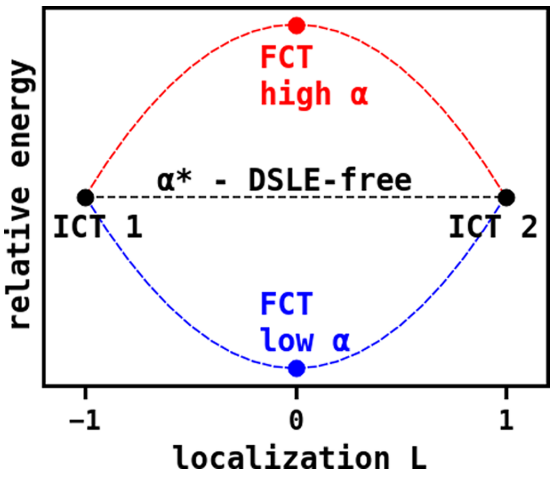

Figure 9. Schematic representation of the relative energies of different solutions, denoted by the associated charge-localization parameter L in the two-molecule system. The two ICT solutions, representing charging of the first molecule while the second one remains uncharged and vice versa, are degenerated in energy. For high values of α, the FCT solution is higher in energy than the ICT solutions (red), whereas for low values of α, it is lower (blue). At the transition value α^*, which marks the DSLE-free situation, FCT and ICT solutions are at the same energy. Note that the dashed lines depicting the evolution of the energy with L are idealized. For example, the FCT solution at high values of α is not necessarily a maximum but might also correspond to a local minimum.

There are two degenerate ICT solutions corresponding to the additional charge localized either on the first (L = +1) or on the second molecule in the unit cell (L = −1). They are denoted as ICT 1 and ICT 2 in Figure 9.

The ideal FCT solution with both molecules equivalently charged marks the transition point between the ICT solutions and must be at a symmetric position relative to both. For the high-α case (the red curve in Figure 9), the FCT solution is energetically unfavorable compared to the ICT solutions. However, because of the symmetry of the energy evolution with

DOI: 10.1021/acs.jpcc.8b03699
J. Phys. Chem. C 2018, 122, 14640−14653

respect to changing the sign of L, it must be a stationary point on the electronic potential energy surface. Thus, conceptually, it has to be accessible as a stable solution in DFT simulations. In the low-α case, the FCT scenario is the energetic minimum and the ICT solutions do not represent stable, stationary points. It is, therefore, usually not possible to enforce an ICT solution for $\alpha < \alpha^*$. This is in line with our results where we are not able to converge an ICT solution for $\alpha = 0.00$ even with asymmetric spin initialization. For $\alpha = 0.25$, which is slightly above α^*, FCT and ICT solutions can be obtained depending on the initialization. Typically, when the symmetry between the molecules is initially broken, the system will converge toward the ICT solution for $\alpha > \alpha^*$, as it is implied by the energy progression in Figure 9. Otherwise, the FCT solution will be obtained. Consistent with the above arguments, we find that for $\alpha = 0.25$, the ICT result is about 0.2 eV per molecule lower in energy. With increasing values of α, convergence of the FCT solution becomes harder and harder, as the energy difference between FCT and ICT solutions becomes larger. Minimal distortions from the perfect symmetry of molecules 1 and 2 already drive the calculations toward the much more stable ICT case. This explains why we have not been able to obtain an FCT solution for $\alpha = 0.50$ and $\alpha = 0.75$.

Figure 9 also gives insights into the situation where an amount of Hartree−Fock exchange corresponding to α^* is used, that is, in the case of a DSLE-free calculation. Then, the energies of FCT and ICT solutions must be degenerate. Therefore, also every linear combination of these solutions is a valid solution with the same energy. This leads to two problems: First, charge can be shifted within the monolayer at no energetic cost, making the SCF notoriously difficult to converge (i.e., while the energy will be converged immediately, the density will not). Second, even when convergence can be achieved, the charge distribution is basically arbitrary and cannot be assigned to either FCT or ICT. This is in line with the above results for $\alpha = 0.25$, which is comparably close to the straight-line value α^*. We find an ICT solution where the localization amounts to only 0.8 instead of 1. As the FCT and ICT solutions are already quite close in energy at this point, we find a solution which is not the ideal ICT scenario but slightly deviates from it.

4.2.4. Estimation of α^* by Comparing Energies of the FCT and ICT Solutions. The fact that at α^*, the FCT and ICT solutions are degenerate provides an additional strategy for estimating the amount of Hartree−Fock exchange required for a DSLE-free functional. As discussed above, it should be conceptually possible to simulate FCT scenarios for all values $\alpha > \alpha^*$. As minimal symmetry distortions prevent the DFT calculations from readily converging into the FCT solution at high values of α, in such cases, symmetry must be enforced. This can be achieved by performing the simulations in a non-spin-polarized manner.

The resulting energy differences between FCT and ICT solutions for different values of α are shown in Figure 10. From these, we can estimate a value of $\alpha^* = 0.03$, where both solutions exhibit equivalent energies. This is satisfactorily in line with our previous results of $\alpha^* = 0.10$ as obtained from enforcing the straight-line condition and again well below the commonly applied $\alpha = 0.25$.

4.3. Impact of α on the Electronic Structure of the TFBQ/Cu Interface. Before discussing how α should be chosen for a given system, we look at a physically different situation, namely, the adsorption of TFBQ on Cu(111). Above,

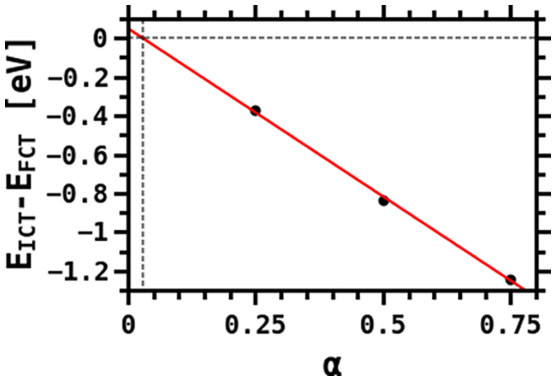

Figure 10. Energy difference between the ICT and FCT solutions as a function of α. The transition point where both solutions exhibit the same energy is deduced from the linear fit depicted in red and lies at $\alpha^* = 0.03$ ($R^2 = 0.9986$).

we found that for the TFBQ/Cu_2O interface, the ICT scenario can always be simulated by applying a sufficiently high value of α. This raises the question whether this effect is system-independent and whether an ICT solution can be found for every system as long as α is high enough. Considering that α^* ought to be reduced by screening effects (vide supra), on metallic surfaces, a value of α^* even smaller than that on Cu_2O should be expected because of the particularly strong screening. Conversely, in a situation in which organic molecules are in direct contact with a metal surface, one would expect an FCT situation because of hybridization effects of the molecules with the substrate. Thus, from the above discussion, it is a priori not clear how α affects the calculated charge-transfer mechanism on a bare metal substrate.

Therefore, we simulate the adsorption of TFBQ on Cu(111). To be able to identify ICT behavior, again a unit cell containing at least two TFBQ molecules is required and an 8×4 surface cell in analogy to the one considered for Cu_2O is applied. The resulting molecule-projected DOSs for different values of α are shown in Figure 11, and the Mulliken charges per molecule are shown in Table 2.

The PBE simulation shows a typical FCT behavior, with both molecules exhibiting equivalent partial charging of the LUMO and, therefore, nonzero DOS at the Fermi level. In addition, both molecules get equally charged with 0.61 electrons. All calculations employing $\alpha > 0.00$ exhibit fully charged LUMOs for both molecules, which lie clearly below the Fermi level, and the molecule-projected DOS at the Fermi level drops to zero. With higher amounts of α, the LUMOs shift to lower energies and are completely filled (in the spin-up and spin-down channels). This suggests that two electrons per molecule have been transferred. The overall transferred charge, however, only amounts to approximately one electron per molecule. This can be explained by back donation from nominally deeper-lying orbitals that hybridize particularly strongly with the substrate.[13,93]

The net transfer of one electron per molecule and the vanishing projected DOS at the Fermi edge point toward an ICT scenario. This is, however, ruled out by the identical structures and charges of the two molecules and by the identical occupations of the spin channels. Furthermore, the amount of

DOI: 10.1021/acs.jpcc.8b03699
J. Phys. Chem. C 2018, 122, 14640−14653

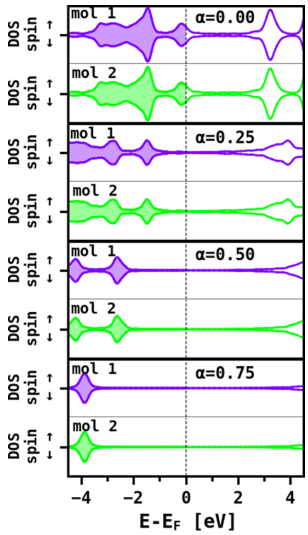

Figure 11. DOSs projected on molecules 1 (purple) and 2 (green) for all applied functionals. Spin-up and spin-down DOSs are drawn in the positive and negative directions in arbitrary units. The energy axis is aligned to the Fermi energy.

Table 2. Mulliken Charges in Electrons per Molecule for Two TFBQ Molecules on the Cu(111) Surface for Different Values of α

	α = 0.00	α = 0.25	α = 0.50	α = 0.75
Mulliken charge molecule 1 [electrons]	0.61	0.88	1.01	1.12
Mulliken charge molecule 2 [electrons]	0.61	0.88	1.01	1.12

charge on each molecule continuously increases with increasing α, which would also not be the case in an ICT situation.

The fundamental difference between the previously discussed adsorption on Cu_2O and that on Cu lies in the hybridization between molecular and substrate states. On Cu_2O, molecule and substrate are electronically largely decoupled, which leads to an ICT scenario even at low values of α. Conversely, on Cu, hybridization between molecule and substrate states appears even at high values of α in spite of the tendency to over-localize charges. Such a strong metal−molecule coupling is in line with the reduced adsorption height the molecule exhibits on Cu in comparison to Cu_2O. (The maximum height difference is found for α = 0.75, where charged TFBQ adsorbs 0.27 Å lower on Cu than on Cu_2O relative to the topmost Cu layer.)

We, therefore, conclude that the strong hybridization appearing between TFBQ and the metallic surface outweighs the effect of stronger screening and causes FCT to appear. Notably, this effect can be described adequately in DFT, with semilocal as well as with hybrid functionals.

5. SUMMARY AND CONCLUSIONS: SUGGESTED CHOICE OF α

In this contribution, we focus on the interplay between the charge-transfer mode across inorganic/organic interfaces and the choice of the DFT functional (i.e., the amount of Hartree−Fock exchange α) used to model it. This is discussed for the example of a monolayer of TFBQ molecules adsorbed on semiconducting Cu_2O and metallic Cu substrates. We show that hybrid functionals exhibit a transition point α^* between spurious over-localization and over-delocalization of charges, favoring either FCT (i.e., all molecules being equally charged) or ICT (i.e., the coexistence of charged and uncharged molecules on the surfaces).

We describe how α^* can be determined in various ways for both the molecule and the interface and show that it is massively reduced by a screening substrate. Our results indicate that the weaker the screening (i.e., the lower the dielectric constant), the higher are the expected values of the transition point α^*. As far as the actually calculated charge-transfer mechanism is concerned, the choice of α relative to α^* fundamentally changes the situation on the semiconducting substrate. This is in contrast to the adsorption on Cu(111), where the functional does not qualitatively change the charge-transfer mechanism. Still, even there it changes the amount of transferred charge and, therefore, influences associated properties, such as the geometry and the adsorption-induced work function change.

This leaves the question how to ideally choose α in the case of weak hybridization. For the example of TFBQ on $Cu_2O(111)$ discussed here, the comparably low value of $\alpha^* \approx 0.1$ that we found implies that most commonly applied hybrid functionals will result in an ICT scenario. This outcome is, however, not necessarily predictive. It is possible to obtain both the FCT and the ICT solutions for values $\alpha > \alpha^*$, which is due to the symmetry of the wave function. However, in that case, the ICT solution is always energetically favorable and, therefore, the relative energies of the solutions are not authoritative.

Then, one might be tempted to conclude that the DSLE-free situation $\alpha = \alpha^*$ would be the ideal choice for reliably predicting the charge-transfer properties of a given interface. This is, however, not the case. At α^*, by definition, the LUMO energies of the molecules in the layer are independent of their occupation. Thus, shifting charge from one molecule to another does not cost energy (geometry relaxations notwithstanding). As a result, every possible localization of transferred charge in the layer results in the same total energy. Consequentially, the charge distribution found by the iterative SCF procedure at α^* is determined by numerics and, basically, arbitrary. It follows from the above that at α^*, ICT and FCT must have the same energy. In hindsight, this is not surprising. There is, in principle, a multitude of ICT solutions; that is, the "charged overlayer" can hop from one site to another. The ensemble average (either time-averaged or spatially averaged) of these ICT solutions is equivalent to an FCT charge distribution. This is formally equivalent to the original derivation of the DSLE principle by Perdew et al.,[53] which rationalized fractional electron numbers by statistical mixtures.

Thus, we arrive at the (somewhat disappointing) conclusion that there is no semilocal or hybrid functional that is universally predictive for the charge-transfer mechanism at weakly interacting interfaces. Also, there appears to be no universally valid recipe that allows constructing such a functional for a specific material combination.

This means that in order to be able to draw insights from computation, some input from experiment is required to determine the prevalent charge-transfer mechanism. The best practice we suggest is to calculate both FCT and ICT for the given interface, for example, by applying a functional with $\alpha < \alpha^*$ and another with $\alpha > \alpha^*$ or by enforcing FCT via spin

DOI: 10.1021/acs.jpcc.8b03699
J. Phys. Chem. C 2018, 122, 14640−14653

restriction for $\alpha > \alpha^*$. By doing so, relevant observables for both scenarios can be calculated. Subsequently, these can be compared to experimentally obtained results. Note that for this comparison, timescales may play an important role; that is, the observables from experiment must be obtained on timescales faster than the supposed charge-hopping times. This is the case, for example, for photoemission experiments or vibrational spectroscopy.

After the charge-transfer mechanism is determined, the corresponding electronic structure can be analyzed to gain valuable insights, for example, into the origin and strength of bonding, charge transfer, and hybridization.

■ ASSOCIATED CONTENT

Supporting Information

The Supporting Information is available free of charge on the ACS Publications website at DOI: 10.1021/acs.jpcc.8b03699.

Details on the impact of geometry optimizations, performed convergence tests, further methodological aspects (spin initialization of molecules and adding charge to the unit cell), calculations with reduced coverage, and localization and charge partitioning schemes (PDF)

■ AUTHOR INFORMATION

Corresponding Author

*E-mail: o.hofmann@tugraz.at.

ORCID

Egbert Zojer: 0000-0002-6502-1721

Oliver T. Hofmann: 0000-0002-2120-3259

Notes

The authors declare no competing financial interest.

■ ACKNOWLEDGMENTS

Financial support by the Austrian Science Fund (FWF) (P28051-N36 and P27868-N36) is gratefully acknowledged. We thank Simon Erker for valuable scientific discussion and computational advice. The computational studies presented have been achieved using the Vienna Scientific Cluster (VSC3).

■ ADDITIONAL NOTE

[a]In the exact functional, the LUMO changes its energy upon infinitesimal filling because of the so-called derivative discontinuity.[53,74−78] Because the semilocal and hybrid functionals do not exhibit this behavior, we neglect this detail here.

■ REFERENCES

(1) Jensen, F. *Introduction to Computational Chemistry*, 3rd ed.; John Wiley & Sons: Chichester, UK, 2017.

(2) Perdew, J. P.; Chevary, J. A.; Vosko, S. H.; Jackson, K. A.; Pederson, M. R.; Singh, D. J.; Fiolhais, C. Atoms, Molecules, Solids, and Surfaces: Applications of the Generalized Gradient Approximation for Exchange and Correlation. *Phys. Rev. B* **1992**, *46*, 6671−6687.

(3) Ernzerhof, M.; Scuseria, G. E. Assessment of the Perdew−Burke−Ernzerhof Exchange-Correlation Functional. *J. Chem. Phys.* **1999**, *110*, 5029−5036.

(4) Staroverov, V. N.; Scuseria, G. E.; Tao, J.; Perdew, J. P. Comparative Assessment of a New Nonempirical Density Functional: Molecules and Hydrogen-Bonded Complexes. *J. Chem. Phys.* **2003**, *119*, 12129−12137.

(5) Perdew, J. P.; Zunger, A. Self-Interaction Correction to Density-Functional Approximations for Many-Electron Systems. *Phys. Rev. B* **1981**, *23*, 5048−5079.

(6) Toher, C.; Filippetti, A.; Sanvito, S.; Burke, K. Self-Interaction Errors in Density-Functional Calculations of Electronic Transport. *Phys. Rev. Lett.* **2005**, *95*, 146402.

(7) Ke, S.-H.; Baranger, H. U.; Yang, W. Role of the Exchange-Correlation Potential in Ab Initio Electron Transport Calculations. *J. Chem. Phys.* **2007**, *126*, 201102.

(8) Cohen, A. J.; Mori-Sánchez, P.; Yang, W. Insights into Current Limitations of Density Functional Theory. *Science* **2008**, *321*, 792−794.

(9) Della Sala, F.; Fabiano, E.; Laricchia, S.; D'Agostino, S.; Piacenza, M. The Role of Exact-exchange in the Theoretical Description of Organic-metal Interfaces. *Int. J. Quantum Chem.* **2010**, *110*, 2162−2171.

(10) Draxl, C.; Nabok, D.; Hannewald, K. Organic/Inorganic Hybrid Materials: Challenges for Ab Initio Methodology. *Acc. Chem. Res.* **2014**, *47*, 3225−3232.

(11) Atalla, V.; Zhang, I. Y.; Hofmann, O. T.; Ren, X.; Rinke, P.; Scheffler, M. Enforcing the Linear Behavior of the Total Energy with Hybrid Functionals: Implications for Charge Transfer, Interaction Energies, and the Random-Phase Approximation. *Phys. Rev. B* **2016**, *94*, 035140.

(12) Braun, S.; Salaneck, W. R.; Fahlman, M. Energy-Level Alignment at Organic/Metal and Organic/Organic Interfaces. *Adv. Mater.* **2009**, *21*, 1450−1472.

(13) Romaner, L.; Heimel, G.; Brédas, J.-L.; Gerlach, A.; Schreiber, F.; Johnson, R. L.; Zegenhagen, J.; Duhm, S.; Koch, N.; Zojer, E. Impact of Bidirectional Charge Transfer and Molecular Distortions on the Electronic Structure of a Metal-Organic Interface. *Phys. Rev. Lett.* **2007**, *99*, 256801.

(14) Duhm, S.; Gerlach, A.; Salzmann, I.; Bröker, B.; Johnson, R. L.; Schreiber, F.; Koch, N. PTCDA on Au(111), Ag(111) and Cu(111): Correlation of Interface Charge Transfer to Bonding Distance. *Org. Electron.* **2008**, *9*, 111−118.

(15) Kröger, I.; Stadtmüller, B.; Stadler, C.; Ziroff, J.; Kochler, M.; Stahl, A.; Pollinger, F.; Lee, T.-L.; Zegenhagen, J.; Reinert, F.; et al. Submonolayer Growth of Copper-Phthalocyanine on Ag(111). *New J. Phys.* **2010**, *12*, 083038.

(16) Edlbauer, H.; Zojer, E.; Hofmann, O. T. Postadsorption Work Function Tuning via Hydrogen Pressure Control. *J. Phys. Chem. C* **2015**, *119*, 27162−27172.

(17) Bokdam, M.; Çakır, D.; Brocks, G. Fermi Level Pinning by Integer Charge Transfer at Electrode-Organic Semiconductor Interfaces. *Appl. Phys. Lett.* **2011**, *98*, 113303.

(18) Çakir, D.; Bokdam, M.; de Jong, M. P.; Fahlman, M.; Brocks, G. Modeling Charge Transfer at Organic Donor-Acceptor Semiconductor Interfaces. *Appl. Phys. Lett.* **2012**, *100*, 203302.

(19) Amsalem, P.; Niederhausen, J.; Wilke, A.; Heimel, G.; Schlesinger, R.; Winkler, S.; Vollmer, A.; Rabe, J. P.; Koch, N. Role of Charge Transfer, Dipole-Dipole Interactions, and Electrostatics in Fermi-Level Pinning at a Molecular Heterojunction on a Metal Surface. *Phys. Rev. B* **2013**, *87*, 035440.

(20) Hofmann, O. T.; Rinke, P.; Scheffler, M.; Heimel, G. Integer versus Fractional Charge Transfer at Metal(/Insulator)/Organic Interfaces: Cu(/NaCl)/TCNE. *ACS Nano* **2015**, *9*, 5391−5404.

(21) Hollerer, M.; Lüftner, D.; Hurdax, P.; Ules, T.; Soubatch, S.; Tautz, F. S.; Koller, G.; Puschnig, P.; Sterrer, M.; Ramsey, M. G. Charge Transfer and Orbital Level Alignment at Inorganic/Organic Interfaces: The Role of Dielectric Interlayers. *ACS Nano* **2017**, *11*, 6252−6260.

(22) Gruenewald, M.; Schirra, L. K.; Winget, P.; Kozlik, M.; Ndione, P. F.; Sigdel, A. K.; Berry, J. J.; Forker, R.; Brédas, J.-L.; Fritz, T.; et al. Integer Charge Transfer and Hybridization at an Organic Semiconductor/Conductive Oxide Interface. http://pubs.acs.org/doi/full/10.1021/jp512153b (accessed Feb 26, 2018).

(23) Gao, W.; Kahn, A. Electronic Structure and Current Injection in Zinc Phthalocyanine Doped with Tetrafluorotetracyanoquinodimethane: Interface versus Bulk Effects. *Org. Electron.* **2002**, *3*, 53−63.

(24) Perdew, J. P.; Burke, K.; Ernzerhof, M. Generalized Gradient Approximation Made Simple. *Phys. Rev. Lett.* **1996**, *77*, 3865−3868.

(25) Perdew, J. P.; Burke, K.; Ernzerhof, M. ERRATA: Generalized Gradient Approximation Made Simple [Phys. Rev. Lett. 77, 3865 (1996)]. *Phys. Rev. Lett.* **1997**, *78*, 1396.
(26) Zhang, Y.; Yang, W. A Challenge for Density Functionals: Self-Interaction Error Increases for Systems with a Noninteger Number of Electrons. *J. Chem. Phys.* **1998**, *109*, 2604−2608.
(27) Mori-Sánchez, P.; Cohen, A. J.; Yang, W. Many-Electron Self-Interaction Error in Approximate Density Functionals. *J. Chem. Phys.* **2006**, *125*, 201102.
(28) Kümmel, S.; Kronik, L. Orbital-Dependent Density Functionals: Theory and Applications. *Rev. Mod. Phys.* **2008**, *80*, 3−60.
(29) Perdew, J. P.; Ruzsinszky, A.; Constantin, L. A.; Sun, J.; Csonka, G. I. Some Fundamental Issues in Ground-State Density Functional Theory: A Guide for the Perplexed. *J. Chem. Theory Comput.* **2009**, *5*, 902−908.
(30) Perdew, J. P.; Ernzerhof, M.; Burke, K. Rationale for Mixing Exact Exchange with Density Functional Approximations. *J. Chem. Phys.* **1996**, *105*, 9982−9985.
(31) Ivády, V.; Armiento, R.; Szász, K.; Janzén, E.; Gali, A.; Abrikosov, I. A. Theoretical Unification of Hybrid-DFT and DFT + U Methods for the Treatment of Localized Orbitals. *Phys. Rev. B* **2014**, *90*, 035146.
(32) Verma, P.; Truhlar, D. G. Does DFT+U Mimic Hybrid Density Functionals? *Theor. Chem. Acc.* **2016**, *135*, 182.
(33) Gani, T. Z. H.; Kulik, H. J. Where Does the Density Localize? Convergent Behavior for Global Hybrids, Range Separation, and DFT +U. *J. Chem. Theory Comput.* **2016**, *12*, 5931−5945.
(34) Hofmann, D.; Kümmel, S. Integer Particle Preference during Charge Transfer in Kohn-Sham Theory. *Phys. Rev. B* **2012**, *86*, 201109.
(35) Adamo, C.; Barone, V. Toward Reliable Density Functional Methods without Adjustable Parameters: The PBE0 Model. *J. Chem. Phys.* **1999**, *110*, 6158−6170.
(36) Blum, V.; Gehrke, R.; Hanke, F.; Havu, P.; Havu, V.; Ren, X.; Reuter, K.; Scheffler, M. Ab Initio Molecular Simulations with Numeric Atom-Centered Orbitals. *Comput. Phys. Commun.* **2009**, *180*, 2175−2196.
(37) Tkatchenko, A.; Scheffler, M. Accurate Molecular Van Der Waals Interactions from Ground-State Electron Density and Free-Atom Reference Data. *Phys. Rev. Lett.* **2009**, *102*, 073005.
(38) Ruiz, V. G.; Liu, W.; Zojer, E.; Scheffler, M.; Tkatchenko, A. Density-Functional Theory with Screened van Der Waals Interactions for the Modeling of Hybrid Inorganic-Organic Systems. *Phys. Rev. Lett.* **2012**, *108*, 146103.
(39) Soon, A.; Todorova, M.; Delley, B.; Stampfl, C. Thermodynamic Stability and Structure of Copper Oxide Surfaces: A First-Principles Investigation. *Phys. Rev. B* **2007**, *75*, 125420.
(40) Önsten, A.; Göthelid, M.; Karlsson, U. O. Atomic Structure of Cu2O(1 1 1). *Surf. Sci.* **2009**, *603*, 257−264.
(41) Xu, Y.; Hofmann, O. T.; Schlesinger, R.; Winkler, S.; Frisch, J.; Niederhausen, J.; Vollmer, A.; Blumstengel, S.; Henneberger, F.; Koch, N.; et al. Space-Charge Transfer in Hybrid Inorganic-Organic Systems. *Phys. Rev. Lett.* **2013**, *111*, 226802.
(42) Hofmann, O. T.; Deinert, J.-C.; Xu, Y.; Rinke, P.; Stähler, J.; Wolf, M.; Scheffler, M. Large Work Function Reduction by Adsorption of a Molecule with a Negative Electron Affinity: Pyridine on ZnO(1010). *J. Chem. Phys.* **2013**, *139*, 174701.
(43) Meyer, B. K.; Polity, A.; Reppin, D.; Becker, M.; Hering, P.; Klar, P. J.; Sander, T.; Reindl, C.; Benz, J.; Eickhoff, M.; et al. Binary Copper Oxide Semiconductors: From Materials towards Devices. *Phys. Status Solidi B* **2012**, *249*, 1487−1509.
(44) Neugebauer, J.; Scheffler, M. Adsorbate-Substrate and Adsorbate-Adsorbate Interactions of Na and K Adlayers on Al(111). *Phys. Rev. B* **1992**, *46*, 16067−16080.
(45) Anderson, P. W. Localized Magnetic States in Metals. *Phys. Rev.* **1961**, *124*, 41−53.
(46) Newns, D. M. Self-Consistent Model of Hydrogen Chemisorption. *Phys. Rev.* **1969**, *178*, 1123−1135.
(47) Lindell, L.; Unge, M.; Osikowicz, W.; Stafström, S.; Salaneck, W. R.; Crispin, X.; de Jong, M. P. Integer Charge Transfer at the Tetrakis(Dimethylamino)Ethylene/Au Interface. *Appl. Phys. Lett.* **2008**, *92*, 163302.
(48) Murdey, R. J.; Salaneck, W. R. Charge Injection Barrier Heights Across Multilayer Organic Thin Films. *Jpn. J. Appl. Phys., Part 1* **2005**, *44*, 3751.
(49) Braun, S.; Salaneck, W. R. Fermi Level Pinning at Interfaces with Tetrafluorotetracyanoquinodimethane (F4-TCNQ): The Role of Integer Charge Transfer States. *Chem. Phys. Lett.* **2007**, *438*, 259−262.
(50) Swart, I.; Sonnleitner, T.; Repp, J. Charge State Control of Molecules Reveals Modification of the Tunneling Barrier with Intramolecular Contrast. *Nano Lett.* **2011**, *11*, 1580−1584.
(51) Png, R.-Q.; Ang, M. C. Y.; Teo, M.-H.; Choo, K.-K.; Tang, C. G.; Belaineh, D.; Chua, L.-L.; Ho, P. K. H. Madelung and Hubbard Interactions in Polaron Band Model of Doped Organic Semiconductors. *Nat. Commun.* **2016**, *7*, 11948.
(52) David Mermin, N. Thermal Properties of the Inhomogeneous Electron Gas. *Phys. Rev.* **1965**, *137*, A1441−A1443.
(53) Perdew, J. P.; Parr, R. G.; Levy, M.; Balduz, J. L. Density-Functional Theory for Fractional Particle Number: Derivative Discontinuities of the Energy. *Phys. Rev. Lett.* **1982**, *49*, 1691−1694.
(54) Stein, T.; Autschbach, J.; Govind, N.; Kronik, L.; Baer, R. Curvature and Frontier Orbital Energies in Density Functional Theory. *J. Phys. Chem. Lett.* **2012**, *3*, 3740−3744.
(55) Kraisler, E.; Kronik, L. Piecewise Linearity of Approximate Density Functionals Revisited: Implications for Frontier Orbital Energies. *Phys. Rev. Lett.* **2013**, *110*, 126403.
(56) Perdew, J. P.; Ruzsinszky, A.; Csonka, G. I.; Vydrov, O. A.; Scuseria, G. E.; Staroverov, V. N.; Tao, J. Exchange and Correlation in Open Systems of Fluctuating Electron Number. *Phys. Rev. A* **2007**, *76*, No. 040501(R).
(57) Vydrov, O. A.; Scuseria, G. E.; Perdew, J. P. Tests of Functionals for Systems with Fractional Electron Number. *J. Chem. Phys.* **2007**, *126*, 154109.
(58) Körzdörfer, T.; Brédas, J.-L. Organic Electronic Materials: Recent Advances in the DFT Description of the Ground and Excited States Using Tuned Range-Separated Hybrid Functionals. *Acc. Chem. Res.* **2014**, *47*, 3284−3291.
(59) Janak, J. F. Proof That $\partial E/\partial ni=\varepsilon$ in Density-Functional Theory. *Phys. Rev. B* **1978**, *18*, 7165−7168.
(60) Cohen, A. J.; Mori-Sánchez, P.; Yang, W. Development of Exchange-Correlation Functionals with Minimal Many-Electron Self-Interaction Error. *J. Chem. Phys.* **2007**, *126*, 191109.
(61) Heaton-Burgess, T.; Yang, W. Structural Manifestation of the Delocalization Error of Density Functional Approximations: C4N+2 Rings and C20 Bowl, Cage, and Ring Isomers. *J. Chem. Phys.* **2010**, *132*, 234113.
(62) Heyd, J.; Scuseria, G. E.; Ernzerhof, M. Hybrid Functionals Based on a Screened Coulomb Potential. *J. Chem. Phys.* **2003**, *118*, 8207−8215.
(63) Heyd, J.; Scuseria, G. E.; Ernzerhof, M. Erratum: "Hybrid Functionals Based on a Screened Coulomb Potential" [J. Chem. Phys.118, 8207 (2003)]. *J. Chem. Phys.* **2006**, *124*, 219906.
(64) Stein, T.; Eisenberg, H.; Kronik, L.; Baer, R. Fundamental Gaps in Finite Systems from Eigenvalues of a Generalized Kohn-Sham Method. *Phys. Rev. Lett.* **2010**, *105*, 266802.
(65) Refaely-Abramson, S.; Baer, R.; Kronik, L. Fundamental and Excitation Gaps in Molecules of Relevance for Organic Photovoltaics from an Optimally Tuned Range-Separated Hybrid Functional. *Phys. Rev. B* **2011**, *84*, 075144.
(66) Kronik, L.; Stein, T.; Refaely-Abramson, S.; Baer, R. Excitation Gaps of Finite-Sized Systems from Optimally Tuned Range-Separated Hybrid Functionals. *J. Chem. Theory Comput.* **2012**, *8*, 1515−1531.
(67) Karolewski, A.; Kronik, L.; Kümmel, S. Using Optimally Tuned Range Separated Hybrid Functionals in Ground-State Calculations: Consequences and Caveats. *J. Chem. Phys.* **2013**, *138*, 204115.
(68) Gledhill, J. D.; Peach, M. J. G.; Tozer, D. J. Assessment of Tuning Methods for Enforcing Approximate Energy Linearity in Range-Separated Hybrid Functionals. *J. Chem. Theory Comput.* **2013**, *9*, 4414−4420.

DOI: 10.1021/acs.jpcc.8b03699
J. Phys. Chem. C 2018, 122, 14640−14653

(69) Sun, H.; Autschbach, J. Influence of the Delocalization Error and Applicability of Optimal Functional Tuning in Density Functional Calculations of Nonlinear Optical Properties of Organic Donor−Acceptor Chromophores. *ChemPhysChem* **2013**, *14*, 2450−2461.
(70) Hofmann, O. T.; Atalla, V.; Moll, N.; Rinke, P.; Scheffler, M. Interface Dipoles of Organic Molecules on Ag(111) in Hybrid Density-Functional Theory. *New J. Phys.* **2013**, *15*, 123028.
(71) Sai, N.; Barbara, P. F.; Leung, K. Hole Localization in Molecular Crystals from Hybrid Density Functional Theory. *Phys. Rev. Lett.* **2011**, *106*, 226403.
(72) Yang, W.; Cohen, A. J.; Mori-Sánchez, P. Derivative Discontinuity, Bandgap and Lowest Unoccupied Molecular Orbital in Density Functional Theory. *J. Chem. Phys.* **2012**, *136*, 204111.
(73) Atalla, V.; Yoon, M.; Caruso, F.; Rinke, P.; Scheffler, M. Hybrid Density Functional Theory Meets Quasiparticle Calculations: A Consistent Electronic Structure Approach. *Phys. Rev. B* **2013**, *88*, 165122.
(74) Perdew, J. P.; Levy, M. Physical Content of the Exact Kohn-Sham Orbital Energies: Band Gaps and Derivative Discontinuities. *Phys. Rev. Lett.* **1983**, *51*, 1884−1887.
(75) Sham, L. J.; Schlüter, M. Density-Functional Theory of the Energy Gap. *Phys. Rev. Lett.* **1983**, *51*, 1888−1891.
(76) Gould, T.; Toulouse, J. Kohn-Sham Potentials in Exact Density-Functional Theory at Noninteger Electron Numbers. *Phys. Rev. A* **2014**, *90*, No. 050502(R).
(77) Rios-Font, R.; Sodupe, M.; Rodríguez-Santiago, L.; Taylor, P. R. The Role of Exact Exchange in the Description of Cu2+−(H2O)n (n = 1−6) Complexes by Means of DFT Methods. *J. Phys. Chem. A* **2010**, *114*, 10857−10863.
(78) Gunnarsson, O.; Lundqvist, B. I. Exchange and Correlation in Atoms, Molecules, and Solids by the Spin-Density-Functional Formalism. *Phys. Rev. B* **1976**, *13*, 4274−4298.
(79) Vydrov, O. A.; Scuseria, G. E. Ionization Potentials and Electron Affinities in the Perdew−Zunger Self-Interaction Corrected Density-Functional Theory. *J. Chem. Phys.* **2005**, *122*, 184107.
(80) Rostgaard, C.; Jacobsen, K. W.; Thygesen, K. S. Fully Self-Consistent GW Calculations for Molecules. *Phys. Rev. B* **2010**, *81*, 085103.
(81) Neaton, J. B.; Hybertsen, M. S.; Louie, S. G. Renormalization of Molecular Electronic Levels at Metal-Molecule Interfaces. *Phys. Rev. Lett.* **2006**, *97*, 216405.
(82) Garcia-Lastra, J. M.; Rostgaard, C.; Rubio, A.; Thygesen, K. S. Polarization-Induced Renormalization of Molecular Levels at Metallic and Semiconducting Surfaces. *Phys. Rev. B* **2009**, *80*, 245427.
(83) Thygesen, K. S.; Rubio, A. Renormalization of Molecular Quasiparticle Levels at Metal-Molecule Interfaces: Trends across Binding Regimes. *Phys. Rev. Lett.* **2009**, *102*, 046802.
(84) Biller, A.; Tamblyn, I.; Neaton, J. B.; Kronik, L. Electronic Level Alignment at a Metal-Molecule Interface from a Short-Range Hybrid Functional. *J. Chem. Phys.* **2011**, *135*, 164706.
(85) Rinke, P.; Qteish, A.; Neugebauer, J.; Scheffler, M. Exciting Prospects for Solids: Exact-Exchange Based Functionals Meet Quasiparticle Energy Calculations. *Phys. Status Solidi B* **2008**, *245*, 929−945.
(86) Blase, X.; Attaccalite, C.; Olevano, V. First-Principles GW Calculations for Fullerenes, Porphyrins, Phtalocyanine, and Other Molecules of Interest for Organic Photovoltaic Applications. *Phys. Rev. B* **2011**, *83*, 115103.
(87) Sinai, O.; Hofmann, O. T.; Rinke, P.; Scheffler, M.; Heimel, G.; Kronik, L. Multiscale Approach to the Electronic Structure of Doped Semiconductor Surfaces. *Phys. Rev. B* **2015**, *91*, 075311.
(88) Erker, S.; Rinke, P.; Moll, N.; Hofmann, O. T. Doping Dependence of the Surface Phase Stability of Polar O-Terminated (0001) ZnO. *New J. Phys.* **2017**, *19*, 083012.
(89) Yang, J.-P.; Bussolotti, F.; Kera, S.; Ueno, N. Origin and Role of Gap States in Organic Semiconductor Studied by UPS: As the Nature of Organic Molecular Crystals. *J. Phys. D: Appl. Phys.* **2017**, *50*, 423002.
(90) Winkler, S.; Amsalem, P.; Frisch, J.; Oehzelt, M.; Heimel, G.; Koch, N. Probing the Energy Levels in Hole-Doped Molecular Semiconductors. *Mater. Horiz.* **2015**, *2*, 427−433.
(91) Mulliken, R. S. Electronic Population Analysis on LCAO−MO Molecular Wave Functions. I. *J. Chem. Phys.* **1955**, *23*, 1833−1840.
(92) Hirshfeld, F. L. Bonded-Atom Fragments for Describing Molecular Charge Densities. *Theor. Chim. Acta* **1977**, *44*, 129−138.
(93) Rangger, G. M.; Hofmann, O. T.; Romaner, L.; Heimel, G.; Bröker, B.; Blum, R.-P.; Johnson, R. L.; Koch, N.; Zojer, E. F4TCNQ on Cu, Ag, and Au as Prototypical Example for a Strong Organic Acceptor on Coinage Metals. *Phys. Rev. B* **2009**, *79*, 165306.

DOI: 10.1021/acs.jpcc.8b03699
J. Phys. Chem. C 2018, 122, 14640−14653

Supporting Information for

Distinguishing between Charge Transfer Mechanisms at Organic/Inorganic Interfaces Employing Hybrid Functionals

Elisabeth Wruss, Egbert Zojer and Oliver T. Hofmann*

Institute of Solid State Physics, NAWI Graz, Graz University of Technology, 8010 Graz, Austria.

Corresponding Author

*o.hofmann@tugraz.at

1. Impact of Geometry Optimization

In this section we discuss the common practice to employ higher-level methods (e.g., hybrid functionals) using geometries obtained at a cheaper level of theory (e.g., semi-local functionals). Here, we illustrate how severely the results can be falsified if a full geometry optimization with the more expensive functional is avoided.

We investigate how problematic this approach is by applying a toy systems of TFBQ on three layers of Cu(111) and Cu_2O(111) substrate in a 4x4 surface unit cell.[a] To ease the following considerations we only allow geometry relaxation of the molecule itself.[b]

At first we considering adsorption on Cu. We perform a cheap PBE geometry optimization and then add a single point PBEh calculation (α=0.25) while retaining the PBE geometry. This will be denoted as the unrelaxed geometry in the following. In the second step we do a full geometry optimization with the hybrid functional. The DOS projected on the molecules for both cases is shown in Figure S1 a.

The PBE geometry used for a hybrid calculation causes a double-peak structure around the Fermi edge. This feature, which is usually indicative of strong chemical interaction,[1–3] disappears after a hybrid geometry optimization.

Tentatively, we explain this behavior by the well-known fact that semi-local functionals underestimate the bond-length alternation in quinoid molecules, i.e. they overestimate the length of double bonds compared to single bonds.[4–7] When a hybrid calculation is performed on top of a semi-local geometry, the elongated double-bonds are already closer

[a] The reduced number of layers for Cu compared to the calculations in the main text makes the alteration of the DOS due to geometry optimization more obvious for this specific system, but we note that it is also present in a system with fully converged substrate, although slightly less pronounced. The alteration of work function and charge transfer due to geometry optimization are not influenced by the number of substrate layers.

[b] We note that we found for the systems presented in the main text that geometry relaxation of the substrate does not cause qualitative alteration of any results. We have additionally checked the influence of substrate relaxation on the current system and have found that neither the observed DOS nor the amount of transferred charge and work function are altered.

to bond breaking, which artificially increases the reactivity of the molecule. This causes the ominous spin-splitting in the DOS.

In addition, the work function of the system is altered by 0.40 eV from 5.73 eV in the unrelaxed case to 5.33 eV in the relaxed case.

Interestingly, the charged transfer toward the molecule is similar in both cases, with the molecule exhibiting a Mulliken charge of 0.84 electrons in the unrelaxed case and 0.87 electrons in the relaxed case. Considering the geometry, we find that the adsorption height of the molecule toward the Cu substrate is reduced by 0.25 Å upon hybrid relaxation.

The change in the work function can arise from the molecular dipole and the bond dipole which occurs upon adsorption on the substrate. The relaxation causes a flattening of the molecule, which contributes with about -0.10 eV to the observed change in work function. We can, therefore, conclude that also the bond dipole must be strongly altered, which we attribute to the higher reactivity of the molecule (see above) and the reduced adsorption height.

Note that similar falsifications of the observables appear for two hybrid calculations when α differs between the performed single-point calculation and the previous geometry optimization.

The situation is even worsened for adsorption on Cu_2O, where the PBE simulation exhibits metallic behavior of the substrate. The PBE geometry is therefore a completely unsuitable starting point for PBEh simulations. For the TFBQ adsorption on Cu_2O, one of the main observables throughout this work is the position of the molecular LUMO. We demonstrate the effect of the use of a PBE geometry for hybrid calculations. The DOS of relaxed and unrelaxed system calculated with PBEh, α=0.50, are shown in Figure S1 b, where the valence band maxima of both calculations are aligned. The LUMO is shifted by 0.80 eV between

unrelaxed and relaxed geometry, which can be assigned to similar effects than discussed before. This means that the errors arising from avoiding full geometry optimization would completely falsify the estimation of α as performed in this work!

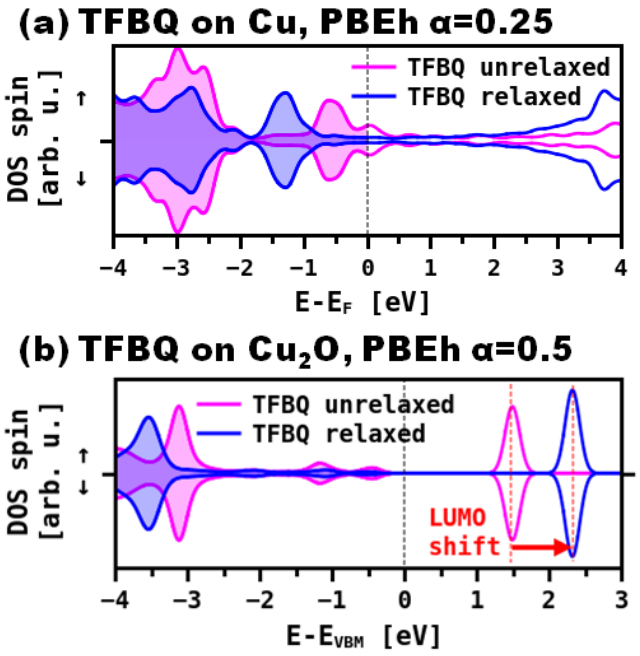

Figure S1: TFBQ adsorbed on Cu (a) and Cu_2O (b). Projected DOS on the TFBQ molecule, calculated with the PBEh functional and different values of α are shown. The magenta curves show PBEh calculations on top of PBE geometries, while the blue curves depict the DOS after full geometry optimization with the corresponding functional. The energies are aligned to the Fermi level in (a) and to the valence band maximum in (b).

2. Verification of Applied Settings

2.1.Lattice Constants

The lattice constants for Cu and Cu_2O were optimized applying all considered functionals, namely PBEh with α=0.00, 0.25, 0.50 and 0.75.

The obtained Cu_2O lattice constants range between 4.3004 Å (α=0.00, PBE) and 4.2430 Å (α=0.75). This corresponds to a variation of approximately 1.3%. To test the influence of the lattice constant on the simulation results, calculations of the Cu_2O substrate applying α=0.00 and α=0.75 were performed with the highest and the lowest obtained lattice constant as well as an average lattice constants a_{Cu2O}= 4.2700 Å. The resulting DOSs were compared and the tests show that (in the for our simulations relevant region of the Cu_2O gap and the surrounding peaks) the DOS remains the same and is not notably shifted in energy (by less than 0.05 eV). We therefore apply the average lattice constant, which is in excellent agreement to experimental results (a_{exp}=4.27 Å).[8]

For Cu, the maximal deviation in the obtained lattice constants amounts to 0.007 Å, which is approximately 0.2% of the total value. Due to this minimal deviation, no further investigations on the influence of the lattice constant on the simulation results are necessary, and an average value of a_{Cu}=3.6300 Å, which is in agreement with experimental results (a_{exp}=3.61 Å), is applied.

2.2.FHI-aims Settings

Convergence tests for the pre-defined FHI-aims settings containing basis sets, integration grids and the numerical accuracy of the Hartree potential ("light", "tight" or "really_tight"),[9] are performed. The investigated parameters re the DOS of the Cu_2O slabs and the work function of Cu the slabs. The smallest possible (111) surface unit cells re used for these tests.

For Cu_2O, this unit cell contains four Cu atoms (and two O atoms) per layer. For Cu, a (111) cell with one atom per layer can be applied.

When calculating Cu_2O(111) with all different applied functionals (α=0.00, 0.25, 0.50 and 0.75) the form of the DOS is unchanged, and the gap size is changed by less than 0.1 eV between “light”, “tight” and “really_tight" .

For the Cu, the surface work function varies by less than 0.1 eV between “light”, “tight” and “really_tight” settings for all applied functionals.

In all cases, “light” settings are, therefore, considered to describe the applied systems sufficiently accurate.

3. Further Methodological Aspects

1.1.Spin Initialization of Molecules

To investigate if an ICT situation (exhibiting spin-splitting of the spin-up and spin-down channels in a molecule) is possible, different spin-initializations on the molecules are tested. The default approach (a superposition of the spherical atomic charge densities in FHI-aims)[9] produces a symmetric spin initialization. For all calculations presented in the main text, an additional initialization creating an asymmetric starting point is applied. This is done by putting an initial magnetic moment of 0.2 μ_B on both O atoms of one molecule in the unit cell. If an ICT scenario is possible, this initialization causes symmetry breaking between molecules and eases integer charging of the initialized molecule.

1.2.Adding Charge to the Unit Cell

To investigate a situation with a charged TFBQ molecule on intrinsic Cu_2O, which offers no free charges, one electron is added to the system. As the calculations are performed using periodic boundary conditions, a compensating positive charge has to be applied. This is done by applying a charged sheet[10,11] of pseudo-atoms which contain no basis functions. The charged sheet is placed below the interface at the bottom of the unit cell to minimize the interaction with the investigated substrate. A distance of at least 7 Å to the lowest lying Cu_2O layer is applied to avoid an overlap with the basis functions of the Cu_2O slab. To guarantee sufficient distance to the periodic replicas in z-direction, the unit cell height is increased to 40 Å for these calculations.

The charged sheet consists of equally distributed pseudo-atoms with only fractional amounts of the atomic charges to add up to one extra electron and one positive charge in the system. 72 pseudo-atoms are applied for the 8x4 unit cell.

The influence of the pseudo-atoms on the occurrences at the surface is tested using an electrostatic model of point charges. The electron potential energy which the point charges in the charged sheet cause on the charged molecule is calculated. It turns out that the occurrences at the interface are not influenced by their presence, as the Cu_2O substrate is effectively separating the charged sheet and the molecular monolayer electrostatically.

4. Reduced Coverage

As we intent to investigate the influence of the surface adsorption, it is also relevant to consider how strongly the straight-line α* is influenced by the presence of neighboring molecules adsorbed on the surface. The physical effects which additionally need to be considered if a molecule adsorbs within a monolayer are screening effects of neighboring molecules and the interface dipoles created by this monolayer of molecules. The interface dipole affects all adsorbed molecules equally, shifting the orbital energies of charged and uncharged molecules. It therefore has no effect on the change in orbital energies with filling, which is relevant for α*.

The screening effects of neighboring molecules, on the other hand, affect the charged, but not the uncharged molecular orbitals, similar to the screening effects of the substrate. In the main text we discusse a loosely packed monolayer with 1 TFBQ molecule per 126 $Å^2$. Due to the already large inter-molecular distance we expect that the surface screening will be dominant and the screening of neighboring molecules will be negligible.

To verify these claims we perform additional, low-coverage calculations in an 8x8 $Cu_2O(111)$ surface unit cell (doubling the unit cell size shown in Figure 1) with only one TFBQ molecule, i.e. with one-quarter of the previous coverage. The distance between molecules amounts to about 25 Å and all inter-molecular interactions can therefore be considered to be negligible. Due to the high computational cost of these large-area calculations and as we are mainly interested if a significant deviation from α* compared to higher coverage appears, only two functionals are considered. In addition, the convergence criterion for the geometry optimization is reduced and forces of 0.03 eV/Å (0.01 eV/Å is used for all other calculations) are considered as converged. The calculations presented in the main text, containing two

TFBQ molecules in the Cu_2O 8x4 unit cell, show that no mentionable difference in the LUMO and SOMO positions appears using this reduced criterion.

The resulting orbital energies of uncharged and charged molecular LUMOs are shown in Figure S2 and we find $\alpha^*=0.08$ (compared to $\alpha^* = 0.10$ for the coverage considered in the main text). We can therefore conclude that the influence of the neighboring molecules is negligible for the considered coverage of our TFBQ on Cu_2O system.

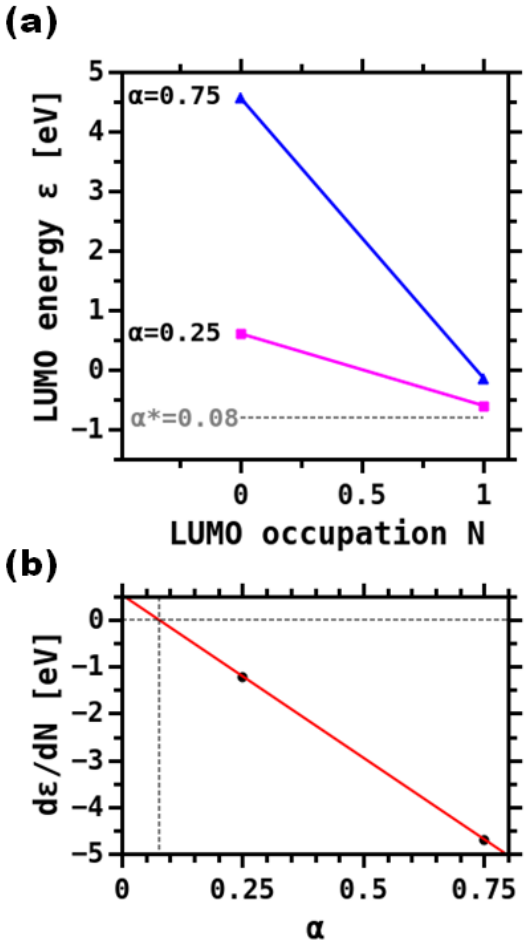

Figure S2: (a) Dependence of the LUMO (SOMO) energy ε (given relative to the upper vacuum level) on its occupation. Two different amounts of α were considered. For every functional the energy values were derived from two different systems, one charged with one electron, while in the other system the molecule remained uncharged. As the energies of two different systems had to be compared, the energies were aligned to the valence band maximum. (b) Change of LUMO energy for all considered values of α. By applying a linear fit the value of α*=0.08 for dε/dN=0 is derived.

5. Localization and Charge Partitioning Schemes

5.1. TFBQ on Cu_2O

The determination of the molecular charges, which are used to determine the localization parameter, is not unambiguous and different approaches can be applied.

In the FCT scenario, we expect to find localization L=0 independent of the applied approach to determine the charge. A localization parameter above 0 points toward symmetry breaking and, thus, charge localization, which indicates an ICT-like situation. We note that dependent on the approach and the overall charge transferred to the layer, the ICT case might not yield L=1. Indeed, if one of the molecule becomes positively charged (due to projection artefacts or hybridization), L could even become larger than 1.

In the main manuscript, we use the Mulliken charges[12] on the TFBQ molecules adsorbed on Cu_2O to determine localization. To exclude the effect of hybridization of lower-lying σ orbitals with the Cu_2O substrate, only negative charges are considered. This ensures that L is always between 0 and 1. The corresponding Mulliken charges for all applied functionals are given in Table S1. To include also an alternative charge partitioning scheme, Hirshfeld charges[13] are listed in Table S2.

Table S1: Mulliken Charges on Molecule 1 and Molecule 2 Given in Electrons for the Adsorption of TFBQ on Cu_2O.

	α=0.00	α=0.25, FCT	α=0.25, ICT	α=0.50	α=0.75
Mulliken charge on molecule 1 [electrons]	0.381	0.231	0.433	0.504	0.579
Mulliken charge on molecule 2 [electrons]	0.382	0.231	0.047	-0.163	-0.145

Table S2: Hirshfeld Charges on Molecule 1 and Molecule 2 Given in Electrons for the Adsorption of TFBQ on Cu_2O.

	α=0.00	α=0.25, FCT	α=0.25, ICT	α=0.50	α=0.75
Hirshfeld charge on molecule 1 [electrons]	0.394	0.365	0.365	0.357	0.353
Hirshfeld charge on molecule 2 [electrons]	0.394	0.365	0.031	-0.228	-0.258

An alternative approach would be to consider only the filling of the LUMO upon adsorption (neglecting all other orbitals). This value can be derived from the so-called molecular-orbital density of states MODOS, where the density of states of the hypothetical free-standing monolayer is projected onto the molecular orbitals.[14] Two exemplary MODOS occupation plots of a FCT and an ICT system (α=0.00 and α=0.75) are given in Figure S3.

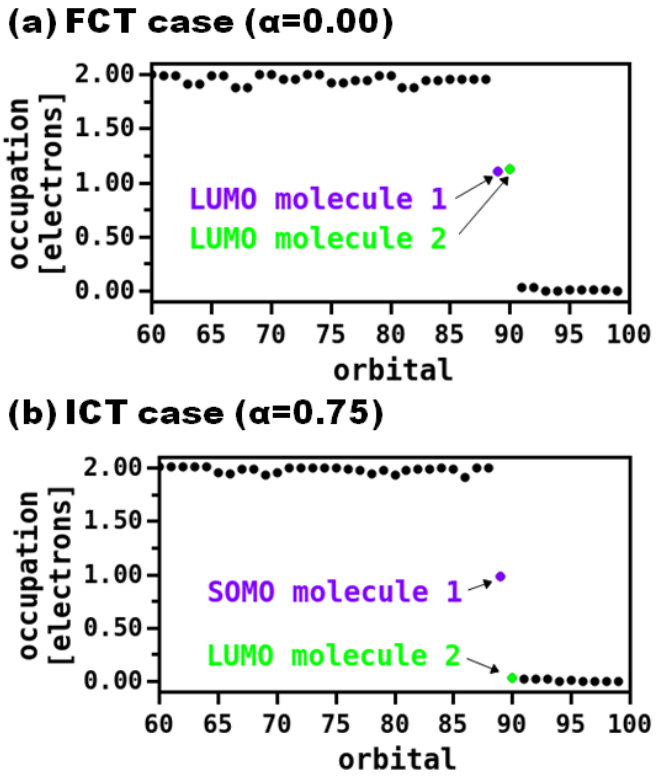

Figure S3: Orbital occupation given in electrons of two TFBQ molecules adsorbed on Cu_2O. (a) is obtained using α=0.00 and shows a prototypical FCT system, while (b) is obtained using α=0.75 and shows a prototypical ICT system.

The LUMO occupation values for all applied functionals are given in Table S3.

Table S3: LUMO Filling of Molecule 1 and Molecule 2 for the Adsorption of TFBQ on Cu_2O.

	α=0.00	α=0.25, FCT	α=0.25, ICT	α=0.50	α=0.75
occupation [electrons]	1.10	0.70	1.02	0.99	0.99
occupation [electrons]	1.13	0.80	0.49	0.07	0.03

To show how the derived localization differs for different partitioning schemes, a comparison is presented in Figure S4. Here, the positive charging of lower-lying orbitals is not excluded in case of Mulliken and Hirshfeld partitioning, which leads to the high localization values for α=0.50 and α=0.75.

Nonetheless, it becomes clear that the conclusions drawn in the main text still hold: For high α, we find that the symmetry between the molecules is broken (corresponding to ICT), whereas for low α, the localization parameter is 0 (corresponding to FCT). At α=0.25, we find two solution, one at L=0 (clear FCT) and one at L>0 (towards ICT).

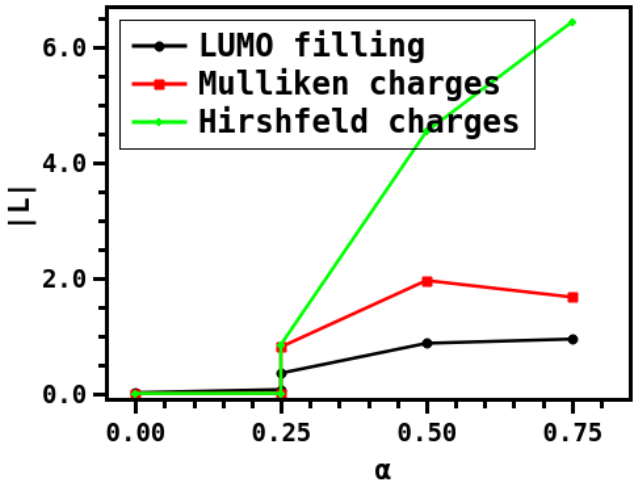

Figure S4: Absolute value of localization L over different values of α is compared for different partitioning schemes.

5.2.TFBQ on Cu

For the adsorption of TFBQ on Cu, the main manuscript lists the Mulliken charges of both molecules with all applied DFT functionals. For the sake of completeness, we provide a comparison of Mulliken charges (Table S4) and Hirshfeld charges (Tables S5) here.

Table S4: Mulliken Charges on Molecule 1 and Molecule 2 Given in Electrons for the Adsorption of TFBQ on Cu.

	α=0.00	α=0.25	α=0.50	α=0.75
Mulliken charge on molecule 1 [electrons]	0.614	0.878	1.014	1.124
Mulliken charge on molecule 2 [electrons]	0.614	0.878	1.014	1.123

Table S5: Hirshfeld charges on molecule 1 and molecule 2 given in electrons for the adsorption of TFBQ on Cu.

	α=0.00	α=0.25	α=0.50	α=0.75
Hirshfeld charge on molecule 1 [electrons]	0.571	0.623	0.643	0.644
Hirshfeld charge on molecule 2 [electrons]	0.571	0.623	0.643	0.644

References

(1) NEWNS, D. M. Self-Consistent Model of Hydrogen Chemisorption. *Phys. Rev.* **1969**, *178* (3), 1123–1135.

(2) Anderson, P. W. Localized Magnetic States in Metals. *Phys. Rev.* **1961**, *124* (1), 41–53.

(3) Grimley, T. B. Chemisorption Theory. In *Progress in Surface and Membrane Science*; Cadenhead, D. A., Danielli, J. F., Rosenberg, M. D., Eds.; Elsevier, 1975; Vol. 9, pp 71–161.

(4) Körzdörfer, T.; Brédas, J.-L. Organic Electronic Materials: Recent Advances in the DFT Description of the Ground and Excited States Using Tuned Range-Separated Hybrid Functionals. *Acc. Chem. Res.* **2014**, *47* (11), 3284–3291.

(5) Körzdörfer, T.; Parrish, R. M.; Sears, J. S.; Sherrill, C. D.; Brédas, J.-L. On the Relationship between Bond-Length Alternation and Many-Electron Self-Interaction Error. *J. Chem. Phys.* **2012**, *137* (12), 124305.

(6) Ho Choi, C.; Kertesz, M.; Karpfen, A. The Effects of Electron Correlation on the Degree of Bond Alternation and Electronic Structure of Oligomers of Polyacetylene. *J. Chem. Phys.* **1997**, *107* (17), 6712–6721.

(7) Jacquemin, D.; Adamo, C. Bond Length Alternation of Conjugated Oligomers: Wave Function and DFT Benchmarks. *J. Chem. Theory Comput.* **2011**, *7* (2), 369–376.

(8) Cuprous Oxide (Cu2O) Crystal Structure, Lattice Parameters. In *Non-Tetrahedrally Bonded Elements and Binary Compounds I*; Madelung, O., Rössler, U., Schulz, M., Eds.; Springer Berlin Heidelberg: Berlin, Heidelberg, 1998; pp 1–3.

(9) Blum, V.; Gehrke, R.; Hanke, F.; Havu, P.; Havu, V.; Ren, X.; Reuter, K.; Scheffler, M. Ab Initio Molecular Simulations with Numeric Atom-Centered Orbitals. *Comput. Phys. Commun.* **2009**, *180* (11), 2175–2196.

(10) Sinai, O.; Hofmann, O. T.; Rinke, P.; Scheffler, M.; Heimel, G.; Kronik, L. Multiscale Approach to the Electronic Structure of Doped Semiconductor Surfaces. *Phys. Rev. B* **2015**, *91* (7), 075311.

(11) Erker, S.; Rinke, P.; Moll, N.; Hofmann, O. T. Doping Dependence of the Surface Phase Stability of Polar O-Terminated (000$\bar{1}$) ZnO. *New J. Phys.* **2017**, *19* (8), 083012.

(12) Mulliken, R. S. Electronic Population Analysis on LCAO–MO Molecular Wave Functions. I. *J. Chem. Phys.* **1955**, *23* (10), 1833–1840.

(13) Hirshfeld, F. L. Bonded-Atom Fragments for Describing Molecular Charge Densities. *Theor. Chim. Acta* **1977**, *44* (2), 129–138.

(14) Nelin, C. J.; Bagus, P. S.; Philpott, M. R. The Nature of the Bonding of CN to Metals and Organic Molecules. *J. Chem. Phys.* **1987**, *87* (4), 2170–2176.

4.3 Preliminary Work on Charge Transfer Properties

In the article presented above, a transition between fractional and integer charge transfer induced by changing the DFT functional was investigated. Alternatively, such a transition should also occur as a consequence of a gradual change of the substrate material from metallic to semiconducting (or insulating). Therefore, the system applied for the charge transfer studies was chosen very carefully, to allow the simulation of such a transition. The choice of adsorbate materials and organic molecules is reviewed briefly in the following, and preliminary results on realizing the transition between ICT and FCT via changing the substrate material is summarized in section 4.4.

Choice of Substrate Material

A material combination which allows a transition from metallic to semiconducting needs to fulfill certain structural conditions. Most importantly, the semiconductor should exhibit a structure that does not fundamentally change the metal crystal structure. Unfortunately, most of the suitable substrate metals (e.g. Zn, Cu) have semiconducting counterparts that transforms into wurzite or zincblende structures (e.g. ZnS, CuCl), and are, therefore, not practical for this purpose.

The choice finally fell on Cu and copper-I-oxide Cu_2O, which exhibits cuprite structure. The Cu atoms keep their fcc structure, while the O atoms form a bcc sub-lattice, shifted by one quarter of the lattice diagonal. The lattice constant is 4.27 Å, which corresponds to an increase of 18% from the Cu lattice constant.[150, 151] The crystal structure is shown in Fig. 27.

Different surfaces of the Cu_2O crystal were examined to find the most suitable one for

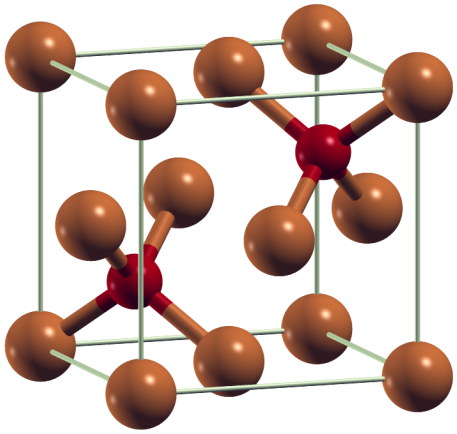

Figure 27: Crystal structure of Cu_2O, which is denoted as cuprite structure. Cu atoms are depicted in brown and O atoms in red.

charge transfer investigations. The requirements were that the surface must be semiconducting (and not become metallic due to surface rearrangements that might occur

during geometry optimization), should be non-polar (as a polar surface would complicate the simulations) and also the surface symmetry was considered. The symmetry is of interest, as matching symmetries of adsorbed molecules and the substrate allow the formation of a well-ordered adsorbate layer more easily. This is very desirable for the present study, as all molecules should adsorb equivalently to allow a comparison of their charge transfer properties.
Several different surfaces were investigated, and the choice finally fell on the (111) surface, which is depicted in Fig. 28. This stepped, mixed-terminated surface is non-polar and exhibits a six-fold symmetry. In contrast to most other examined surfaces, it is stable and does not rearrange.[150, 151, 152] In addition, no metallic surface states appeared upon relaxation and the surface stays semiconducting upon surface relaxation, which was not the case for most other investigated Cu_2O surfaces.

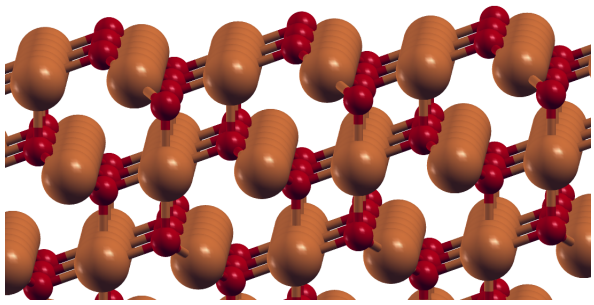

Figure 28: Surface structure of the $Cu_2O(111)$ surface, with Cu atoms depicted in brown and O atoms depicted in red.

Choice of Molecule
All preliminary calculations to investigate charge transfer on Cu_2O were performed with tetracyanoehthylene TCNE, which is shown in Fig. 29. Due to its small size (which allows the simulation of several molecules in one unit cell), the strong electron accepting character, and its LUMO lying in the gap of Cu_2O (for a large region of α), it appeared to be ideal. However, during full geometry optimizations it turned out that adsorption on Cu_2O leads to a pronounced deformation of the molecule due to strong bonding of the four N atoms to surface Cu atoms. As the symmetries of the chosen (111) surface and molecule did not agree well (due to four bonding N atoms and the almost quadratic shape, TCNE is close to a four-fold symmetry), the adsorption geometries were not reproducible, and the appearance of a well-ordered film appeared very unlikely. An upright standing geometry did also not appear to be stable at loose packing densities.
Therefore, TCNE was exchanged for the tetrafluoro-1,4-benzoquinone TFBQ (shown in Fig. 26), which can bind with two O atoms to the surface. It has previously been simulated on Cu(111) and was found to adsorb in a flat-lying geometry.[153]
As discussed in the article above, TFBQ adsorbs on Cu and Cu_2O by binding of the

molecular O atoms to surface Cu atoms, which results in similar binding properties for both substrates. In addition, it exhibits a LUMO in the Cu_2O gap at a large range of α values.

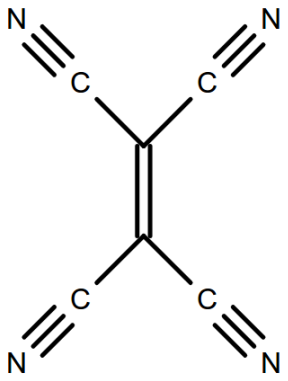

Figure 29: Structure of tetracyanoehthylene TCNE.

4.4 Further Investigations and Outlook on Charge Transfer

As mentioned previously, a part of the original project plan about investigating different charge transfer properties was to gradually modify the substrate in a way that a transition between FCT and ICT could be investigated. By changing the nature of the substrate from metallic to semiconducting, the DOS at the Fermi edge should be decreased and it can be monitored how this influences the charge transfer processes occurring at the interface. The similarity of the metallic and semiconducting substrate materials Cu and Cu_2O should allow for a smooth transition between the different substrate materials, e.g. by adding O atoms to the slab one by one. As a fist step, it was tested how the binding properties of the adsorbed TFBQ changes upon stretching Cu to the Cu_2O lattice constant, to allow to eventually insert O atoms step by step and, hence, model the metal-semiconductor transition. As discussed previously for Au and Ag (see section 3.4.6), the d-band of metals is narrowed upon stretching. However, the interface DOS showed that bonding and charge transfer properties between TFBQ and Cu stayed essentially the same for stretched Cu. It should, therefore, be possible to gradually transform the substrate from Cu to Cu_2O, or vice versa.
Several tests investigating charge transfer between different substrate configurations and TFBQ were performed, with one molecule in the unit cell.
By investigating the molecular orbital density of states MODOS,[154] it was possible to identify which peaks in the DOS can be assigned to which molecular orbital, as the position and form of the molecular LUMO was of interest.
The tests presented in the following were obtained with $\alpha = 0.50$. This high value was chosen to ensure the occurrence of integer charge transfer.
On Cu, fractional charge transfer with a completely filled molecular LUMO was found,

as shown in Fig. 30a. On $Cu_2O(111)$ in its original, O-terminated structure, the molecule remains mostly uncharged. This becomes clear from the DOS in Fig. 30c, where the molecular LUMO, which lies at about E_{VBM}+1.5 eV, is empty. However, the small peaks at about E_{VBM}-1.0 eV, which can also be assigned to the LUMO, as well as the substrate contribution at the energy of the LUMO in the gap indicate some hybridization between substrate and molecule. This is because of the binding appearing between the molecular O-atoms to surface Cu-atoms, which is also clearly visible in the adsorbate geometry.
Additionally, a situation with the topmost O layer removed from $Cu_2O(111)$, as shown in Fig. 30b, was considered. In that case, the molecule binds quite strongly to the substrate, and the LUMO is almost completely filled. However, a small split-off peak at approximately E_{VBM}1.75 eV appears, which is also assigned to the molecular LUMO, and the presence of a strong substrate contribution at this energy indicates strong hybridization.

Although these results do not yet allow for a conclusive interpretation of the change in charge transfer upon different substrate configurations, the splitting of the molecular LUMO into an occupied and an unoccupied part, but without spin splitting as it appears in case of ICT, is an interesting effect. This splitting had been found to be significantly stronger before full, functional-specific geometry optimization of the system. Most likely, the geometry relaxation led to a more saturated configuration of the Cu_2O surface atoms, which weakened the hybridization with the TFBQ molecule and also the corresponding LUMO splitting.
Therefore, in the spirit of the gradual change between Cu and Cu_2O, another intermediate step between these two situation was considered. Fig. 31 shows the DOS of TFBQ on O-terminated Cu_2O, where only one surface O atom was removed directly below the molecule. Subsequently, the geometry of the system was fully relaxed. This configuration was calculated with $\alpha = 0.25$, as this value had been shown to suffice for achieving ICT for TFBQ on Cu_2O.[6]
The molecular LUMO, obtained from the MODOS, is indicated in red in Fig. 31. Its splitting is very pronounced here. This appears to be a characteristic effect for the situation on Cu_2O with (partly) removed surface O atoms, where the molecule exhibits rather strong hybridization with the substrate, but the charge reservoir is small and limits the charge transfer toward the molecule. A possible interpretation of the splitting is that the LUMO splits into a bonding and anti-bonding state upon hybridization with a surface band.[155, 156].
These results give a first notion about the transition between FCT and ICT caused by substrate tuning, and call for a more detailed study of such effects. This should lead to a deeper understanding of the different charge transfer mechanism, how they depend on the substrate composition, and how this is described within DFT.

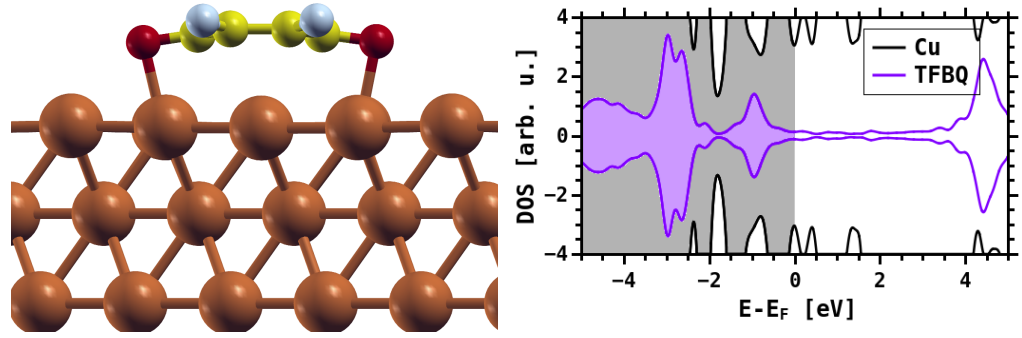

(a) TFBQ on Cu

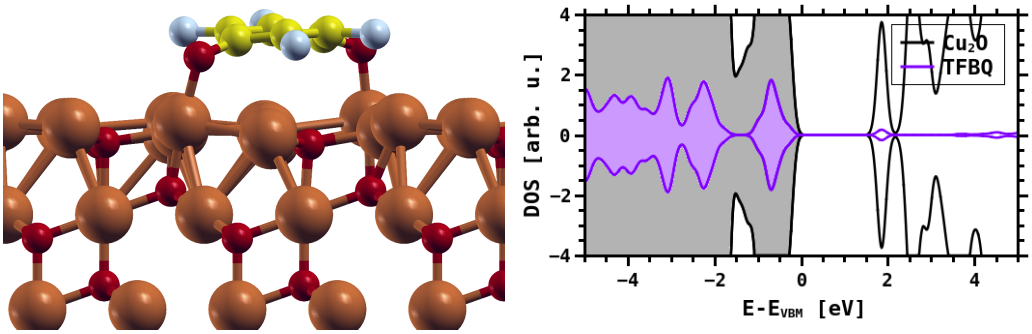

(b) TFBQ on Cu_2O - Cu-terminated

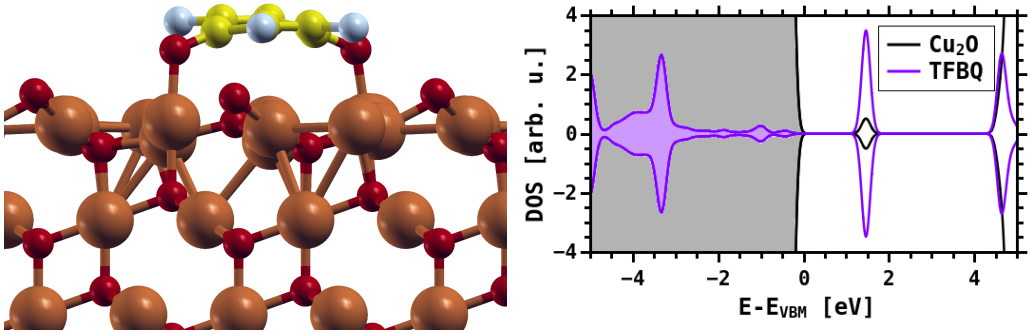

(c) TFBQ on Cu_2O - O-terminated

Figure 30: Geometries and DOSs of TFBQ adsorbed on Cu, Cu-terminated Cu_2O and O-terminated Cu_2O. The energies are aligned to the Fermi level (Cu) or to valence band maximum (Cu_2O).

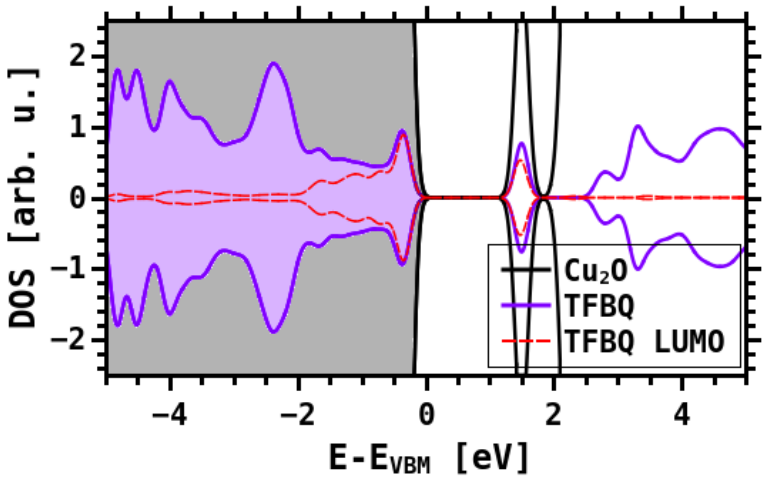

Figure 31: DOS of TFBQ adsorbed on O-terminated Cu_2O, with one surface O atom removed directly below the molecule. The molecular LUMO is indicated in red. The energy is aligned to the valence band maximum.

5 Magnetic Properties at Interfaces: Transition-Metal Phthalocyanines CuPc and CoPc on Ag(111)

The adsorption on a surface can modify the magnetic properties of a molecule. An example was shown in section 4, where charge transfer from the substrate resulted in a spin-splitting of the adsorbate orbitals in case of ICT systems. The appearance of molecular magnetic effects can depend strongly on the charge localization and is, therefore, influenced by the applied DFT functional.
To study magnetic effects at interfaces, transition metal phthalocyanines (TMPc) adsorbed on a metal substrate were simulated.
For the work on this project, I was also supervised by David A. Egger (University of Regensburg, Germany).

Such TMPc adsorption systems have been the subject of several extensive experimental and theoretical studies, as they exhibit good chemical stability and film growth properties.[157, 158, 159] TMPcs mostly adsorb in a flat-lying manner on metals and have been shown to grow well-ordered films on many metallic substrates.[24, 25, 27, 160, 161, 162, 163] The interchangeable central metal ion strongly influences the properties of the molecule. [162, 164, 165, 166] In most cases, the adsorption of such TMPcs, their geometric properties as well as several electronic properties (e.g. work function modification, charge transfer) can be described well within DFT.[24, 25, 162, 166] An additional interesting aspect are their magnetic properties upon adsorption. While the appearance of magnetic polarization of the molecules upon adsorption on ferromagnetic substrates is to be expected,[167, 168, 169, 170] another appealing aspect that has not yet draw so much attention are their magnetic properties upon adsorption on non-magnetic substrates. It has been shown that in several examples of metal phthalocyanines adsorbed on non-metallic substrates, the magnetic moment of the molecules is quenched.[171, 172, 173]. However, some studies, e.g. by Stepanow and Mugarza et al. [164, 165, 174, 175, 176] present experimental work on curious magnetic effects of metal phthalocyanines adsorbed on non-magnetic substrates. Although simulations were included in these works, no full computational description of the magnetic effects was achieved. The question arises if and how well these properties can be described from simulation, namely standard DFT methodologies, as applied here.

Preliminary Work on CuPc/Ag(111)
I have performed simulations of CuPc on Ag(111) during my master thesis,[23] which were published in combination with experimental data.[25] The DFT calculations were performed with the semi-local PBE and the range-separated hybrid HSE06 functional. There, it was found that the simulated molecular magnetization and DOS depends on the applied functional. In the semi-local calculation, the intrinsic magnetic moment of the CuPc molecule, which amounts to $\mu \approx 1\ \mu_B$ in gas phase, was conserved upon

adsorption. The hybrid functional, on the other hand, exhibited a curious increase of the magnetic moment to $\mu \approx 2\ \mu_B$.

Investigation of CuPc/Ag(111) and CoPc/Ag(111)
The scope of the present work was to investigate the occurrence of these different magnetic solutions in more detail, elucidate the physical aspects of such magnetic effects and how they can be described in DFT.
For the CuPc molecule, it was investigated which solutions can be created and how their appearance depends on the applied functional. To gain more insight into the physical situation underlying the appearance of different magnetic solutions, another similar system, namely CoPc on Ag(111) was also investigated here. The choice fell on CoPc, as experimental results indicate that its magnetic moment is quenched upon adsorption on Ag, which is in sharp contrast to the CuPc/Ag results.[165, 177, 178]
The chosen interface systems were simulated with different (semi-local and hybrid) functionals. The obtained magnetic solutions were analyzed to find out (i) whether they are physically reasonable, and (ii) which one is most likely to appear in experiments. A detailed comparison and ratification with experimental findings on similar systems from literature was done and it was examined if it is possible to predict these results from simulation.
In addition, the influence of the choice of functional on the appearing solutions was investigated and is discussed in the following.
It was found that the obtained magnetic solutions are not strictly linked to a specific functional, in contrast to the findings in presented in Ref. [25].
The obtained data demonstrates that the interaction of the central metal ion with the substrate and the interaction of the ligands with the substrate play a significant role for the magnetic moments the molecules exhibits after adsorption. This appears to be the reason for the difference between the CuPc and the CoPc adsorption systems.

5.1 System and Methodology

The investigated systems consisted of the CuPc and CoPc molecules (see Fig. 32) adsorbed on the Ag(111) substrate.

5.1.1 Substrate

During an extensive testing phase, different adsorption configurations and also substrate orientations, namely Ag(111) and Ag(100), were considered. The Ag(100) surface would have been preferable, as it (i) has a four-fold symmetry like the molecule, (ii) allows the use of a small 5x5 surface unit cell and (iii) is used in several experimental studies. Unfortunately, it was not possible to obtain all desired magnetic solutions

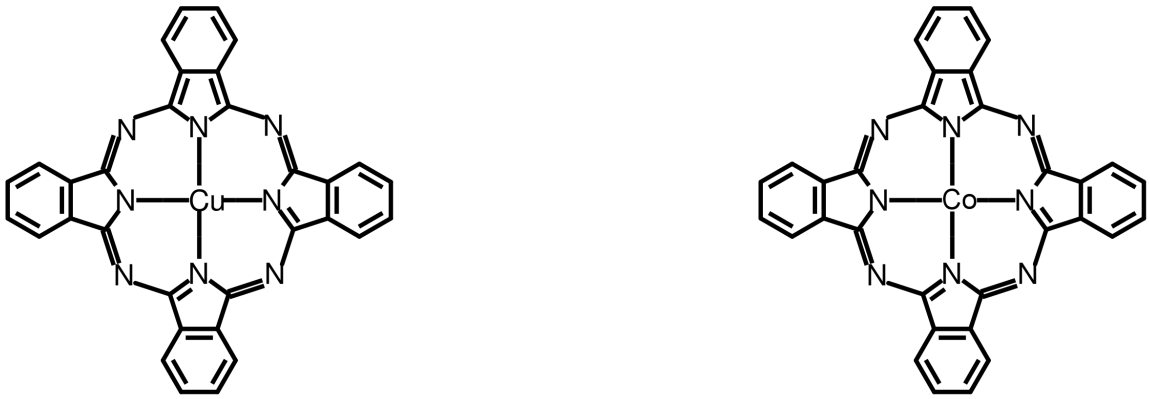

(a) CuPc (b) CoPc

Figure 32: Structure of the copper phthalocyanine CuPc and cobalt phthalocyanine CoPc molecules.

(see below) on this surface. This will be discussed in detail in section 5.5. Therefore, the three-fold symmetric Ag(111) surface was applied.
The substrate lattice constant was optimized with all different functionals used in this study. By applying the Birch-Murnaghan equation,[106] a PBE lattice constant of 4.150 Å was found (compared to a literature value of 4.079 Å [127]). For the hybrid calculations, the change in lattice constant amounted to less than 0.2%. As this minimal variation is irrelevant for the performed simulations, the PBE lattice constant was applied throughout.
The slab contained three layers of Ag substrate, which was the highest possible layer setting that was still computationally feasibly. Applying more layers, the number of atoms in the unit cell would have become too large to perform hybrid calculations on the available computational infrastructure. To make sure that this comparably low number does not falsify any obtained results, several tests were performed. The work function of the substrate upon adding more layers was tested and it was found that it is converged within 0.05 eV. In addition, calculations with reduced computational settings (to allow the use of more layers of substrate) showed that the obtained (magnetic) solutions are stable upon varying the number of layers.

5.1.2 Unit Cell and Adsorption Position

Consistent with previously performed calculations on the CuPc/Ag(111) system [23, 25], a $5 * 3\sqrt{3}$ (111) surface unit cell was chosen. This cell is rectangular and has, with the optimized lattice constant, edge lengths of 14.7 Å x 15.2 Å. The CoPc molecule, which showed similar size and binding geometries (see below) during test calculations, was adsorbed in the same unit cell. The geometry of the applied cell is well in line

with experimental results presented in Refs. [27, 159, 179].
To find the ideal adsorption position of the molecules on the Ag(111) substrate, different configurations were applied as starting points for geometry optimizations. The central metal atom of the molecule was placed above an on-top, bridge, a fcc hollow and a hcp hollow position. Geometry optimizations led to a lateral shift of the molecule in all cases, moving it to an adsorption position between hollow and bridge site (both for CuPc and CoPc). By comparing the total energies it was found that the configurations shown in Fig. 33, with the central atom close to the hcp hollow and bridge site, are favorable compared to the position close to the fcc hollow site.
The rotation of the molecule with respect to the axis perpendicular to the Ag surface turned out to be a soft degree of freedom, as no significant energy differences could be obtained after geometry optimizations from different starting rotations. Only a a small preference of an alignment of the outer Pc rings along the $<1\underline{1}0>$ and the perpendicular $<\underline{1}1\underline{2}>$ directions could be determined, as the molecules roughly aligned along those substrate directions during geometry optimizations (see Fig. 33).
The CuPc and CoPc geometries obtained from these geometry optimizations were applied as starting points for all calculations discussed in the following.
Because of the huge computational effort of hybrid calculations, it was not possible to perform these tests on adsorption positions also with the HSE functional. However, the geometry optimization tests presented in section 5.5 did not show any tendency of the molecule to move to another adsorption position during the hybrid optimization. Therefore, it is assumed that the adsorption positions obtained using PBE are suitable also for the hybrid calculations.

5.1.3 Choice of DFT Functionals

For several phthalocyanine molecules it has been shown that the description of the electronic structure cannot be done properly by just applying a standard, semi-local GGA functional.[9, 93, 94] This is mostly due to the (single electron) self-interaction error SIE present in DFT, which can cause energy shifts of the molecular states (see section 2.3).[65, 180, 181] The effect of this error is different for differently localized orbitals, i.e. more strongly localized orbitals are also affected more strongly.[63] As a result, not only the absolute energies, but also the orbital ordering can be altered.[9]
In case of large metal phthalocyanine molecules, the influence of the SIE is particularly problematic. This is because the delocalized π-orbitals in the molecular backbone and the strongly localized metal-centered states on the central metal atom lie close in energy. Due to their different localization, these states are shifted differently by the SIE, which can falsify the orbital ordering in the valence region.
In previous works, it was found that different magnetic solutions for CuPc/Ag can be found and that the obtained solutions depend on the applied DFT functional.[23, 25] To investigate the interplay of magnetic solution and functional choice in more detail, the considered system were simulated with various functionals in the present work.

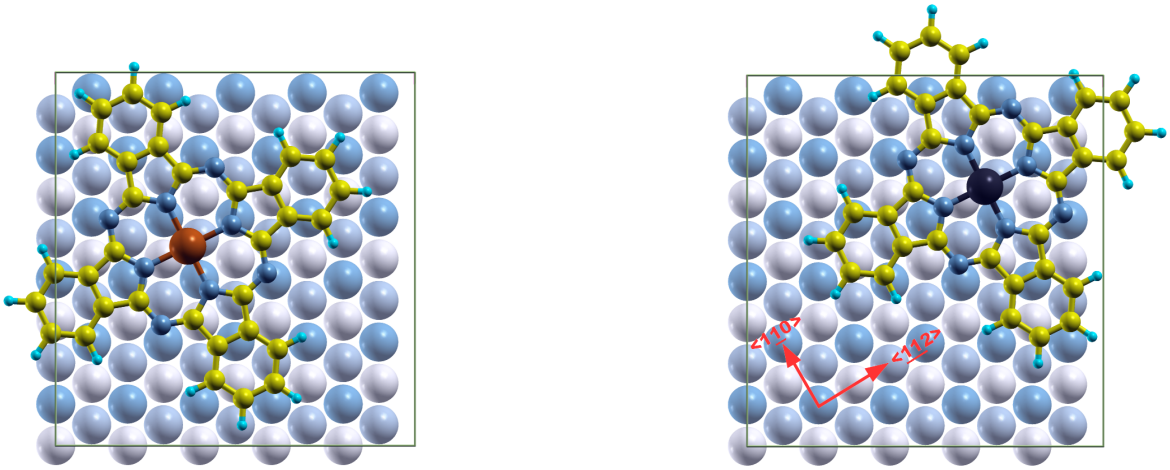

(a) CuPc

(b) CoPc

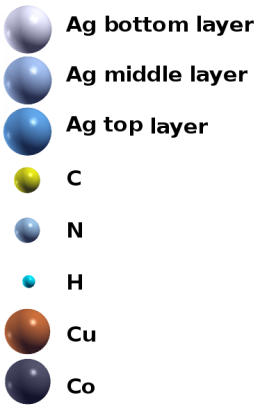

(c) elements

Figure 33: Adsorption position of CuPc and CoPc on the Ag(111) surface. To identify the adsorption position, different Ag layers are displayed in different colors.

Two different functional types were applied, namely the semi-local PBE functional [44] and the range-separated hybrid HSE functional family [45, 99] with different amounts α of Hartree-Fock exchange. The choice fell on a range-separated hybrid functional, as the application of computational costly Hartree-Fock exchange only in the short-range region (determined by the exchange screening parameter ω) significantly decreases the total computational cost compared to a hybrid functional without range separation, such as PBE0 [44, 182] (or PBEh [44]). In addition, the HSE functional (and especially the HSE06 functional, see below) have been shown to perform well for organic molecules.[183] For molecular CuPc and similar metal phthalocyanine systems, it has been found that the relative orbital ordering is described very well within the HSE06 functional.[9, 93, 94]. It also has been shown to yield at least qualitatively correct

results for solids.[184, 185] The benefit of lower computational costs stands against the disadvantage of an additional free parameter, which can be tuned and makes the obtained results harder to interpret.
The most widely applied set of HSE parameters is denoted as HSE06 [186], which applies an amount of 25% Hartree-Fock exchange in the short range, with an exchange screening parameter $\omega = 0.11$ Bohr^{-1}. In the present study, parameter tuning was limited to the amount of Hartree-Fock exchange α, while ω was left at the default HSE06 value. To ensure that the range separation does not falsify the obtained results, test calculations applying PBE0 (which uses $\alpha = 0.25$ as HSE06, but no range separation) of CuPc and CoPc on Ag(111) were performed. In all cases, the obtained results were similar to the the ones obtained using HSE, especially with respect to the magnetic properties of the adsorbed molecules.
It should be mentioned that even with the applied settings, the performed calculations where on the verge of computational feasibility (with the available computational infrastructure) due to the use of hybrid functionals for such large surface unit cells.

5.1.4 DFT Methodology

All calculations discussed in the following results sections (section 5.2 and 5.3) were obtained applying the FHI-aims simulation package [58]. A Γ-centered k-point grid of 3x3x1 k-points was applied, combined with the suggested "tight" FHI-aims settings.[58] These settings ensured that the substrate work function was converged to below 0.05 eV.
Note that also VASP calculations on the systems in question were performed, but did not yield conclusive results. Why that was the case and also several of these calculations are discussed in section 5.5.1 on the influence of the applied DFT code.

Broadening Width
Gaussian broadening[101] was applied.
Extensive tests on the influence of the broadening on the magnetic moment in the unit cell were conducted, as it had been shown in my Master Thesis that a change in broadening width can change the total magnetic moment of a unit cell.[23] This effect is caused by a magnetization of the substrate at low broadening widths, which is a known effect for metals and has, e.g., also been observed for Au clusters, where a magnetization only appeared with sufficiently low broadening widths.[187]
For the CoPc/Ag(111) system, the impact of the broadening on the magnetic moment of the Ag substrate was particularly strong. At $\alpha = 0.30$, a solution was found where the total system magnetic moment amounted to $\mu = 0.09\ \mu_B$ and the magnetic moment of the Ag substrate was zero, using a broadening of 0.1 eV. For a reduced broadening of 0.05 eV, this value increased to $\mu = 0.61\ \mu_B$, due to significantly stronger magnetization of the substrate. The substrate magnetization clearly gets "smeared out" if a

larger broadening width is applied.
However, for a broadening of 0.1 eV, the magnetization of the adsorbate molecule, which is the main observable here, was not influence by the broadening width and the substrate magnetization amounted to less than 0.15 μ_B in all investigated cases. Therefore, this value was applied in all calculations presented below.

Geometry Optimizations
In principle, studying the electronic structure of a system should only be done after a full geometry optimization with the corresponding functional (see section 4). This is especially true in case of charge transfer systems, as transferred charge can have a huge impact on the geometry. However, in case of large hybrid functional calculations, this is a problematic aspect due to the associated high computational cost. Performing full geometry relaxations can, therefore, often become forbiddingly expensive. For molecular systems as CuPc, it has been argued, e.g. by N. Marom and coworkers,[93, 94, 188] that it is sufficient to perform geometry optimizations with significantly less costly semi-local functionals such as PBE. Subsequently, single-point hybrid calculations to determine the electronic structure can be performed on top of these geometries. However, in my recent work on charge transfer systems, see Ref. [6] and section 4, we have shown how significantly the electronic structure can be falsified upon using PBE geometries as a basis for hybrid single-point calculations.
This constitutes a dilemma for the present systems, as the immense computational effort for every calculation makes geometry optimizations computationally almost impossible.
The results presented in the following sections on CuPc and CoPc on Ag(111) do not include full geometry optimizations applying the corresponding hybrid functionals, but are all based on the PBE geometries as discussed above. However, full geometry optimizations will be part of forthcoming investigations performed on these system. Preliminary results on geometry optimizations are presented in section 5.5.3. The results indicate that the electronic and magnetic properties relevant here are not qualitatively modified upon geometry relaxation starting from PBE geometries.

5.2 Obtained Solutions: CuPc on Ag(111)

As mentioned before, the CuPc/Ag(111) system has been shown to exhibit different magnetic solutions in DFT.[25] The previously published results were obtained using the VASP code.[97] Two different solutions were found, namely one where the magnetic moment of the gas phase molecule $\mu = 1\ \mu_B$ is conserved upon adsorption, and one where the magnetic moment of the molecule is almost doubled ($\mu \approx 2\ \mu_B$) upon adsorption. In the previous work, the solutions were strictly linked to specific DFT functionals: While the $\mu = 1\ \mu_B$ solution (from now on denoted as spin-1 solution)

was only found when applying PBE, the $\mu \approx 2\ \mu_B$ solution (from now on denoted as spin-2 solution) was only found when applying HSE06.
By performing FHI-aims calculations and focusing on the magnetic properties, a third solution could be obtained where the magnetic moment of the molecule is quenched and goes to 0 upon adsorption (from now on denoted as spin-0 solution). In the following, the properties of these three solutions as well as the circumstances under which they appear will be discussed.
In contrast to the previous findings, the appearance of a specific solutions was not directly linked to a specific functional. While it was found that the admixture of Hartree-Fock exchange can stabilize or destabilize the solutions, all three were found using the HSE06 functional at $\alpha = 0.25$. The DOSs projected onto the adsorbed molecules of all three magnetic solutions obtained with this functional are shown in Fig. 34.
In the following, the discussion of the three different observed magnetic solutions is done on the basis of these HSE06 calculations. Later on, in section 5.2.4, also the results obtained with differing functionals will be discussed.

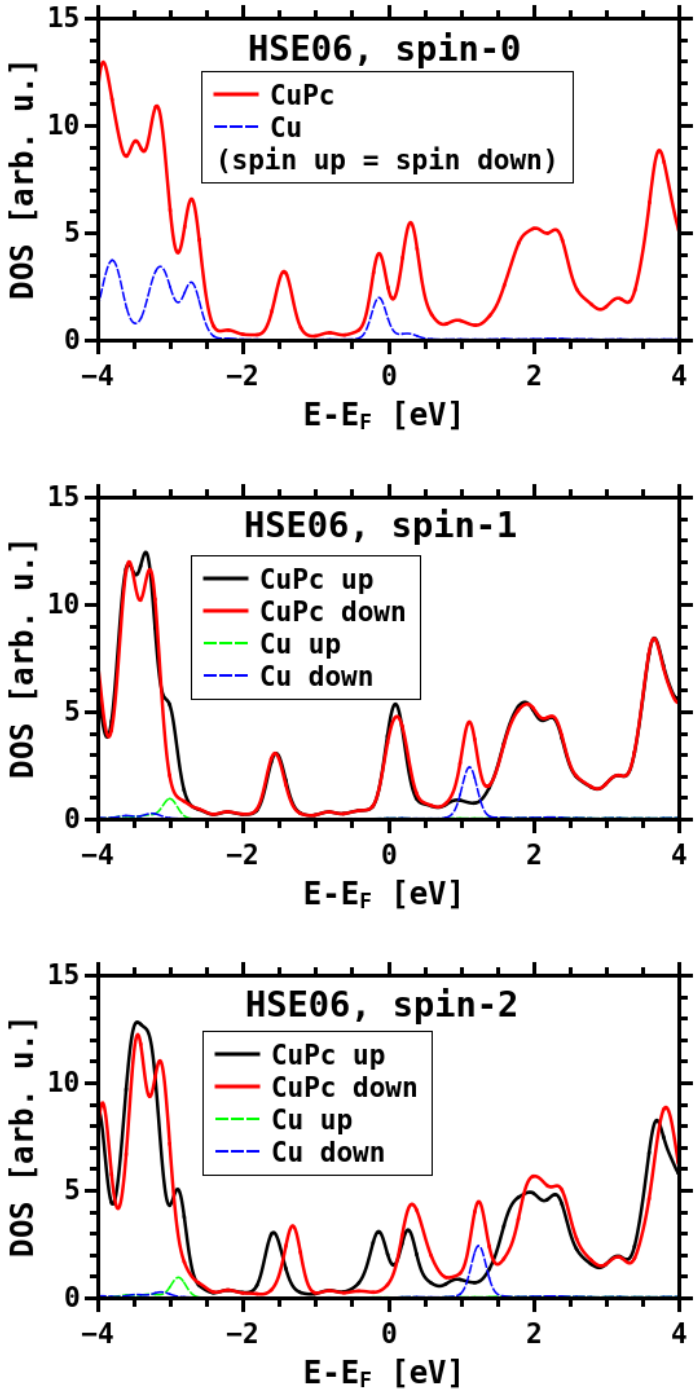

Figure 34: DOS projected onto the CuPc molecule adsorbed on Ag(111) for all obtained magnetic solutions with the HSE06 functional. The spin up and spin down DOSs are shown in black and red, respectively. In addition, the DOSs projected on the central Cu atoms are shown with dashed green (spin up) and blue (spin down) lines. The energies are aligned to the Fermi level.

5.2.1 CuPc on Ag(111): Spin-0 Solution

As shown in Fig. 34, the spin-up and spin-down DOSs of the CuPc molecule on Ag(111) are perfectly aligned in the spin-0 case. This is in contrast to the gas phase CuPc molecule, which exhibits one unpaired electron on the central Cu atom and, therefore, has a singly occupied and singly unoccupied peak (see Fig. 35). By adding up the Hirshfeld charges [189] on the molecule, a total charging of 0.81 electrons was found.
The analysis of the spin per atom showed that the magnetic moment on the Cu atom goes to (almost) zero (μ = -0.000011 μ_B). The magnetic moments on all other molecular atoms are similarly close to zero and can, therefore, be considered negligible. This suggests a situation, where charge from the substrate is transferred toward the central Cu atom and quenches the molecular magnetic moment.
As the magnetic moment is completely quenched, one would expect that one electron per molecule must be transferred, rather than only 0.81 electrons. However, this deviation is most likely a consequence of (i) the molecular hybridization with the substrate, which does not allow a direct assignment of charges to either molecule or substrate any longer and (ii) the charge partitioning, which is not unambiguous and can be defined according to different schemes, e.g. Hirshfeld charges or Mulliken charges.[190]
This spin-0 solution could be found with all applied functionals, namely PBE, HSE06 with $\alpha = 0.25$ and HSE with $\alpha = 0.35$.

5.2.2 CuPc on Ag(111): Spin-1 Solution

The DOS of the spin-1 solution (shown in Fig. 34) exhibits metal-centered Cu orbitals close to the Fermi level. These stem from the unpaired spin which is also present in the gas phase molecule and lie at -3.01 and 1.11 eV relative to the Fermi level (see green and blue Cu peaks in the DOS, Fig. 34).
To find out how similar the states of the adsorbed molecule are to the ones of the uncharged gas phase molecule, gas phase calculations were performed and the occupations are shown in Fig. 35. The gas phase DOS shows the corresponding occupied α-spin (green) and β-spin states (blue) below and above the Fermi level, respectively. Due to the strong localization of this orbital, it is strongly shifted in energy by the SIE, which explains its different location in the PBE and the HSE06 calculations. The occupied (spin up) peak is shifted from -0.3 eV to -1.8 eV, and the unoccupied (spin down) peak is shifted from 0.8 eV to 2.4 eV relative to the valence band maximum upon changing the functional from PBE to HSE06.
The molecular spin is very similar for the surface-adsorbed molecule (μ = 1.02 μ_B) and the gas phase molecule (μ = 1.00 μ_B). This solution, therefore, appears to leave the molecule in a largely unperturbed manner. However, the DOS at the Fermi edge indicates charge transfer toward the former molecular LUMO of about one electron. This was confirmed by the analysis of the Hirshfeld charges, which showed a charging

of of the molecule with 1.13 electrons.
To obtain a better picture of the magnetic configuration of the molecule, the spin per atom was read out (from the Mulliken analysis) and is presented in Fig. 36. The location of magnetic moments on the central Cu atom and the closest N atoms clearly resembles the situation of the gas phase CuPc molecule. It appears that the transferred charge does not affect the unpaired electron on the Cu atom, but goes to the C-N molecular ligands, which is also suggested by the DOS.
This spin-1 solution was found with both PBE and HSE06, but could not be obtained for HSE with higher values of α, e.g. $\alpha = 0.35$. It also was the solution toward which PBE calculations most easily converged (especially with the VASP code, see section 5.5.1).
The fact that this solution becomes less likely with higher amounts of Hartree-Fock exchange indicates that it is linked to the charge localization. The strong hybridization between the molecular ligands and the substrate, in combination with charge overdelocalization from semi-local (or low-α hybrid functionals) allows a spin-unpolarized charging of molecular ligand states. For higher amount of Hartree-Fock exchange, the charge is more localized and this solution is no longer stable.

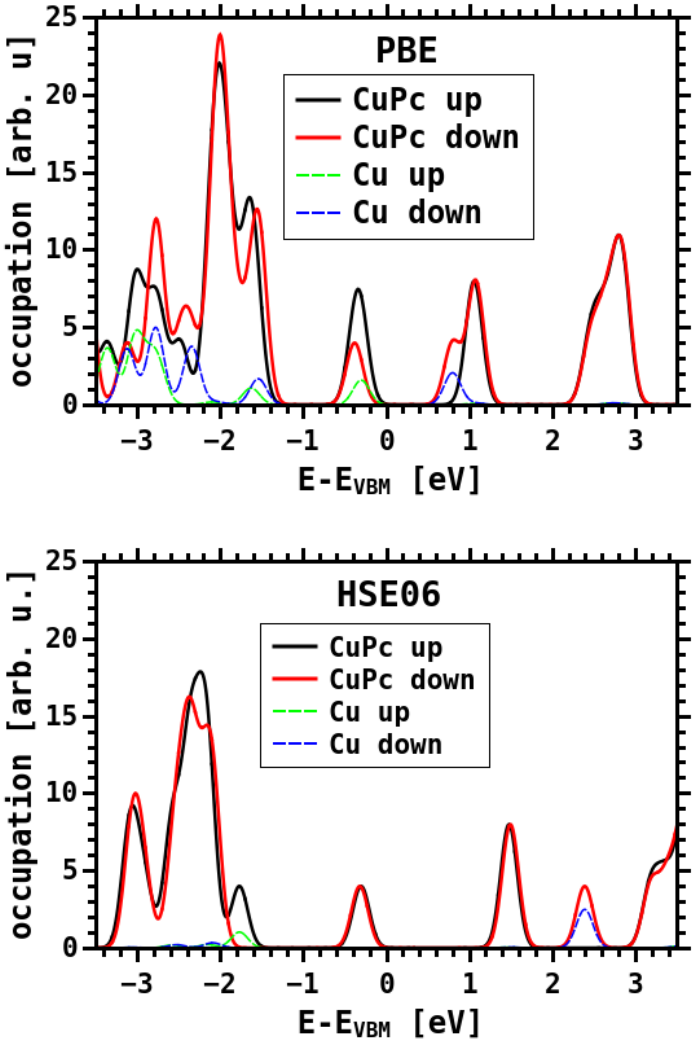

Figure 35: Orbital occupation of the neutral CuPc molecule in gas phase, calculated with PBE and HSE06. The spin up and spin down occupations are shown in black and red, respectively. The energy is aligned to the valence band maximum.

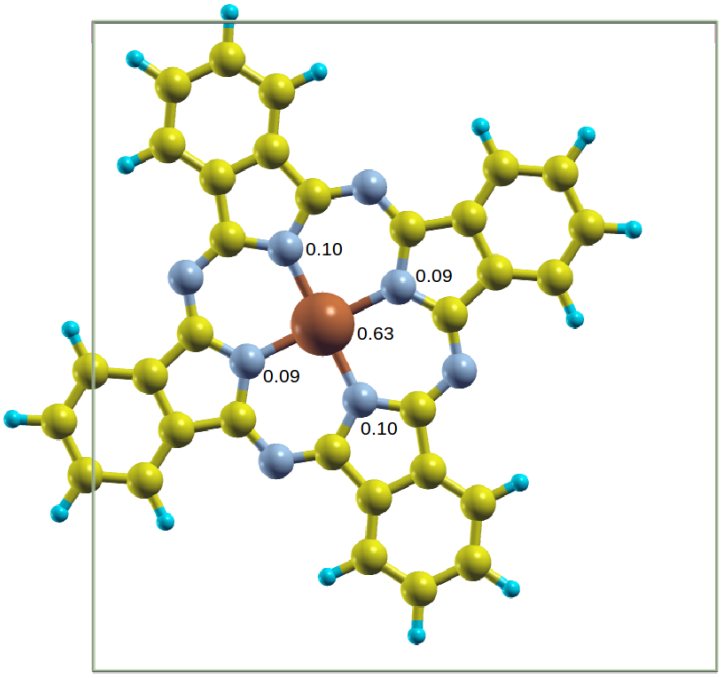

Figure 36: Per-atom spin analysis of CuPc/Ag(111) in the spin-1 configuration. All spins above $\mu = 0.05\ \mu_B$ are given in multiples of μ_B next to the corresponding atoms.

5.2.3 CuPc on Ag(111): Spin-2 Solution

The DOS of the spin-2 solution (see Fig. 34) exhibits several interesting features. First of all, it is noticeable that the spin-split peak of singly occupied Cu, which is also visible in gas phase and in the spin-1 solution, is still present. This is in contrast to the spin-0 solution. Additionally, a curious, spin-split double-peak structure appears around the Fermi edge. The assigned orbital appears to be the former molecular LUMO (a ligand π-state) and indicates a charging of the molecule upon adsorption. The Hirshfeld charge analysis showed an additional molecular charge of 0.81 electrons, similar to the other solutions. Finally, the molecular HOMO exhibits a splitting between its spin up and spin down channels of about 0.30 eV. As indicated by the large differences in spin up and spin down density of states, the molecule exhibits an enhanced net magnetic moment of $\mu = 1.85\ \mu_B$. To shed light on the spin distribution on the molecular atoms, the per-atom spin analysis is shown in Fig. 37. Clearly, the magnetic moment of the Cu atom remains unperturbed and that the spin arises from magnetic moments on the ligands, located on the outer N and inner C atoms. It appears that upon charging, only one spin channel is occupied, and the additional molecular spin aligns in parallel to the Cu spin. To find out if this parallel alignment is a robust property, several tests were performed which where initialized toward a so-called open-shell singlet configuration, where the ligand spin would be aligned anti-parallel to the the Cu spin (see spin-0.1 solution for CoPc below). However, such an anti-parallel solution could never be obtained.

Another property that becomes visible from the spin-per-atom analysis is a symmetry breaking in the spin distribution, which does not reflect the four-fold symmetry of the Pc molecule. This effect is discussed in more detail in section 5.2.5 in combination with the charge rearrangements upon adsorption.

The split peaks around the Fermi edge stem from ligand states and do not exhibit a contribution from the central Cu atom. This splitting indicates a situation with a partially filled orbital, where Coulomb repulsion (characterized by the on-site repulsion term U) causes a splitting of states which are singly occupied from those which are double occupied.[164, 165, 191, 192] The splitting amounts to 0.45 eV with HSE06 (and 0.64 eV with HSE $\alpha = 0.35$, see Fig. 38). A similar feature for CuPc adsorbed on Ag(100) was seen experimentally by Mugarza et al., where the splitting amounted to 0.65 eV (see Ref. [165] and section 5.4). The correlation effects leading to such features are captured within hybrid functionals, but not within semi-local DFT.[191, 192] In accordance with that, the spin-2 solution could only be found in hybrid calculations applying $\alpha = 0.25$ and $\alpha = 0.35$, but not by using PBE (although extensive test were performed trying to obtain this solution also with this functional). The amount of Hartree-Fock exchange, as employed in hybrid functionals, is related to the Coulomb repulsion U, which explains why the peak splitting widens upon the use of a higher amount of Hartree-Fock exchange.[193, 194, 195]

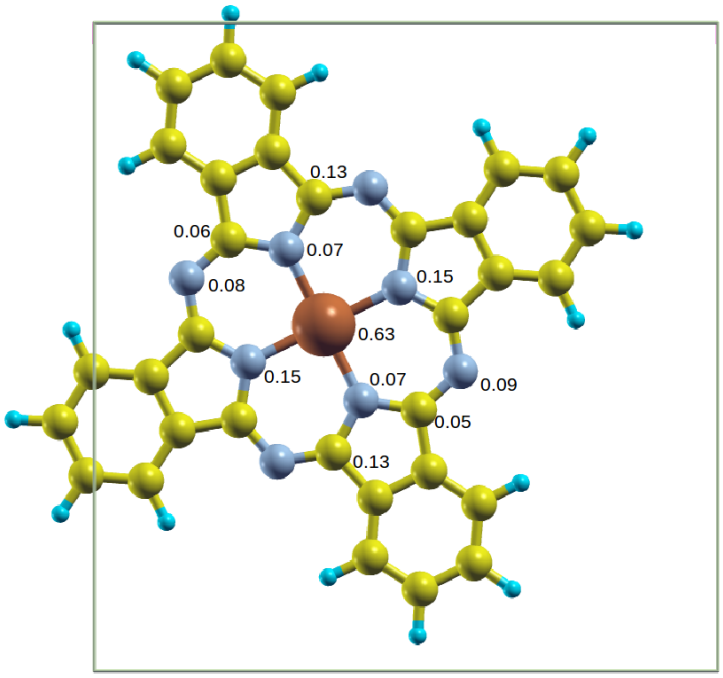

Figure 37: Per-atom spin analysis of CuPc/Ag(111) in the spin-2 configuration. All spins above $\mu = 0.05\ \mu_B$ are given in multiples of μ_B next to the corresponding atoms.

5.2.4 Dependence of Result on the Applied Functional

As mentioned previously, not only HSE06 calculations, but also PBE ($\alpha = 0.00$) and HSE calculations with $\alpha = 0.35$ were performed. While with HSE06, all three different magnetic solutions could be obtained, this was not the case with higher and lower α values. PBE calculations never resulted in the spin-2 solutions, and HSE calculations with $\alpha = 0.35$ never yielded the spin-1 solution.
Additionally to these settings, also higher values of $\alpha = 0.40$ and $\alpha = 0.50$ were tested, but did not lead to converged results. The reason for these problems at high α values appeared to be the metallic substrate, which did no easily converge any more. As these high-α calculations did not converged, they could not be fully interpreted. However, by observing the molecular spins during the calculations it appeared that trends toward both spin-0 and spin-2 solutions, but not toward the spin-1 solution occurred.
In the following, the results of all converged calculations are summarized and their DOSs (Fig. 38), total energies (Tab. 10), Hirshfeld charges (Tab. 11) and total spins (Tab. 12) are shown.

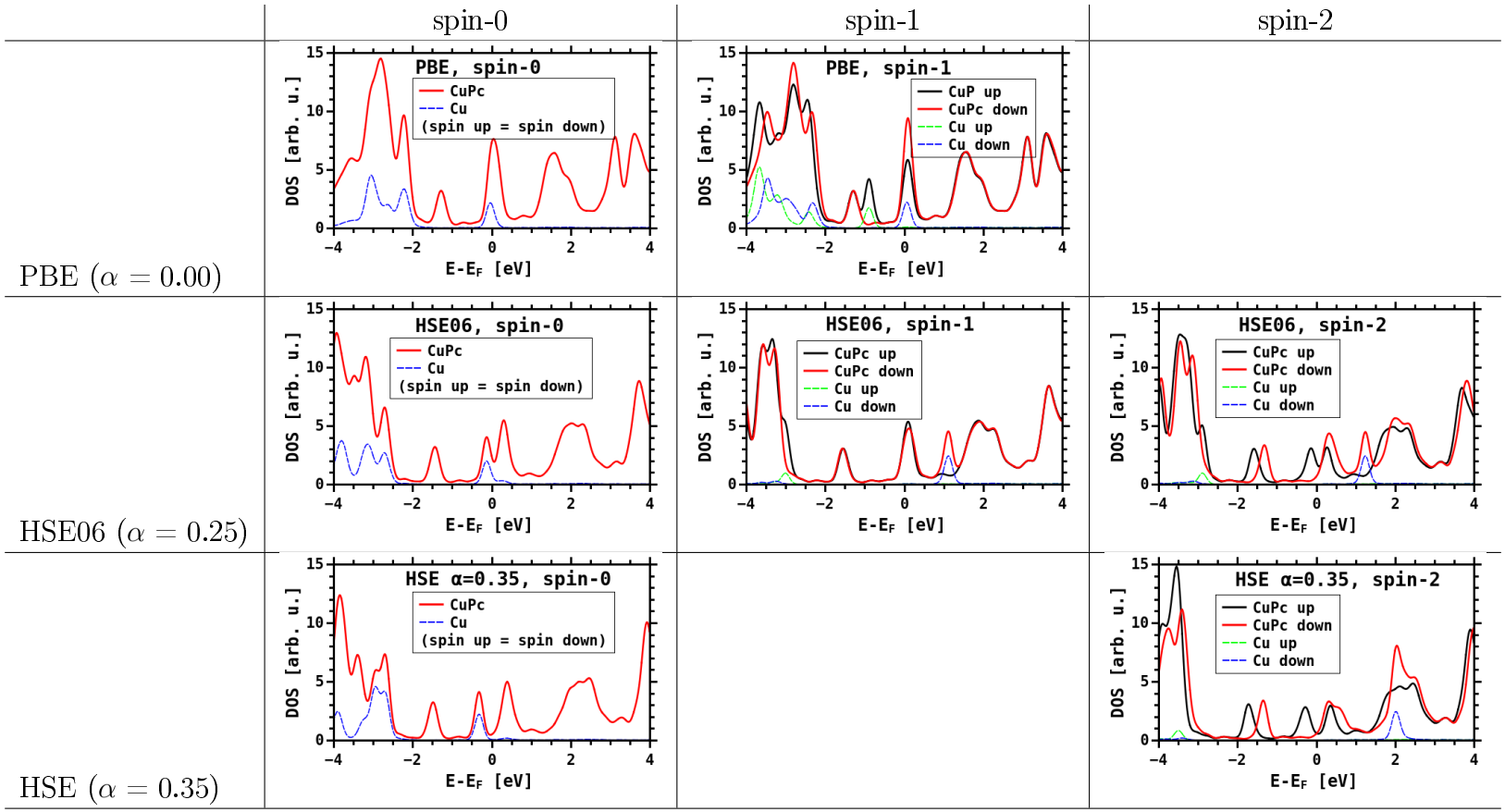

Figure 38: DOSs projected onto the the CuPc molecules adsorbed on Ag(111) for all obtained magnetic solutions with all different applied functionals. The spin up and spin down DOSs are shown in black and red, respectively. In addition, the DOSs projected on the central Cu atoms are shown with dashed green (spin up) and blue (spin down) lines. The energies are aligned to the Fermi level. Note that the spin-2 solution could not be obtained with PBE, while the spin-1 solution could not be obtained with HSE $\alpha = 0.35$.

Table 10: Total energies in eV of all different magnetic solutions with all applied functionals. Note that the spin-2 solution could not be obtained with PBE, while the spin-1 solution could not be obtained with HSE $\alpha = 0.35$.

	PBE ($\alpha = 0.00$)	HSE06 ($\alpha = 0.25$)	HSE ($\alpha = 0.35$)
total energy spin-0 [eV]	-13265507.475	-13265602.949	-13265722.929
total energy spin-1 [eV]	-13265507.620	-13265603.618	-
total energy spin-2 [eV]	-	-13265603.681	-13265723.915

Table 11: Hirshfeld charges on the CuPc molecule in electrons for different solutions and obtained with different functionals. This value was not evaluated in all calculations.

	PBE ($\alpha = 0.00$)	HSE06 ($\alpha = 0.25$)
Hirshfeld charge spin-0 [electrons]	0.80	0.81
Hirshfeld charge spin-1 [electrons]	0.79	1.13
Hirshfeld charge spin-2 [electrons]	-	0.81

Table 12: Total spin on the CuPc molecule in multiples of Bohr magneton μ_B, of all different magnetic solutions with all applied functionals.

	PBE ($\alpha = 0.00$)	HSE06 ($\alpha = 0.25$)	HSE ($\alpha = 0.35$)
energy spin-0 [eV]	0.00	0.00	0.00
energy spin-1 [eV]	0.94	1.01	-
energy spin-2 [eV]	-	1.85	1.91

5.2.5 Comparison of Different Solutions for CuPc/Ag(111)

The distinguishing feature between the three previously discussed solutions appears to be the spin distribution on the atoms in the CuPc molecule. In all three cases, about one electron is transferred from the substrate to the molecule. The spin-0 solution is most straightforward to interpret. Hybridization with the substrate and charge transfer toward the molecule lead to the filling of the spin-split orbital of the central Cu atom, which results in perfect alignment of spin up and spin down DOS.
In case of the spin-1 solution, the DOS exhibits indications for charge transfer toward the molecular LUMO, but the spin state of the molecule appears to be largely undisturbed. Similar to the isolated molecule, it exhibits an unpaired magnetic moment on the central Cu atom and the closest N atoms, with about 0.6 μ_B on the Cu and 0.1 μ_B on every surrounding N atom. The transferred charge on the ligands is distributed between both spin channels, and, therefore, does not influence the total magnetic moment of the molecule.
The situation is more complex for the spin-2 solution. The charge transfer from the substrate goes toward the molecular ligands, just like in the spin-1 solution. Also, the unpaired spin on the Cu atom is preserved, which is visible from both the DOS and the spin-per-atom analysis. However, the molecule exhibits an additional magnetic moment, which amounts to about 0.8 μ_B. This additional magnetic moment is, according to the DOS and the spin-per-atom analysis, located on the molecular C-N ligands. This means that, in contrast to the spin-1 solution, the transferred charge goes to only one spin channel of the molecule. This additional magnetic moment aligns parallel to the spin of the central Cu atom, which causes a net increase of the molecular magnetic moment.
Additionally, for this solution, the spin distribution on the molecule shows that a symmetry breaking appears and the the four-fold symmetry of the molecule is no longer preserved. This could appear for different reasons. The most obvious reason for such a symmetry breaking would be that the symmetries of substrate and molecule do not agree. However, it has been seen in some test calculations performed for CuPc on Ag(100), which exhibits the same four-fold symmetry as the molecule, that the spin-2 solution with the corresponding symmetry breaking seems to appear also on that surface. Another approach would be to considers the orbital symmetries of the molecule. According to gas phase calculations of CuPc performed by N. Marom and coworkers,[9] the LUMO of CuPc calculated with HSE06 is the e_g orbital, which does not preserve the four-fold symmetry of the molecule. It is, of course, not clear if this orbital ordering found in the gas phase persist upon adsorption. However, a situation where the filling of an orbital that breaks the four-fold molecular symmetry is a likely scenario. As a next step to analyze the spin-2 situation, the occupied orbitals should be plotted, which would allow to directly interpret which orbital gets filled in this configuration.
Additional insights can be gained from looking at the charge rearrangements that appear in the system upon adsorption. The charge rearrangements can be calculated by subtracting the charge density of the slab and the free-standing monolayer from the

charge density of the combined system:

$$\Delta\rho = \rho_{system} - \rho_{slab} - \rho_{monolayer} \tag{7}$$

The resulting plots for all three magnetic configurations, applying the HSE06 functional, are shown in Fig. 39.
For both the spin-1 and the spin-2 solution, the four-fold molecular symmetry is not reflected in the charge rearrangements. In the spin-1 case, it is reduced to a two-fold symmetry. For spin-2, the charge rearrangements could also be interpreted to be slightly chiral (see the charge accumulation on the upper and lower pyrrole rings), which is also seen experimentally by Mugarza el al.[165] The charge rearrangements in this case clearly bear resemblance to the CuPc e_g orbital as presented in Ref. [9].
While for the spin-1 and spin-2 solutions, charge depletion around the central Cu becomes visible, the spin-0 solution clearly exhibits charge accumulation in this region. These results suggest that a coupling between the Ag substrate and the molecular Cu atom appears for the spin-0 case. Although the DFT results do no give any insights into the charging process itself, this suggests that the charge transfer might happen through this channel for the spin-0 solution. In the other two solutions, the coupling is stronger between the substrate and the ligands of the molecule, and charge transfer most likely appears mainly in this region.
The appearance of these three different magnetic solutions raises several questions. Most importantly one would want to find out whether they are all physically meaningful and whether it is possible to determine a most favorable solution from simulations, which would then be expected to appear in experiments.
To discuss if the solutions are physically meaningful, it is helpful to compare them to gas phase results of the CuPc molecule. The spin-0 solutions corresponds to a closed shell singlet solution of CuPc, while the spin-2 solution is an open-shell triplet. In gas phase, also an open-shell singlet can be found, where the spin on the ligands aligns anti-parallel to the Cu spin. As mentioned previously, this solution could not be stabilized in the surface calculations performed here.
Comparing the energies for the gas phase singlet and triplet configurations, it was found that, applying PBE, the singlet is about 0.8 eV lower in energy. With HSE06, on the other hand, the triplet solution becomes favorable and lies 0.15 eV lower than the singlet.
No gas phase analogy to the spin-1 solution is obtainable. This solution is, most likely, only possible due to the (strong) hybridization with the surface. As mentioned previously, it appearance might be an consequence of charge over-localization in functionals with low amount of Hartree-Fock exchange, as it was not found in calculations applying higher values of α. It is possible that the spin-1 solution is a saddle point between the spin-0 and spin-2 solution. By applying higher values of α, these solutions differ stronger in energy, which destabilizes the saddle point in between. A similar situation was discussed for FCT and ICT solutions, where the FCT solution is a saddle point between two ICT solutions (see section 4). Therefore, it is very likely that the spin-1 solution is not physically relevant.

The obvious approach to compare the the different solutions is to compare their total energies. However, this comparison is complicated by the fact that the energy differences between the three solutions differ, depending on the applied functional. A similar effect was found for FCT and ICT solutions of TFBQ on Cu_2O, as discussed in section 4. The received energies for all obtained solutions are shown in Tab. 10. In the total energies, a clear trend is observable, with the spin-2 solution being the most favorable one for both HSE calculations, and the spin-1 solution more favorable than the spin-0 solution with HSE06. Additionally, this trend appears to become more clear with increasing α, as the energy difference between spin-0 and spin-2 increases from 0.73 eV for HSE06 to 0.99 eV for HSE $\alpha = 0.35$.
However, the spin-2 solution being favorable in the considered range of α does not allow to be predictive, as the ideal α value for the system is unknown. In addition, as already discussed in the methodological section, to be predictive it would be necessary to perform full geometry optimizations of for every system, i.e. for every solution with every applied value of α. However, this was, so far, not feasible with the available computational resources. Results on the performed preliminary geometry optimizations are given in section 5.5.3.
Therefore, at this point the conclusion is that while the spin-2 solution appears to be most likely from calculations performed here, further input is necessary to be able to make a clear statement on the spin spate of CuPc on Ag(111).

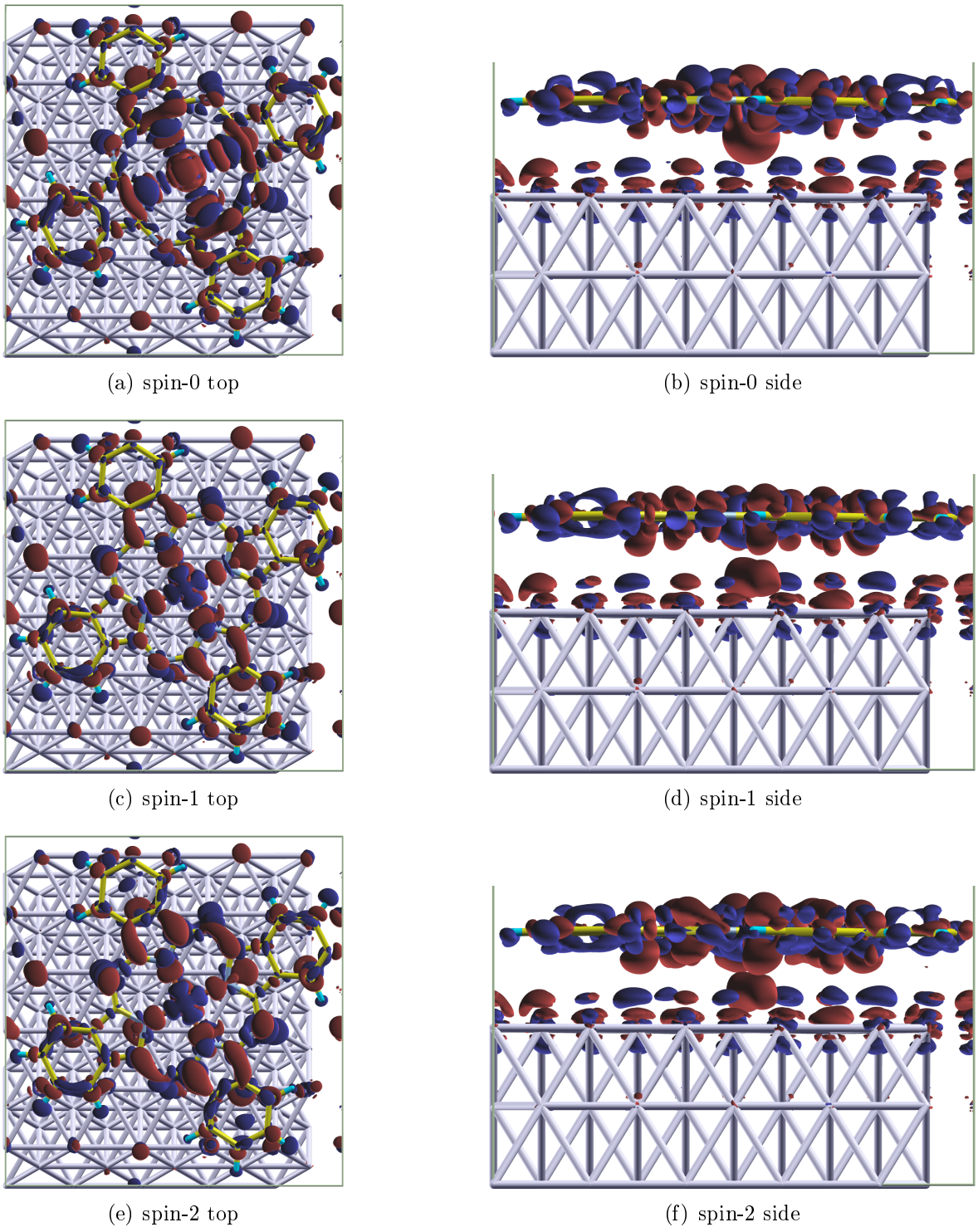

(a) spin-0 top

(b) spin-0 side

(c) spin-1 top

(d) spin-1 side

(e) spin-2 top

(f) spin-2 side

Figure 39: Charge rearrangements upon adsorption of the CuPc molecule on the Ag(111) surface for the three different magnetic configurations, calculated with HSE06. Red regions indicate charge accumulation, while blue regions indicate charge depletion. The isovalue was set to 0.006 eV/Å^3.

5.3 Obtained Solutions: CoPc on Ag(111)

The appearance of different magnetic solutions for CuPc upon adsorption on Ag raised the question whether such effect occurs for all similar molecules, which exhibit a non-zero magnetic moment in the gas phase, or a contrasting behavior could be observed. For CuPc, several experimental results show the persistence of the magnetic moment upon adsorption, while for CoPc on Ag, the gas phase magnetic moment appears to be quenched. Among other results, the absence of a Kondo Peak for adsorbed CoPc points toward a situation with no unpaired electron close to the Fermi level.[164, 165, 174, 177] Therefore, CoPc on Ag(111) was chosen as an alternative system to be compared to the results obtained for CuPc on Ag(111).
Extensive tests on the CoPc/Ag(111) and CoPc/Ag(100) systems showed that on the (100) surface, similar to the situation of CuPc on Ag(100), convergence is troublesome to achieve. Therefore, only the CoPc/Ag(111) interface was investigated in more depth. In contrast to the situation for CuPc/Ag(111), the magnetic moment of the molecule was always reduced upon adsorption. Nonetheless, two different magnetic solutions were found. Although the total molecular magnetic moment of both solutions is close to zero, the analysis of the DOS and spin per atom uncovers that they differ significantly. In the following, the solutions are denoted as spin-0.0 and spin-0.1 solution.
A comparison between those two solutions was only possible at the value $\alpha = 0.30$, because only with this setting, full convergence could be obtained for both. Fig. 40 shows the DOSs of both solutions, as obtained with HSE $\alpha = 0.30$, and the following sections discuss these solutions in detail. More details on solutions obtained with other functionals are then given in section 5.3.3.

5.3.1 CoPc on Ag(111): Spin-0.0 Solution

This solution is very similar to the spin-0 solution found for CuPc/Ag(111). The sum of Hirshfeld charges on the molecule show that the charge transfer amounts to 0.87 electrons. The spin goes to zero on all atoms, and the DOS (see Fig. 40) suggests that charge is transferred to the central Co atom, as no spin-split peak remains upon adsorption and the spin-up and spin-down DOSs are perfectly aligned. At the Fermi level, the molecular DOS goes to zero, which indicates the complete filling of a molecular state upon adsorption.
This solution was found with all applied functionals (semi-local and hybrid) for CoPc on Ag(111).

5.3.2 CoPc on Ag(111): Spin-0.1 Solution

Similar to the spin-0.0 solution, in this second case, charge of slightly below one electron (0.86 electrons) is transferred to the CoPc molecule upon adsorption according

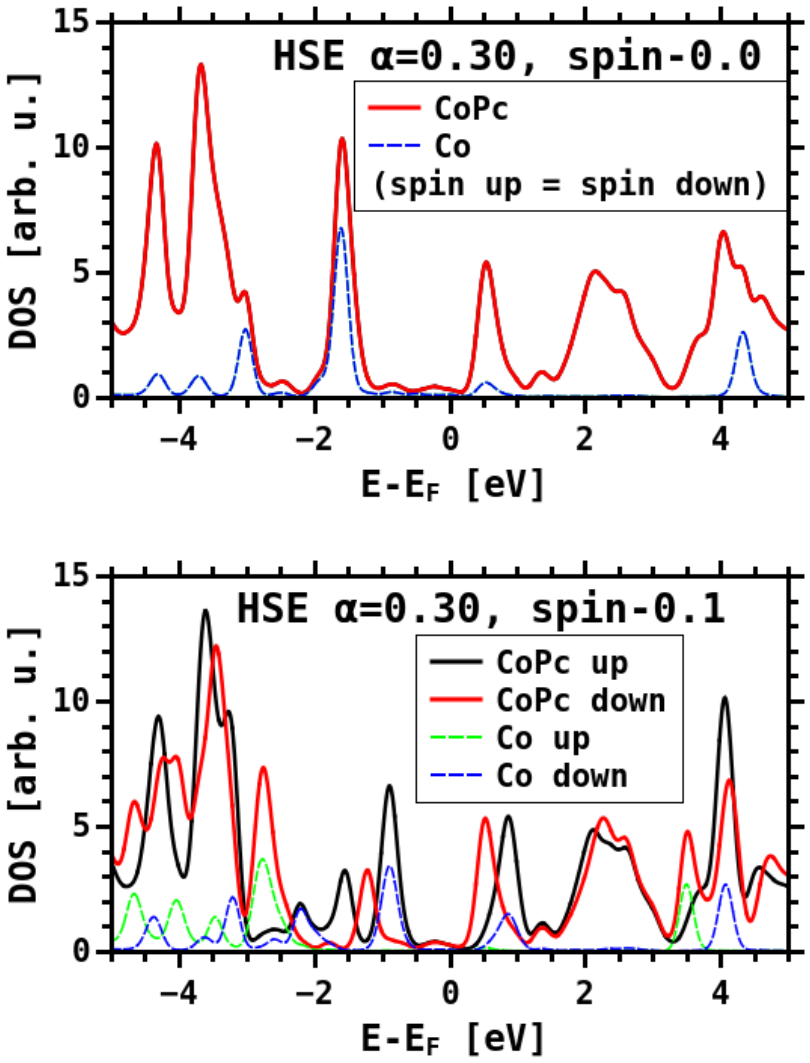

Figure 40: DOS of the CoPc molecule adsorbed on Ag(111) for both obtained magnetic solutions with the HSE $\alpha = 0.30$ functional. The spin up and spin down DOSs are shown in black and red, respectively. Additionally, the DOS projected onto the central Co atom is shown in dashed lines in green (spin up) and blue (spin down). Note that for the spin-0.0 solution, spin up and spin down are perfectly aligned. The energies are aligned to the Fermi level.

to the Hirshfeld analysis. The molecular magnetic moment goes to almost zero and amounts to $\mu = 0.06\ \mu_B$ applying HSE $\alpha = 0.30$. The DOS, however, looks very different from the one obtained for the spin-0.0 solution. The spin up and spin down channels are occupied very differently. Fig. 40 includes also the DOS projected on the central Co atom, and the spin-split Co peak at about 0.75 eV indicates that the Co spin is not quenched in this case. Several additional spin-split peaks prevail around the

Fermi level. It is not a priory clear what the electronic configuration of the adsorbed molecule is and why the total molecular magnetic moment is so strongly reduced upon adsorption. The analysis of the spin per atom allowed to shed light on this matter. Fig. 41 depicts how the spins are distributed in the adsorbed CoPc. Similar to the non-zero magnetic solutions of CuPc, the spin of the central Co atom amounts to μ = 0.69 μ_B. There are only very small spins of μ = 0.02 μ_B on the surrounding N atoms. This magnetic moment of the central region is compensated by a negative magnetic moment on the inner C atoms of the ligands, which amounts to about μ = -0.08 μ_B per atom. Due to the opposite signs, the total molecular magnetic moment cancels to almost zero. This spin distribution indicates that the charge transfer goes to the outer ligands of the molecule.
As mentioned previously, this solution could, so far, only be obtained with the HSE α = 0.30 functional.

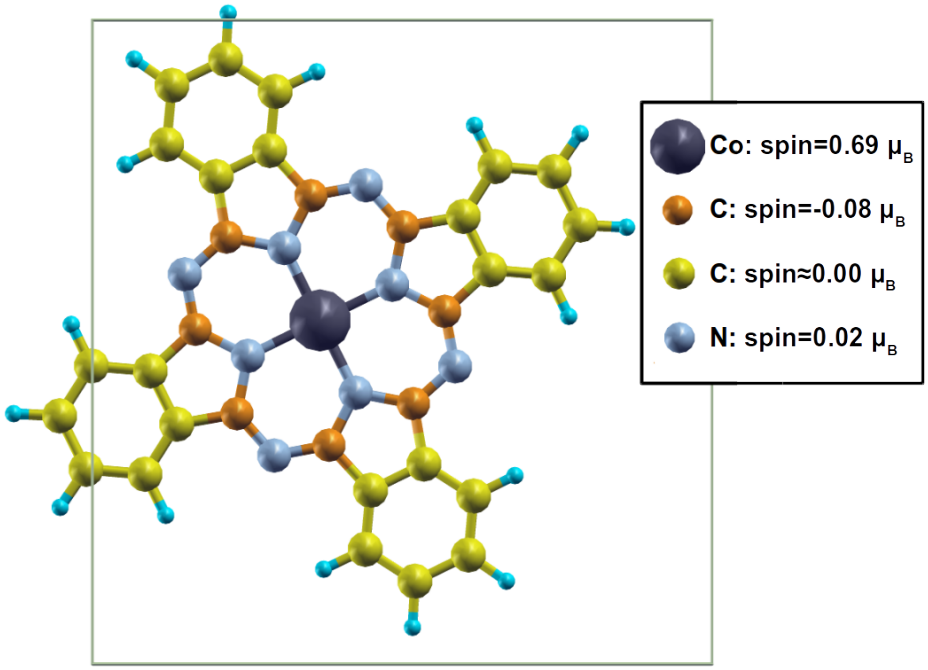

Figure 41: Per-atom spin analysis of CoPc on Ag(111) in the spin-0.1 configuration. All spins above μ = 0.01 μ_B are given in multiples of μ_B. All N atoms exhibit the same spin of μ = 0.02 μ_B. The inner C atoms, which exhibit a spin of μ = -0.08 μ_B are depicted in orange, while the C atoms with a spin close to zero are depicted in yellow.

5.3.3 Dependence of Result on the Applied Functional

While the spin-0.0 solution was found with all tested functionals, including PBE and HSE with α values between $\alpha = 0.20$ and $\alpha = 0.40$, the spin-0.1 solution could, so far, only be converged using $\alpha = 0.30$. However, this might be caused by the sensibility of the different magnetic solutions on the exact computational settings like spin initialization and broadening, and more extensive tests might be necessary to achieve convergence also at different α values.
Also higher values $\alpha = 0.50$ and $\alpha = 0.65$ were tested, applying several different input settings (varying the broadening, spin initialization and mixing parameters of the DFT calculation). However, similar to the situation of CuPc/Ag(111), these calculations could not be converged.
The DOSs of all converged calculations are summarized in Fig. 13.
An interesting feature that should be noted here is the shift of Co-assigned peaks. Two peaks assigned to the central Co atom are found closely below the Fermi level. While the larger one is shifted by less than 1 eV upon changing the applied value of α (between -1.05 eV in the PBE $\alpha = 0.00$ calculations to -1.93 eV in the HSE $\alpha = 0.40$), the second peak is shifted by more than 2 eV from -1.43 eV with PBE to -3.57 eV with HSE $\alpha = 0.40$. This stronger shifting upon increasing α indicates stronger charge localization.

5.3.4 Comparison of Different Solutions for CoPc on Ag(111)

The two obtained solutions for CoPc/Ag(111) do not differ in terms of charge transfer to the molecule (which amounts to approximately one electron) or molecular magnetic moment, but exhibit different electronic structures. This difference arises from the location of the transferred charge in different regions of the molecule. The spin-0.0 solution is a closed-shell scenario similar to the CuPc spin-0 case, where charge is transferred to the central Co atom. In the open-shell spin-0.1 solution, charge is transferred to the molecular ligands. However, in contrast to the CuPc situation, which exhibits a triplet state with $\mu \approx 2\ \mu_B$, the ligand spin of CoPc aligns anti-parallel to the metal spin. Therefore, a so-called open-shell singlet configuration arises, where the total magnetic moment of the molecule goes to (almost) zero. Numerous tests were performed to obtain the open-shell triplet configuration also for adsorbed CoPc, but this result could never be obtained.
The charge rearrangements upon adsorption of CoPc on Ag(111) are shown in Fig. 42, where red regions depict charge accumulation, while blue regions show charge depletion. Surprisingly, they are rather similar for both solutions, with the strongest rearrangements appearing in the region of the central Co atom (as well as above and below it). This indicates that the charge transfer, in contrast to the CuPc situation, takes place mainly via hybridization of the Co atom with the Ag substrate, rather than via the ligands. For the open-shell spin-0.1 solution, the central feature is a little

	spin-0.0	spin-0.1
PBE ($\alpha = 0.00$)	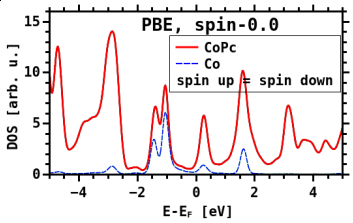	
HSE $\alpha = 0.20$	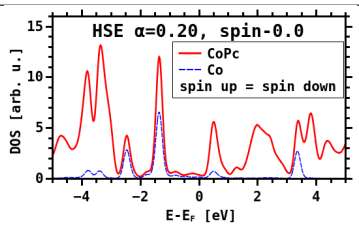	
HSE06 ($\alpha = 0.25$)	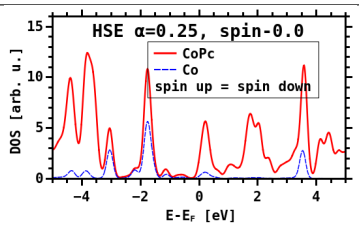	
HSE $\alpha = 0.30$	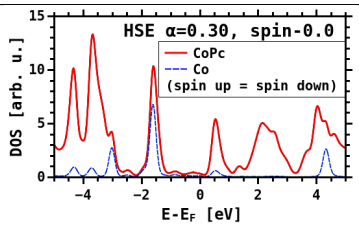	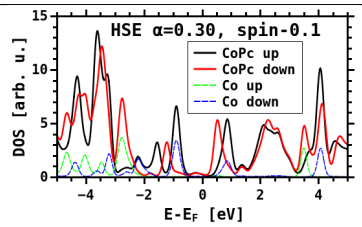
HSE $\alpha = 0.35$	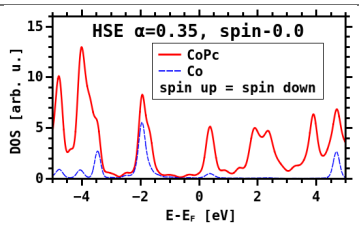	
HSE $\alpha = 0.40$	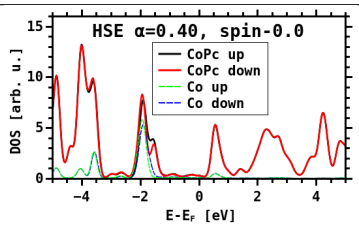	

Table 13: DOS of the CoPc molecule adsorbed on Ag(111) for both obtained magnetic solutions with all different applied functionals. The spin up and spin down DOSs are shown in black and red, respectively. In addition, the DOSs projected on the central Co atoms are shown with dashed green (spin up) and blue (spin down) lines. The energies are aligned to the Fermi level.

weaker, and more charge accumulation on the ligands is visible.
Tab. 14 summarizes energies, Hirshfeld charges and spin on the molecule for CoPc on Ag(111) calculated with HSE $\alpha = 0.30$. The energy difference (of about 0.02 eV) between the two magnetic solutions is negligible. Additionally, as already discussed for the CuPc system, a comparison of the energies of different solutions alone is not instructive, as they strongly depend on the applied functional. Unfortunately, in the case of CoPc it was so far also not possible to obtain both solutions for different α values, which would at least allow to observe a trend in the total energies.

Table 14: Comparison of total energies, Hirshfeld charges and molecular spin of the CoPc/Ag(111) system obtained with HSE $\alpha = 0.30$.

HSE $\alpha = 0.30$	energy [eV]	Hirshfeld charge [electrons]	molecular spin [μ_B]
spin-0.0	-13258478.962	0.83	0.00
spin-0.1	-13258478.984	0.86	0.06

To reach a better understanding of the obtained solutions, gas phase calculations of the neutral and anion CoPc molecule were performed with HSE $\alpha = 0.30$. In contrast to CuPc, where no clear gas phase equivalent for the spin-1 solution is obtainable, for CoPc it is possible to calculated gas phase equivalents of both surface solutions. The obtained orbital occupations are shown in Fig. 43. A comparison of the energies of the open-shell and the closed-shell singlet solutions showed that the open shell configuration is by 2.08 eV favorable in energy. However, while for CuPc, the orbital ordering of the gas phase anion appears to be similar to that of the Ag-adsorbed molecule, this is not the case for CoPc. Comparing the orbital ordering in gas phase to the DOS of the adsorbed molecule for the spin-0.1 open shell solution shows that the highest occupied orbital is strongly Co-derived on the surface, while it is a spin-split ligand orbital in the gas phase. A strong contribution of Co to the highest occupied orbital of the adsorbed molecule appears for both solutions, which is in good agreement with experimental results, e.g. by Salomon and coworkers.[177] Therefore, the gas phase results here do not yield instructive input for the determination of the surface-adsorbed situation of CoPc.
Note that for systems where strong orbital reordering appears, the DFT approach has to be applied with extra caution, as it might easily miss such effects. This is the case as the obtained orbital ordering depends on the applied amount of Hartree-Fock exchange, as can be seen in the DOSs obtained with different amounts of Hartree-Fock exchange shown before.
Therefore, for CoPc, it is unfortunately not possible to obtain enough insights from this theoretically obtained data to draw conclusions which of the obtained solutions is more likely to be found from experiments.

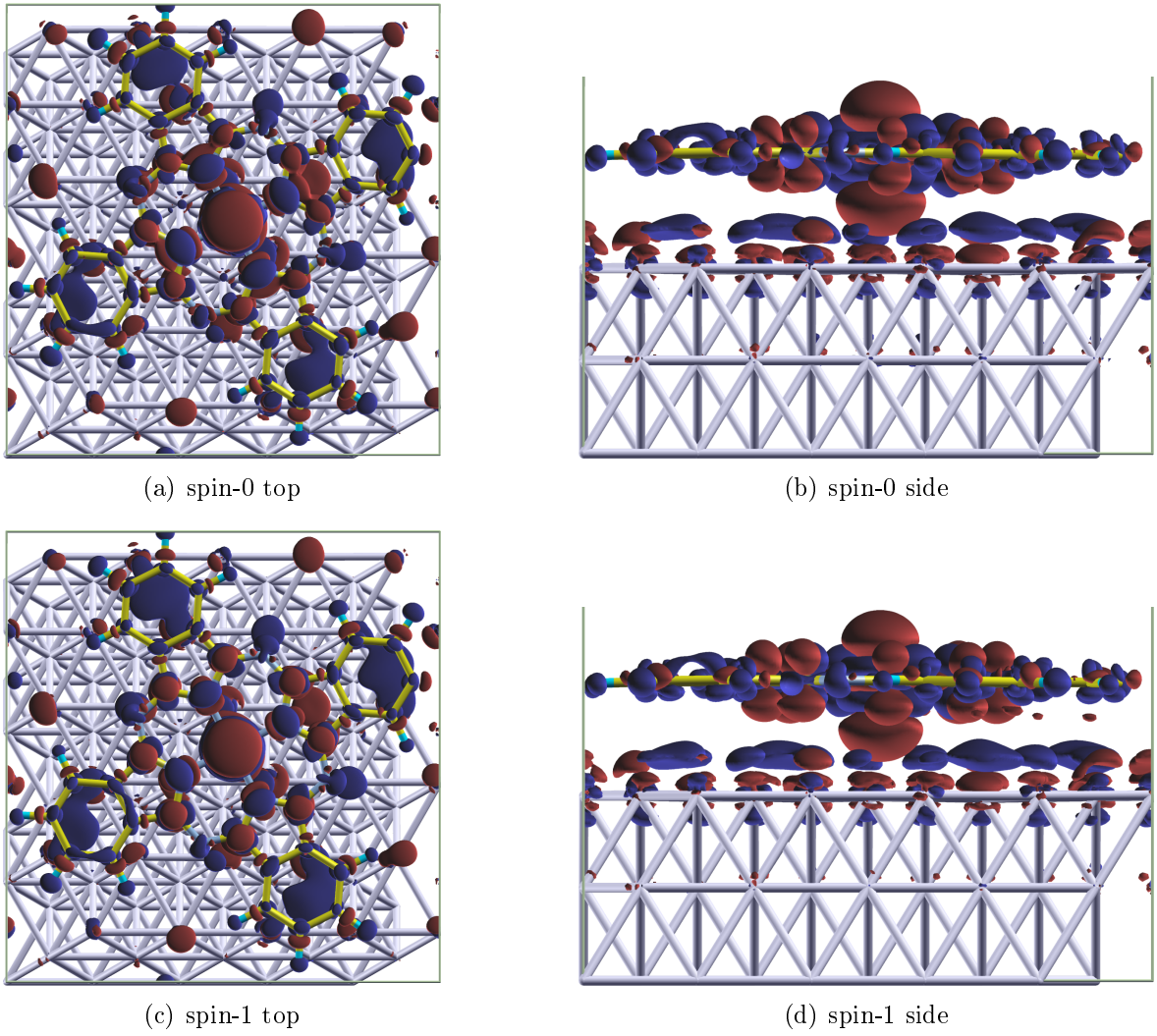

(a) spin-0 top

(b) spin-0 side

(c) spin-1 top

(d) spin-1 side

Figure 42: Charge rearrangements upon adsorption of the CoPc molecules on the Ag(111) surface for both different magnetic configurations. Red regions indicate charge accumulation, while blue regions indicate charge depletion. The isovalue was set to 0.006 eV/Å^3.

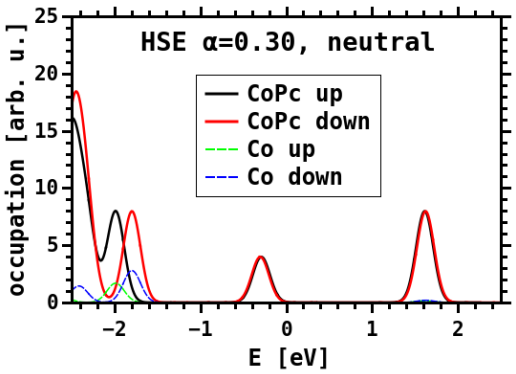

(a) neutral

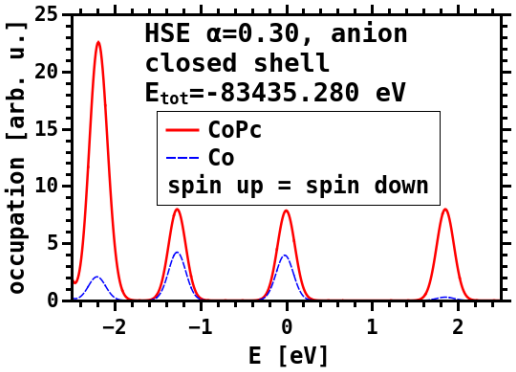

(b) closed-shell anion

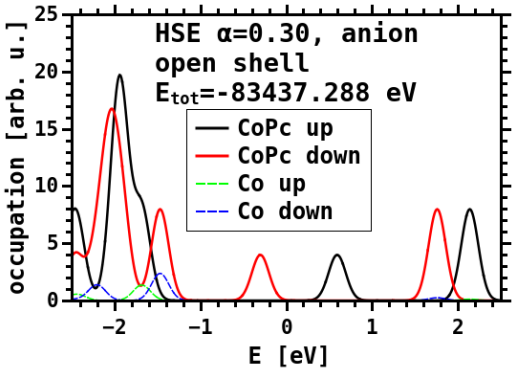

(c) open-shell anion

Figure 43: Gas phase orbital occupation of CoPc calculated for the neutral molecule and anion with HSE $\alpha = 0.30$. Spin up and spin down are shown in black and red, respectively. Additionally, the occupation of of the central Co atom is shown in green (spin up) and blue (spin down). The energy is aligned to the valence band maximum.

5.4 Comparison to Literature and Experimental Results

The performed DFT simulations unfortunately do not provide conclusive answers which magnetic solution of CuPc and CoPc is most likely to appear on Ag substrates. Therefore, a comparison of the obtained results to experimental data is required.
CuPc and CoPc adsorbed on coinage metal substrates have been extensively discussed in literature, presenting both experimental and theoretical insights. Some of these studies focused on the magnetic properties of CuPc and CoPc on Ag surfaces [164, 165, 174, 176, 177, 178, 196] and also several other surfaces.[167, 171, 175, 192, 196, 197, 198, 199, 200, 201, 202, 203]
An additional interesting aspect is the tuning of spin states of such molecules, which was discussed by Krull et al. [196] and Stepanow et al. [176]. There, spin tuning of different TMPc molecules adsorbed on Ag surfaces was obtained by adding electrons to the molecules by alkali metal doping.
In the following, the relevant literature is reviewed and the results obtained in this work are discussed in the context of previous experimental and theoretical findings. The most relevant publications are the following:

- Stepanow et al. (*Giant spin and orbital moment anisotropies of a Cu-phthalocyanine monolayer*) explored the magnetic properties of submonolayers of CuPc on Ag(100) by performing x-ray magnetic circular dichroism (XMCD) experiments. Indications for an enhanced magnetic moment of the molecule upon adsorption were found.[174]

- Mugarza et al. (*Spin coupling and relaxation inside molecule-metal contacts*) studied different metal phthalocyanine molecules adsorbed on Ag(100) by scanning tunneling microscopy STM and reviewed the origins, intra-molecular densities and coupling of the spin magnetic moments.[164]

- Stepanow et al. (*Mixed-valence behavior and strong correlation effects of metal phthalocyanines adsorbed on metals*) investigated CoPc and FePc on Au(111). They performed XMCD measurements to investigate local magnetic moments and conducted ligand field multiplet calculations to properly describe magnetic correlation effects. Although no direct comparison with the present work is possible due to the different substrate material, this study is still highly interesting in the present context, as the coupling of central Co atom to the substrate metal as a consequence of the molecular orbital symmetry is discussed.[175]

- Mugarza et al. (*Electronic and magnetic properties of molecule-metal interfaces: Transition-metal phthalocyanines adsorbed on Ag(100)*) applied scanning tunneling spectroscopy STS and DFT to study the molecule-metal interactions and magnetic properties of various different transition metal-phthalocyanines. They

found that while the molecular magnetic moment for CoPc (and FePc) is reduced upon adsorption, for CuPc (and NiPc) it is enhanced.[165]

- Salomon et al. (*Electronic structure of CoPc adsorbed on Ag(100): Evidence for molecule-substrate interaction mediated by Co 3d orbitals*) applied both photoelectron spectroscopy PES and GW calculations to investigate charge transfer and corresponding interfaces states of CoPc on Ag(100).[177]

Unfortunately, most studies were not performed on (111) but rather on (100) surfaces, which has been shown to be problematic to reproduce in DFT, as discussed before. This has to be kept in mind when drawing conclusions from comparing the results obtained in this thesis to the above discussed literature.

It should be noted here that, in accordance with the results of CuPc and CoPc on Ag(111) discussed above, several experimental and computational results reported that the adsorbed TMPcs receive about one electron from Ag substrates. [164, 165, 177]

5.4.1 CuPc on Ag

For CuPc on Ag the main question is whether the high-spin state, denoted as spin-2 solution, can also be found experimentally. This magnetic solution exhibits an unpaired spin both on the central Cu atom and on the ligands of the Pc molecule.
The appearance of such an unpaired ligand spin which arises from charge transfer upon adsorption is confirmed by Mugarza et al. in two different studies.[164, 165] In these contributions, the differential conductance dI/dV spectra of the adsorbed molecule on the outer and inner molecular region were investigated and it was found that the ligand spin appears after adsorption and is delocalized over the peripheral atoms of the CuPc molecule. An additional indication for a magnetic moment on the ligands is the occurrence of a Kondo peak.
They also showed that this ligand spin is independent of the spin on the central metal atom. The outer π-orbitals and the metal-centered d orbitals do not interact strongly, which leads to an isolated coexistence of the ligand spin and the metal spin.[164, 165]
The next interesting question is whether also indications for the parallel alignment of these spins can be found, as such an alignment appears in the DFT calculations and leads to the increased total magnetic moment of the molecule. In Refs. [164] and [165], Mugarza et al. stated that the magnetic moment of the CuPc molecule increases upon adsorption. This was reasoned by the appearance of a Kondo peak at zero bias, which was interpreted as an indication for a magnetic triplet ground state. To achieve such a magnetic ground state, the metal and ligand spins must align in parallel. Mugarza et al. reasoned that this alignment is a consequence of intra-molecular exchange coupling

between the d states of Cu and the π states of the ligands.[164, 165]
These findings are in excellent agreement with our results and confirm the appearance of a high-spin state of the CuPc molecule upon adsorption on Ag.
An additional confirmation for the spin-2 solution of CuPc is given by the electronic structure STS measurements by Mugarza et al.,[165] where it was found that the charge transfer appearing from the Ag substrate toward the molecule goes to the former molecular LUMO. This results in a double-peak structure around the Fermi level, separated by about 0.65 eV. This was interpreted as a partially filled orbital, where the Coulomb repulsion U causes a separation of single occupied and and double occupied states [164, 165, 192]. As discussed in section 5.2.3, the DFT results of CuPc in the spin-2 configuration also showed this double peak structure, separated by 0.45 eV with HSE06 ($\alpha = 0.25$) and 0.64 eV with HSE $\alpha = 0.35$. In accordance with the literature results, these splitted states are not assigned to the central Cu atom, but to the molecular ligands (see Fig. 34).
In section 5.2.3 it was already discussed that the relevant correlation effects causing such features are not described within standard semi-local DFT such as PBE [191, 192] but require either hybrid functionals, as it was done here, or so-called DFT+U methods.[165, 192] The amount of Hartree-Fock exchange, as employed in hybrid functionals, is related to the Coulomb repulsion term U in the Hubbard model, as employed in DFT+U. [44, 193]
In accordance with that, Mugarza et al.[164] reported that they were not able to reproduce this double-peak structure by performing DFT calculations using LDA due to underestimation of correlation effects. In a later work, Mugarza et al.[165] applied GGA+U, which still did not give the full picture for CuPc on Ag. In contrast to the present work, they only obtained one solution, which appears to be similar to the spin-1 case reported here. Therefore, their results do not reproduce the charging of the ligands and the U-splitting at the Fermi edge, which they found experimentally. Additionally, the magnetic moment of the adsorbed CuPc molecule could not be reproduced within their DFT calculations, but was close to $\mu = 1\ \mu_B$, as in the spin-1 solution presented here. It is not clear how well the results obtained in this work could be obtained by applying DFT+U as used by Mugarza et al., especially as (i) the three obtained solutions lie close in energy for most values of α and might therefore be hard to converge and (ii) the ideal choice of the U parameter is not a priori clear,[192] similar to the ideal amount of Hartree-Fock exchange.
Summarizing the results on CuPc on Ag discussed in literature, it can be concluded that the magnetic spin-2 case corresponds well to what is found in various experiments. It remains to discuss why the charge transfer of about one electron, which causes the magnetic state of the adsorbed CuPc molecule, does not directly go to the central Cu atom and cause quenching of the molecular magnetic moment. Stepanow et al. (Ref. [174]) found that the central Cu atom exhibits no significant hybridization with the underlying Ag substrate, which is a consequence of the symmetry of the molecular orbitals of the Cu ion, which lie within the molecular plane. Due to this geometric hindrance for charge transfer between the substrate and the central metal atom,

charge transfer to the molecule can only occur through the outer molecular region, as the ligands do hybridize with the underlying substrate.[164, 174] This corresponds to the interpretation of the charge rearrangements of CuPc upon adsorption on Ag as presented in section 5.2.5, where it was argued that no strong hybridization between the Cu atom and the Ag substrate seems to appear.
Stepanow et al. also found that the Cu 3d states remain unoccupied upon adsorption, which again agrees well with the DOS of CuPc on Ag(111) shown in Fig. 34, where the Cu states close to the Fermi edge remain spin-split upon adsorption for the spin-2 solution.[174] The ligand spin was assigned to be located at the orbital corresponding to the molecular $2e_g$ orbital, which suggests that the charge transfer occurs toward this state. This agrees with the findings that this state is the molecular LUMO in gas phase [9] and indicates that no complete reordering of the molecular states upon adsorption (and charging) occurs.[164, 165]

5.4.2 CoPc on Ag

In contrast to the situation of CuPc adsorption, where the central Cu atom does not hybridize with an Ag substrate, the Co atom of CoPc molecules does exhibit hybridization with Ag.[161, 171, 175, 177, 201]. Salomon et al. [177] showed that in case of a monolayer CoPc adsorbing on Ag(100), the substrate interaction mainly appears via the central metal atom, which receives charge from the substrate.[177, 204] This can, e.g. be shown from experiment by investigating the interface states which contribute to the charge transfer from the photoionization cross section.[177] Similar results were obtained by Stepanow et al. for CoPc adsorbing on Au(111) in Ref. [175], where it was stated that the symmetry of the central metal 3d states is responsible for charge transfer between the Au substrate and the molecule, as it leads to an overlap between Co and substrate states.
The suggested partly-filled orbital, which forms a bond with the substrate corresponds to the d_{z^2} molecular orbital, which lies perpendicular to the molecular plane.[175, 177] Salomon et al. [177] suggested that the coupling between Co d states and the substrate appears due to this geometric issue, where the molecular orbital derived from the d_{z^2} orbital sticks out from the molecular plane. Consequentially, this leads to a significant contribution of this Co orbital to the "new" HOMO of the surface-adsorbed molecule. These findings agree well with the results obtained here. First, the charge transfer toward an orbital lying perpendicular to the molecular plane can be seen in the charge rearrangements upon CoPc adsorption as shown in Fig. 42. Second, the DOS projected on the adsorbed CoPc molecule shown in Fig. 40 show a significant contribution of Co states to the highest molecular state, both for the open-shell and the closed-shell configuration. The closest Co state is found at -1.62 eV in the HSE $\alpha = 0.35$ results for the closed-shell spin-0.0 solution and at -0.90 eV for the open-shell spin-0.1 solution. In Ref. [177], this state was found at -1.0 eV. In contrast to the discussion in Ref. [177], the DFT results obtained in this work agree reasonably well with experiment

results, although the position of the Co-derived peaks does not agree perfectly, which is a consequence of their dependence on the applied amount of Hartree-Fock exchange. While for CuPc adsorbed on Ag, experimental results indicate an enhanced magnetic moment, for the CoPc on Ag, experiments indicate a quenching of the molecular magnetic moment.[165, 177, 178] This quenching also appear for CoPc on Au(111).[175] However, this does not settle the question whether the simulated open-shell or closed-shell singlet configuration of the molecule appears, as they both lead to a molecular magnetic moment close to zero. Several available studies in literature also discussed both of these magnetic solutions.[165, 177] In Ref. [165], Mugarza et al. found that the total spin of the adsorbed CoPc molecule goes to zero and assumed an antiferromagetic coupling of a spin located on the Co d states and a second spin on the molecular ligands, which leads to a total spin close to zero. This corresponds to the the open-shell singlet discussed here. However, they suggested the open-shell situation relying mainly on GGA+U calculations, where only the open-shell solution was found. Therefore, it is not clear whether this claim is trustworthy and whether the existence of alternative solutions was missed in their simulations, as the computational results of the open-shell configuration are not well supported by their experimental results.
The experimental absence of Kondo peaks (which can not be captured within standard DFT [3, 7, 203, 205]) could be an indication for the closed-shell scenario, as the open-shell singlet does have unpaired spins close to the Fermi level.[171, 203] However, the absence of a Kondo peak is merely an indication, and not a solid proof for a non-magnetic ground state, as e.g. the Kondo temperature might be too low to allow the experimental detection of a Kondo peak.[165, 175, 206]
Salomon et al. suggested that upon adsorption, the CoPc molecule gets charged and a non-trivial charge redistribution appears.[177] By performing G_0W_0 calculations of the gas phase molecule, they found two different possibilities for the CoPc anion: an open-shell singlet and a closed-shell configuration, which corresponds to the solutions for the adsorbed CoPc found in this work. By comparing the G_0W_0 results to experimental data, they concluded that the open-shell singlet configuration does not agree well with photoemission spectroscopy data and the closed-shell configuration is most likely to appear on the Ag(100) surface.
Considering the orbital reordering, Salomon et al. found that the HOMO of the anion (which would supposedly be the orbital that gets filled upon adsorption) does not correspond to LUMO of the neutral molecule, which is the 2-fold symmetric e_g orbital. Rather, the Co-centered a_{1g} orbital gets filled and represents the HOMO of the adsorbed molecule.[177, 207] This is consistent with our findings, as the highest occupied peak of the spin-0.0 solution is a Co-derived orbital. Also, the observed charge rearrangements of CoPc adsorption on Ag preserve the 4-fold symmetry of the molecule, see Fig. 42. In case of filling of a two-fold symmetric orbital as e_g, a symmetry breaking should appear in the charge rearrangement, as it is the case for the spin-2 configuration of CuPc on Ag(111) (see Fig. 39).
In conclusion, literature states that the molecular magnetic moment of CoPc adsorbed on Ag is quenched, and indicates that the closed shell spin-0.0 solution appears. How-

ever, the available literature is not perfectly conclusive regarding the latter point.

5.5 Further Calculations of CuPc and CoPc on Ag Surfaces

As mentioned previously, the systems investigated here were not at all straightforward to calculate, as the hybrid calculations are extremely time-consuming and the specific magnetic solutions could often not be obtained right away. Therefore, numerous calculations with different settings, on different surfaces and also with a different DFT code were performed. These tests are summarized briefly in the following.

5.5.1 Dependence of Result on the Applied DFT Code

Originally, the investigation of CuPc on Ag(111) was performed applying the Vienna ab initio simulation package VASP [97]. The obtained results were presented in Ref. [25]. In that work, the spin-1 solution was found applying PBE, and the spin-2 solution applying HSE06. Extensive tests performed later showed that the spin-1 solution could also be found with HSE06, and that no direct linking between functional and magnetic solutions exists. Interestingly, CuPc on Ag(111) could never be converged into the closed-shell spin-0 solution in VASP, neither with PBE nor with HSE06.
In contrast to that, on the Ag(100) surface, also the spin-0 solution was found applying VASP with the PBE functional. Further tests for this surface with VASP showed that both the spin-1 and spin-2 solution seem to appear with HSE06, but most calculations could not be fully converged.
For CoPc on Ag(111), the VASP HSE06 calculations led to convergence into the open-shell spin-0.1 solution, and the closed-shell solution could not be obtained. Only on the Ag(100) surface, the closed shell spin-0.0 solution could also be found with VASP and HSE06. In that case, some calculations showed a trend toward an open-shell solution, but no convergence could be reached.
The VASP results clearly showed that the different obtained magnetic solutions are not direct linked to specific functionals. However, it turned out to be hard to control the convergence toward specific solutions with VASP. Therefore, it was decided to switch to FHI-aims, which should supposedly allow an easier control of the magnetic moment of specific atoms, and therefore allow easier convergence toward specific solutions. However, it should be noted here that the failure to obtain all different solutions in VASP does not at all mean that they cannot be obtained within this code. More likely, the initializations and settings of the calculations would need to be done in a different way, which was, unfortunately, not found by the author.
To make sure that no significant differences in the way that the molecules are described within FHI-aims and VASP influence the results, the DOSs of the molecular CuPc monolayer in the applied unit cells was compared for both codes. Such differences could arise, e.g. because of applying underconverged settings in one of the codes. The

resulting DOSs are shown in Fig. 44. Note that the different applied broadenings lead to the different peak widths. Still, these results show that for the CuPc monolayer, the description in VASP and FHI-aims is very similar and no significant discrepancies should arise in the surface calculations.

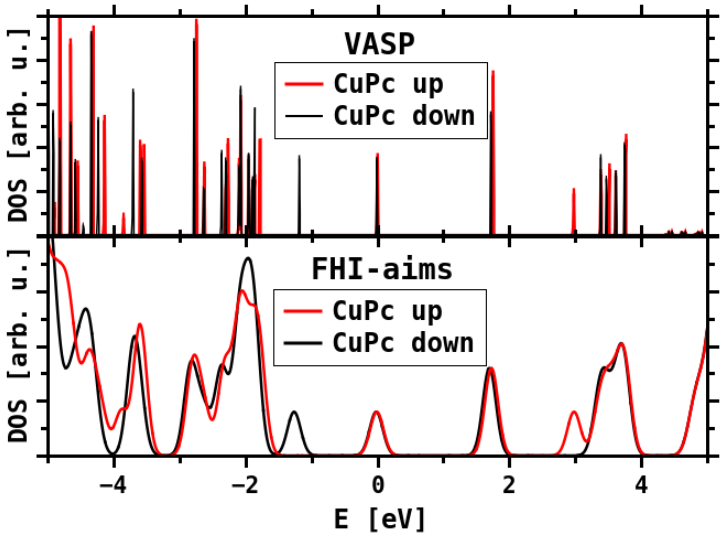

Figure 44: Comparison of DOSs of one free-standing monolayer of CuPc in VASP and FHI-aims. The spin-up and spin-down values are shown in red and black, respectively.

5.5.2 CuPc and CoPc on Ag(100)

Studying the adsorption of CuPc and CoPc on the Ag(100) surface would have had the benefits of (i) the same symmetry of surface and molecule and (ii) being directly comparable to most experimental results. In addition, a smaller surface unit cell could have been applied. In the VASP calculations performed previously it had been shown that also on the Ag(100) surface different magnetic solutions for CuPc and CoPc adsorption could be found, although not all solutions could be converged. Therefore, FHI-aims tests were performed with CuPc adsorbed on Ag(100) in a 5x5 surface unit cell.
Unfortunately, calculations at this surface turned out to be extremely tedious due to SCF convergence problems. It was found that while for CuPc both the spin-0 and spin-1 solution could be found after extensive testing including different initializations and settings (e.g. broadening method and broadening width), calculations showing trends toward the spin-2 solution could never be converged. To exclude that the convergence issues arise from a too close packing of the molecules, the unit cell was enlarged to a 7x7 surface unit cell. Still, convergence remained to be tedious and could not be achieved for the spin-2 solution.

In summary, the observed trend on the Ag(100) surface was that three different magnetic solutions similar to the ones appearing on Ag(111) exist. However, due to the problematic convergence of Ag(100) calculations, only calculations on the Ag(111) surface were pursued.

5.5.3 Geometry Relaxations

It has been discussed in the previous section on charge transfer (Section 4) that hybrid calculations on top of PBE geometries might lead to artifacts in the electronic structure of a system. In case of the systems discussed here, performing full geometry optimizations with hybrid functionals is quite problematic due to the large system size and the corresponding huge computational effort. However, to make sure that the obtained results are not falsified by the applied PBE geometries, several geometry optimization steps were performed for both systems and all magnetic solutions.
Note that the obtained geometries are not fully converged, and functionals with different amounts of Hartree-Fock exchange were used for these first geometry optimization tests. This is the case as in some of the geometry optimizations, the magnetic moment of the system could not be preserved from one geometry steps to the next, i.e. the system could not be easily converged toward one specific magnetic solution. However, this appears to be an initialization problem which should be solvable by further tests, including varying starting geometries and different initializations of the magnetic moments of the molecular atoms.
For CuPc, the spin-2 solution could, so far, not be optimized with the HSE06 functional, but only with a higher amount of Hartree-Fock exchange, namely $\alpha = 0.35$, where this solution is more stable. The spin-0 and spin-1 solutions were optimized with HSE06. For CoPc, both solutions were optimized with the HSE $\alpha = 0.30$ functional, which was also applied in the calculations presented previously and which was the only one that gave a stable open-shell spin-0.1 solution. The closed-shell solution could also be optimized with the HSE06 functional.
In all cases, between 5 and 10 geometry optimization steps were performed to find out whether the DOS exhibits significant changes upon these optimizations. In previously performed geometry optimizations of TFBQ on Cu and Cu_2O, which were presented in section 4, it was found that large changes in the DOS tend to appear already after the first few geometry optimization steps. Therefore, it is to be expected that already these tentative optimizations performed here give a good estimation of how strongly the geometry influences the electronic structure of the investigated systems. However, it should be noted that full geometry optimizations still need to be performed to receive a full picture of the investigated systems, as alterations in the electronic structure due to the use of a GGA geometry in a hybrid calculation could appear as a consequence of changes in bond lengths, which are described differently within different functionals.[53, 181, 208, 209]
The comparison of the DOS obtained applying the PBE geometry and after several

geometry optimizations steps are depicted in Fig. 45 for CuPc on Ag(111) and in Fig. 46 for CoPc on Ag(111). The applied functionals and maximum remaining forces are given for every hybrid-optimized system. While the geometry convergence is already quite good for the spin-0 and spin-1 solutions of CuPc and both solutions of CoPc (below 0.07 eV/Å; full convergence is usually considered to be reached for a maximum remaining force below 0.01 eV/Å), the remaining forces are still quite high for CuPc in the spin-2 solution. However, the trend that can be deduced from these preliminary optimizations is that while small peak shifts and changes in peak heights appear, no qualitative change in the DOS can be observed and the results obtained using PBE geometries appear to be qualitatively correct.

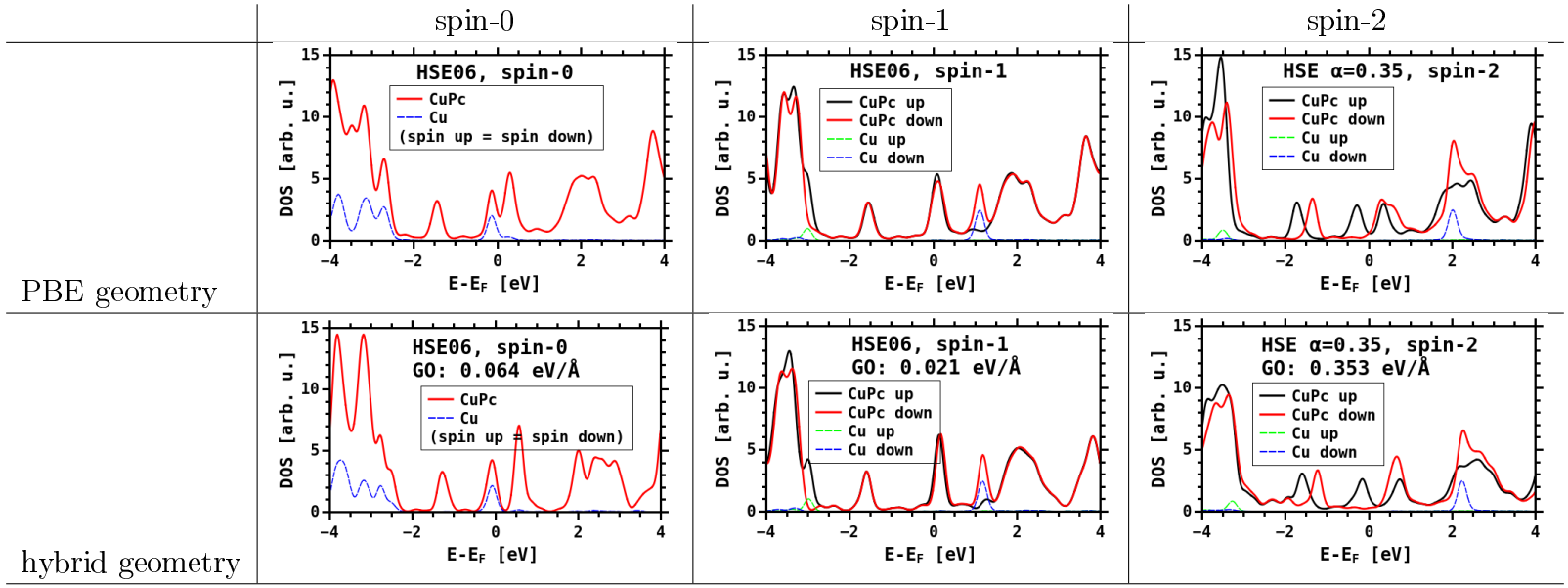

Figure 45: DOS projected on the CuPc molecule on Ag(111) in the PBE geometries (top) and after several geometry optimization steps with the corresponding hybrid functional (bottom). The applied functionals and the maximal remaining forces are indicated directly in the graphs. Spin up and spin down DOSs are shown in black and red, respectively. Additionally, the DOS projected on the Cu atom is shown in blue (spin up) and green (spin down). The energy is aligned to the Fermi energy.

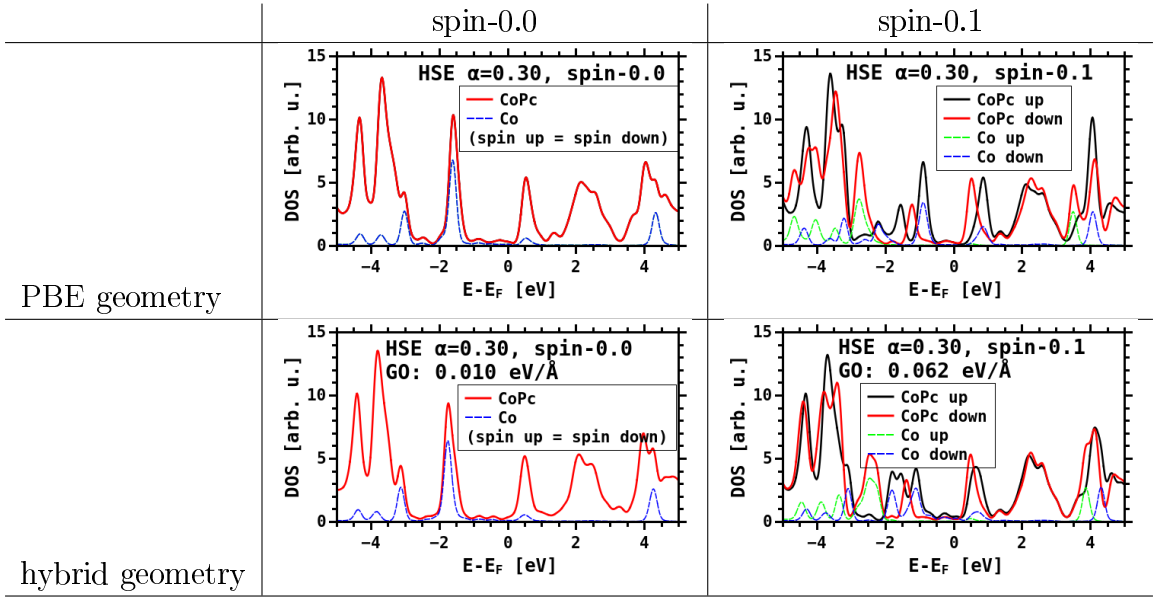

Figure 46: DOS projected on the CoPc molecule on Ag(111) in the PBE geometries (top) and after several geometry optimization steps with the HSE $\alpha = 0.30$ functional (bottom). The maximal remaining forces are indicated directly in the graphs. Spin up and spin down DOSs are shown in black and red, respectively. Additionally, the DOS projected on the Cu atom is shown in green (spin up) and blue (spin down). The energy is aligned to the Fermi energy.

5.6 Conclusion and Outlook on Magnetic Properties of CuPc and CoPc on Ag(111)

Upon adsorption on Ag(111), both CuPc and CoPc receive about one electron from the substrate. The localization of this transferred charge leads to different magnetic solutions of the adsorbed molecules. While CuPc on Ag(111) exhibits three different magnetic solutions, for CoPc on Ag(111), two magnetic solutions were found. After extensive testing with different initializations, it appears likely that only these solutions are stable on the surface.
For both molecules, a "trivial" spin = 0 solution was found. Also, for both molecules a solution appeared, where charge is transferred to the ligands, while the metal spin remains untouched. While this open-shell scenario results in a triplet configuration for CuPc, as the spins align anti-parallel, it results in an singlet configuration for CoPc, where the spins align parallel. For CuPc, an additional solution was found, where only the spin of the central metal atom is preserved, but the charge transfer toward the ligands does not result in additional spin polarization.

Different Behavior of CuPc and CoPc upon Adsorption
The different magnetic properties of the two regarded TMPc molecules upon adsorption were investigated, and it was shown to originate from differences in the d states of the employed central metal atom, which is in accordance with literature findings.[171, 175, 177, 192] Comparing the charge rearrangements which occur upon adsorption for both molecules offers insights into the coupling between substrate and molecule. Such a comparison is shown in Fig. 47 for CuPc on Ag in the triplet spin-2 solution and for CoPc on Ag in the open-shell singlet spin-0.1 solution.
For CuPc, no strong feature protruding from the molecular backbone appears, only some charge accumulation below the Cu atom is visible. This is in contrast to CoPc, where strong charge accumulation above and below the central Co atom appears. This stronger coupling between Co and the Ag substrate indicates a charge transfer channel between the central metal atom and the substrate, which does not exist for CuPc on Ag(111).
In the context of molecule-substrate interaction, it is interesting to regard the molecular states which get occupied upon adsorption. In case of CuPc, the triplet spin-2 case appears to be the most relevant solution (see below), and is, therefore, considered here. In this scenario, the highest occupied state of the adsorbed molecule is a ligand state without contribution from the central Cu atom. Due to its symmetry, it can be assigned to the molecular e_g orbital. For CoPc, both obtained solutions exhibit a highest occupied state with a strong Co contribution that can be assigned to the molecular a_{1g} orbital.
In the spin-2 solution for CuPc and the spin-0.1 solutions for CoPc, both molecules exhibit a ligand and a metal spin.The intermolecular alignment of the two spins is different, namely parallel for CuPc, and anti-parallel for CoPc. This difference between

CuPc and CoPc can be interpreted in terms of different crystal-field splittings of the central atoms. The stronger splitting of the Co atom favors a low-spin state, while the splitting is lower for Cu and favors a hight-spin state.[174, 176]

Prediction of a Magnetic Solution from Simulation

Obtaining a conclusive answer which magnetic solution is most stable is, unfortunately, very difficult based on simulation alone. This is due to the shortcomings of DFT, where the use of semi-local functionals neglects relevant correlation effects, while hybrid functionals offer free tuning parameters, which can strongly influence the results. Especially for the systems investigated here, the self-interaction error is very problematic, as strongly localized and delocalized states lie close in energy. Due to their different localization, they are shifted differently by the self-interaction error.[9, 93] This is more problematic for CoPc than for CuPc, as the strongly localized metal-centered state is the one hybridizing with the substrate and receiving charge upon adsorption. In addition, CoPc appears to exhibit strong orbital reordering upon adsorption, which is also discussed in literature.[177]

As argued in section 4, the choice of the amount of Hartree-Fock exchange is not a straightforward task for charge transfer systems. Also, the approach applied for TFBQ on Cu_2O, where a system-specific value α is obtained by a series of hybrid calculations, is unfeasible for these large phthalocyanine systems because of its computational cost.[6] Due to these complications, for the description of the magnetic properties of TMPcs on metals, DFT has to be applied with great caution. One needs to be aware that several different solutions might exist, and that the received results depends strongly on the applied functional, magnetic initialization and computational settings. Additionally, the most easily received solutions have, for these systems, been shown to not necessarily be the most energetically favorable ones. And finally, when comparing the energies of different solutions one has to keep in mind that which solution is energetically favorable might strongly depend on the amount of Hartree-Fock exchange.

Relevance of Different Magnetic Solutions

As the above discussed complications do not allow to predict a magnetic solutions from simulations alone, comparison to experimental results is necessary, and an extensive discussion of literature reports of the investigated systems was done.

For CuPc on Ag(111), it can be concluded that the triplet spin-2 solution is the most likely scenario. It exhibits several features, including the enhanced total magnetic moment and the peak-splitting around the Fermi edge, that compare very well to experimental results.[165] In simulations, it is the energetically favorable solution already for low values of Hartree-Fock exchange α, and gets stabilized upon increasing this value.

For CoPc on Ag(111), on the other hand, the outcome is, unfortunately, not so clear. The DFT results do not allow a final answer on which solution is more likely for the above given reasons, and also the comparison to experimental results does not allow a

clear answer, as contrary results exist. However, by comparing the work by Salomon et al.,[177] which is the most extensive study on a comparable system that the author is aware of, the closed-shell spin-0.0 solution appears to be the more stable one.

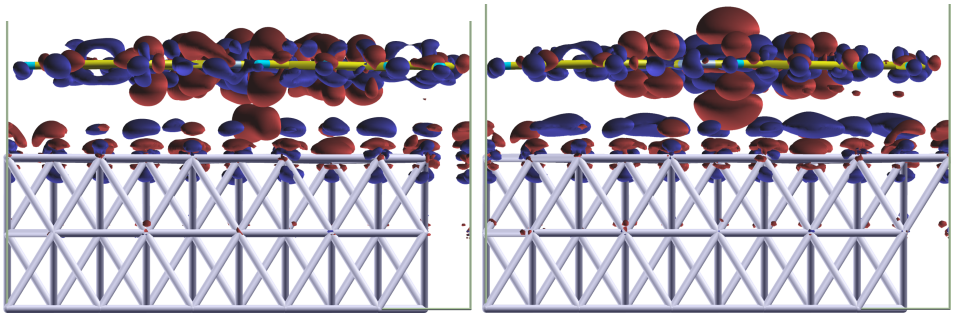

(a) CuPc spin-2 (b) CuPc spin-01

Figure 47: Comparison of charge rearrangements upon adsorption for CuPc and CoPc on Ag(111), with red regions indicating charge accumulation, while blue regions indicate charge depletion. For CuPc adsorption, the triplet spin-2 solution is shown, while for CoPc adsorption, the open-shell singlet spin-0.1 solution is shown. The isovalue was set to 0.006 eV/Å^3.

Outlook

To improve the reliability of the obtained results, the next step would be to perform full geometry optimizations of the investigated systems. Also, a detailed analysis of the relevant orbitals on the surface, and a comparison of those to the gas phase molecular orbitals will lead to a deeper understanding of the electronic structures, especially for the CoPc/Ag(111) system.

6 Summary

The starting point for the computational description of inorganic/organic interfaces is the determination of the system geometry. Therefore, being able to perform reliable geometry optimizations is of major importance for the simulation of such interfaces, which is the topic of section 3 of this work.
At first, the GADGET geometry optimization tool is discussed. In the course of this thesis, several new implementations were included, which should allow for better simulations of molecule adsorption on surfaces, especially for upright standing molecules and nonplanar molecular geometries. Easier and more direct coordinate definition was implemented, which allows to chose the applied coordinates in a suitable way for a specific system. The use of cartesian coordinates for the description of crystalline substrates has proven to speed up simulations for several test systems, where the substrate is not deformed strongly upon adsorption. Not all implemented functionalities seem to lead to great benefits, namely the use of vdW-derived long-range coordinates, which did not speed up optimizations as hoped. However, the new functionalities and also a better understanding of geometry optimizations in DFT were of great benefit for the simulation of interface systems with non-trivial geometry, such as the nonplanar phthalocyanines.
For a proper optimization of the different configurations of the GaClPc molecule on Cu(111), the use of GADGET turned out to be crucial. The adsorption behavior of this system was investigated with dispersion-corrected DFT, trying to reach full comparability of simulated and experimental XSW and UPS results.
The interpretation of adsorption heights from XSW carries some degree of ambiguity, due to the heights being given modulo the interlayer distance of the underlying substrate.[210, 211] Therefore, the application of simulations was necessary to reach a comprehensive understanding of the molecular adsorption on Cu(111).
Originally, the GaClPc molecule was simulated in two different configurations, Cl-up and Cl-down. However, they both did not reproduce the experimental XSW adsorption heights. This revealed that the adsorption process must be more complicated than initially assumed. Therefore, a third configuration, with the Cl atom detached from the rest of the molecule (adsorbing isolated from it on the Cu substrate), was considered. For this configuration, good agreement between simulation and experiment on the adsorption heights was obtained for all atomic species. Furthermore, the Cl-diss scenario exhibits the lowest adsorption energy of the three investigated scenarios.
Another curious effect of the GaClPc/Cu(111) system is that its work function modification $\Delta\Phi$ turned out to be very similar for the Cl-down and Cl-diss scenarios, despite their different molecular dipoles. This is due to the fact that the molecular dipoles are compensated by the bond dipole arising upon molecular adsorption. This effect appears in systems which exhibit Fermi-level pinning of the molecular LUMO, where the interface work function becomes independent of the work function of the underlying substrate.[11, 14, 212, 213, 214] For the Cl-up configuration, the molecular dipole

is not compensated as it lies above the molecular pinning levels. The contributions to the work function modification from the molecular dipole and the bond dipole arising upon adsorption for the different configurations is depicted in Fig. 48.
The comparison of the different work function modifications to experimental data showed that GaClPc adsorption primarily happens in the Cl-up configuration and that Cl dissociation is caused by annealing.
The GaClPc/Cu(111) system serves as an excellent example for the complications that

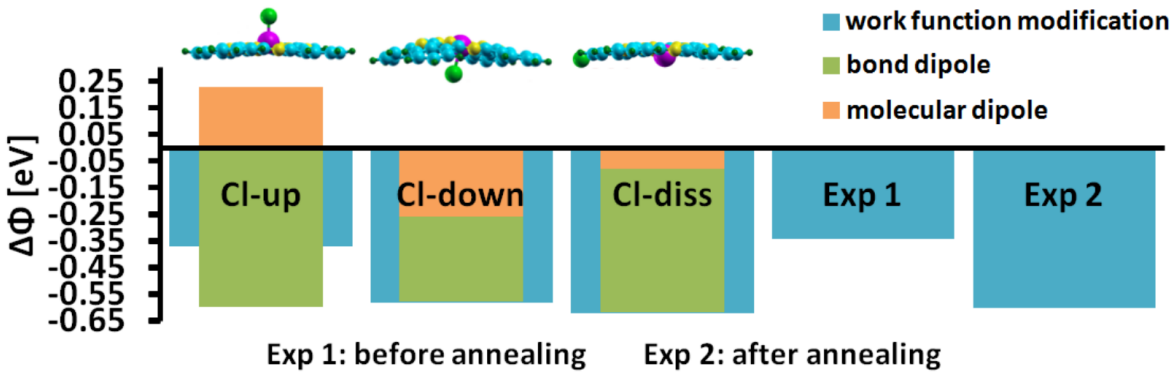

Figure 48: Contributions to the total work function modifications $\Delta\Phi$ of GaClPc adsorbed on Cu in different configuration. The experimental values before and after annealing are given for reference.

can arise when comparing experimental and simulated results of interface systems. It also demonstrates the huge benefits of reliable vdW correction methods in DFT, which allow full geometry optimizations of such interfaces. Only by reviewing several different scenarios and taking into account experimental and simulated data on both geometry and electronic structure, it was possible to finally achieve a comprehensive picture of the adsorption process of GaClPc on Cu(111).
A related system is chlorinated SnPc, where the final adsorption configuration of the molecule was also not a priori clear. In a similar manner as for GaClPc, the interpretation of the experimental data required quantum-mechanical simulations.
Several different adsorption scenarios, including $SnCl_2Pc$, SnPc and SnClPc in Cl-up and Cl-down configuration, were investigated. By comparing the simulation results to experimental structures from STM and adsorption heights from XSW, the configuration proposed based on experiments could be verified. It was concluded that the SnClPc molecule adsorbs in a Cl-down configuration, with the Cl atom penetrating the Ag substrate.
Different vacancy configurations were tested and while the exact configuration could not be determined (as several configurations gave quite similar results), it became clear that at least three surface Ag atoms have to be removed to obtain adsorption heights close to the experimentally observed ones. An energy estimation for binding energies confirmed that such vacancy formation upon adsorption is also energetically reasonable.

While both above discussed phthalocyanine molecules exhibit different adsorption configurations due to their nonplanar geometries, also for planar, flat lying molecules, different adsorption scenarios can appear, depending on their bonding to the substrate. For P2O on Ag(111), the goal was to investigate the appearance of two different situations, namely strongly bonded chemisorption and weakly bonded physisorption. While the molecule was experimentally found to exhibit physisorption, simulation results indicate chemisorption. As the agreement with experiments for similar systems is typically very good, it appeared likely that the system is close to a transition point between those two scenarios, and a little change should suffice to switch from on to the other. Several different approaches to change the interaction between substrate and molecule were tested, including alloying to change the substrate work function, and changes in the substrate lattice constant to modify the chemical interaction of the molecular O atoms to the Ag surface. However, none of these tested handles caused a change in the adsorption scenario, and the hypothesis of the system being close to a transition point had to be discarded. The most likely reason for the disagreement between simulation and experiment appeared to be a restructuring of the surface, e.g., the formation of adatoms, which bind to the adsorbed molecules.
For the description of geometric properties of organic molecules adsorbed on inorganic surfaces, it is clearly beneficial to combine experimental and computational results. Especially for non-trivial geometries like the nonplanar phthalocyanines, the number of possible adsorption configurations can easily become too large for a clear interpretation just from one approach. The above examples demonstrate, how these two approaches can ideally complement each other to reach a throughout understanding of the inorganic/organic interfaces in question.
In addition, the discussed systems highlight the interplay of geometric and electronic properties, e.g. for the GaClPc/Cu(111) system, where the molecular dipole can be compensated, depending on its relative position. Only after the adsorption geometry is known, a reliable description of the electronic properties of a system is possible.

One of the main factors characterizing the electronic structure of the discussed interfaces is charge transfer between substrate and molecule.
For the survey of the charge transfer properties at interfaces, also the choice of the DFT functional is of major importance. This is discussed in section 4. As an exemplary system, tetrafluoro-benzoquinone (TFBQ) on metallic (Cu) and semiconducting (Cu_2O) substrates was investigated. For such systems, the occurrence of two different charge transfer mechanisms, fractional charge transfer FCT and integer charge transfer ICT, is typical.[11] A major part of this study was to discuss why and how the charge transfer mechanism is influenced by the applied DFT functional. Subsequently, the systems were simulated with different functionals, and the interplay of physical properties and functional was evaluated.
It was shown that the substantial influence of the DFT methodology on the charge transfer mechanisms stems from the influence the choice of DFT functional has on

the charge localization. In the case of FCT, a hybrid state spreading over the substrate (mostly pristine metals [20, 26, 27]) as well as the adsorbed molecular layer is formed.[11] The transferred charge is delocalized over the whole adsorbate layer, with all molecules becoming fractionally charged. In case of ICT, substrate and adsorbate are decoupled and share no charges. Then, charge transfer can only appears in integer numbers, and the transfered charge is localized on individual molecules.[11, 28]
The influence of the DFT functional arises from the fact that charge is localized differently with different functionals. While standard semi-local functionals tend to over-delocalize charge,[3, 7, 54, 63, 87, 149] hybrid functionals minder this effect, but, in case of high amounts of Hartree-Fock exchange α, the opposite problem of charge over-localization can appear.[90, 215] Therefore, different functionals can (incorrectly) favor specific charge transfer mechanisms.
For the investigated systems, hybrid functionals were applied, with the parameter α tuned such that a self-interaction free situation without spurious over-localization or over-delocalization of charges was reached.[46, 65, 216, 217]
The corresponding value α^* was evaluated for the gas phase molecule, as well as adsorbed on the Cu_2O substrate. It was found that α^* is significantly decreased upon surface adsorption on Cu_2O, depending strongly on the surface screening and, hence, the polarizability of the substrate material. However, it was also shown that while on the semiconductor, both the amount of transfered charge and also the charge transfer mechanism were influenced by α, on the metallic Cu substrate, only the amount, but not the mechanism, was altered. The charge transfer mechanism can be clearly seen in the molecular DOS, as ICT systems exhibit spin splitting. This is depicted in Fig. 49, which shows the DOSs of the TFBQ/Cu_2O and the TFBQ/Cu systems evaluated with different functionals. While for TFBQ/Cu_2O a sufficiently high amount of α leads to ICT, the TFBQ/Cu system always exhibits FCT.
Different methods to evaluate α^* were applied, including enforcement of the straight-line condition,[46, 90] and also comparing the energies of FCT and ICT solutions. It was shown that for a given system and a given value of α, these different solutions can be obtained by applying different initializations of the molecules in the DFT calculation. The numerical reasons for the appearance of both charge transfer scenarios at the same value of α were discussed, based on charge localization within the system. This led to a comprehensive understanding of the numerical description and the influence of the functional on the charge transfer mechanisms in DFT. It also demonstrated that the use of the system-specific α^* is not the ideal choice to describe a given system, as with this setting, all possible charge distributions exhibit the same energy. Consequential, it was concluded that DFT is, unfortunately, not predictive concerning the charge transfer mechanism in many cases. Anyhow, it was possible to suggest different approaches how DFT can be used to gain insights into charge transfer at surfaces even in such problematic cases.
As these investigations required full geometry optimizations for every system and every applied functional, also their significance could be demonstrated. It was shown that the frequently applied approach of using geometries derived with semi-local functionals for

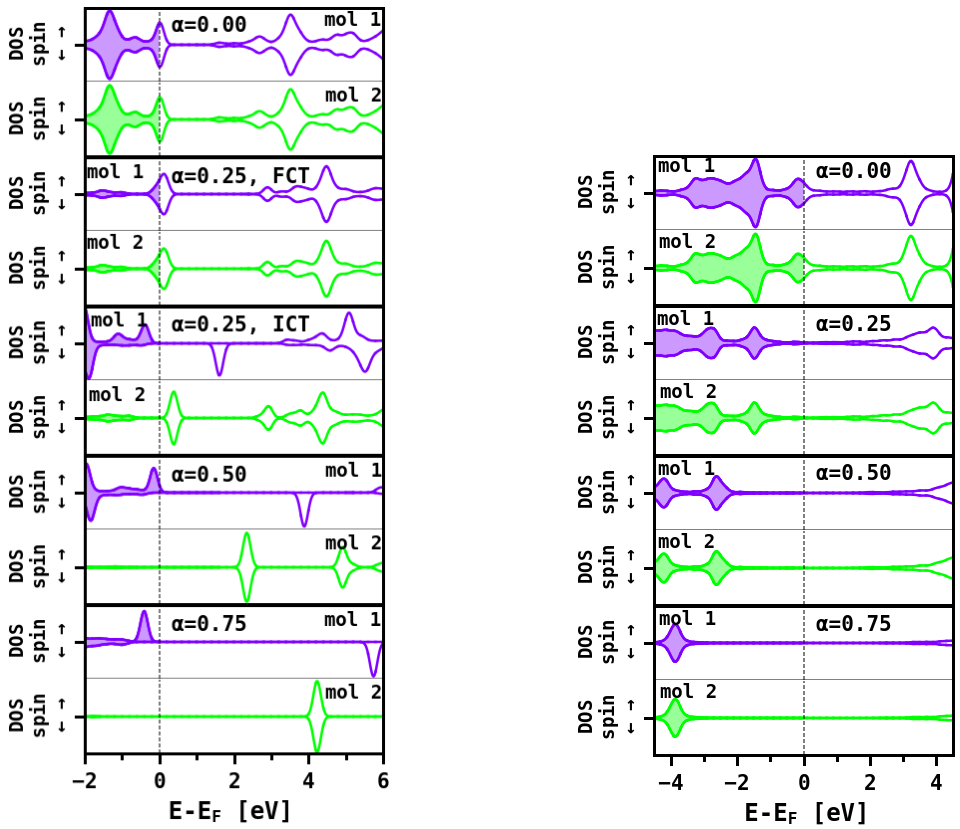

(a) TFBQ on Cu_2O (b) TFBQ on Cu

Figure 49: For systems of TFBQ/Cu_2O and TFBQ/Cu containing two molecules in the unit cell, the DOSs projected on both molecules are shown (in purple and green), as presented in Ref. [6]. Different amounts of Hartree-Fock exchange α were applied. The spin-up and spin-down DOSs are given in arbitrary unit and are drawn in the positive and negative directions, respectively. For TFBQ/Cu_2O and α=0.25, both FCT and ICT solutions are shown.

hybrid single-point calculations can completely falsify the derived electronic structures of charge-transfer systems.

This in-depth analysis of how simulated charge transfer mechanism are influenced by the choice of the functional highlights the interplay of the physical properties of a system and the DFT methodology. The obtained results put the common practice of applying standard DFT functionals with a fixed value of α for all different sorts of systems into question.

In addition, preliminary work on charge transfer tuning via the substrate material was done. A gradual change between the two substrates Cu and Cu_2O should enable monitoring the transition between FCT and ICT from a different perspective. While it is not clear yet, whether the applied system is ideal to investigate this property, it

appears to be a promising approach to reach a deeper understanding of FCT and ICT processes at interfaces depending on the nature of the substrate.

The localization of the charge transferred to adsorbed molecules is not only crucial for the observed charge transfer mechanism, but can also influence the magnetic properties of the interface. This was discussed for the example of two different transition metal phthalocyanines, namely CuPc and CoPc, adsorbed on Ag(111). Upon adsorption, they exhibit changes in their magnetic moments as a consequence of charge transfer from the substrate. An extensive study on how such magnetic effects are described in DFT is presented in section 5.
For both considered systems, various magnetic states of the surface-adsorbed molecules were found. Similar to the previous study on charge transfer, an influence of the choice of DFT functionals on the outcome was observed.
The occurrence of the different solutions, their physical relevance and how they depend on the applied DFT functional was investigated in detail. In addition, it was discussed why the two systems exhibit different magnetic properties despite of their similarities. Both molecules exhibit a non-zero magnetic moment in the gas phase due to an unpaired spin at the central metal atom. They also both receive approximately one electron from the substrate upon adsorption. In case of CuPc/Ag, three solutions could be obtained, with the gas phase spin getting either quenched, preserved, or enhanced. For CoPc/Ag, on the other hand, the magnetic moment of the molecule was always quenched upon adsorption, but two different electronic structures were observed. The appearance of these different magnetic solutions was found to depend on the applied DFT functional as well as on the magnetic initialization of the calculations.
At first, the electronic structures accompanying the different magnetic solutions were analyzed. For both systems, a solution without any molecular magnetic moment was found, where the unpaired spin of the central metal atom was compensated by charge transfer directly to the this atom. Also for both molecules, another solution with charge transfer to the ligands of the molecule was obtained, which resulted in an additional ligand spin. While for CuPc/Ag, the ligand charging led to a triplet solution, with the ligand spin aligning parallel to the metal spin, for CoPc/Ag, the ligand spin aligned anti-parallel, resulting in an open-shell singlet solution.
This raised the question which of the obtained solutions for each molecule is the most reasonable result that should also be expected to be found experimentally. As mentioned previously, the simulations were done with different functionals, namely semi-local PBE and hybrid HSE with different amounts of Hartree-Fock exchange α. Not all solutions could be obtained with all applied functionals. While the closed shell solution (with charge transfer to the central metal atom) could be found with all functionals in both bases, the open shell solutions (with charge transfer to the molecular ligands) were only obtained with hybrids. This could be assigned to correlation effects, namely on-site repulsion,[164, 165, 191, 192] which are not accounted for in semi-local functionals like PBE. And not only the appearance of the different magnetic solutions

was found to be functional-dependent, but also their relative energies. Therefore, it was not possible to predict an energetically favorable solution from simulation alone, which is a similar situation as for the previously discussed charge transfer studies. By comparing the electronic structure and the spin distribution of the different magnetic solutions to experimental data, the open-shell high-spin solution for CuPc/Ag and the closed shell solution for CoPc/Ag could be validated.
This allowed an interpretation of their electronic properties and a further comparison to experimental results, focusing on the differences of the two investigated systems, which result in the occurrence of different magnetic solutions. The appearance of a high-spin state for CuPc/Ag, but not for CoPc, can be assigned to different crystal field splittings of the central metal atoms.[174, 176] Also the coupling between substrate and molecules is different for the two systems. The charge rearrangements upon adsorption revealed that the molecular Co atom couples to the Ag substrate, while the molecular Cu does not, and charge transfer in the latter case presumably mainly appear through the molecular ligands.
This study demonstrated how magnetic properties of surface-adsorbed molecules can be investigated with DFT. However, great caution in the interpretation of the results must be applied, as different stable solutions might appear, and various initializations should, therefore, be tested. Although the functional dependence of the results prevented the prediction of a specific magnetic solution in the present case, the DFT results allowed to study the electronic properties of the systems in detail. Thereby, insights into the physical effects causing the appearance of molecular magnetic moments upon adsorption could be provided.

In summary, this thesis discusses DFT simulations of several challenging examples of inorganic/organic interfaces. It was shown that the choice of DFT functional as well as an adequate initialization of calculations can be of huge importance, as these factors often affect the obtained results, concerning both geometric and electronic properties. The influence of DFT methodology on the description of charge transfer and magnetic effects was analyzed in detail. These studies demonstrated that the predictive power of DFT is limited for observables which are functional dependent, and that the choice of functional and also the interpretation of certain results has to be handled with great care. In several cases, no unambiguous final solution could be obtained from simulation and made a comparison to experimental data necessary. Nonetheless, it was demonstrated that also for such problematic examples, DFT results provide valuable insights, as they allow to fully interpret experimental results and provide atomistic insights into the electronic and geometric structures of the considered interfaces.

Bibliography

[1] Frank Jensen. *Introduction to Computational Chemistry*. John Wiley & Sons Ltd., 3rd edition, February 2017.

[2] Claudia Draxl, Dmitrii Nabok, and Karsten Hannewald. Organic/Inorganic Hybrid Materials: Challenges for ab Initio Methodology. *Accounts of Chemical Research*, 47(11):3225–3232, November 2014.

[3] Aron J. Cohen, Paula Mori-Sánchez, and Weitao Yang. Insights into Current Limitations of Density Functional Theory. *Science*, 321(5890):792–794, August 2008.

[4] Tomáš Bučko, Jürgen Hafner, and János G. Ángyán. Geometry optimization of periodic systems using internal coordinates. *The Journal of Chemical Physics*, 122(12):124508, March 2005.

[5] Claudia Ambrosch-Draxl, Dmitrii Nabok, Peter Puschnig, and Christian Meisenbichler. The role of polymorphism in organic thin films: oligoacenes investigated from first principles. *New Journal of Physics*, 11(12):125010, 2009.

[6] Elisabeth Wruss, Egbert Zojer, and Oliver T. Hofmann. Distinguishing between Charge-Transfer Mechanisms at Organic/Inorganic Interfaces Employing Hybrid Functionals. *The Journal of Physical Chemistry C*, 122(26):14640–14653, July 2018.

[7] Aron J. Cohen, Paula Mori-Sánchez, and Weitao Yang. Challenges for Density Functional Theory. *Chemical Reviews*, 112(1):289–320, January 2012.

[8] Navit Dori, Mahesh Menon, Lennart Kilian, Moritz Sokolowski, Leeor Kronik, and Eberhard Umbach. Valence electronic structure of gas-phase 3,4,9,10-perylene tetracarboxylic acid dianhydride: Experiment and theory. *Physical Review B*, 73(19):195208, May 2006.

[9] Noa Marom, Oded Hod, Gustavo E. Scuseria, and Leeor Kronik. Electronic structure of copper phthalocyanine: A comparative density functional theory study. *The Journal of Chemical Physics*, 128(16):164107, April 2008.

[10] Hisao Ishii, Kiyoshi Sugiyama, Eisuke Ito, and Kazuhiko Seki. Energy Level Alignment and Interfacial Electronic Structures at Organic/Metal and Organic/Organic Interfaces. *Advanced Materials*, 11(8):605–625, June 1999.

[11] Slawomir Braun, William R. Salaneck, and Mats Fahlman. Energy-Level Alignment at Organic/Metal and Organic/Organic Interfaces. *Advanced Materials*, 21(14-15):1450–1472, April 2009.

[12] V. De Renzi, R. Rousseau, D. Marchetto, R. Biagi, S. Scandolo, and U. del Pennino. Metal Work-Function Changes Induced by Organic Adsorbates: A Combined Experimental and Theoretical Study. *Physical Review Letters*, 95(4):046804, July 2005.

[13] Slawomir Braun, Michel P. de Jong, Wojciech Osikowicz, and William R. Salaneck. Influence of the electrode work function on the energy level alignment at organic-organic interfaces. *Applied Physics Letters*, 91(20):202108, November 2007.

[14] Oliver T. Hofmann, David A. Egger, and Egbert Zojer. Work-Function Modification beyond Pinning: When Do Molecular Dipoles Count? *Nano Letters*, 10(11):4369–4374, November 2010.

[15] A. Gerlach, T. Hosokai, S. Duhm, S. Kera, O. T. Hofmann, E. Zojer, J. Zegenhagen, and F. Schreiber. Orientational Ordering of Nonplanar Phthalocyanines on Cu(111): Strength and Orientation of the Electric Dipole Moment. *Physical Review Letters*, 106(15):156102, April 2011.

[16] Elisabeth Wruss, Oliver T. Hofmann, David A. Egger, Elisabeth Verwšter, Alexander Gerlach, Frank Schreiber, and Egbert Zojer. Adsorption Behavior of Nonplanar Phthalocyanines: Competition of Different Adsorption Conformations. *The Journal of Physical Chemistry C*, 120(12):6869–6875, March 2016.

[17] Oliver T. Hofmann, Jan-Christoph Deinert, Yong Xu, Patrick Rinke, Julia Stähler, Martin Wolf, and Matthias Scheffler. Large work function reduction by adsorption of a molecule with a negative electron affinity: Pyridine on ZnO($10\bar{1}0$). *The Journal of Chemical Physics*, 139(17):174701, November 2013.

[18] Hans Lüth. *Solid Surfaces, Interfaces and Thin Films*. Springer International Publishing, 6 edition, 2015.

[19] J. P. Muscat and D. M. Newns. Chemisorption on metals. *Progress in Surface Science*, 9(1):1–43, January 1978.

[20] Lorenz Romaner, Georg Heimel, Jean-Luc Brédas, Alexander Gerlach, Frank Schreiber, Robert L. Johnson, Jörg Zegenhagen, Steffen Duhm, Norbert Koch, and Egbert Zojer. Impact of Bidirectional Charge Transfer and Molecular Distortions on the Electronic Structure of a Metal-Organic Interface. *Physical Review Letters*, 99(25):256801, December 2007.

[21] Georg Heimel, Ferdinand Rissner, and Egbert Zojer. Modeling the Electronic Properties of π-Conjugated Self-Assembled Monolayers. *Advanced Materials*, 22(23):2494–2513, April 2010.

[22] Shashank S. Harivyasi, Oliver T. Hofmann, Nahid Ilyas, Oliver L. A. Monti, and Egbert Zojer. van der Waals Interaction Activated Strong Electronic Coupling at the Interface between Chloro Boron-Subphthalocyanine and Cu(111). *The Journal of Physical Chemistry C*, 122(26):14621–14630, July 2018.

[23] Elisabeth Wruss. Master Thesis: Influence of van der Waals interactions on the adsorption of flat-lying organic molecules on metallic surfaces, April 2014.

[24] David A. Egger, Victor G. Ruiz, Wissam A. Saidi, Tomáš Bučko, Alexandre Tkatchenko, and Egbert Zojer. Understanding Structure and Bonding of Multilayered Metal-Organic Nanostructures. *The Journal of Physical Chemistry C*, 117(6):3055–3061, February 2013.

[25] Yu Li Huang, Elisabeth Wruss, David A. Egger, Satoshi Kera, Nobuo Ueno, Wissam A. Saidi, Tomáš Bučko, Andrew T. S. Wee, and Egbert Zojer. Understanding the Adsorption of CuPc and ZnPc on Noble Metal Surfaces by Combining Quantum-Mechanical Modelling and Photoelectron Spectroscopy. *Molecules*, 19(3):2969–2992, March 2014.

[26] S. Duhm, A. Gerlach, I. Salzmann, B. Bröker, R. L. Johnson, F. Schreiber, and N. Koch. PTCDA on Au(111), Ag(111) and Cu(111): Correlation of interface charge transfer to bonding distance. *Organic Electronics*, 9(1):111–118, February 2008.

[27] Ingo Kröger, Benjamin Stadtmüller, Christoph Stadler, Johannes Ziroff, Mario Kochler, Andreas Stahl, Florian Pollinger, Tien-Lin Lee, Jörg Zegenhagen, Friedrich Reinert, and Christian Kumpf. Submonolayer growth of copper-phthalocyanine on Ag(111). *New Journal of Physics*, 12(8):083038, 2010.

[28] Oliver T. Hofmann, Patrick Rinke, Matthias Scheffler, and Georg Heimel. Integer versus Fractional Charge Transfer at Metal(/Insulator)/Organic Interfaces: Cu(/NaCl)/TCNE. *ACS Nano*, 9(5):5391–5404, May 2015.

[29] Menno Bokdam, Deniz Cakir, and Geert Brocks. Fermi level pinning by integer charge transfer at electrode-organic semiconductor interfaces. *Applied Physics Letters*, 98(11):113303, March 2011.

[30] Deniz Cakir, Menno Bokdam, Michel P. de Jong, Mats Fahlman, and Geert Brocks. Modeling charge transfer at organic donor-acceptor semiconductor interfaces. *Applied Physics Letters*, 100(20):203302, May 2012.

[31] P. Amsalem, J. Niederhausen, A. Wilke, G. Heimel, R. Schlesinger, S. Winkler, A. Vollmer, J. P. Rabe, and N. Koch. Role of charge transfer, dipole-dipole interactions, and electrostatics in Fermi-level pinning at a molecular heterojunction on a metal surface. *Physical Review B*, 87(3):035440, January 2013.

[32] Michael Hollerer, Daniel Lüftner, Philipp Hurdax, Thomas Ules, Serguei Soubatch, Frank Stefan Tautz, Georg Koller, Peter Puschnig, Martin Sterrer, and Michael G. Ramsey. Charge Transfer and Orbital Level Alignment at Inorganic/Organic Interfaces: The Role of Dielectric Interlayers. *ACS Nano*, 11(6):6252–6260, June 2017.

[33] Linda Lindell, Mikael Unge, Wojciech Osikowicz, Sven Stafström, William R. Salaneck, Xavier Crispin, and Michel P. de Jong. Integer charge transfer at the tetrakis(dimethylamino)ethylene/Au interface. *Applied Physics Letters*, 92(16):163302, April 2008.

[34] Marco Gruenewald, Laura K. Schirra, Paul Winget, Michael Kozlik, Paul F. Ndione, Ajaya K. Sigdel, Joseph J. Berry, Roman Forker, Jean-Luc Brédas, Torsten Fritz, and Oliver L. A. Monti. Integer Charge Transfer and Hybridization at an Organic Semiconductor/Conductive Oxide Interface, February 2015.

[35] P. Hohenberg and W. Kohn. Inhomogeneous Electron Gas. *Physical Review*, 136(3B):B864–B871, November 1964.

[36] Richard M. Martin. *Electronic Structure: Basic Theory and Practical Methods*. Cambridge University Press, Cambridge, UK, 2004.

[37] W. Kohn and L. J. Sham. Self-Consistent Equations Including Exchange and Correlation Effects. *Physical Review*, 140(4A):A1133–A1138, November 1965.

[38] Mel Levy, John P. Perdew, and Viraht Sahni. Exact differential equation for the density and ionization energy of a many-particle system. *Physical Review A*, 30(5):2745–2748, November 1984.

[39] John P. Perdew. Density functional theory and the band gap problem. *International Journal of Quantum Chemistry*, 28(S19):497–523, March 1985.

[40] John P. Perdew and Karla Schmidt. Jacob's ladder of density functional approximations for the exchange-correlation energy. *AIP Conference Proceedings*, 577(1):1–20, July 2001.

[41] John P. Perdew, Kieron Burke, and Matthias Ernzerhof. Generalized Gradient Approximation Made Simple. *Physical Review Letters*, 77(18):3865–3868, October 1996.

[42] John P. Perdew, Kieron Burke, and Matthias Ernzerhof. Generalized Gradient Approximation Made Simple [Phys. Rev. Lett. 77, 3865 (1996)]. *Physical Review Letters*, 78(7):1396–1396, February 1997.

[43] Jianmin Tao, John P. Perdew, Viktor N. Staroverov, and Gustavo E. Scuseria. Climbing the Density Functional Ladder: Nonempirical Meta–Generalized Gradient Approximation Designed for Molecules and Solids. *Physical Review Letters*, 91(14):146401, September 2003.

[44] John P. Perdew, Matthias Ernzerhof, and Kieron Burke. Rationale for mixing exact exchange with density functional approximations. *The Journal of Chemical Physics*, 105(22):9982–9985, December 1996.

[45] Jochen Heyd, Gustavo E. Scuseria, and Matthias Ernzerhof. Hybrid functionals based on a screened Coulomb potential. *The Journal of Chemical Physics*, 118(18):8207–8215, May 2003.

[46] Oliver T. Hofmann, Viktor Atalla, Nikolaj Moll, Patrick Rinke, and Matthias Scheffler. Interface dipoles of organic molecules on Ag(111) in hybrid density-functional theory. *New Journal of Physics*, 15(12):123028, 2013.

[47] Ester Livshits and Roi Baer. A well-tempered density functional theory of electrons in molecules. *Physical Chemistry Chemical Physics*, 9(23):2932–2941, June 2007.

[48] Tamar Stein, Helen Eisenberg, Leeor Kronik, and Roi Baer. Fundamental Gaps in Finite Systems from Eigenvalues of a Generalized Kohn-Sham Method. *Physical Review Letters*, 105(26):266802, December 2010.

[49] Sivan Refaely-Abramson, Roi Baer, and Leeor Kronik. Fundamental and excitation gaps in molecules of relevance for organic photovoltaics from an optimally tuned range-separated hybrid functional. *Physical Review B*, 84(7):075144, August 2011.

[50] Leeor Kronik, Tamar Stein, Sivan Refaely-Abramson, and Roi Baer. Excitation Gaps of Finite-Sized Systems from Optimally Tuned Range-Separated Hybrid Functionals. *Journal of Chemical Theory and Computation*, 8(5):1515–1531, May 2012.

[51] Andreas Karolewski, Leeor Kronik, and Stephan Kümmel. Using optimally tuned range separated hybrid functionals in ground-state calculations: Consequences and caveats. *The Journal of Chemical Physics*, 138(20):204115, May 2013.

[52] Jonathan D. Gledhill, Michael J. G. Peach, and David J. Tozer. Assessment of Tuning Methods for Enforcing Approximate Energy Linearity in Range-Separated Hybrid Functionals. *Journal of Chemical Theory and Computation*, 9(10):4414–4420, October 2013.

[53] Thomas Körzdörfer and Jean-Luc Brédas. Organic Electronic Materials: Recent Advances in the DFT Description of the Ground and Excited States Using Tuned Range-Separated Hybrid Functionals. *Accounts of Chemical Research*, 47(11):3284–3291, November 2014.

[54] Paula Mori-Sánchez, Aron J. Cohen, and Weitao Yang. Many-electron self-interaction error in approximate density functionals. *The Journal of Chemical Physics*, 125(20):201102, November 2006.

[55] Joachim Paier, Martijn Marsman, and Georg Kresse. Why does the B3lyp hybrid functional fail for metals? *The Journal of Chemical Physics*, 127(2):024103, July 2007.

[56] Matthias Ernzerhof and Gustavo E. Scuseria. Assessment of the Perdew-Burke-Ernzerhof exchange-correlation functional. *The Journal of Chemical Physics*, 110(11):5029–5036, March 1999.

[57] P. E. Blöchl. Projector augmented-wave method. *Physical Review B*, 50(24):17953–17979, December 1994.

[58] Volker Blum, Ralf Gehrke, Felix Hanke, Paula Havu, Ville Havu, Xinguo Ren, Karsten Reuter, and Matthias Scheffler. Ab initio molecular simulations with numeric atom-centered orbitals. *Computer Physics Communications*, 180(11):2175–2196, November 2009.

[59] G. Kresse and J. Furthmüller. Efficiency of ab-initio total energy calculations for metals and semiconductors using a plane-wave basis set. *Computational Materials Science*, 6(1):15–50, July 1996.

[60] G. Kresse and D. Joubert. From ultrasoft pseudopotentials to the projector augmented-wave method. *Physical Review B*, 59(3):1758–1775, January 1999.

[61] Manish Jain, James R. Chelikowsky, and Steven G. Louie. Reliability of Hybrid Functionals in Predicting Band Gaps. *Physical Review Letters*, 107(21):216806, November 2011.

[62] John P. Perdew, Robert G. Parr, Mel Levy, and Jose L. Balduz. Density-Functional Theory for Fractional Particle Number: Derivative Discontinuities of the Energy. *Physical Review Letters*, 49(23):1691–1694, December 1982.

[63] Stephan Kümmel and Leeor Kronik. Orbital-dependent density functionals: Theory and applications. *Reviews of Modern Physics*, 80(1):3–60, January 2008.

[64] Jiří Klimeš and Angelos Michaelides. Perspective: Advances and challenges in treating van der Waals dispersion forces in density functional theory. *The Journal of Chemical Physics*, 137(12):120901, September 2012.

[65] J. P. Perdew and Alex Zunger. Self-interaction correction to density-functional approximations for many-electron systems. *Physical Review B*, 23(10):5048–5079, May 1981.

[66] Wei Liu, Alexandre Tkatchenko, and Matthias Scheffler. Modeling Adsorption and Reactions of Organic Molecules at Metal Surfaces. *Accounts of Chemical Research*, 47(11):3369–3377, November 2014.

[67] Michael Rohlfing, Ruslan Temirov, and Frank Stefan Tautz. Adsorption structure and scanning tunneling data of a prototype organic-inorganic interface: PTCDA on Ag(111). *Physical Review B*, 76(11):115421, September 2007.

[68] Victor G. Ruiz, Wei Liu, Egbert Zojer, Matthias Scheffler, and Alexandre Tkatchenko. Density-Functional Theory with Screened van der Waals Interactions for the Modeling of Hybrid Inorganic-Organic Systems. *Physical Review Letters*, 108(14):146103, April 2012.

[69] Stefan Grimme, Jens Antony, Stephan Ehrlich, and Helge Krieg. A consistent and accurate ab initio parametrization of density functional dispersion correction (DFT-D) for the 94 elements H-Pu. *The Journal of Chemical Physics*, 132(15):154104, April 2010.

[70] Axel D. Becke and Erin R. Johnson. A density-functional model of the dispersion interaction. *The Journal of Chemical Physics*, 123(15):154101, October 2005.

[71] Alexandre Tkatchenko and Matthias Scheffler. Accurate Molecular Van Der Waals Interactions from Ground-State Electron Density and Free-Atom Reference Data. *Physical Review Letters*, 102(7):073005, February 2009.

[72] M. Dion, H. Rydberg, E. Schröder, D. C. Langreth, and B. I. Lundqvist. Van der Waals Density Functional for General Geometries. *Physical Review Letters*, 92(24):246401, June 2004.

[73] O. Anatole von Lilienfeld and Alexandre Tkatchenko. Two- and three-body interatomic dispersion energy contributions to binding in molecules and solids. *The Journal of Chemical Physics*, 132(23):234109, June 2010.

[74] Milton W. Cole, Darrell Velegol, Hye-Young Kim, and Amand A. Lucas. Nanoscale van der Waals interactions. *Molecular Simulation*, 35(10-11):849–866, September 2009.

[75] Alexandre Tkatchenko, Robert A. DiStasio, Roberto Car, and Matthias Scheffler. Accurate and Efficient Method for Many-Body van der Waals Interactions. *Physical Review Letters*, 108(23):236402, June 2012.

[76] Reinhard J. Maurer, Victor G. Ruiz, and Alexandre Tkatchenko. Many-body dispersion effects in the binding of adsorbates on metal surfaces. *The Journal of Chemical Physics*, 143(10):102808, June 2015.

[77] Filipp Furche and Troy Van Voorhis. Fluctuation-dissipation theorem density-functional theory. *The Journal of Chemical Physics*, 122(16):164106, April 2005.

[78] D. C. Langreth and J. P. Perdew. The exchange-correlation energy of a metallic surface. *Solid State Communications*, 17(11):1425–1429, December 1975.

[79] O. Gunnarsson and B. I. Lundqvist. Exchange and correlation in atoms, molecules, and solids by the spin-density-functional formalism. *Physical Review B*, 13(10):4274–4298, May 1976.

[80] Filipp Furche. Molecular tests of the random phase approximation to the exchange-correlation energy functional. *Physical Review B*, 64(19):195120, October 2001.

[81] Filipp Furche. Developing the random phase approximation into a practical post-Kohn-Sham correlation model. *The Journal of Chemical Physics*, 129(11):114105, September 2008.

[82] Dmitrij Rappoport, Nathan R. M. Crawford, Filipp Furche, and Kieron Burke. Approximate Density Functionals: Which Should I Choose? In *Encyclopedia of Inorganic Chemistry*. American Cancer Society, 2009.

[83] E. M. Lifshitz. The theory of molecular attractive forces between solids. *Soviet Phys. JETP*, Vol: 2, January 1955.

[84] E. Zaremba and W. Kohn. Van der Waals interaction between an atom and a solid surface. *Physical Review B*, 13(6):2270–2285, March 1976.

[85] Martin Willenbockel, Reinhard J. Maurer, Christopher Bronner, Michael Schulze, Benjamin Stadtmüller, Serguei Soubatch, Petra Tegeder, Karsten Reuter, and F. Stefan Tautz. Coverage-driven dissociation of azobenzene on Cu(111): a route towards defined surface functionalization. *Chemical Communications*, 51(83):15324–15327, 2015.

[86] Wei Liu, Friedrich Maaß, Martin Willenbockel, Christopher Bronner, Michael Schulze, Serguei Soubatch, F. Stefan Tautz, Petra Tegeder, and Alexandre Tkatchenko. Quantitative Prediction of Molecular Adsorption: Structure and Binding of Benzene on Coinage Metals. *Physical Review Letters*, 115(3):036104, July 2015.

[87] Yingkai Zhang and Weitao Yang. A challenge for density functionals: Self-interaction error increases for systems with a noninteger number of electrons. *The Journal of Chemical Physics*, 109(7):2604–2608, August 1998.

[88] Aron J. Cohen, Paula Mori-Sánchez, and Weitao Yang. Development of exchange-correlation functionals with minimal many-electron self-interaction error. *The Journal of Chemical Physics*, 126(19):191109, May 2007.

[89] Tim Heaton-Burgess and Weitao Yang. Structural manifestation of the delocalization error of density functional approximations: C4n+2 rings and C20 bowl, cage, and ring isomers. *The Journal of Chemical Physics*, 132(23):234113, June 2010.

[90] Viktor Atalla, Igor Ying Zhang, Oliver T. Hofmann, Xinguo Ren, Patrick Rinke, and Matthias Scheffler. Enforcing the linear behavior of the total energy with hybrid functionals: Implications for charge transfer, interaction energies, and the random-phase approximation. *Physical Review B*, 94(3):035140, July 2016.

[91] Oleg A. Vydrov, Gustavo E. Scuseria, and John P. Perdew. Tests of functionals for systems with fractional electron number. *The Journal of Chemical Physics*, 126(15):154109, April 2007.

[92] John P. Perdew, Adrienn Ruzsinszky, Gábor I. Csonka, Oleg A. Vydrov, Gustavo E. Scuseria, Viktor N. Staroverov, and Jianmin Tao. Exchange and correlation in open systems of fluctuating electron number. *Physical Review A*, 76(4):040501, October 2007.

[93] Noa Marom and Leeor Kronik. Density functional theory of transition metal phthalocyanines, I: electronic structure of NiPc and CoPc-self-interaction effects. *Applied Physics A*, 95(1):159–163, December 2008.

[94] Noa Marom and Leeor Kronik. Density functional theory of transition metal phthalocyanines, II: electronic structure of MnPc and FePc-symmetry and symmetry breaking. *Applied Physics A*, 95(1):165–172, April 2009.

[95] J. Hubbard. Electron correlations in narrow energy bands. *Proc. R. Soc. Lond. A*, 276(1365):238–257, November 1963.

[96] Vladimir I. Anisimov, F. Aryasetiawan, and A. I. Lichtenstein. First-principles calculations of the electronic structure and spectra of strongly correlated systems: the LDA + U method. *Journal of Physics: Condensed Matter*, 9(4):767, 1997.

[97] G. Kresse and J. Furthmüller. Efficient iterative schemes for ab initio total-energy calculations using a plane-wave basis set. *Physical Review B*, 54(16):11169–11186, October 1996.

[98] Jörg Neugebauer and Matthias Scheffler. Adsorbate-substrate and adsorbate-adsorbate interactions of Na and K adlayers on Al(111). *Physical Review B*, 46(24):16067–16080, December 1992.

[99] Jochen Heyd, Gustavo E. Scuseria, and Matthias Ernzerhof. Erratum: "Hybrid functionals based on a screened Coulomb potential" [J. Chem. Phys.118, 8207 (2003)]. *The Journal of Chemical Physics*, 124(21):219906, June 2006.

[100] M. Methfessel and A. T. Paxton. High-precision sampling for Brillouin-zone integration in metals. *Physical Review B*, 40(6):3616–3621, August 1989.

[101] C. L. Fu and K. M. Ho. First-principles calculation of the equilibrium ground-state properties of transition metals: Applications to Nb and Mo. *Physical Review B*, 28(10):5480–5486, November 1983.

[102] Hendrik J. Monkhorst and James D. Pack. Special points for Brillouin-zone integrations. *Physical Review B*, 13(12):5188–5192, June 1976.

[103] Anton Kokalj. Computer graphics and graphical user interfaces as tools in simulations of matter at the atomic scale. *Computational Materials Science*, 28(2):155–168, October 2003.

[104] Ion Vasilief. QtiPlot, November 2011.

[105] F. D. Murnaghan. The Compressibility of Media under Extreme Pressures. *Proceedings of the National Academy of Sciences*, 30(9):244–247, September 1944.

[106] Francis Birch. Finite Elastic Strain of Cubic Crystals. *Physical Review*, 71(11):809–824, June 1947.

[107] Elisabeth Verwüster, Oliver T. Hofmann, David A. Egger, and Egbert Zojer. Electronic Properties of Biphenylthiolates on Au(111): The Impact of Coverage Revisited. *The Journal of Physical Chemistry C*, 119(14):7817–7825, April 2015.

[108] Anna M. Track, Ferdinand Rissner, Georg Heimel, Lorenz Romaner, Daniel Käfer, Asif Bashir, Gerold M. Rangger, Oliver T. Hofmann, Tomáš Bučko, Gregor Witte, and Egbert Zojer. Simultaneously Understanding the Geometric and Electronic Structure of Anthraceneselenolate on Au(111): A Combined Theoretical and Experimental Study. *The Journal of Physical Chemistry C*, 114(6):2677–2684, February 2010.

[109] Ferdinand Rissner, David A. Egger, Lorenz Romaner, Georg Heimel, and Egbert Zojer. The Electronic Structure of Mixed Self-Assembled Monolayers. *ACS Nano*, 4(11):6735–6746, November 2010.

[110] David A. Egger, Ferdinand Rissner, Gerold M. Rangger, Oliver T. Hofmann, Lukas Wittwer, Georg Heimel, and Egbert Zojer. Self-assembled monolayers of polar molecules on Au(111) surfaces: distributing the dipoles. *Physical Chemistry Chemical Physics*, 12(17):4291–4294, 2010.

[111] Thomas C. Taucher, Iris Hehn, Oliver T. Hofmann, Michael Zharnikov, and Egbert Zojer. Understanding Chemical versus Electrostatic Shifts in X-ray Photoelectron Spectra of Organic Self-Assembled Monolayers. *The Journal of Physical Chemistry C*, 120(6):3428–3437, February 2016.

[112] Elisabeth Verwüster, Elisabeth Wruss, Egbert Zojer, and Oliver T. Hofmann. Exploring the driving forces behind the structural assembly of biphenylthiolates on Au(111). *The Journal of Chemical Physics*, 147(2):024706, July 2017.

[113] H. Bernhard Schlegel. Geometry optimization. *Wiley Interdisciplinary Reviews: Computational Molecular Science*, 1(5):790–809, May 2011.

[114] Roland Lindh, Anders Bernhardsson, Gunnar Karlström, and Per-Åke Malmqvist. On the use of a Hessian model function in molecular geometry optimizations. *Chemical Physics Letters*, 241(4):423–428, July 1995.

[115] Thomas H. Fischer and Jan Almlof. General methods for geometry and wave function optimization. *The Journal of Physical Chemistry*, 96(24):9768–9774, November 1992.

[116] Gregor Witte, Simon Lukas, Paul S. Bagus, and Christof Wöll. Vacuum level alignment at organic/metal junctions: "Cushion" effect and the interface dipole. *Applied Physics Letters*, 87(26):263502, December 2005.

[117] Ramón Cuadrado, Jorge I. Cerdá, Yongfeng Wang, Ge Xin, Richard Berndt, and Hao Tang. CoPc adsorption on Cu(111): Origin of the C4 to C2 symmetry reduction. *The Journal of Chemical Physics*, 133(15):154701, October 2010.

[118] B. Amin, S. Nazir, and U. Schwingenschlögl. Molecular distortion and charge transfer effects in ZnPc/Cu(111). *Scientific Reports*, 3, April 2013.

[119] Shih-Hsin Chang, Stefan Kuck, Jens Brede, Leonid Lichtenstein, Germar Hoffmann, and Roland Wiesendanger. Symmetry reduction of metal phthalocyanines on metals. *Physical Review B*, 78(23):233409, December 2008.

[120] H. Karacuban, M. Lange, J. Schaffert, O. Weingart, Th. Wagner, and R. Möller. Substrate-induced symmetry reduction of CuPc on Cu(1 1 1): An LT-STM study. *Surface Science*, 603(5):L39–L43, March 2009.

[121] Jakub D. Baran and J. Andreas Larsson. Structure and Energetics of Shuttlecock-Shaped Tin-Phthalocyanine on Ag(111): A Density Functional Study Employing Dispersion Correction. *The Journal of Physical Chemistry C*, 116(17):9487–9497, May 2012.

[122] B. V. Andryushechkin, V. V. Cherkez, E. V. Gladchenko, G. M. Zhidomirov, B. Kierren, Y. Fagot-Revurat, D. Malterre, and K. N. Eltsov. Structure of chlorine on Ag(111): Evidence of the (3x3) reconstruction. *Physical Review B*, 81(20):205434, May 2010.

[123] H. I. Li, K. Pussi, K. J. Hanna, L.-L. Wang, D. D. Johnson, H.-P. Cheng, H. Shin, S. Curtarolo, W. Moritz, J. A. Smerdon, R. McGrath, and R. D. Diehl. Surface Geometry of C60 on Ag(111). *Physical Review Letters*, 103(5):056101, July 2009.

[124] H. Piao, K. Adib, and Mark A. Barteau. A temperature-programmed X-ray photoelectron spectroscopy (TPXPS) study of chlorine adsorption and diffusion on Ag(111). *Surface Science*, 557(1):13–20, May 2004.

[125] Nahid Ilyas, Shashank S. Harivyasi, Percy Zahl, Rocio Cortes, Oliver T. Hofmann, Peter Sutter, Egbert Zojer, and Oliver L. A. Monti. Sticking with the Pointy End? Molecular Configuration of Chloro Boron-Subphthalocyanine on Cu(111). *The Journal of Physical Chemistry C*, 120(13):7113–7121, April 2016.

[126] Stefan Müllegger, Wolfgang Schöfberger, Mohammad Rashidi, Thomas Lengauer, Florian Klappenberger, Katharina Diller, Kamuran Kara, Johannes V. Barth, Eva Rauls, Wolf Gero Schmidt, and Reinhold Koch. Preserving Charge and Oxidation State of Au(III) Ions in an Agent-Functionalized Nanocrystal Model System. *ACS Nano*, 5(8):6480–6486, August 2011.

[127] Wheeler P. Davey. Precision Measurements of the Lattice Constants of Twelve Common Metals. *Physical Review*, 25(6):753–761, June 1925.

[128] G. M. Lamble, R. S. Brooks, S. Ferrer, D. A. King, and D. Norman. Surface structural determination for a weakly ordered and a disordered phase of Cl on Ag(111). *Physical Review B*, 34(4):2975–2978, August 1986.

[129] Katrin Forster-Tonigold and Axel Groß. A systematic DFT study of substrate reconstruction effects due to thiolate and selenolate adsorption. *Surface Science*, 640:18–24, October 2015.

[130] Diana Otálvaro, Thijs Veening, and Geert Brocks. Self-Assembled Monolayer Induced Au(111) and Ag(111) Reconstructions: Work Functions and Interface Dipole Formation. *The Journal of Physical Chemistry C*, 116(14):7826–7837, April 2012.

[131] G. Heimel, S. Duhm, I. Salzmann, A. Gerlach, A. Strozecka, J. Niederhausen, C. Bürker, T. Hosokai, I. Fernandez-Torrente, G. Schulze, S. Winkler, A. Wilke, R. Schlesinger, J. Frisch, B. Bröker, A. Vollmer, B. Detlefs, J. Pflaum, S. Kera, K. J. Franke, N. Ueno, J. I. Pascual, F. Schreiber, and N. Koch. Charged and metallic molecular monolayers through surface-induced aromatic stabilization. *Nature Chemistry*, 5(3):187–194, March 2013.

[132] Lothar Nordheim. Zur Elektronentheorie der Metalle. I. *Annalen der Physik*, 401(5):607–640, 1931.

[133] Andreas Jeindl. Influence of molecule size on surface polymorph formation: An ab-initio study with machine learning, 2018.

[134] Michael Scherbela, Lukas Hörmann, Andreas Jeindl, Veronika Obersteiner, and Oliver T. Hofmann. Charting the energy landscape of metal/organic interfaces via machine learning. *Physical Review Materials*, 2(4):043803, April 2018.

[135] G. Mercurio, E. R. McNellis, I. Martin, S. Hagen, F. Leyssner, S. Soubatch, J. Meyer, M. Wolf, P. Tegeder, F. S. Tautz, and K. Reuter. Structure and Energetics of Azobenzene on Ag(111): Benchmarking Semiempirical Dispersion Correction Approaches. *Physical Review Letters*, 104(3):036102, January 2010.

[136] Alberto Ambrosetti, Anthony M. Reilly, Robert A. DiStasio, and Alexandre Tkatchenko. Long-range correlation energy calculated from coupled atomic response functions. *The Journal of Chemical Physics*, 140(18):18A508, February 2014.

[137] J. Furthmueller, G. Kresse, and M. Marsman. VASP the GUIDE. Computational Physics, Faculty of Physics, Universitaet Wien, 2012.

[138] Oedoen Farkas and H. Bernhard Schlegel. Methods for optimizing large molecules. Part III. An improved algorithm for geometry optimization using direct inversion in the iterative subspace (GDIIS). *Physical Chemistry Chemical Physics*, 4(1):11–15, January 2002.

[139] Ajit Banerjee, Noah Adams, Jack Simons, and Ron Shepard. Search for stationary points on surfaces. *The Journal of Physical Chemistry*, 89(1):52–57, January 1985.

[140] Jorge Nocedal and S. Wright. *Numerical Optimization*. Springer Series in Operations Research and Financial Engineering. Springer-Verlag, New York, 2 edition, 2006.

[141] Wei Liu, Javier Carrasco, Biswajit Santra, Angelos Michaelides, Matthias Scheffler, and Alexandre Tkatchenko. Benzene adsorbed on metals: Concerted effect of covalency and van der Waals bonding. *Physical Review B*, 86(24):245405, December 2012.

[142] Herbert B. Michaelson. The work function of the elements and its periodicity. *Journal of Applied Physics*, 48(11):4729–4733, November 1977.

[143] M. Chelvayohan and C. H. B. Mee. Work function measurements on (110), (100) and (111) surfaces of silver. *Journal of Physics C: Solid State Physics*, 15(10):2305, 1982.

[144] Günter Gottstein. *Physikalische Grundlagen der Materialkunde*. Springer-Lehrbuch. Springer-Verlag, Berlin Heidelberg, 3 edition, 2007.

[145] Charles Kittel. *Einführung in die Festkörperphysik*. De Gruyter, Berlin, Boston, 13., korrigierte auflage. reprint 2017 edition, 2002.

[146] M. Mavrikakis, B. Hammer, and J. K. Nørskov. Effect of Strain on the Reactivity of Metal Surfaces. *Physical Review Letters*, 81(13):2819–2822, September 1998.

[147] Gerold M. Rangger, Oliver T. Hofmann, Lorenz Romaner, Georg Heimel, Benjamin Bröker, Ralf-Peter Blum, Robert L. Johnson, Norbert Koch, and Egbert Zojer. F4tcnq on Cu, Ag, and Au as prototypical example for a strong organic acceptor on coinage metals. *Physical Review B*, 79(16):165306, April 2009.

[148] Fabio Della Sala, Eduardo Fabiano, Savio Laricchia, Stefania D'Agostino, and Manuel Piacenza. The role of exact-exchange in the theoretical description of organic-metal interfaces. *International Journal of Quantum Chemistry*, 110(12):2162–2171, March 2010.

[149] John P. Perdew, Adrienn Ruzsinszky, Lucian A. Constantin, Jianwei Sun, and Gábor I. Csonka. Some Fundamental Issues in Ground-State Density Functional Theory: A Guide for the Perplexed. *Journal of Chemical Theory and Computation*, 5(4):902–908, April 2009.

[150] Anneli Önsten, Mats Göthelid, and Ulf O. Karlsson. Atomic structure of Cu2o(1 1 1). *Surface Science*, 603(2):257–264, January 2009.

[151] Chiara Gattinoni and Angelos Michaelides. Atomistic details of oxide surfaces and surface oxidation: the example of copper and its oxides. *Surface Science Reports*, 70(3):424–447, November 2015.

[152] Aloysius Soon, Mira Todorova, Bernard Delley, and Catherine Stampfl. Thermodynamic stability and structure of copper oxide surfaces: A first-principles investigation. *Physical Review B*, 75(12):125420, March 2007.

[153] Hermann Edlbauer, Egbert Zojer, and Oliver T. Hofmann. Postadsorption Work Function Tuning via Hydrogen Pressure Control. *The Journal of Physical Chemistry C*, 119(48):27162–27172, 2015.

[154] C. J. Nelin, P. S. Bagus, and M. R. Philpott. The nature of the bonding of CN to metals and organic molecules. *The Journal of Chemical Physics*, 87(4):2170–2176, August 1987.

[155] D. M. Newns. Self-Consistent Model of Hydrogen Chemisorption. *Physical Review*, 178(3):1123–1135, February 1969.

[156] T. B. Grimley. Chemisorption Theory. *Progress in Surface and Membrane Science*, 9:71–161, January 1975.

[157] Tamotsu Inabe and Hiroyuki Tajima. PhthalocyaninesVersatile Components of Molecular Conductors. *Chemical Reviews*, 104(11):5503–5534, November 2004.

[158] Martin Knupfer and Heiko Peisert. Electronic properties of interfaces between model organic semiconductors and metals. *physica status solidi (a)*, 201(6):1055–1074, April 2004.

[159] J. Michael Gottfried. Surface chemistry of porphyrins and phthalocyanines. *Surface Science Reports*, 70(3):259–379, November 2015.

[160] Christoph Stadler, Sören Hansen, Ingo Kröger, Christian Kumpf, and Eberhard Umbach. Tuning intermolecular interaction in long-range-ordered submonolayer organic films. *Nature Physics*, 5(2):153–158, February 2009.

[161] Pierluigi Gargiani, Marco Angelucci, Carlo Mariani, and Maria Grazia Betti. Metal-phthalocyanine chains on the Au(110) surface: Interaction states versus d-metal states occupancy. *Physical Review B*, 81(8):085412, February 2010.

[162] J. D. Baran, J. A. Larsson, R. A. J. Woolley, Yan Cong, P. J. Moriarty, A. A. Cafolla, K. Schulte, and V. R. Dhanak. Theoretical and experimental comparison of SnPc, PbPc, and CoPc adsorption on Ag(111). *Physical Review B*, 81(7):075413, February 2010.

[163] Benjamin Stadtmüller, Ingo Kröger, Friedrich Reinert, and Christian Kumpf. Submonolayer growth of CuPc on noble metal surfaces. *Physical Review B*, 83(8):085416, February 2011.

[164] Aitor Mugarza, Cornelius Krull, Roberto Robles, Sebastian Stepanow, Gustavo Ceballos, and Pietro Gambardella. Spin coupling and relaxation inside molecule-metal contacts. *Nature Communications*, 2:490, October 2011.

[165] A. Mugarza, R. Robles, C. Krull, R. Korytár, N. Lorente, and P. Gambardella. Electronic and magnetic properties of molecule-metal interfaces: Transition-metal phthalocyanines adsorbed on Ag(100). *Physical Review B*, 85(15):155437, April 2012.

[166] Jakub D. Baran and J. Andreas Larsson. Theoretical Insights into Adsorption of Cobalt Phthalocyanine on Ag(111): A Combination of Chemical and van der Waals Bonding. *The Journal of Physical Chemistry C*, 117(45):23887–23898, November 2013.

[167] C. Iacovita, M. V. Rastei, B. W. Heinrich, T. Brumme, J. Kortus, L. Limot, and J. P. Bucher. Visualizing the Spin of Individual Cobalt-Phthalocyanine Molecules. *Physical Review Letters*, 101(11):116602, September 2008.

[168] Emilia Annese, Jun Fujii, Ivana Vobornik, Giancarlo Panaccione, and Giorgio Rossi. Control of the magnetism of cobalt phthalocyanine by a ferromagnetic substrate. *Physical Review B*, 84(17):174443, November 2011.

[169] Ying-Shuang Fu, Qi-Kun Xue, and Roland Wiesendanger. Spin-Resolved Splitting of Kondo Resonances in the Presence of RKKY-Type Coupling. *Physical Review Letters*, 108(8):087203, February 2012.

[170] Emilia Annese, Carlos E. ViolBarbosa, Giorgio Rossi, and Jun Fujii. CoPc 2d and 1d Arrangement on a Ferromagnetic Surface. *Langmuir*, 32(21):5300–5305, May 2016.

[171] Aidi Zhao, Qunxiang Li, Lan Chen, Hongjun Xiang, Weihua Wang, Shuan Pan, Bing Wang, Xudong Xiao, Jinlong Yang, J. G. Hou, and Qingshi Zhu. Controlling the Kondo Effect of an Adsorbed Magnetic Ion Through Its Chemical Bonding. *Science*, 309(5740):1542–1544, September 2005.

[172] L. Gao, W. Ji, Y. B. Hu, Z. H. Cheng, Z. T. Deng, Q. Liu, N. Jiang, X. Lin, W. Guo, S. X. Du, W. A. Hofer, X. C. Xie, and H.-J. Gao. Site-Specific Kondo Effect at Ambient Temperatures in Iron-Based Molecules. *Physical Review Letters*, 99(10):106402, September 2007.

[173] Ying-Shuang Fu, Shuai-Hua Ji, Xi Chen, Xu-Cun Ma, Rui Wu, Chen-Chen Wang, Wen-Hui Duan, Xiao-Hui Qiu, Bo Sun, Ping Zhang, Jin-Feng Jia, and Qi-Kun Xue. Manipulating the Kondo Resonance through Quantum Size Effects. *Physical Review Letters*, 99(25):256601, December 2007.

[174] S. Stepanow, A. Mugarza, G. Ceballos, P. Moras, J. C. Cezar, C. Carbone, and P. Gambardella. Giant spin and orbital moment anisotropies of a Cu-phthalocyanine monolayer. *Physical Review B*, 82(1):014405, July 2010.

[175] S. Stepanow, P. S. Miedema, A. Mugarza, G. Ceballos, P. Moras, J. C. Cezar, C. Carbone, F. M. F. de Groot, and P. Gambardella. Mixed-valence behavior and strong correlation effects of metal phthalocyanines adsorbed on metals. *Physical Review B*, 83(22):220401, June 2011.

[176] Sebastian Stepanow, Alberto Lodi Rizzini, Cornelius Krull, Jerald Kavich, Julio C. Cezar, Flora Yakhou-Harris, Polina M. Sheverdyaeva, Paolo Moras, Carlo Carbone, Gustavo Ceballos, Aitor Mugarza, and Pietro Gambardella. Spin Tuning of Electron-Doped Metal-Phthalocyanine Layers. *Journal of the American Chemical Society*, 136(14):5451–5459, April 2014.

[177] E. Salomon, P. Amsalem, N. Marom, M. Vondracek, L. Kronik, N. Koch, and T. Angot. Electronic structure of CoPc adsorbed on Ag(100): Evidence for molecule-substrate interaction mediated by Co 3d orbitals. *Physical Review B*, 87(7):075407, February 2013.

[178] Zhenyu Li, Bin Li, Jinlong Yang, and Jian Guo Hou. Single-Molecule Chemistry of Metal Phthalocyanine on Noble Metal Surfaces. *Accounts of Chemical Research*, 43(7):954–962, July 2010.

[179] Marius Toader, Pavel Shukrynau, Martin Knupfer, Dietrich R. T. Zahn, and Michael Hietschold. Site-Dependent Donation/Backdonation Charge Transfer at the CoPc/Ag(111) Interface. *Langmuir*, 28(37):13325–13330, September 2012.

[180] T. Körzdörfer, S. Kümmel, N. Marom, and L. Kronik. When to trust photoelectron spectra from Kohn-Sham eigenvalues: The case of organic semiconductors. *Physical Review B*, 79(20):201205, May 2009.

[181] T. Körzdörfer. On the relation between orbital-localization and self-interaction errors in the density functional theory treatment of organic semiconductors. *The Journal of Chemical Physics*, 134(9):094111, March 2011.

[182] Carlo Adamo and Vincenzo Barone. Toward reliable density functional methods without adjustable parameters: The PBE0 model. *The Journal of Chemical Physics*, 110(13):6158–6170, March 1999.

[183] Jochen Heyd and Gustavo E. Scuseria. Assessment and validation of a screened Coulomb hybrid density functional. *The Journal of Chemical Physics*, 120(16):7274–7280, April 2004.

[184] Jochen Heyd and Gustavo E. Scuseria. Efficient hybrid density functional calculations in solids: Assessment of the Heyd-Scuseria-Ernzerhof screened Coulomb hybrid functional. *The Journal of Chemical Physics*, 121(3):1187–1192, July 2004.

[185] Iann C. Gerber, János G. ángyán, Martijn Marsman, and Georg Kresse. Range separated hybrid density functional with long-range Hartree-Fock exchange applied to solids. *The Journal of Chemical Physics*, 127(5):054101, August 2007.

[186] Aliaksandr V. Krukau, Oleg A. Vydrov, Artur F. Izmaylov, and Gustavo E. Scuseria. Influence of the exchange screening parameter on the performance of screened hybrid functionals. *The Journal of Chemical Physics*, 125(22):224106, 2006.

[187] Mathis Gruber, Georg Heimel, Lorenz Romaner, Jean-Luc Brédas, and Egbert Zojer. First-principles study of the geometric and electronic structure of au_{13} clusters: Importance of the prism motif. *Physical Review B*, 77(16):165411, April 2008.

[188] Noa Marom, Xinguo Ren, Jonathan E. Moussa, James R. Chelikowsky, and Leeor Kronik. Electronic structure of copper phthalocyanine from g_0w_0 calculations. *Physical Review B*, 84(19):195143, November 2011.

[189] F. L. Hirshfeld. Bonded-atom fragments for describing molecular charge densities. *Theoretica chimica acta*, 44(2):129–138, June 1977.

[190] R. S. Mulliken. Electronic Population Analysis on LCAO-MO Molecular Wave Functions. I. *The Journal of Chemical Physics*, 23(10):1833–1840, October 1955.

[191] R. C. Albers, N. E. Christensen, and A. Svane. Hubbard- U band-structure methods. *Journal of Physics: Condensed Matter*, 21(34):343201, 2009.

[192] Iulia Emilia Brumboiu, Soumyajyoti Haldar, Johann Lüder, Olle Eriksson, Heike C. Herper, Barbara Brena, and Biplab Sanyal. Influence of Electron Correlation on the Electronic Structure and Magnetism of Transition-Metal Phthalocyanines. *Journal of Chemical Theory and Computation*, 12(4):1772–1785, April 2016.

[193] Viktor Ivády, Rickard Armiento, Krisztián Szász, Erik Janzén, Adam Gali, and Igor A. Abrikosov. Theoretical unification of hybrid-DFT and DFT + U methods for the treatment of localized orbitals. *Physical Review B*, 90(3):035146, July 2014.

[194] Pragya Verma and Donald G. Truhlar. Does DFT+U mimic hybrid density functionals? *Theoretical Chemistry Accounts*, 135(8):182, August 2016.

[195] Terry Z. H. Gani and Heather J. Kulik. Where Does the Density Localize? Convergent Behavior for Global Hybrids, Range Separation, and DFT+U. *Journal of Chemical Theory and Computation*, 12(12):5931–5945, December 2016.

[196] Cornelius Krull, Robles Roberto, Aitor Mugarza, and Pietro Gambardella. Site- and orbital-dependent charge donation and spin manipulation in electron-doped metal phthalocyanines | Nature Materials. *Nature Materials*, 12:337–343, January 2013.

[197] Zhenpeng Hu, Bin Li, Aidi Zhao, Jinlong Yang, and J. G. Hou. Electronic and Magnetic Properties of Metal Phthalocyanines on Au(111) Surface: A First-Principles Study. *The Journal of Physical Chemistry C*, 112(35):13650–13655, September 2008.

[198] Xi Chen, Ying-Shuang Fu, Shuai-Hua Ji, Tong Zhang, Peng Cheng, Xu-Cun Ma, Xiao-Long Zou, Wen-Hui Duan, Jin-Feng Jia, and Qi-Kun Xue. Probing Superexchange Interaction in Molecular Magnets by Spin-Flip Spectroscopy and Microscopy. *Physical Review Letters*, 101(19):197208, November 2008.

[199] Benjamin W. Heinrich, Cristian Iacovita, Thomas Brumme, Deung-Jang Choi, Laurent Limot, Mircea V. Rastei, Werner A. Hofer, Jens Kortus, and Jean-Pierre Bucher. Direct Observation of the Tunneling Channels of a Chemisorbed Molecule. *The Journal of Physical Chemistry Letters*, 1(10):1517–1523, May 2010.

[200] Xi Chen and M. Alouani. Effect of metallic surfaces on the electronic structure, magnetism, and transport properties of Co-phthalocyanine molecules. *Physical Review B*, 82(9):094443, September 2010.

[201] Jens Brede, Nicolae Atodiresei, Stefan Kuck, Predrag LaziÄĞ, Vasile Caciuc, Yoshitada Morikawa, Germar Hoffmann, Stefan Blügel, and Roland Wiesendanger. Spin- and Energy-Dependent Tunneling through a Single Molecule with Intramolecular Spatial Resolution. *Physical Review Letters*, 105(4):047204, July 2010.

[202] Benjamin Siegert, Andrea Donarini, and Milena Grifoni. Nonequilibrium spin crossover in copper phthalocyanine. *Physical Review B*, 93(12):121406, March 2016.

[203] Yu Wang, Xiao Zheng, Bin Li, and Jinlong Yang. Understanding the Kondo resonance in the d-CoPc/Au(111) adsorption system. *The Journal of Chemical Physics*, 141(8):084713, August 2014.

[204] Martin Schmid, Andre Kaftan, Hans-Peter Steinrück, and J. Michael Gottfried. The electronic structure of cobalt(II) phthalocyanine adsorbed on Ag(111). *Surface Science*, 606(11-12):945–949, June 2012.

[205] Justin P. Bergfield, Zhen-Fei Liu, Kieron Burke, and Charles A. Stafford. Bethe Ansatz Approach to the Kondo Effect within Density-Functional Theory. *Physical Review Letters*, 108(6):066801, February 2012.

[206] Jens Kügel, Michael Karolak, Jacob Senkpiel, Pin-Jui Hsu, Giorgio Sangiovanni, and Matthias Bode. Relevance of Hybridization and Filling of 3d Orbitals for the Kondo Effect in Transition Metal Phthalocyanines. *Nano Letters*, 14(7):3895–3902, July 2014.

[207] Pierluigi Gargiani, Antonio Calabrese, Carlo Mariani, and Maria Grazia Betti. Control of Electron Injection Barrier by Electron Doping of Metal Phthalocyanines. *The Journal of Physical Chemistry C*, 114(28):12258–12264, July 2010.

[208] Cheol Ho Choi, Miklos Kertesz, and Alfred Karpfen. The effects of electron correlation on the degree of bond alternation and electronic structure of oligomers of polyacetylene. *The Journal of Chemical Physics*, 107(17):6712–6721, November 1997.

[209] Denis Jacquemin and Carlo Adamo. Bond Length Alternation of Conjugated Oligomers: Wave Function and DFT Benchmarks. *Journal of Chemical Theory and Computation*, 7(2):369–376, February 2011.

[210] J. Zegenhagen. Surface structure determination with X-ray standing waves. *Surface Science Reports*, 18(7-8):202–271, October 1993.

[211] D. P. Woodruff. Surface structure determination using x-ray standing waves. *Reports on Progress in Physics*, 68(4):743, April 2005.

[212] I. G. Hill, A. Rajagopal, A. Kahn, and Y. Hu. Molecular level alignment at organic semiconductor-metal interfaces. *Applied Physics Letters*, 73(5):662–664, August 1998.

[213] Xavier Crispin, Victor Geskin, Annica Crispin, Jérôme Cornil, Roberto Lazzaroni, William R. Salaneck, and Jean-Luc Brédas. Characterization of the Interface Dipole at Organic/ Metal Interfaces. *Journal of the American Chemical Society*, 124(27):8131–8141, July 2002.

[214] Norbert Koch. Organic Electronic Devices and Their Functional Interfaces. *ChemPhysChem*, 8(10):1438–1455, July 2007.

[215] D. Hofmann and S. Kümmel. Integer particle preference during charge transfer in Kohn-Sham theory. *Physical Review B*, 86(20):201109, November 2012.

[216] Tamar Stein, Jochen Autschbach, Niranjan Govind, Leeor Kronik, and Roi Baer. Curvature and Frontier Orbital Energies in Density Functional Theory. *The Journal of Physical Chemistry Letters*, 3(24):3740–3744, December 2012.

[217] Eli Kraisler and Leeor Kronik. Piecewise Linearity of Approximate Density Functionals Revisited: Implications for Frontier Orbital Energies. *Physical Review Letters*, 110(12):126403, March 2013.